Real-time reporting of marine ecosystem metrics from active acoustic sensors

Robert Edward Blackwell

Thesis submitted in partial fulfilment of the requirements for the degree of Doctor of Philosophy.

University of East Anglia

School of Environmental Sciences

December 15, 2020

"They that go down to the sea in ships, that do business in great waters;
These see the works of the Lord, and his wonders in the deep."

Psalm 107:23-24.

Abstract

Marine autonomous vehicles (MAVs) carrying active acoustic sensors (echosounders) are being used for ecosystem research, but high data volumes are presenting challenges for data storage, processing and communication. One of the appeals of autonomous vehicles is directing them to regions of interest and receiving data in real-time, but current satellite networks have insufficient bandwidth for real-time acoustic data transmission. We seek solutions using data compression or summarisation.

We first explore the use of generic, lossless data compression algorithms (e.g. ZIP) and find that they do not deliver the necessary reduction in data size. We then convert acoustic data to echograms and examine the role of colour palettes in echogram interpretation, but image compression is still unsatisfactory.

Using echosounder data from the Southern Ocean ecosystem at South Georgia, collected by research vessels (which are easier to work with and more readily available than MAV acoustic data), we compute acoustic summary metrics and assess their correlation to independent ecosystem indices. There is a strong correlation between *abundance* and traditional krill density estimates ($r = 0.83$, $p < 0.01$) and *location* (centre of mass of acoustic backscatter) and chlorophyll ($r = -0.7$, $p < 0.01$) suggesting that acoustic summaries could be used as concise ecosystem descriptors.

Aliased seabed is a corruption caused by acoustic reflections and its removal is an example of an acoustic processing step that is currently undertaken manually. We use modern machine learning techniques and develop

a conventional algorithm to detect aliased seabed automatically in single frequency, split-beam echosounder data without the need for bathymetry.

Finally, we demonstrate an unsupervised acoustic data processing system (RAPIDKRILL) that can transmit acoustically derived ecosystem indicators in real-time via the Iridium satellite network. The technology is fully autonomous, low-cost, and could be further developed for use on MAVs.

Contents

Note to examiners

This PhD work was funded by the Next Generation Unmanned Systems Science (NEXUSS) Centre for Doctoral Training (CDT) and is a blend of experimental science and systems engineering. The CDT handbook, *NEXUSS information for students and supervisors*[1] states:

"The PhD projects that NEXUSS students are engaged in may differ from traditional science or traditional engineering PhD projects. This means that outputs from these PhDs will not solely be scientific discoveries, nor hardware developed. The NEXUSS CDT firmly supports the idea of PhDs that are a blend of traditional science and traditional engineering, and expects that advisory panels will adjust expectations to account for this approach, while still upholding their host institution's requirement for what constitutes a PhD."

---

[1] https://bit.ly/2VOAORh, accessed April 2020.

Acknowledgements

List of abbreviations

ARM - Advanced RISC Machines is a computer processor architecture.

AS - In fisheries acoustics, an Attenuated Signal has reduced amplitude, often caused by bubbles in the water.

ASB - Aliased SeaBed is a corruption in acoustic data caused by unwanted reflections from the seabed.

ASV - An Autonomous Surface Vehicle is a kind of marine autonomous vehicle.

AUV - An Autonomous Underwater Vehicle is a kind of marine autonomous vehicle.

BN - Background Noise is the noise floor caused by natural and anthropogenic sound.

CVD - Colour Vision Deficiency is more commonly known as colour blindness.

CN - Combined Noise is a general term for all noise in a fisheries acoustic system.

CNN - A Convolutional Neural Network is a class of deep neural network commonly used in image processing.

CPU - A Central Processing Unit is the part of a computer used to execute computer programs.

CSV - Comma Separated Value is a data representation format in which individual data are delimited by commas.

CTD - An oceanographic instrument used to measure Conductivity, Temperature and Depth.

CW - A Continuous Wave is a signal of constant amplitude and frequency.

DVM - Diurnal Vertical Migration describes the vertical movement of zooplankton between the surface (at night to feed) and depth (during the day to avoid predation).

EDSU - An Elementary Distance Sampling Unit is the length of cruise track over which acoustic measurements are averaged to form a single sample.

EK400, EK60, EK80 - Simrad scientific echosounder model numbers.

FM - Frequency Modulation is the process of varying the frequency of an electromagnetic wave to encode a signal.

FPGA - A Field Programmable Gate Array is a semiconductor device whose hardware can be programmatically reconfigured after manufacturing.

GPRS - General Packet Radio Service (GPRS) is a packet oriented mobile communication data standard.

GPU - A Graphics Processing Unit is a semiconductor device originally designed for fast manipulation of images for display purposes. However, a GPU can also be used for fast linear algebra.

IN - Impulse Noise consists of noise spikes seen in fisheries acoustic data.

IOT - An Internet of Things is a system of internetworked sensors and devices.

MAV - Marine Autonomous Vehicle.

NASC - Nautical Area Scattering Coefficient (m^2nmi^{-2}).

PAR - Photosynthetically Available Radiation is a spectral range that can be sampled as a proxy for photosynthesis.

PCA - Principal Component Analysis is an exploratory data analysis method used to assess variability in multivariate data.

SBD - Short Burst Data is a very low bandwidth, low cost satellite communication system provided by Iridium LLC. Message size is 270 bytes mobile terminated, and 340 bytes mobile originated.

SHAPES - SHoal Analysis And Patch Estimation System is a method for finding and measuring animal aggregations in fisheries acoustic data.

SMB - Server Message Block is an Internet protocol providing file sharing.

SOC - A System on Chip combines nearly all components of a traditional computer in a single integrated circuit.

SONAR - SOund Navigation And Ranging is the technology that enables echosounders.

TCP/IP - Transmission Control Protocol / Internet Protocol interconnects network devices on the Internet.

TN - Transient Noise in fisheries acoustic data is noise lasting for several pings and may be due to waves on the hull.

TRL - Technology Readiness Level is a scale for measuring technology maturity.

TS - Target Strength is a measure of the acoustic reflection from a sonar target.

TVG - Time Varied Gain is a compensation for signal strength attenuation.

UDP - User Datagram Protocol is an Internet protocol providing simple, connectionless but unreliable communication.

USB - Universal Serial Bus is a common interface that enables wired communication between devices and a host controller.

USV - An Unmanned Surface Vehicle is a kind of marine autonomous vehicle.

WG-FAST - Working Group on Fisheries Acoustics Science and Technology.

WiFi - Wireless Fidelity allows devices to connect and communicate with one another wirelessly within an area of a few tens of metres.

XML - eXtensible Markup Language is a text-based data representation format that is intended to be both machine readable and human readable.

List of Figures

List of Tables

Chapter 1

Introduction

> "(this) is or should be our main scientific activity – studying the structure of information and the structure of problem solving processes"
>
> John McCarthy (1974)

Sound is the most effective method for sensing the underwater marine environment (Fernandes *et al.*, 2002). Active acoustic sampling from research vessels is one of the principle tools for marine ecosystems analysis (Simmonds and MacLennan, 2005; Benoit-Bird and Lawson, 2016), but research vessels are expensive resources. The new polar research vessel, the RRS Sir David Attenborough, is reportedly costing £200 million (HM Government, 2015). Ship time is also expensive, both financially (£20k - £30k per day) and in terms of environmental impact (emissions from marine diesel engines). Ships are also limited for safety reasons (for example, they can't work in very rough weather, in areas at risk from piracy, or near calving glaciers).

Marine autonomous vehicles (MAVs) have been proposed as more cost-effective and flexible alternatives to ships (Griffiths, 2002), and one of the appeals of MAVs is the potential to direct them to any region of interest and receive data in real-time. An autonomous underwater vehicle (AUV) such as an ocean glider (Eriksen *et al.*, 2001; Rudnick, 2016) might cost less

than £150k. AUVs have been deployed in a growing number of marine science studies and will continue to play an increasingly important role in the exploration and monitoring of the oceans (Wynn *et al.*, 2014). The ocean glider community has grown rapidly (Testor *et al.*, 2019). National ocean observation agencies have invested in developing glider observing capability, and as of 2019, there were reportedly about 400–500 gliders in the world actively being used to better observe the ocean.

Fisheries acoustic echosounders have been used on MAVs (e.g. Guihen *et al.*, 2014; Benoit-Bird *et al.*, 2018), but they generate large amounts of data and communication bandwidth is limited in marine environments (Guihen *et al.*, 2014). Current practice is to store acoustic data locally for retrieval and analysis once the MAV is recovered. This leaves missions liable to data loss in the event of vehicle loss and limits adaptive sampling and reactive survey management strategies. The problem is becoming more acute with the introduction of newer broadband instruments with higher data rates. Large acoustic data volumes are already complex and costly to maintain (Wall, Jech and McLean, 2016), but much more data are required if we are to address key marine science questions (Meredith *et al.*, 2013; Kennicutt *et al.*, 2014). Therefore, effective methods for reducing the size of fisheries acoustic data are urgently required.

1.1 Fisheries acoustics

Fishing is an important source of food, nutrition and income, having a total global fish production of 171 million tonnes in 2016 (Food and Agriculture Organization of the United Nations, 2018), but fisheries management entails challenges including governance, sustainability, illegal fishing and climate change (Sumaila, 2012).

Fisheries acoustics, supported by net haul data, is the principle means of measuring animal abundance, distribution and biomass (Simmonds and MacLennan, 2005). Echosounders use sonar (originally an acronym for SOund Navigation And Ranging), transmitting pulses of sound and mea-

suring the magnitude, phase and delay of received responses. The transmitter and the receiver are often one and the same device, referred to as a transducer and typically operate at frequencies between 18 and 333 kHz. When a sound wave insonifies a target, some of the energy is absorbed, some scattered and some is reflected back towards the transducer. The transmission time, when adjusted for hydrographic conditions, is proportional to the range of the target. The received signal can be analysed to infer information about biology in the water column. Echosounder operation is modelled using the sonar equation (1.1) (Urick, 1967).

$$\text{SL} - 2\text{TL} + \text{TS} - (\text{NL} - \text{DI}) = \text{DT} \qquad (1.1)$$

SL is the source level of the transmitted signal, TL is the transmission loss in each direction, TS is the target strength, NL is the background noise level, DI is the directivity index of the transducer and DT, the detection threshold. The left-hand side of the equation is the signal to noise ratio that must reach the detection threshold for a target to be detected. All units are in decibels (a logarithmic ratio scale) rather than SI units, because values can be very large or very small, covering many orders of magnitude.

Beam spreading reduces the resolution of an echosounder with distance to target. It is impossible to differentiate between individual target fish in the far field and so volume backscatter is calculated by integrating the received signal. This allows the intensity of animal aggregations to be measured. A time varied gain (TVG) function is applied to amplify the signal and compensate for range. Frequently, acoustic data are presented as echograms, images synthesised from detected backscatter plotted by depth and time, displaying a vertical cross-section of the water column as in Figure 1.1.

Different species exhibit different backscattering effects at different frequencies depending on their biological characteristics, including presence of a shell, swim bladder or skeleton (Korneliussen and Ona, 2003). Frequencies can therefore be selected to enable species differentiation and identification. Narrowband, continuous wave (CW) echosounders transmit and receive
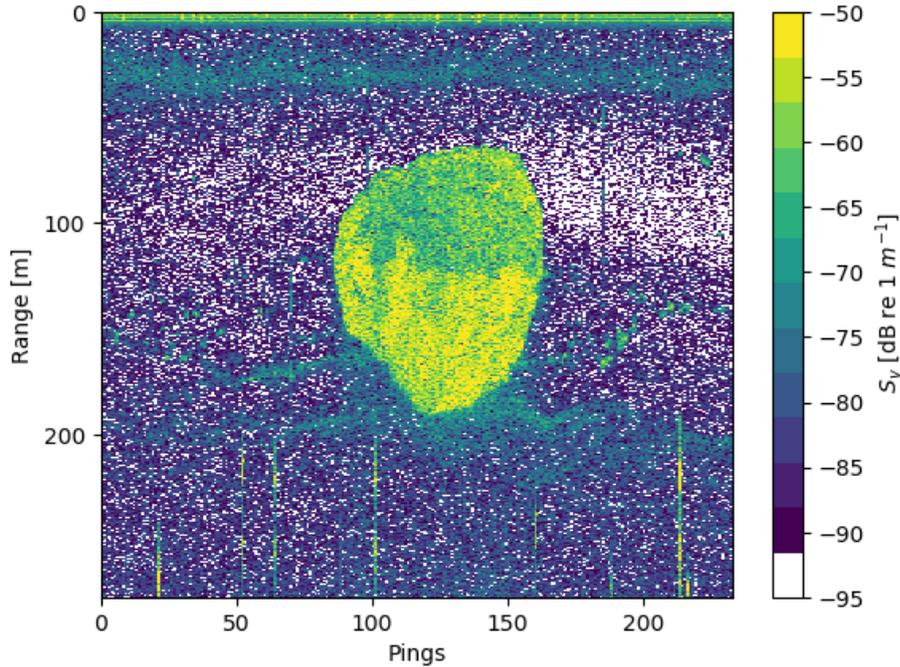
Figure 1.1: An example echogram depicting an Antarctic krill swarm. The swarm is about 150 m in height and 1 km in plan. Data collected using a Simrad EK60 scientific echosounder (120 kHz, ping interval $I_T = 2$ s, nominal speed = 10 kts) onboard RRS James Clark Ross, Cruise JR230, Southern Ocean, December 2009.

sound pulses at single frequencies. Broadband, or wideband, echosounders use frequency modulated (FM) pulses called chirps (originally an acronym for Compressed High Intensity Radar Pulse), comprising a range of frequencies (Fassler *et al.*, 2015). A split-beam echosounder has a transducer that is divided into four parts, thereby using phase difference to measure target direction (often referred to as split-beam angle).

If a target school or swarm is homogeneous, then estimates of abundance and biomass can be made based on knowledge of the scattering properties of an individual animal (Horne, 2000). In practice, acoustic responses often come from heterogeneous, unknown targets that are difficult to distinguish, making automated species identification challenging. The problem of determining characteristics of a target, based on backscatter is known as the

inverse scattering problem.

Following an acoustic survey, echosounder data are typically post processed using interactive software (Foote *et al.*, 1991) to:

- convert the received signal to target strength or mean volume backscattering coefficient;
- remove noise;
- detect and segment targets;
- estimate animal abundance.

Received signal is converted to volume backscattering coefficient (S_v) based on the sonar equation[1]. Adjustments are applied following instrument calibration (Demer *et al.*, 2015). The signal inevitably includes unwanted noise from physical, biological and artificial sources. Along with ambient and anthropogenic acoustic noise, ships are a source of electromagnetic noise. Signal processing techniques (Vaseghi, 2008) are often employed for noise reduction, removal and correction (e.g. Ryan *et al.*, 2015).

Target detection identifies regions of interest within echograms using manual, semi-automated or automated classification. Expert manual interpretation of echograms is often referred to as scrutinisation. Target detection may include:

- comparison of frequency responses to the scattering properties of different species (Madureira, Everson and Murphy, 1993; Korneliussen and Ona, 2003);
- thresholding of backscattering strength;
- pattern recognition based on the shape of targets;
- application specific algorithms, e.g. shoal analysis and patch estimation system (SHAPES) (Coetzee, 2000).

Finally, net hauls are typically used to validate target identification and parameterise target strength models that are then used to convert acoustic

---

[1]The sonar equation for a Simrad EK60 echosounder is given in Appendix A.

backscatter to animal abundance or biomass.

Fisheries acoustic surveys are typically conducted from research vessels, but autonomous underwater vehicles (Guihen *et al.*, 2014), unmanned surface vessels (Manley, 2008) and fishing vessels (Godø *et al.*, 2014; Watkins *et al.*, 2016) offer alternative options. AUVs in particular are often electromagnetically and acoustically quieter than ships, and allow close range measurement from within the ocean interior rather than from the surface. Moline *et al.* (2015) describe a deployment of an echosounder on a REMUS 600 to examine the biology of animals in the mesopelagic zone (600–1200 m), Guihen *et al.* (2014) describe the use of a Seaglider to make acoustic measurements of zooplankton and Suberg *et al.* (2014) assess the use of gliders for both passive and active acoustic sampling. Greene *et al.* (2014) envisage a time when fleets of gliders contribute to acoustic biomass surveys. Real-time communication is key to this vision, enabling coordinated activity and dynamic, adaptive sampling (Maxwell *et al.*, 2015).

In this thesis, we consider Antarctic krill as an ecosystem exemplar and use echosounder recordings from around South Georgia in the South Atlantic, where krill is the dominant species.

1.2 Antarctic krill

Antarctic krill, *Euphausia superba* is a type of zooplankton found in the Southern Ocean. It is one of the most abundant species on Earth, supplying the Southern Ocean fishery (Nicol and Foster, 2016) and performing a central role in Sub-Antarctic food webs (Trathan and Hill, 2016). Zooplankton are known to contribute to the biological carbon pump (Giering *et al.*, 2014) and are vulnerable to climate change (Flores *et al.*, 2012). Despite these factors, the species remains under sampled, and production and biomass estimates remain uncertain (Atkinson *et al.*, 2009).

The distribution of Antarctic krill is bounded by the polar front; therefore, krill habitat is estimated to cover some 19×10^6 km^2 (Atkinson *et al.*, 2009).

Krill behaviour is complex, making it hard to build statistical models of distribution and abundance. Surveys of Antarctic krill typically take place from research ships. Direct sampling using net hauls allows accurate species identification, but suffers from bias due to avoidance, which is dependent on net type and depth (Everson, 2008). Acoustic sampling uses backscatter as a proxy for abundance and allows sampling over large areas but can be ambiguous in terms of species identification (Demer and Conti, 2005). Net sampling is often used to ground-truth acoustic sampling (Siegel, 2016) and current krill estimates show a total biomass of 379 million tonnes. (Atkinson *et al.*, 2009).

The Western Core Box (WCB) is an annual ship-based survey, conducted near South Georgia by the British Antarctic Survey, collecting echosounder and net haul data (Fielding *et al.*, 2014). The data are primarily used to study Antarctic krill (Figure 1.2), and we make extensive use of these data in this thesis.

The Commission for the Conservation of Antarctic Marine Living Resources (CCAMLR) is responsible for management of the Antarctic krill fishery and for setting annual, precautionary catch limits (currently 5.6 million tonnes). The fishery is the largest by tonnage in the Southern Ocean (approximately 300 kilo-tonnes annually), with krill being used for aquaculture, fish bait and nutritional supplements for human consumption. Its management regime faces challenges in terms of increasing demand, new harvesting technology and environmental change (Nicol and Foster, 2016).

The management of the Antarctic krill fishery, as implemented by CCAMLR, requires large scale biomass estimates. At the Scotia Sea scale, this is undertaken as part of multinational, multi-ship surveys and has been completed three times (1981, 2000 and 2019: Trathan *et al.*, 1995; Watkins *et al.*, 2004; Krafft *et al.*, 2019). In between these large surveys, the interannual context has been sampled at the regional level (Reiss *et al.*, 2008; Fielding *et al.*, 2014; Krafft *et al.*, 2018). As the cost of ship time increases, managers are looking for alternative platforms to undertake
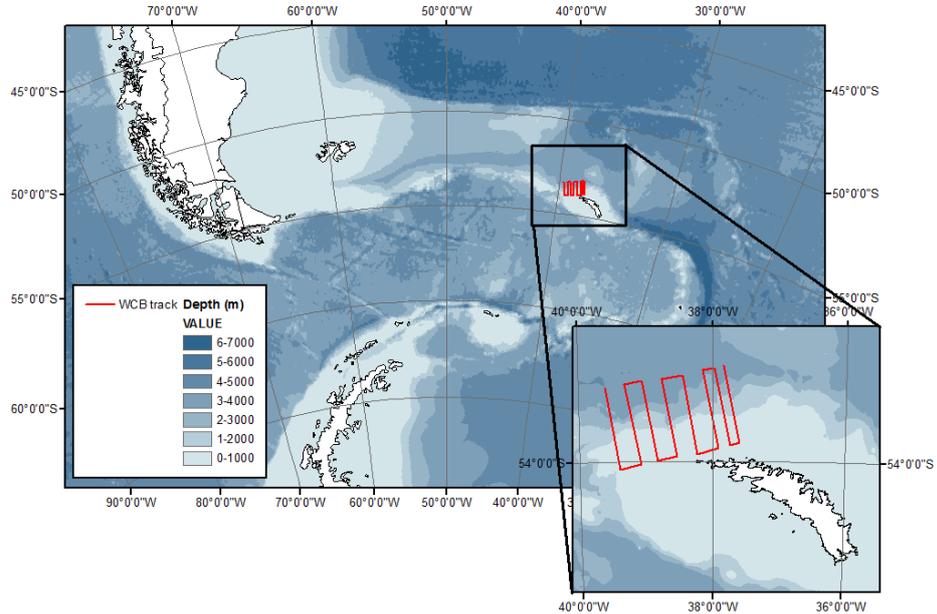
Figure 1.2: The Western Core Box survey. Transects are shown in red and we refer to them as 1.1, 1.2, 2.1, 2.2, 3.1, 3.2, 4.1 and 4.2 from west to east respectively).

acoustic surveys, including fishing vessels (Godø *et al.*, 2014; Watkins *et al.*, 2016) and autonomous vehicles (Guihen *et al.*, 2014).

1.3   Ocean gliders

Autonomous Underwater Vehicles (AUVs) are underwater marine autonomous vehicles that are driven through the water by propulsion systems controlled and piloted by an onboard computer, and manoeuvrable in three dimensions (Von Alt, 2003). They are distinguished from remotely operated vehicles (ROVs) by being untethered. The operational characteristics of AUVs allow them to explore under ice (Asper *et al.*, 2011), work in dangerous areas (Piontkovski *et al.*, 2017) and explore phenomena from different vantage points (Guihen *et al.*, 2014).

Ocean gliders are a self-contained, battery powered AUVs that use small changes in their buoyancy to affect a vertical movement. (Eriksen *et al.*, 2001; Rudnick, 2016). This method is more power efficient than traditional engine propulsion systems, extending endurance and allowing them to serve as a quiet platform for acoustic applications (Guihen, 2018). Horizontal motion is achieved by adjusting the glider's attitude (moving the battery to affect the centre of gravity) and using the hydrodynamic body shape and wings to provide lift and to glide. This results in a sawtooth trajectory of dives that allows profiling of the water column. Gliders are a derivative of Argo floats, a global array of free-drifting floats that profile the water column (Roemmich *et al.*, 2009).

A wide range of sensor packages have been integrated with gliders allowing measurement of ocean variables including temperature, salinity, dissolved oxygen, fluorescence, photosynthetically available radiation (PAR), current, nitrate, turbulence, acidity and acoustics. These variables allow physical, chemical and biological ecosystem indicators to be tracked over time to assess changes and trends in marine ecosystems. Ocean gliders are increasingly being seen as an important component of the Global Ocean Observing System (Liblik *et al.*, 2016).

When underwater, a glider is unsupervised, relying only on instructions from an onboard, embedded microcomputer system. Manual, operator intervention occurs when the glider is at the surface and able to communicate. In the case of the Seaglider[2], an operator or "pilot'' connects via the Internet to a base station using a secure shell[3], sending command files and retrieving sensor sample files. The glider communicates with the base station using the Iridium satellite communication network (Pratt *et al.*, 1999). Pilots are usually keen to minimise the time that a glider is at the surface to reduce the risk of collision and damage. This limits the opportunity for transmission of sensor data. Data are postprocessed using motion sensor information to cor-

---

[2]Seaglider Product Specification, https://bit.ly/2V8LJnd, accessed April 2020.

[3]SSH(1) BSD General Commands Manual, https://man.openbsd.org/ssh, accessed April 2020.

rect for the flight model, sensor lag and differences in upcast and downcast sensor attitude.

A key consideration for any glider mission is endurance (how long can the mission last and how far can the glider go?). These factors are limited by battery power and current drain. The power budget is consumed by the control, buoyancy variation, sensor and communication subsystems. The probability of a shallow underwater glider surviving a thirty-day mission without a premature mission end is 0.59 (Brito, Smeed and Griffiths, 2014). The risk of data loss due to vehicle failure gives rise to a cost-benefit judgement involving value of data, cost of communication, power for onboard processing and time at surface. In general, we would like to transmit a backup of the data as quickly as possible.

1.4 Maritime data communication

The fundamental problem of communication is that of reproducing at one point, either exactly or approximately, a message selected at another point (Shannon, 1948). Figure 1.3 depicts a generalised communications system where messages flow from an information source and a transmitter converts them to a signal on a noisy channel. A receiver receives the signal, reproduces the message and delivers it to a destination. Throughput is limited by the bandwidth of the channel which is limited by noise. Data compression and decompression can be implemented at the transmitter and the receiver respectively.

The size of data is usually measured in bits (binary digits). A Kilobit (Kb) is 1024 bits (note the capital K) and a kilobit (kb) is 10^3 bits. The bandwidth of a channel (the data transmission rate) is measured in bits per second (bps), Kilobits per second (Kbps, 1024 bps), kilobits per second (kbps, 10^3 bps) or Megabits per second (Mbps, 10^6 bps). A byte is 8 bits, a Kilobyte (KB) is 1024 bytes, and a kilobyte (kB) is 10^3 bytes. This can be a source of confusion, but the rule is that K means 1024, k means 10^3, b means bit and B means byte. All other prefixes correspond to the SI system.
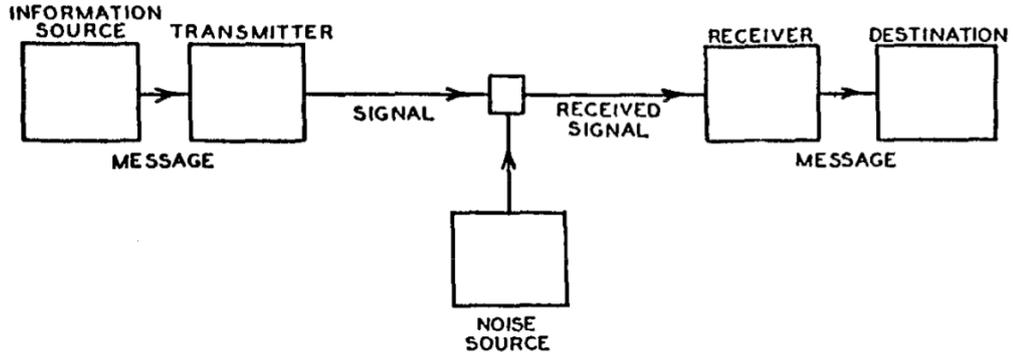
Figure 1.3: Schematic diagram of a general communications system (from Shannon, 1948).

Unfortunately, there is a woeful lack of accuracy, precision and consistency in equipment specification and literature when quoting data rates.

The principle options for marine telemetry systems are underwater acoustic communication within the ocean interior, or radio communication from the surface (Bekkadal, 2009). Sea water is a very difficult medium to use for the transmission of signals (Hilliard Jr, 1960). Radio frequency and light waves are strongly attenuated by water and acoustic communication is hampered by complex channel characteristics such as fading, multipath propagation, variable delay, refraction and attenuation (Catipovic, 1990; Akyildiz, Pompili and Melodia, 2005). Acoustic modems offer point-to-point communication of up to a few kilometres, and network topologies can be formed by means of repeater nodes (Sozer, Stojanovic and Proakis, 2000), but bandwidth is low (typically less than about 10 kbps) and communication suffers from propagation delays.

Radio frequency (RF) communication at the surface, requires line-of-sight between the transmitter and the receiver. Very High Frequency (VHF, 30 – 300 MHz) and below are impractical for AUVs because of antenna size (typically > 1 m) but Ultra High Frequency (UHF, above 300 MHz) solutions exist, offering communication of up to about 20 kbps) over distances less than about 10 km with antennae measured in centimetres (e.g. Free-

wave[4]). Satellite communication systems typically use higher frequencies with smaller antennae (e.g. L band, $1-2$ GHz). The satellite azimuth must be high enough not to be affected by sea surface waves. For this reason, polar orbiting satellites are often more advantageous than geostationary satellites, particularly when operating at high latitudes such as the Southern Ocean (Maral and Bousquet, 2011). As an example, Iridium data modems[5], providing a circuit-switched channel with a bandwidth of 2.4 Kbps, are installed on both Seaglider and Slocum gliders. New technology could improve bandwidth (e.g. Iridium are currently testing their new Certus 9770 transceiver which could provide a 35-fold speed increase), but there are physical limits to antenna size and stability, and the applicability for autonomous vehicles remains to be seen.

Broadband Internet systems are also available, but these can be expensive and typically require dishes or large antenna systems to be mounted at a high elevation, making them unsuitable for MAVs. Terrestrial mobile data networks such as GPRS are only accessible from some coastal waters.

1.5 Data compression

In a digital system, messages, consisting of *symbols* for transmission, are typically represented as a sequence of bits. *Data compression* (or more correctly, source coding) reduces the bandwidth required to transmit data by encoding information using fewer bits than the original representation (MacKay, 2003). *Information theory* is the mathematical study of information coding (Shannon, 1948). An encoding may be *lossless* (in which case no information is lost and the process is reversible), or *lossy* (in which case information judged to be of low importance is irreversibly removed). Some scientists use the terms *data thinning* or *data decimation* to mean data reduction; both can be regarded as forms of lossy compression. The *compression ratio* is the ratio of the size of the uncompressed data to the

---

[4]https://www.freewave.com/, accessed April 2020.
[5]Iridium Communications Inc, https://www.iridium.com/, accessed April 2020.

size of the compressed data.

The Kolmogorov complexity of a message is the length of the shortest computer program in any programming language that produces that message as output, and it can be shown to have the highest (optimal) compression ratio (Kolmogorov, 1963). The decoding of a message requires the receiver to have both the transmitted program, and an interpreter for the predetermined programming language. The programming language can be a general-purpose programming language, or it can be a language optimised for a specific domain. Unfortunately, there are no known algorithms for finding Kolmogorov complexity and therefore, no general methods for optimal compression.

Compression algorithms can use the fact that not all symbols occur equiprobably and the most frequent can be coded with shorter bit sequences (e.g. Huffman encoding, Huffman, 1952). Lempel-Ziv methods look for repeated symbol sequences and use pointers to remove repetition (Ziv and Lempel, 1977, 1978). There is also a large literature covering image compression, with algorithms such as JPEG (Wallace, 1992) being commonly used in digital cameras and PNG[6] being used for Internet applications.

1.6 Science as a form of lossy data compression

We live in an era of big data, in which scientific experiments routinely require collection and analysis of large data sets (Mayer-Schönberger and Cukier, 2013). The Problem, Plan, Data, Analysis and Conclusion (PPDAC) structure has been suggested as a way of representing the scientific problem-solving process (Wild and Pfannkuch, 1999; Spiegelhalter, 2019). Problems are posed, experiments are planned, data are collected and anal-

---

[6]Portable Network Graphics (PNG) Specification, W3C/ISO/IEC version, http://www.libpng.org/pub/png/spec/iso/, accessed April 2020.

ysed, leading to conclusions that may in turn generate further problems (Figure 1.4).
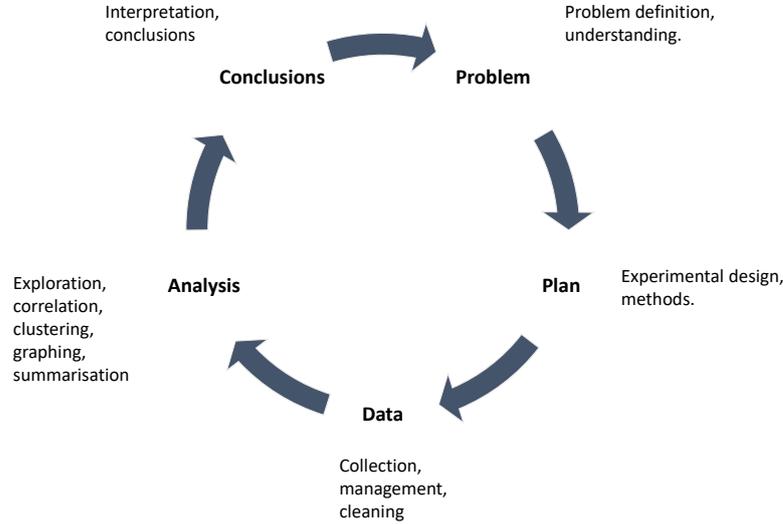
Figure 1.4: The PPDAC model of statistical thinking in empirical enquiry, adapted from Wild and Pfannkuch (1999).

The Analysis and Conclusion phases of PPDAC can be considered as a form of data compression. Analysis usually entails methods such as grouping (clustering), classification, correlation and graphing - all forms of data summarisation. Results are interpreted, leading to conclusions which are often simply confirmation or rejection of hypotheses. As an example, consider the existence or otherwise of the Standard Model Higgs boson particle in physics. The ATLAS detector at the Large Hadron Collider recorded 300 trillion proton–proton collisions. Following extensive computation and analysis, it was concluded that the new particle exists (Aad *et al.*, 2012). This can be seen as a lossy compression ratio of > 300 trillion!

1.7 Our research question

We ask: "Can we find acoustic data compression and summarisation algorithms that could be deployed alongside echosounders on marine au-

tonomous vehicles, to deliver real-time ecosystem indicators?"

1.8 Thesis structure

In Chapter 2, we explore the use of generic data compression algorithms (e.g. ZIP) to reduce the size of acoustic data. We convert acoustic data to echograms to look at image compression, examining the use of colour palettes in echogram interpretation (Chapter 3).

We go on to consider the possibility of processing and summarising acoustic data onboard marine autonomous vehicles, which poses three key problems:

1. Whilst summary acoustic metrics have already been proposed, it is not clear which are descriptive of marine ecosystems;

Using echosounder data from the Southern Ocean ecosystem at South Georgia, collected by research vessels (which are easier to work with and more readily available than MAV acoustic data), we compute acoustic metrics and assess their correlation to independent ecosystem indices (Chapter 4).

2. Current acoustic processing techniques require supervision by experts and are difficult to automate;

Aliased seabed is a corruption caused by acoustic reflections from the seabed. Aliased seabed detection and removal is an example of an acoustic processing step that is currently undertaken manually. We use modern machine learning techniques and a conventional algorithm to detect aliased seabed in single frequency, split-beam echosounder data without the need for bathymetry (Chapter 5).

3. Current acoustic processing software is typically desktop-based, interactive and and unsuitable for unsupervised, embedded, autonomous operation.

We demonstrate an unsupervised acoustic data processing system (RAPID-KRILL) that connects to an echosounder and reports real-time, acoustically derived metrics from ships of opportunity (e.g. fishing vessels) using the

Iridium satellite network (Chapter 6). The technology is fully autonomous, low-cost, and could be further developed for use on marine autonomous vehicles.

Finally, we present conclusions and suggestions for future work (Chapter 7).

Chapter 2

Compression of fisheries acoustic data

> "The most important tool of the theoretical physicist is his wastebasket."
>
> Albert Einstein

In this chapter, we consider whether general-purpose compression techniques are effective for reducing the size of fisheries acoustic data.

2.1 Introduction

Echosounders are routinely used in fisheries acoustics to survey marine ecosystems. (Simmonds and MacLennan, 2005; Benoit-Bird and Lawson, 2016). Sound pulses ("pings") are transmitted towards a target and the intensity and phase angle of the received signal are measured, integrated and recorded. Data are stored as a matrix of signal samples indexed by depth (or range) and along track distance. Echosounders are usually deployed onboard research vessels, but fishing vessels (Godø *et al.*, 2014; Watkins *et al.*, 2016) and marine autonomous vehicles (Guihen *et al.*, 2014; Mordy *et al.*, 2017) are increasingly being used to extend spatial and temporal sampling.

Large acoustic data volumes, amounting to many terabytes, are already

costly and complex to maintain, with manual processing becoming overwhelming and impractical (Wall, Jech and McLean, 2016). Echosounders generate large amounts of data, and this is a particular challenge for marine autonomous vehicles (MAVs), where communication networks have limited bandwidth. If an echo sounder is operated with a transmit pulse interval (I_T), and generates n samples per ping, with k bits per sample then the data rate R, usually measured in kilobits per second (kbps), is given by (2.1). New broadband sensors such as the Simrad WBT Mini can produce as much as 70 GB per day (6.48 Mbps, Benoit-Bird *et al.*, 2018) but satellite communication channels typically only have a bandwidth of 2.4 kbps (e.g. Iridium).

$$R = \frac{n \times k}{I_T} \tag{2.1}$$

Whenever a communication system is bandwidth limited, there can be only two possible solutions: add more bandwidth or reduce the amount of data transmitted. Increasing bandwidth to ocean areas is often expensive or impractical. Electromagnetic (radio frequency) communication is not possible underwater where acoustic communication is also short range or very low bandwidth. Above water, radio frequency communication is difficult because of the need to raise an antenna above the waves. Satellite communication is possible, but high bandwidth requires stable antenna systems which are unsuitable for platforms smaller than a ship. We would therefore like to reduce the size of acoustic data for storage and transmission.

At the time of writing, four terabyte, USB (Universal Serial Bus) disk drives are routinely used to transfer acoustic data between shipborne echo sounders and data centres. The principal communication between MAVs and control stations is by low earth orbit satellite communication. The glider must be at the surface to transmit, where it is vulnerable to collision with shipping or sea ice and could drift away from intended waypoints. These risks, and the cost of maritime data communication, require that we minimise time at the surface and consequent transmission times. Current practice is to store

data locally for retrieval and analysis once the MAV is recovered, leaving missions liable to data loss in the event of vehicle loss (Guihen *et al.*, 2014).

There are at least three studies that have looked at compression of acoustic data: Amblas *et al.* (2016) explore lossless compression of multibeam echosounder data and show compression ratios of up to 1.8. Wu, Zielinski and Bird (1997) claim lossless compression ratios of between 2 and 3 for hydroacoustic image data. Beaudoin (2010) applies JPEG compression to Simrad echosounder data, reporting compression ratios of up to 20 using lossy compression.

In this chapter we attempt to quantify current and near future requirements for data compression in fisheries acoustics. We apply conventional lossless compression algorithms to data collected from a Simrad EK60 echosounder. We convert data to matrices of power and assess the effects of numeric precision on survey results and data size. Finally, we convert data to echograms and assess the efficacy of image compression algorithms.

2.2 Methods

To estimate current and near future data collection rates for echosounders, we considered three representative instruments:

1. An Imagenex, single beam, 120 kHz CW ES853 echosounder mounted on a Kongsberg Sea Glider (Guihen *et al.*, 2014). The device measured backscatter to a range of 100 m with 0.5 m bins, generating 200 7 bit values per ping at a pulse interval, $I_T = 0.6$ s. This echosounder was selected for its compact size and modest power requirements, but lack of split-beam or broadband capability limits its usefulness;

2. A Simrad EK60, split-beam echosounder mounted on a research vessel (e.g. Fielding *et al.*, 2014). The EK60 stores each sample as a pair of short (two byte) integers (a total of four bytes) for each transducer frequency. Bin size is variable, but a typical pulse duration of 1.024 ms gives a range resolution of 19.2 cm (Simrad, 2012). Assuming single

frequency operation, this yields 5200 samples for 1000 m with a transmit pulse interval, $I_T = 2\,$s. Despite being obsolete, this echosounder is still widely used on research vessels;

3. A Simrad EK80 broadband echosounder where each sample is four complex numbers (one for each of the four transducer quadrants). Each complex number consists of two 32 bit floating point values. A sample is therefore represented as 4 quadrants × 2 × 4 bytes = 32 bytes. Again, we assume single frequency operation with 5200 samples per ping and a transmit pulse interval, $I_T = 2\,$s. This echosounder architecture is state-of-the-art, with EK80 being fitted to new research vessels and WBT Mini to a wide range of MAVs.

To test various compression strategies, we used 125 Simrad EK60 38 kHz transects recorded from the Western Core Box survey (2003 - 2019, Fielding *et al.*, 2014, Section 1.2). Simrad echosounder data are usually stored in RAW format (Simrad, 2012), which can also contain metadata, and data from other instruments (e.g. a Global Positioning System receiver). To avoid our study being instrument specific, we converted each acoustic transect to a matrix of volume backscattering coefficient (S_v) using SimradEk60.jl[1]. Calibration corrections (S_a) were determined and applied annually using standard sphere techniques (Demer *et al.*, 2015). Sound speed (c) and absorption (α) were determined from cruise CTD stations undertaken during each cruise (Francois and Garrison, 1982), averaged over the top 250 m of the water column. Finally, we saved the transect matrices in uncompressed binary format.

Many data analysis tools (e.g. Python[2], MATLAB[3] and R[4]) now use 64 bit, double precision floating point numbers by default. If this precision could be reduced to 32 bits, then total uncompressed data size would immediately be halved (Overton, 2001). To test the effect of varying numeric precision,

---

[1]https://github.com/EchoJulia/SimradEK60.jl, accessed April 2020.
[2]https://www.python.org/, accessed April 2020.
[3]https://www.mathworks.com, accessed April 2020.
[4]https://www.r-project.org, accessed April 2020.

we computed mean volume backscattering coefficient (S_v) for each transect using both 64 bit and 32 bit floating point arithmetic and noted the maximum numerical error (The SimradEK60.jl software can be compiled to use either 64 bit or 32 bit floating point types).

To test the efficacy of general-purpose compression programs, we applied zip (version 3.0), bzip2 (version 1.0.8), xz (version 5.2.4) and gzip (version 1.10) to each of the transect binary files, comparing compression ratios. The CPU execution time was measured for each program (User + Sys time) for all 125 transects on a Linux AMD64 system, kernel version 5.3.0-26.

Echograms quantise acoustic data (usually volume backscattering coefficient, S_v or target strength (TS) by means of a colour map and are therefore a form of lossy compression. We used EchogramImages.jl[5] to convert transects to echograms (scale bar -95 dB and -50 dB). We tested two common colour schemes: Simrad EK500 (12 colours) and Viridis (256 colours). The resulting echograms are images which we converted to PNG and lossless JPEG to explore the additional compression achieved by image compression algorithms.

2.3   Results

Table 2.1: Echosounders ordered by data generation rate. For example, an EK60 generates 83.20 kilobits per second, which is 37.44 Megabytes per hour. This data rate is 33.85 times higher than the capacity of an Iridium channel and would require a compression ratio of 406 to transfer two hours of samples in ten minutes. The Iridium data rate is shown for comparison purposes.

Echosounder	kbps	MBph	$\times$ Iridium	Compression
ES853	2.33	1.05	0.95	11
Iridium	2.46	1.11	1.00	12
EK60	83.20	37.44	33.85	406
EK80	665.60	299.52	270.83	3250

[5]https://github.com/EchoJulia/EchogramImages.jl, accessed April 2020.

The Imagenex echosounder generates data at a rate of 2.3 kbps, the Simrad EK60 83.2 kbps and the Simrad EK80 665.6 kbps. Sending two hours of samples in ten minutes over an Iridium channel would require a compression ratio of 406 for EK60 and 3250 for EK80 (Table 2.1).

The maximum error when computing mean volume backscattering coefficient (S_v) using 32 bit arithmetic compared to using 64 bit arithmetic was 1.8e−5. It is unusual for S_v to be quoted to more than two significant figures after the decimal point, and so we proceeded to use a 32 bit representation for all S_v samples.

Of the general-purpose file compression programs tested, xz provided the highest compression ratio (2.21) but had the slowest execution time (14 431 s; Table 2.2). Zip was the fastest (1409 s), but had the lowest compression ratio (1.19). Image compression algorithms achieved higher compression ratios, with PNG performing better that JPEG in both cases. Of the echogram image compression methods, echograms using the EK500 colour scheme, saved as PNG had the highest compression ratio (23.72).

Compression ratios are not the same across transects (e.g. EK500 PNG, 23.72 ±0.48), showing that compression is dependent on the size and nature of the data itself. Similarly, echogram compression ratios are dependent on the choice of colour palette.

2.4   Discussion

All three echosounders that we considered generate data at a higher rate than can be reasonably transmitted by an Iridium satellite modem. Although the Imagenex echosounder only generates 2.3 kbps (compared with a 2.4 kbps channel), a glider can only transmit data whilst at the sea surface and has to transmit other mission data too (e.g. GPS and other instrument data). Such an arrangement would limit data collection to about half the vehicle's deployment time. Pilots are usually keen to minimise the time that a glider is at the surface to reduce the risk of collision and damage, and to

Table 2.2: Mean compression ratios for general-purpose file compression tools and echogram image processing applied to 125 38 kHz acoustic transects from the Western Core Box 2003 - 2019. The mean transect uncompressed file size was 273.09 MB ±13.62 MB.

Method	Compression Ratio	CPU time (s)
Zip	1.19 ±0.01	1409
Gzip	1.19 ±0.01	1456
Bz2	1.44 ±0.01	3198
Xz	2.21 ±0.03	14431
EK500 JPG	5.01 ±0.1	2885
Viridis JPG	6.6 ±0.12	2968
Viridis PNG	10.47 ±0.24	5700
EK500 PNG	23.72 ±0.48	3325

maximise dive time and data collection.

None of the compression ratios seen in this study is sufficient to allow data communication across an Iridium 2.4 kbps channel, except perhaps EK500 PNG. The highest lossless compression ratio achieved with the general-purpose file compression programs was 2.21 (using xz). These results show similar compression ratios to earlier studies (Wu, Zielinski and Bird, 1997; Amblas *et al.*, 2016). The best image compression ratio of 23.72 was achieved with an echogram using EK500 colours and PNG format (Table 2.2). However, this would still require a glider to be at the surface for about one hour in every 24 purely for the transmission of echosounder data, which would increase its susceptibility to currents and collision.

Whilst literature such as Wall, Jech and McLean (2016) raises legitimate concerns about increasing acoustic data volumes, Equation 2.1 shows that the growth is linear $(\mathcal{O}(n))$ with data size being directly proportional to the number of samples. Data rates are larger for more sophisticated echosounders (6.48 Mbps for the EK80), but this is not the crisis that would have been the case had we seen polynomial or exponential growth. Whilst the number of echosounders in use is likely to grow through more widespread sampling, this growth seems unlikely to be polynomial or

exponential either.

The compression ratios required in practice may be larger than those shown in Table 2.1. Benoit-Bird *et al.* (2018) reported that a glider deployed, Simrad WBT broadband echosounder can generate 70 GB per day with two transducers collecting CW samples. This is an order of magnitude more in terms of data rate than our EK80 estimates above. However our estimates only included single frequency samples and did not include auxiliary data such as GPS or other instrumentation. Even so, the results highlight the large difference between required data compression ratios and those offered by general-purpose data compression techniques.

Single precision floating point arithmetic gave sufficient precision when calculating mean volume backscattering coefficient, providing an immediate, effective compression ratio of two. Double precision floating point numbers are stored using 64 bits (eight bytes), whilst single precision floating point numbers use 32 bits (four bytes). This data reduction not only halves the size of memory and disk required to store acoustic data, it also reduces acoustic data processing time by halving input and output.

The compression ratio depends on the size and nature of the data itself. Table 2.2 shows variability in compression ratios between transects. Compression algorithms identify repetition in the data and can therefore compress homogenous sections more effectively than inhomogeneous sections. This makes it hard to know exactly what compression ratios can be achieved in practice.

Echogram image compression ratios depends on the choice of colour palette. The EK500 echogram stored as PNG resulted in a compression ratio of 23.72, whilst the Viridis echogram PNG resulted in only 10.47. The EK500 colour scheme has only 12 colours (compared to Viridis 256) and this reduced variability obviously yields higher compression at the expense of precision. We might have expected JPEG to yield higher compression ratios than PNG, but JPEG is optimised for photographs (where there is usually a wide range of luminance in the detail) and here we are using it for echograms (where

there is a limited range of colours). Our results suggest that echograms can provide an effective form of lossy compression, but raise questions about the number and type of colours that should be used (a theme we explore further in Chapter 3).

Whilst compression ratio is a measure of the effectiveness of a compression algorithm, other factors, including time and resources required for execution, should also be considered. Designers of embedded systems for autonomous underwater vehicles must be mindful of power requirements and it may be desirable to trade off compression ratios against computation and communication resources. All the compression schemes tested enable more efficient and cost-effective disk storage, allowing scientists to more easily capture larger data sets.

It is clear that lossy compression is required if we are to dramatically increase compression ratios, but decisions about which data could be discarded are highly application specific. For example, an application for estimating krill biomass might require krill swarm dimensions, but would not need pelagic fish schools. In science, there is a danger that data are discarded that may prove useful for subsequent analyses. Ideally, all data should be preserved, with lossy compression only being employed for expediency of results.

2.5   Next steps

In this thesis, we make extensive use of echograms for acoustic data presentation and inspection, and so we would like to resolve the questions raised in this chapter concerning echogram colour maps. In the next chapter we assess echogram colour maps and optimise the visual appearance of echograms before going on to look at acoustic data summarisation in Chapter 4.

Chapter 3

Colour maps for fisheries acoustic echograms

> "The chief function of colour should be to serve expression."
>
> Henri Matisse

In the last chapter, we converted acoustic data to echograms and used image compression to reduce data storage and transmission time. Echograms are widely used in fisheries acoustics, but the visual appearance and effectiveness of echograms depends on their colour map. In this chapter, we optimise our choice of echogram colour maps before using echograms for further data analysis.

This chapter is based on a paper of the same name, published in ICES Journal of Marine Science (R. E. Blackwell *et al.*, 2019).

3.1 Introduction

Echosounders are routinely used in marine science to survey the underwater environment. Sound pulses ("pings") are transmitted into the water and reflections from targets (e.g. seabed, plankton, zooplankton, fish) are measured, integrated and recorded. Signals are typically recorded as power,

in watts, and converted to target strength (TS), or volume backscattering strength (S_v), in decibels, to study the distribution, abundance and behaviour of animals (Simmonds and MacLennan, 2005).

Acoustic data are recorded as a matrix of signals $X(i, j)$ where i is the range index and j the along-track distance index. $X(i, j)$ can be mapped to pixels $\mathbf{c}(i, j)$, where $\mathbf{c}(i, j)$ is usually a three-dimensional colour vector, to form a digital image (an echogram) using colours drawn from a colour map. A colour map, $C = \{\mathbf{c}_1, \mathbf{c}_2, ..., \mathbf{c}_k\}$, is an ordered set of k colours used to assign numbers to colours such that $\mathbf{c}(i, j) \in C$. The range of X to be visualised (determined by the scale bar) is divided into k equal bins, and pixels are mapped accordingly. The available radiometric resolution of an echogram reduces as k reduces, and an echogram often has lower dynamic resolution than the original acoustic data. Changing the colours in an echogram affects the visual appearance of its content in the same way that changing the colours in a photograph would change the appearance of its subject.

The first fisheries acoustic echograms were published in the 1930s (e.g. Sund, 1935). Early systems used "wet" paper processes to record measurements and these produced monochromatic images (Mitson, 1983). By the 1980s, computers could store echograms in memory and display them on monochrome cathode ray tubes (CRT) or print them using dry photographic processes. By the 1990s, echograms could be rendered in colour using colour CRT monitors, and the Bergen Echo Integrator (BEI) included purposely designed colour maps (Foote *et al.*, 1991). The Simrad EK500 was one of the first scientific echosounders to have an attached colour display, but the hardware had only four bit planes, of which one was used for fixed lines, limiting the number of available colours to 12. Colour dot-matrix printers and pen plotters were available, but also had a limited range of colours (e.g. Figure 3.1).

As the number of available display colours increased, k increased, enabling the Simrad EK80 colour map based on EK500. As of 2019, we now have
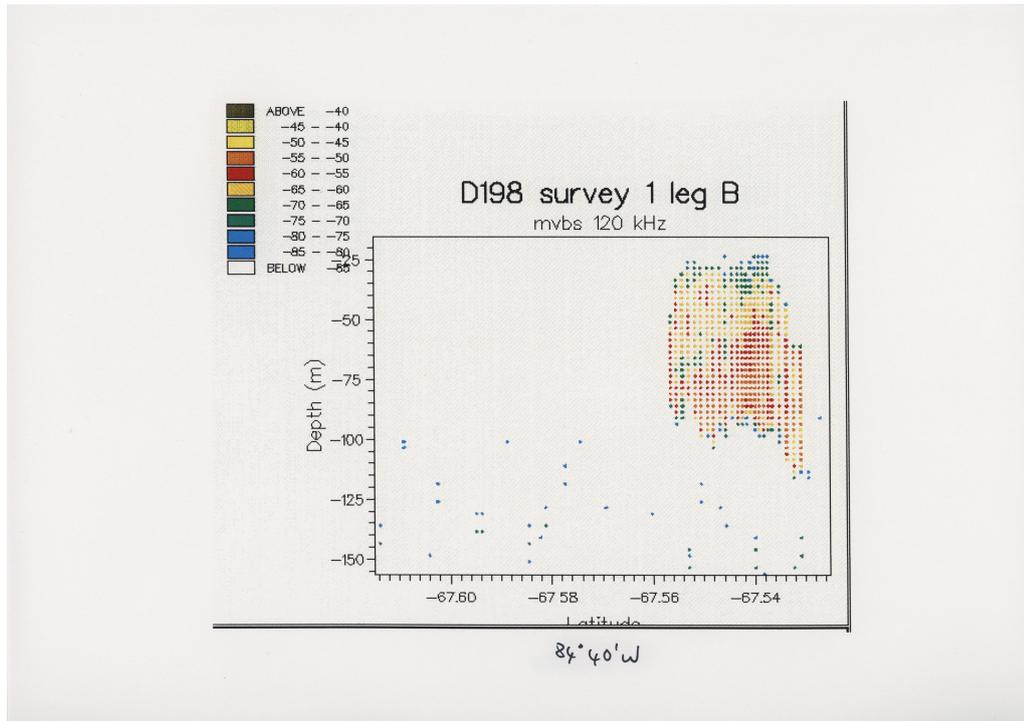
Figure 3.1: An echogram dating from 1992, rendered using a colour plotter. Note the limited colour and spatial resolution. Data recorded using a Simrad EK400 (120 kHz) connected to a Biosonics Echo Signal Processor, during cruise D198, RRS Discovery, Bellingshausen Sea, 1992 (Archives ref: 2001/5).

high definition monitors that use light emitting diodes (LEDs) and colour laser printers; both can render echograms in millions of colours. This gives rise to a wide variety of colour map options (Figure 3.2).

Acoustic data analysis still entails echogram interpretation by skilled fisheries acousticians. Echograms are postprocessed to remove unwanted signal and noise (Ryan *et al.*, 2015), before identifying acoustic targets and quantifying distribution, abundance and behaviour. Thresholding is a common way of discriminating targets from surrounding backscatter, with thresholds set based on visual interpretation of echograms and the scattering characteristics of target species, validated by target fishing (Korneliussen, 2018). Whilst automated, unsupervised algorithms exist for some aspects of fish-
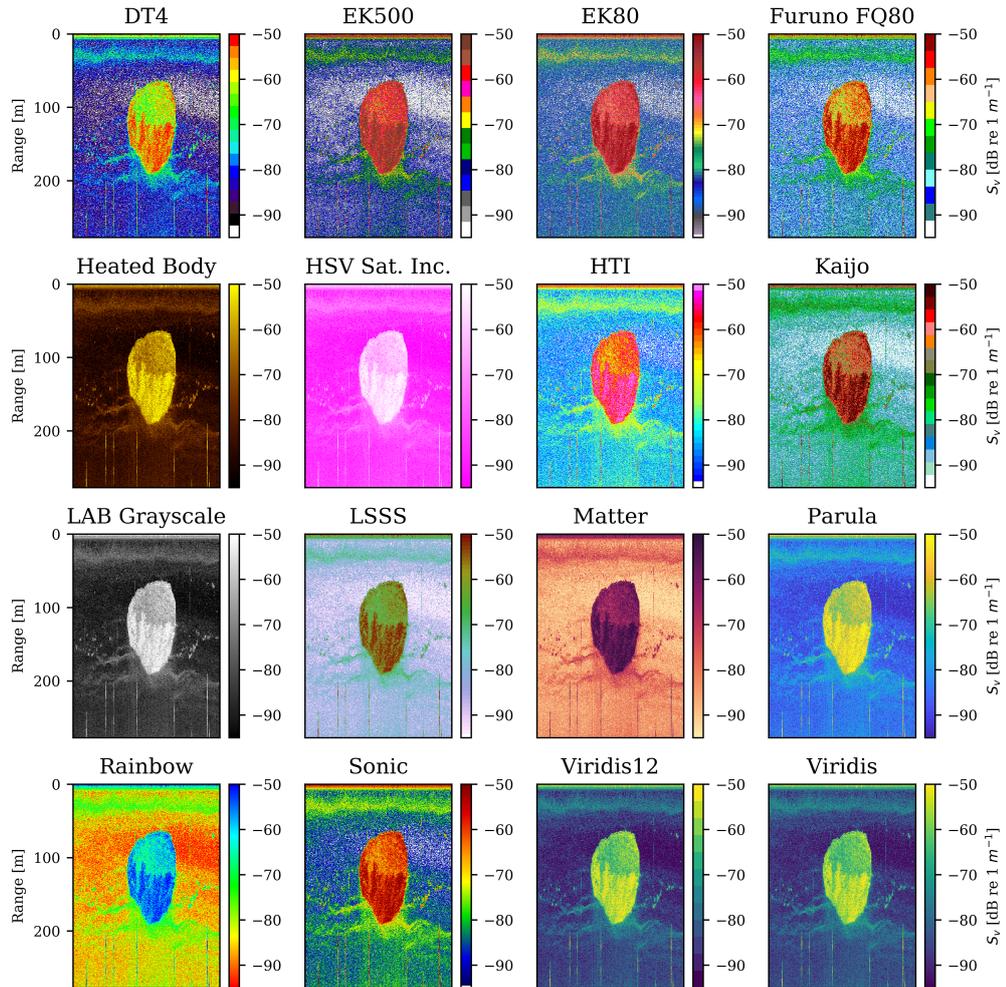
Figure 3.2: Echograms depicting an Antarctic krill swarm plotted using a selection of colour maps. The swarm is about 150 m in height and 1 km in plan. Data collected using a Simrad EK60 scientific echosounder (120 kHz, ping interval $I_T = 2s$, nominal speed = 10 kts) onboard RRS James Clark Ross, Cruise JR230, Southern Ocean, December 2009.

eries acoustic data processing, much work is still undertaken manually using graphical, interactive software such as Echoview® (Echoview Software Pty Ltd), Large Scale Survey System (LSSS) (Korneliussen *et al.*, 2016), MOVIES (Trenkel *et al.*, 2009) or ESP3 (Ladroit 2017)[1]. It is therefore important that echogram data are displayed faithfully, clearly and consistently,

---

[1]https://sourceforge.net/projects/esp3, accessed April 2020.

and that colour maps are chosen to optimise human-computer interaction.

The visual representation of data has a powerful effect on the perception and interpretation of the structure of those data (Rogowitz, Treinish and Bryson, 1996). Our ability to perceive the details of a visual scene is determined by the relative size and contrast of the detail present (Campbell and Robson, 1968). Studies in medical imaging have shown that poorly designed colour maps can lead to imprecise readings and inaccurate interpretation (Borkin *et al.*, 2011). Colour map choice affects the visual appearance of an echogram (Figure 3.2), but the colour map used by a particular fisheries acoustician may be based on a number of factors: the colour map may have been chosen to optimise a particular detection, comparison, or estimation task; the display software may only provide a default colour map or a limited choice; the user may have been trained using a particular colour map and now have experience, familiarity and learned expertise specific to that map; or the user may simply have a subjective preference.

Pseudo coloured images are used to show *metric* (or value) information as well as *form* (shape and structure) (Ware, 1988). In psychophysical tests, greyscale colour maps better revealed form, whilst colourful maps better revealed metric. To create a colour map that reveals both metric and form, the colour sequence should increase monotonically in luminance and use a range of hues. The hues provide accurate readings from a key, while the luminance conveys form. Greyscale is therefore best for detecting shape in echo traces, and colour for presenting backscattering strength (Foote *et al.*, 1991). Based on Ware (1988), Foote *et al.* (1991) combined greyscale and red-blue as a colour map option for BEI and this is the origin of the default echogram colour map in LSSS.

Colour maps may be either qualitative (sometimes called categorical) (where colour represents a category but does not imply magnitude), sequential (where colour implies ordering and magnitude), diverging (where colour implies ordering and magnitude in two directions from a central value) or cyclical (where colour implies ordering in "wrap around" data) (Brewer, 2015).

Echograms of S_v or TS which are intended to represent the magnitude of acoustic backscatter should therefore use a sequential colour map.

The human vision system is complex and there is a huge literature on colour perception (for a primer, see Baylor, 1995). Colour is not intrinsic to objects, and we perceive colour using reflected light which varies depending on lighting conditions. Light energy entering the eye has two fundamental dimensions: intensity, which determines brightness, and frequency which determines colour. The eye consists of rods and cones which are sensitive to intensity and frequency respectively. We can perceive millions of colours (Judd and Wyszecki, 1975), but different people perceive colour in different ways as demonstrated by the 2015 internet sensation known as #thedress where some audiences reported dress colours as blue and black, and others as gold and white (Gegenfurtner, Bloj and Toscani, 2015).

The "Which Blair Project" provides a quick visual test for evaluating colour maps (Rogowitz and Kalvin, 2001). In psychophysical testing, the perceptual quality of colour maps was assessed by using them to render a photograph of a human face. A strong correlation was found between the perceived naturalness of images, luminance monotonicity and the suitability of colour maps for rendering continuous scalar data.

Colour spaces organise colours within a vector space. For example, the RGB colour space organises colours according to their red, green and blue components. Standard RGB (sRGB) is commonly used for computer displays which mix red green and blue light additively on a black screen to produce images. CMY colour spaces are used for print media, mixing cyan, magenta and yellow ink on a white page to produce colours subtractively. These colour spaces are device-dependent, with different screens, cameras, scanners and printers producing different colours. A colour space is said to be perceptually uniform if a small perturbation to a component value is equally perceptible across the range of that value (Poynton, 1996), however neither RGB nor CMY colour spaces have this property. The CIELAB colour space was designed by the International Commission on Illumina-

tion (CIE) to have approximate perceptual uniformity by describing any colour in a device independent manner using three dimensions, L^* for lightness (black-white), a^* for green-red and b^* for blue–yellow (Robertson, 1977, 1990). Euclidean distances in CIELAB colour space can be used to approximate the magnitude of perceived colour differences making it useful for the measurement and comparison of colours (Brainard, 2003) and the perceptual uniformity of colour maps.

Colour maps such as *Rainbow* have been widely criticised for a lack of perceptual uniformity (Borland and Ii, 2007). MathWorks™ changed its default MATLAB™ colour map from *Rainbow* to *Parula* in 2014 (revised in 2017) and Matplotlib (Hunter, 2007) to *Viridis* in 2016. Both *Parula* and *Viridis* have been carefully designed for colour contrast consistency, accessibility for viewers with red-green colour-blindness, and legibility when printed in monochrome. Some scientific disciplines employ specialised colour maps tailored to the subject matter. Many oceanographic publications use *cmocean* (Thyng *et al.*, 2016) and the *Brewer colour maps* are commonly used in geography (Brewer, 2015). These colour maps have also been designed explicitly with colour contrast consistency in mind.

Based on the evidence from Ware (1988), Brewer (2015) and Borland and Ii (2007), we conclude that echogram colour maps for displaying quantitative acoustic backscatter should be colourful, sequential and perceptually uniform. In this chapter, we measure whether fisheries acoustic colour maps are colourful, sequential and perceptually uniform using CIELAB. We compare our results with colour maps used by the wider scientific community and make recommendations concerning colour map selection for the presentation and interpretation of fisheries acoustic echograms.

3.2 Materials and methods

A selection of fisheries acoustic echogram colour maps was obtained from echosounder data collection and processing systems. These include *BioSonics DT4*, *Simrad EK500*, *Simrad EK80*, *Furuno FQ80*, *HTI*, *Kaijo* and *Sonic*

from Echoview, and *LSSS*, the default colour map from the Large Scale Survey System. It is common for echogram colour maps to have dark and light variants by using black or white as a background colour. These background colours were excluded from our analyses.

Data science tools include modern colour maps which were designed for colour contrast consistency, and so for comparison, we also selected *Matter* from cmocean, *Parula* from MATLAB, and *Viridis* from matplotlib. A subsampled version of *Viridis* having 12 colours, $\{\mathbf{c}_1, \mathbf{c}_{24}, \mathbf{c}_{47}, ..., \mathbf{c}_{254}\}$ called *Viridis12* was created to test the effect of reducing the number of colours (k). All colours were converted into CIELAB colour space using the Colors.jl software library[2].

The colour maps from Rogowitz and Kalvin (2001) were recreated and included in our analyses.[3] For *LAB Grayscale*, *Heated Body*, *Rainbow*, *HSV Grayscale*, *HSV Saturation (increasing)* and *HSV Saturation (decreasing)*, we recreated the colour maps programmatically in accordance with their descriptions in the paper. For *Isoluminant Rainbow* and *LAB Isoluminant Saturation*, we scanned the colour maps from the paper, adjusted L^* to ensure isoluminance, and interpolated to find 100 colours for each map.

One hundred journal papers matching the search term "fisheries echogram", published after 2009 in the ICES Journal of Marine Science, were examined (Appendix H). Echogram colour maps were identified by visual inspection. A paper was attributed to a colour map if that colour map occurred at least once in the paper. If a paper contained more than one colour map, it was attributed to all colour maps present.

Colourfulness is the subjective human perception of the variety and intensity of colours in an image, with greyscale images being not colourful and rainbow images being highly colourful. We determined the colourfulness of each colour map by using it to plot a sample echogram (Figure 3.2) and measuring the colourfulness of the resulting image according to Hasler and

---

[2]https://github.com/JuliaGraphics/Colors.jl, version v0.9.5.
[3]The colour maps used in The Which Blair Project are no longer available and were reconstructed following advice from the original author.

Süsstrunk ([2003]). They used non expert viewers to rate the colourfulness of a set of natural images and fitted a statistical model yielding a metric $\hat{M}^{(3)}$ described in ([3.1]), where R is the image red channel (0-255), G is the green channel (0-255) and B is the blue channel (0-255). $\hat{M}^{(3)} = 0$ means not colourful, $\hat{M}^{(3)} = 15$ slightly colourful, $\hat{M}^{(3)} = 33$ moderately colourful, $\hat{M}^{(3)} = 45$ averagely colourful, $\hat{M}^{(3)} = 59$ quite colourful, $\hat{M}^{(3)} = 82$ highly colourful and $\hat{M}^{(3)} = 109$ extremely colourful.

$$
\begin{aligned}
\hat{M}^{(3)} &= \sigma_{rgyb} + 0.3 \cdot \mu_{rgyb}, \\
\sigma_{rgyb} &= \sqrt{\sigma_{rg}^2 + \sigma_{yb}^2}, \\
\mu_{rgyb} &= \sqrt{\mu_{rg}^2 + \mu_{yb}^2}, \\
rg &= R - G, \\
yb &= \frac{R + G}{2} - B
\end{aligned}
\tag{3.1}
$$

A colour map is sequential if it is monotonically increasing in luminance (Rogowitz and Kalvin, [2001]; Brewer, [2015]). The Spearman rank correlation coefficient can be used to measure the monotonicity of an ordered set of numbers. We used the Spearman rank correlation coefficient of lightness, $(r_s(\{\mathbf{c}_{L^*} \mid \mathbf{c} \in C\}, \{1...k\})$ if $\mu_{\Delta L^*} > 0)$ to measure monotonicity and thus determine whether a colour map is sequential. A colour map is sequential and monotonically increasing in lightness if $r_s = 1$ and sequential and monotonically decreasing in lightness if $r_s = -1$.

The CIEDE2000 colour distance metric (ΔE_{00}^*) is a refinement to the CIELAB Euclidean distance metric (Witt, [2007]). We defined a colour map as perceptually uniform if CIEDE2000 colour distances were uniform across the colour map range. The Pearson correlation coefficient of CIEDE2000 colour distances, from the first colour to each of the other colours in turn $\rho(\{\Delta E_{00}^*(\mathbf{c}_1, \mathbf{c}) \mid \mathbf{c} \in \{\mathbf{c}_2, ..., \mathbf{c}_k\}\}, \{1...k-1\}))$, was used to determine linearity of colour distance. A colour map was defined as perceptually uniform if $\rho = 1$.

3.3 Results

Of the 100 journal papers analysed, 78 contained data from a Simrad instrument. Echoview was used for analysis in 48 papers, LSSS in 11 and MOVIES in 4. The *EK500* (34%) and "Rainbow" (16%) colour maps were the most frequently used for echograms, followed by *LSSS* (8%), "Greyscale" (7%) and "Other" (14%).
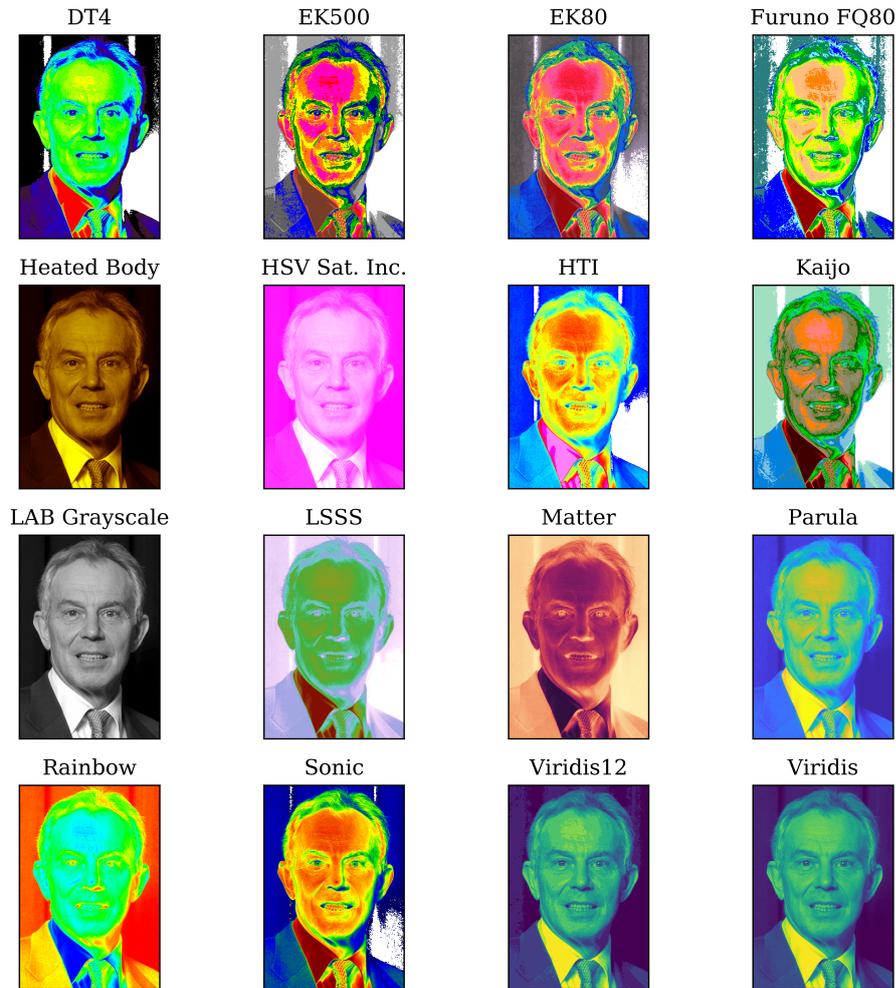
Figure 3.3: A human face rendered using a selection of colour maps. According to Rogowitz & Kalvin (2001), those images that appear most natural use colour maps better suited to visualising continuous scalar data.

Each colour map under test was used to render a photograph of a human

face as in the Which Blair Project (Rogowitz and Kalvin, 2001) (Figure 3.3). There is a large variation in the naturalness of the images and the results appear to be consistent with Rogowitz and Kalvins' observation that *LAB Grayscale* and *Heated Body* produce more natural images than either *HSV Saturation Increasing* or *Rainbow*.
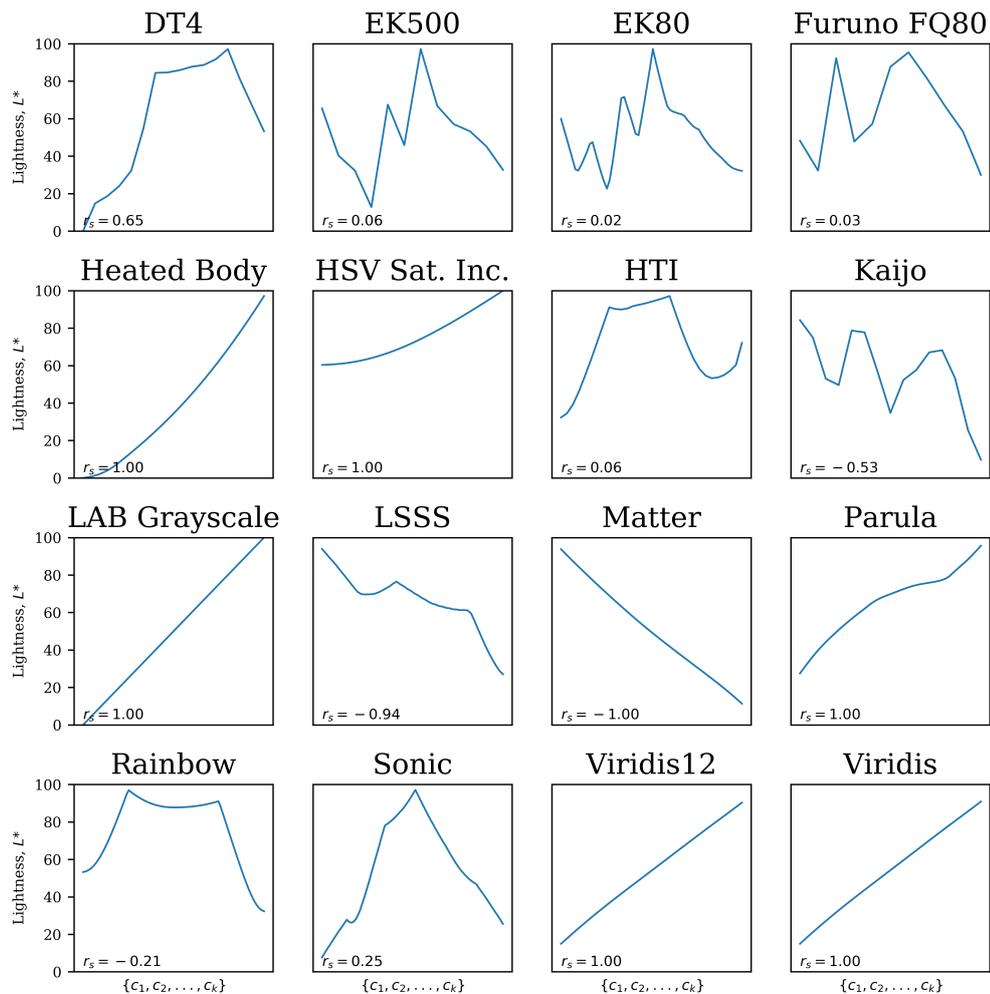
Figure 3.4: Lightness by colour sequence for each colour map. r_s is the Spearman rank correlation coefficient (1.0 or -1.0 for a sequential colour map).

Table 3.1: Colour maps ordered by lightness monotonicity (r_s) and perceptual uniformity (ρ). The first column is the colour map name with a superscript indicating its origin ((1) from Rogowitz and Kalvin(2001), (2) a fisheries acoustic colour map or (3) a modern colour map designed for colour contrast consistency). k is the number of colours; $\hat{M}^{(3)}$ is colourfulness; r_s is the Spearman rank correlation coefficient of lightness (L^*) (-1.0 or 1.0 indicates a sequential colour map) and ρ is the Pearson correlation coefficient of CIEDE2000 colour distance (1.0 indicates perfect perceptual uniformity).

Name	k	$\hat{M}^{(3)}$	r_s	ρ
LAB Iso. Sat.[1]	100	35		0.96
Iso. Rainbow[1]	100	62		0.67
EK80[2]	64	151	0.02	0.28
Furuno FQ80[2]	11	186	0.03	0.78
EK500[2]	12	186	0.06	0.26
HTI[2]	31	235	0.06	0.24
Rainbow[1]	100	236	-0.21	0.46
Sonic[2]	96	193	0.25	0.34
Kaijo[2]	15	165	-0.53	0.83
DT4[2]	16	198	0.65	0.70
LSSS[2]	52	79	-0.94	0.95
HSV Sat. Dec.[1]	100	93	-1.00	0.94
Heated Body[1]	100	82	1.00	0.97
HSV Sat. Inc.[1]	100	125	1.00	0.98
Parula[3]	64	158	1.00	0.98
LAB Grayscale[1]	100	0	1.00	0.99
Viridis[3]	256	95	1.00	0.99
Viridis12[3]	12	91	1.00	0.99
HSV Grayscale[1]	100	0	1.00	0.99
Matter[3]	256	83	-1.00	1.00

All of the fisheries acoustics colour maps bar *LSSS* are extremely colourful ($\hat{M}^{(3)} > 109$). LSSS is quite colourful ($\hat{M}^{(3)} = 79$). *Parula* is the most colourful of the modern colour maps, being extremely colourful ($\hat{M}^{(3)} = 158$), but most are quite colourful ($\hat{M}^{(3)} > 59$) or highly colourful ($\hat{M}^{(3)} > 82$). The *Rainbow* colour map is the most colourful ($\hat{M}^{(3)} = 236$) and the isoluminant colour maps the least colourful (*LAB Isoluminant Saturation*, $\hat{M}^{(3)} = 35$ and *Isoluminant Rainbow*, $\hat{M}^{(3)} = 62$) not including the grey scales. In general, fisheries acoustic colour maps are more colourful than modern colour maps.

Using r_s, we determine those colour maps which are sequential (Table 3.1, Figure 3.4). None of the fisheries acoustic colour maps is sequential, but *LSSS* comes closest ($r_s = -0.94$). Of the sequential colour maps, *Heated Body, HSV Saturation (Increasing), Parula, LAB Grayscale, Viridis, Viridis12* and *HSV Grayscale* are monotonically increasing ($r_s = 1.00$). Whereas *Matter* and *HSV Saturation (Decreasing)* are monotonically decreasing ($r_s = -1.00$).

None of the fisheries acoustic colour maps is perceptually uniform ($\rho = 1$), but *LSSS* comes closest ($\rho = 0.95$). *Matter* is perfectly perceptually uniform ($\rho = 1.00$), but *LAB Grayscale, Viridis, Viridis12* and *HSV Grayscale* are approximately perceptually uniform ($\rho \approx 1.00$).

The colour maps contain between 11 and 256 individual colours (k), with *Furuno FQ80* having 11 colours and *Viridis* having 256 colours. Notably, reducing the number of colours in the *Viridis* colour map to 12 (*Viridis12*), did not change whether it was sequential, did not reduce its perceptual uniformity, and had only a small effect on its colourfulness. The colourfulness ($\hat{M}^{(3)}$) of a colour map is not proportional to its length (k).

3.4   Discussion

The purpose of an echogram image is to effectively convey acoustic information to a human viewer. Echosounder receivers are sensitive and have a very

high dynamic range. It is typical to use a logarithmic scale (decibels) to make power measurements easier to work with, and to allow sufficient colour contrast between values in an echogram display. The logarithmic scale is monotonically increasing and it is reasonable to require equal perceptual contrast increments per decibel across the colour map range.

The choice of colour map has a substantial effect on the appearance of an image and the detail revealed (Campbell and Robson, 1968). The Which Blair Project used a subjective test (image naturalness) to assess colour maps (Rogowitz and Kalvin, 2001); in this chapter, colour maps are ordered by objective measures of lightness monotonicity (r_s) and uniformity of colour distance (ρ) with consistent results. We use these measurements to compare colour maps from fisheries acoustics with modern colour maps designed for colour contrast consistency.

Although sequential colour maps are widely recommended for visualising continuous scalar data such as S_v and TS (Rogowitz and Kalvin, 2001), none of the fisheries acoustic colour maps tested is sequential. When a colour map is not sequential, greater-than and less-than relationships are not immediately evident (Borland and Ii, 2007). Non-sequential colour maps can introduce false gradients that can covertly exaggerate features in some regions, whilst minimising features elsewhere (Thyng *et al.*, 2016).

Rainbow echogram colour maps are still used in the fisheries acoustic literature (16%), despite being widely criticised for their lack of perceptual uniformity (Borland and Ii, 2007). In our tests, some fisheries acoustic colour maps (*Simrad EK80*, *Simrad EK500*, *HTI* and *Sonic*) were shown to have even lower perceptual uniformity than the *Rainbow* colour map used by Rogowitz and Kalvin (2001). Like *Rainbow*, these fisheries acoustics colour maps lack perceptual ordering, have uncontrolled luminance variation and non-data dependent gradients. Non perceptually uniform colour maps can hinder the effective visualisation and interpretation of data by confusing, obscuring and misleading (Borland and Ii, 2007).

The Simrad EK500 scientific echosounder was introduced in 1989 and is

now obsolete, but the *EK500* colour map is still widely used (34%), and was even applied to Simrad EK80 data in one of our examined papers. The *EK500* colour map appears to be closely related to *Rainbow* and may have been intended to make colour bars easy to read. Despite its popularity and familiarity, we have shown that the *EK500* colour map is not sequential ($r_s = 0.06$) and has highly uneven perceptual contrast over its range ($\rho = 0.26$). Echoview was used in 48% of the papers, but *EK500* is not the Echoview default, suggesting that users are making a conscious choice of colour map. Simrad instruments were used in 78% of the papers examined, and this may help to explain the continued popularity of *EK500*.

Of the fisheries acoustics colour maps tested, *LSSS* is closest to being sequential ($r_s = -0.94$) and perceptually uniform ($\rho = 0.95$). *LSSS* originates from the combined greyscale and red-blue colour map designed by Foote *et al.* (1991). Like *LSSS*, modern colour maps such as *Parula* and *Viridis* are designed to combine monotonic luminance with a range of hues (Ware, 1988), but are more colourful, truly sequential and have better perceptual uniformity.

Sequential colour maps with high perceptual uniformity tend to have lower colourfulness than perceptually uneven colour maps, e.g. *Viridis* ($\hat{M}^{(3)} = 95$) versus *Rainbow* ($\hat{M}^{(3)} = 236$). It is natural to want colourful echograms, but the lack of perceptual ordering of the rainbow colours red, orange, yellow, green, blue, indigo and violet, gives rise to a trade-off between colourfulness and perceptual uniformity. It would be difficult or impossible to simply adjust existing echogram colour schemes to improve their perceptual uniformity. All of the fisheries acoustics colour maps, except *LSSS*, are highly colourful and this may help to explain their continued popularity.

The number of colours (k) in the colour maps tested did not influence whether colour maps were sequential, their degree of perceptual uniformity nor the colourfulness of resulting echograms. Our methods work irrespective of k. As k decreases so does the radiometric resolution of resulting images (compare *Viridis12* to *Viridis* in Figure 3.3). As k decreases so does

the number of colours on the scale bar which may make it easier to read (compare *Viridis12* to *Viridis* in Figure 3.2). However, care must be taken when using colour maps with reduced k that reduced radiometric resolution in echograms does not hide important detail.

More than half of the colour maps tested have increasing lightness ($r_s > 0$) but *Kaijo*, *LSSS* and *Matter* have strongly decreasing lightness ($r_s < -0.5$). This causes them to look much more like colour negative film images in Figure 3.3. Whilst both monotonically increasing and monotonically decreasing colour maps are considered sequential, it is interesting to compare *Viridis* and *Matter* in Figure 3.2. The former uses lightness to indicate more intense volume backscatter at the bottom of the krill swarm, whilst the latter uses darkness to imply density. For echograms that have been processed for noise removal, monotonically increasing colour maps may be more suited to computer screens (less bright light), and monotonically decreasing colour maps more suited to print media (less ink).

Greyscale colour maps are used in the literature that we analysed (7%), but it is unclear whether the objective was to portray morphological aspects of the data (Ware, 1988) or simply to reduce printing costs. Unlike greyscale, *Viridis* and *Parula*, some fisheries acoustics colour maps are highly non-sequential ($r_s \rightarrow 0$) and do not maintain legibility when reproduced in monochrome.

About eight percent of men and 0.4 percent of women have colour vision deficiency (CVD) (Spalding, 1999). When we presented our preliminary results at the Working Group for Fisheries Acoustic Science and Technology (WGFAST) in 2019, a number of fisheries acousticians told us that they had CVD and preferred greyscale colour maps for accessibility. The greyscale colour maps tested here are sequential ($r_s = 1.00$) and approximately perceptually uniform ($\rho \approx 1.00$). Tufte (1983) suggests that colour often generates graphical puzzles and that grey shades may be superior for the presentation of quantitative data; however, there is evidence that we can only distinguish limited shades of grey and potentially millions of

colours (Poynton, 1996). Greyscale echograms may be a good choice for accessibility, but *Viridis* and *Parula* have been designed with CVD in mind, and users without CVD may benefit from a wider colour palette. Colour maps can be adjusted for observers with particular CVD variants (Jefferson and Harvey, 2006).

Echograms are sometimes used to show regions segmented according to categories (e.g. fish, zooplankton, seabed or noise) or multi-frequency characteristics (e.g. Jech and Michaels, 2006). Such qualitative data require qualitative colour maps (Brewer, 2015). Qualitative colour maps are purposely designed to be colourful and use high perceptual contrast between colours to distinguish categories. Where categorisation is based on signal intensity (e.g. target strength or acoustic backscattering strength), there is a natural desire for the colour map to be both sequential and qualitative. Our results show that perceptually uniform colour maps tend to be less colourful than non-perceptually uniform, but that colour maps such as *Parula* can provide a compromise.

Split-beam echosounders, described by Foote, Aglen and Nakken (1986), also record phase angle data diverging from 0°, which can be displayed using a diverging colour map. *DT4* has a single turning point and is thus diverging, but its lightness profile is not symmetric (Figure 3.4). Despite having three turning points, the *Sonic* colour map has a sharp central peak in its lightness profile and could be used as a diverging colour map (Figure 3.4). However, *Sonic* is not perceptually uniform and better diverging colour maps are widely available. Good diverging colour maps are symmetrical, having exactly one turning point in their lightness profile, and have colourful, sequential and perceptually uniform legs (e.g. *cmocean balance*).

As echosounder resolution and precision increases, echogram data contain ever more detail (e.g. the Simrad EK80 has a range resolution of centimetres, Lavery *et al.*, 2017). The echogram shown in Figure 3.1 has low spatial resolution and low radiometric resolution, but a modern computer monitor may display more than 240 dots per inch with millions of colours. Colour maps

should be chosen carefully to make best use of the available display capability; however, we have reached a point where the human vision system may not be able to discriminate all the features present in an echogram image. As range and power resolution increases, the use of computational methods for echogram segmentation, classification and interpretation (Korneliussen, 2018) will likely become more effective than manual methods.

The CIELAB colour space and CIEDE2000 colour distance measurements are approximations of human visual perception. The effectiveness of a colour map is also influenced by factors including simultaneous contrast (Ware, 1988), lighting environment (Baylor, 1995) and the eye's dark adaptation. Still, the methods presented here offer simple, reliable and objective measures for assessing and comparing colour maps.

None of the colour maps tested is extremely colourful, sequential and perceptually uniform, so there is no single colour map that meets every requirement. Modern colour maps are available from other scientific disciplines (e.g. Thyng *et al.*, 2016; Hunter, 2007; Brewer, 2015) that are not yet widely implemented in fisheries acoustic software, but may offer additional choice and advantages over traditional fisheries acoustic colour maps. We hope that Table 3.1 and the methods herein will allow fisheries acousticians to make more informed decisions when selecting echogram colour maps.

3.5   Recommendations

When using echograms to detect morphological structure in acoustic data, sequential, perceptually uniform greyscale colour maps are recommended.

When using echograms to present quantitative data (e.g. S_v or TS) colour maps should be colourful, sequential and perceptually uniform. Of the fisheries acoustic colour maps tested, *LSSS* comes closest to being sequential and perceptually uniform. However, modern colour maps have been specifically designed for colour contrast consistency, accessibility for viewers with red-green colour-blindness, and legibility when printed in monochrome

(e.g. *Viridis*, *Parula*).

When using echograms to present diverging data (e.g. split-beam angle), diverging colour maps should be used, with symmetrical legs, each being colourful, sequential and perceptually uniform.

When using echograms to present categorical data (e.g. fish schools, seabed), qualitative colour maps should be used.

Chapter 4

Acoustic indices of ecosystem variability at South Georgia

> "If you torture the data long enough, it will confess."
>
> Ronald H. Coase, Essays on Economics and Economists.

In Chapter 2 we used compression algorithms to reduce acoustic data size, but compression ratios were unsatisfactory. We are forced to try summarising acoustic data, a theme we explore in this chapter.

4.1 Introduction

Marine ecosystems vary over multiple spatial and temporal scales (Dickey, 1991). Ecological processes are influenced by local weather parameters and large-scale patterns of climate variability, affecting marine biology and fish stocks through both direct and indirect pathways (Stenseth *et al.*, 2002). Identifying change and the drivers of change in ecosystems is key to their study and management.

Climatic drivers of variability in the Southern Ocean include the Southern Annular Mode (SAM) and the El Niño–Southern Oscillation (ENSO) (Meredith *et al.*, 2008). Positive SAM is associated with warm winds di-

rected towards the South Pole, decreased sea ice (Stammerjohn *et al.*, 2008), and increased ocean mixing (Lovenduski and Gruber, 2005). The El Niño–Southern Oscillation (ENSO) exerts an irregular, periodic influence that increases temperature and reduces sea ice near the Antarctic Peninsula.

The Southern Ocean is undergoing major changes as a result of anthropogenically driven climate change (Rogers *et al.*, 2019). Increasing ocean temperatures, ocean acidification, changes in sea ice characteristics and consequent impacts on marine biota have been observed for at least the last thirty years (Constable *et al.*, 2014). The ecosystem is complex with significant regional variability and non-linear, indirect biotic relationships that are difficult to quantify (Gutt *et al.*, 2015).

Antarctic krill *Euphausia superba* (henceforth krill) is the dominant mid-trophic-level species in the Southern Ocean (Murphy *et al.*, 2016). It is prey to a wide range of predators including whales, birds, seals and fish (Trathan and Hill, 2016). Krill help to remove carbon dioxide from the atmosphere as part of a biological carbon pump, consuming phytoplankton in surface waters and repackaging this carbon into rapidly sinking faecal pellets (Giering *et al.*, 2014; Belcher *et al.*, 2019). Seventy percent of the Southern Ocean krill population is contained in the Atlantic sector (Atkinson *et al.*, 2008), with the population originating from the Peninsula (Hofmann *et al.*, 1998), the region showing the greatest temperature increase and sea ice reduction (Meredith *et al.*, 2008). Krill is also the target of the largest Southern Ocean fishery, being used for aquaculture as well as human consumption (Nicol and Foster, 2016). These combined pressures have led ecologists to highlight the vulnerability of krill and the Southern Ocean ecosystem (Schiermeier, 2010; Flores *et al.*, 2012).

The British Antarctic Survey has been measuring krill in the South Georgia region since 1996 (Fielding *et al.*, 2014). The Western Core Box (WCB, Section 1.2) is an annual ship based survey undertaken each austral summer collecting echosounder and net haul data. It is primarily used to make an estimate of krill density (*KLD*). However, this creates just a single value each

year to represent a population of krill with complex patterns of distribution and abundance. We would like to study the whole ecosystem rather than a single species. Alternative acoustic indices have been proposed including *density* (mean volume backscattering strength), *abundance* (area backscattering strength), *location* (centre of mass), *occupied* area (proportion occupied), *evenness* (equivalent area) and *aggregation* (index of aggregation) (Urmy, Horne and Barbee, 2012). These measures (henceforth Echometrics) have been successfully applied to mooring data at Monterey Bay (Urmy, Horne and Barbee, 2012) and survey data in the Gulf of Mexico (D'elia *et al.*, 2016) to describe ecosystems in terms of both animal abundance and behaviour. In these cases, Echometrics revealed strong seasonal cycles and variability in diurnal vertical migration.

In this chapter we ask whether Echometrics are effective indicators of ecosystem variability at South Georgia. We compute Echometrics from WCB data (2003 to 2019) and compare our results to the recently updated, krill density time series after Fielding *et al.* (2014). Finally, we examine correlation between Echometrics and independent indices of local environmental, and large-scale climatic forces.

4.2 Materials and methods

4.2.1 Western Core Box data

Western Core Box data (Simrad EK60, 120 kHz, 2003 - 2019) were selected to allow us to study acoustic trends over nearly two decades (Table 4.1). The survey area was originally chosen for its proximity to concurrent predator studies at South Georgia. Each survey consisted of eight 80 km transects run in daylight hours, alternately in on and off shelf directions at a nominal speed of 10 knots with a fixed ping rate, $I_T = 2\,$s (Figure 1.2). Power settings varied between years but were consistent within year.

Table 4.1: Western Core Box cruises by survey year.

Year	Cruise	Date	Transects	Notes
2003	JR82	Feb 2003	7	Transect 3.2 corrupted
2004	JR96	Jan 2004	8	
2005	JR116	Jan 2005	8	
2006	JR140	Jan 2006	8	
2007	JR162	Dec 2006	6	Reduced due to weather
2008				No survey
2009	JR188	Jan 2009	8	
2010	JR228	Dec 2009	8	
2011	JR245	Dec 2010	8	
2012	JR260	Jan 2012	8	
2013	JR280	Dec 2012	8	
2014	JR291	Dec 2013	8	
2015	JR304	Dec 2014	8	
2016	JR15002	Dec 2015	8	
2017	JR16003	Dec 2016	8	
2018	JR17002	Jan 2018		No EK60 120 kHz data
2019	DY098	Jan 2019	8	

4.2.2 Acoustic data processing

Data were first converted to volume backscattering coefficient (S_v) using EchoJulia[1]. Off effort acoustic data (i.e. data collected between transects) were discarded. Calibration corrections (S_{ac}) were determined annually using standard sphere techniques (Demer *et al.*, 2015). Sound speed (c) and absorption (α) were determined from cruise CTD stations undertaken during each cruise (Francois and Garrison, 1982), averaged over the top 250 m of the water column. Calibration corrections are given in Appendix B.

Before calculating Echometrics, noise was detected and removed using EchoPy[2] (an assessment of the impact of noise removal on results is given in Section 4.6.2). Impulse Noise (IN), defined as noise "spikes" of less than

---

[1]https://github.com/EchoJulia/SimradEK60.jl, accessed April 2020.
[2]https://github.com/bas-acoustics/echopy, accessed April 2020.

one ping in duration, was identified with a two-sided comparison method using a resolution of 5 m vertical bins and a 10 dB threshold (Ryan *et al.*, 2015). Attenuated Signal (AS), defined as signal of lower amplitude due to bubbles, was identified by comparing the deviation of each ping from S_v data within the 100 to 200 m range, using a 30 ping average and -6 dB threshold (Ryan *et al.*, 2015). Samples detected as noise were regarded as "empty water" and replaced with -999 dB which is approximately 0 in the linear domain.

Transient noise (TN) may result from sounds generated in bad weather when waves collide with the hull of the ship, and last for several pings. TN was identified by comparing S_v data from each ping to a block in a reference layer at far range. If the ping median is greater than the block median by a user defined threshold (30 dB), the ping is masked until transient noise disappears, or until some minimum range (100 m) is reached. The method is implemented in EchoPy.

Background noise (BN) was detected and subtracted following the method described by De Robertis and Higginbottom (2007) (5 m vertical bins, 20 pings, $\text{Noise}_{max} = -125$ dB), as implemented in EchoPy. The seabed and below (SB) was excluded using a maximum S_v bottom pick followed by manual inspection, and correction where necessary. Aliased seabed (ASB) is caused by seabed reverberation from preceding pings coinciding with echoes from the current ping, and was replaced manually with -999 dB following echogram scrutinisation, as was other obvious corruption. All manual inspection, scrutinisation and classification was undertaken using the GNU Image Manipulation Program (GIMP).[3]

The top 20 m of range was excluded to avoid surface noise and near field effects. The range of analysis was also restricted to 250 m because data from 2003 to 2006 were collected to a range of only 300 m and it is common to consider the top 250 m in krill surveys (e.g. Fielding *et al.*, 2014).

To remove bias from zooplankton undertaking diurnal vertical migration

---

[3]https://www.gimp.org, version 2.10.8.

(movement from depth to the surface at night), all data before maritime sunrise and after maritime sunset were discarded. The local time of each ping relative to the solar noon was calculated using Astral.[4]

It is common practice in fisheries acoustics to downsample data using spatial averaging (sometimes called binning or bucketing) to reduce the effect of noise extrema, account for the linearity principle (which requires a minimum number of samples to ensure stochasticity of animal orientation) and to reduce local variability. However, we have concerns about the sensitivity of volume backscattering coefficient (S_v) results to the choice of bin size (for examples and discussion, see Appendix G). This study does not use results to derive biological abundance or biomass estimates and can therefore maintain the native resolution of the data. This preserves the spatial variability of the signal in all subsequent calculations.

4.2.3 Echometrics

From the metrics proposed by Urmy, Horne and Barbee (2012), we calculated *density*, *abundance*, *location*, *dispersion*, *occupied*, *evenness* and *aggregation* on a ping-by-ping basis (Table 4.2 [5]). *Density* and *abundance* are measures of the intensity of the reflected acoustic signal. *Location*, being the centre of mass of the signal, indicates the water column depth from which reflections originate. *Dispersion* is a measure of the spatial distribution of the signal. *Occupied* is the proportion of the water column with reflected signal greater than some threshold value s_v^{thresh} which we set to -90 dB re $1\,\mathrm{m}^{-1}$ after Urmy, Horne and Barbee (2012). *Aggregation* and *evenness* are indications of whether the signal is grouped or evenly distributed. Urmy, Horne and Barbee (2012) also mention a layer structure metric, but this was not adequately described algebraically and so was not used. Annual summaries were calculated to assess interannual variability using the mean of all ping values for that year (the mean in the linear domain was used

---

[4]https://github.com/sffjunkie/astral, accessed April 2020.
[5]N.B. The equation for occupied was specified incorrectly in Urmy, Horne and Barbee (2012) but can be deduced from the context and is corrected here.

for decibel measures). A principal component analysis was undertaken to assess the degree of collinearity among metrics.

Table 4.2: Echometrics used for summarising active acoustic data. z represents depth and $s_v(z)$ the volume backscattering coefficient at depth z. H is the total water column depth.

Variable	Description	Equation	Unit
Density	Mean volume backscattering strength	$S_v = 10\log_{10}\left(\frac{\int s_v(z)\mathrm{d}z}{H}\right)$	dB re $1\,\mathrm{m}^{-1}$
Abundance	Area backscattering strength	$S_a = 10\log_{10}(\int s_v(z)\mathrm{d}z)$	dB re $1\,\mathrm{m}^2\ \mathrm{m}^{-2}$
Location	Centre of mass	$\mathrm{CM} = \dfrac{\int z s_v(z)\mathrm{d}z}{\int s_v(z)\mathrm{d}z}$	m
Dispersion	Inertia	$I = \dfrac{\int (z - \mathrm{CM})^2 s_v(z)\mathrm{d}z}{\int s_v(z)\mathrm{d}z}$	m^{-2}
Occupied	Proportion occupied	$P_{occ} = \dfrac{|s_v(z) > s_v^{thresh}|}{|z|}$	
Evenness	Equivalent area	$\mathrm{EA} = \dfrac{(\int s_v(z)\mathrm{d}z)^2}{\int s_v(z)^2\mathrm{d}z}$	m
Aggregation	Index of aggregation	$\mathrm{IA} = \dfrac{\int s_v(z)^2\mathrm{d}z}{(\int s_v(z)\mathrm{d}z)^2}$	m^{-1}

Echometrics were compared to other environmental indices using correlation analysis. The Pearson correlation coefficient (r) is a measure of the linear correlation between two variables X and Y, where 1 is total positive linear correlation, 0 is no linear correlation, and -1 is total negative linear correlation. The critical value of r at $p = 0.05$ with $N = 15$ is 0.514 (Kanji, 2006) and so we consider correlations $r > 0.514$ as significant. The Spearman's rank correlation coefficient (r_s) is a measure of the monotonic dependence between variables X and Y and an indicator of non-linear correlation. Values of $r_s > 0.525$ are significant at $p = 0.05$. We interpret Pearson's correlation coefficient (r) and Spearman's rank correlation coefficient (r_s) according to Table 4.3 from (Fowler, Cohen and Jarvis, 1998).

Table 4.3: Interpretation of the strength of a correlation.

Coefficient (positive or negative)	Meaning
0.00 to 0.19	A very weak correlation
0.20 to 0.39	A weak correlation
0.40 to 0.69	A modest correlation
0.70 to 0.89	A strong correlation
0.90 to 1.00	A very strong correlation

4.2.4 Comparison with krill metrics

The Echometrics were compared to krill density estimates (KLD, $\mathrm{g\,m^{-2}}$) and krill length calculated from the same WCB time series, after Fielding *et al.* (2014). We used the median krill length (KLM, mm) as a measure of central tendency of the distribution. Atkinson *et al.* (2006) report average krill length of 40 mm at South Georgia, and so we used the proportion of krill with length < 40 mm as a measure of small (possibly juvenile) krill ($KL40$).

All correlation plots use a blue line to show the simple linear regression fit, with a grey shaded area showing the standard error on either side of the line.

4.2.5 Comparison with local environmental variables

Whitehouse, Priddle and Brandon (2000) showed interannual variability of chlorophyll-a and phytoplankton (a key source of food for krill) and so the Echometrics were compared to in situ, cotemporal measurements of chlorophyll (CHL, $\mathrm{mg\,m^{-3}}$). Echometrics were also compared with sea surface temperature (SST, ºC) and mixed layer depth (MLD, m) (Table 4.4). The nearest temporal measurement to the Western Core Box centroid (38º 30 W, 53º 30 S) was used.

Table 4.4: Independent environmental indices.

Variable	Source
CHL	Chlorophyll ($\mathrm{mg\,m^{-3}}$) obtained from the OCEANCOLOUR GLO CHL L4 REP OBSERVATIONS 009 082 product, 4 km resolution, available from the E.U. Copernicus Marine Environment Monitoring Service at https://marine.copernicus.eu, (accessed September 2019).
ENSO	The El Niño 3.4 region temperature anomaly obtained from the NOAA National Weather Service Climate Prediction Center, http://www.cpc.ncep.noaa.gov/data/indices/sstoi.indices, (accessed September 2019).
SAM	Monthly SAM obtained from British Antarctic Survey, http://www.nerc-bas.ac.uk/public/icd/gjma/newsam.1957.2007.txt, (accessed September 2019).
SST	Sea Surface temperature (ºC) obtained from the NOAA Optimum Interpolation Sea Surface Temperature V2 monthly mean data, 0.25 degree resolution, available from https://www.ncdc.noaa.gov/oisst, (accessed September 2019).
MLD	Mixed layer depth (m) obtained from the GLOBAL REANALYSIS PHY 001 030 monthly product, 0.083 degree resolution, available from the E.U. Copernicus Marine Environment Monitoring Service at https://marine.copernicus.eu, (accessed September 2019).
SII	Sea ice extent (millions $\mathrm{km^2}$) in the preceding September, 25 km resolution, obtained from Fetterer, F., K. Knowles, W. N. Meier, M. Savoie, and A. K. Windnagel. 2017, updated daily. Sea Ice Index, Version 3. Boulder, Colorado USA. NSIDC: National Snow and Ice Data Center. doi: https://doi.org/10.7265/N5K072F8, (accessed September 2019).

4.2.6 Comparison with larger scale, climatic variables

Fielding *et al.* (2014) showed higher krill density following colder sea surface temperature in the preceding August and so the Echometrics were compared with August SST (*SST'*). The indices were also compared to other larger scale, climatic factors: *SAM*, *ENSO*, peak seasonal chlorophyll (*CHL'*), and September sea ice extent (*SII*). September sea ice extent was chosen based on typical maximum mean circumpolar sea ice extent reported by Holland (2014).

4.2.7 Impact of survey parameters

We also examined aspects of the survey to determine possible bias. Most traditional survey results are derived from the magnitude of acoustic backscatter and so we looked at the impact on *abundance* caused by differences

in:

- Direction of sampling transect (North to South versus South to North);
- Within day timing of transect (sampling in the morning (before the solar noon) versus afternoon);
- Decadal timing of the survey (sampling before 2011 versus after);
- Seasonal timing of the survey (start date before 29 December (early season) versus after (late season)).

4.3 Results

4.3.1 Interannual variability of Echometrics

All Echometrics vary by survey year (Figure 4.1; Section 4.6.1). *Density* and *abundance* show a decrease between 2003 and 2019 (Figure 4.2). A principal component analysis shows that 76% of variability described by the Echometrics is explained by the first two principal components (*PC1*, *PC2*), and 97% by the first four (Figure 4.3). *PC2* shows decrease in a similar pattern to that observed for *density* and *abundance*.

Figure 4.4 shows how the individual metrics are aligned with the first two principal components and each other. *Density* and *abundance* are similar, broadly aligned with *PC2*, and highly correlated ($r = 0.995$). *Location* is closely aligned with *PC1* and therefore orthogonal to *density* and *abundance*. *Aggregation* is the reciprocal of *evenness*. *Dispersion* and *location* are the opposite of *occupied*. Survey years 2005 and 2010 are highly separated along *PC1* and this is consistent with *abundance* and *density* plots (Figure 4.1).
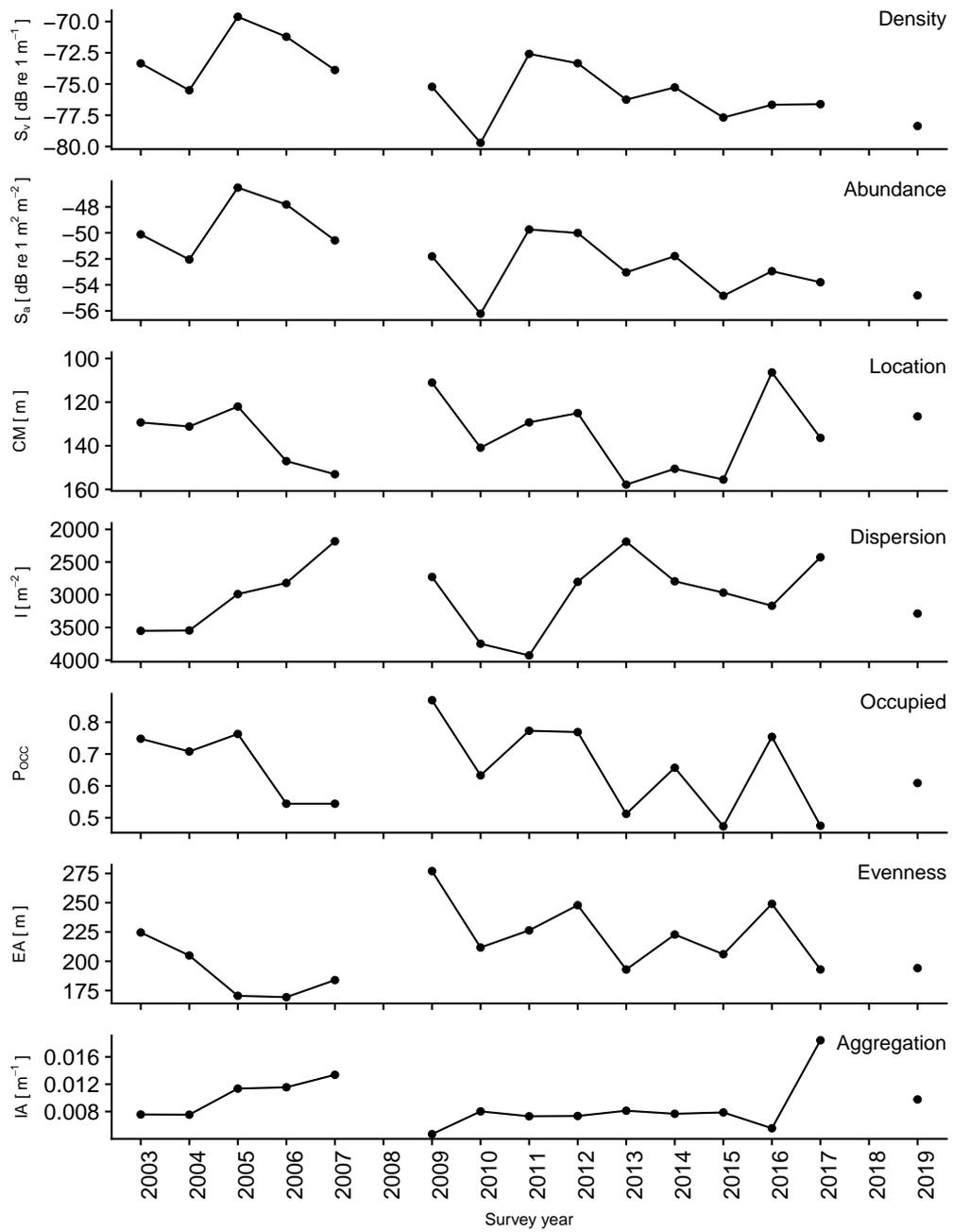
Figure 4.1: Western Core Box Echometrics by survey year.

55
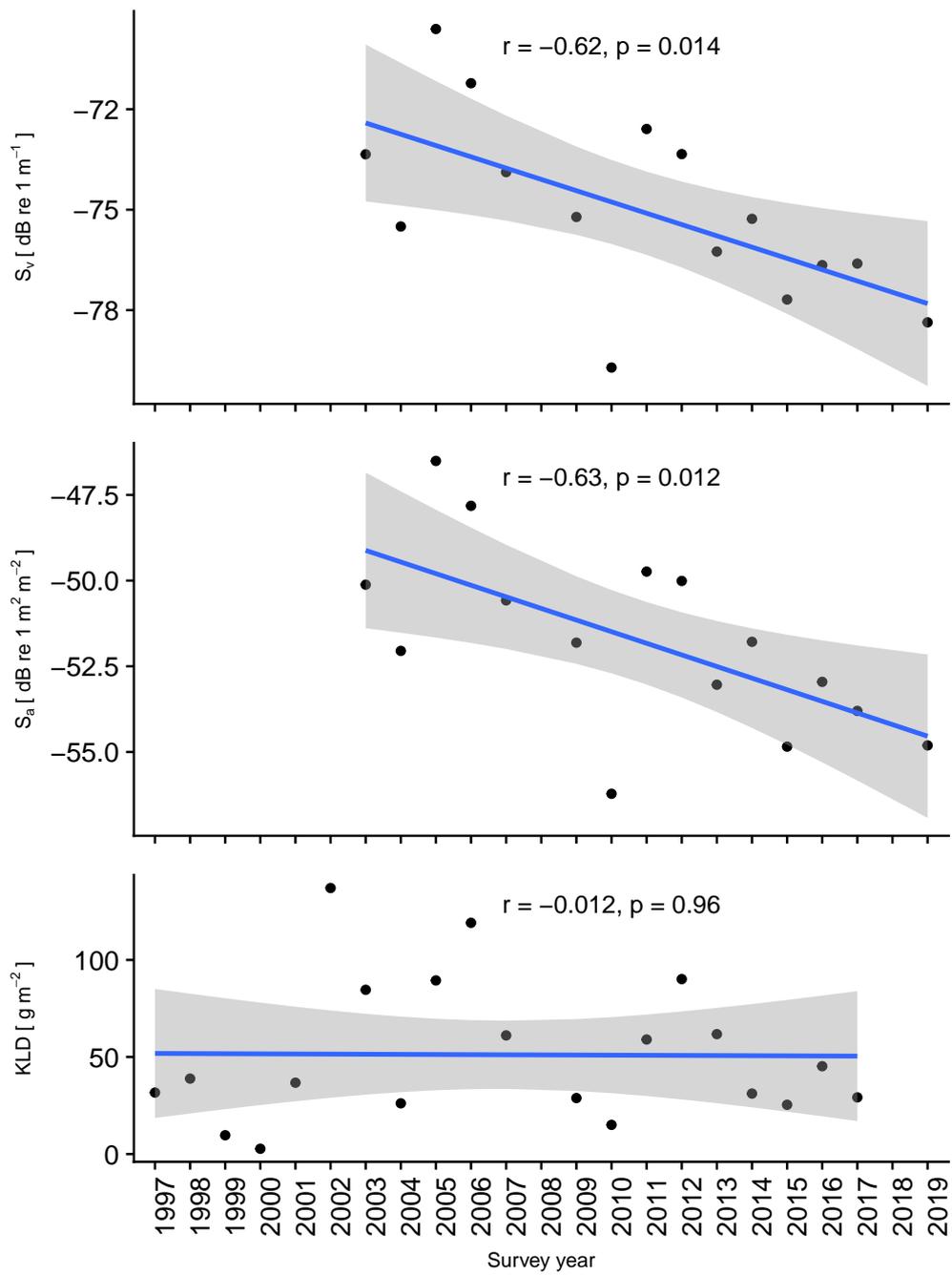
Figure 4.2: Density (S_v), abundance (S_a) and krill density (KLD) by survey year.
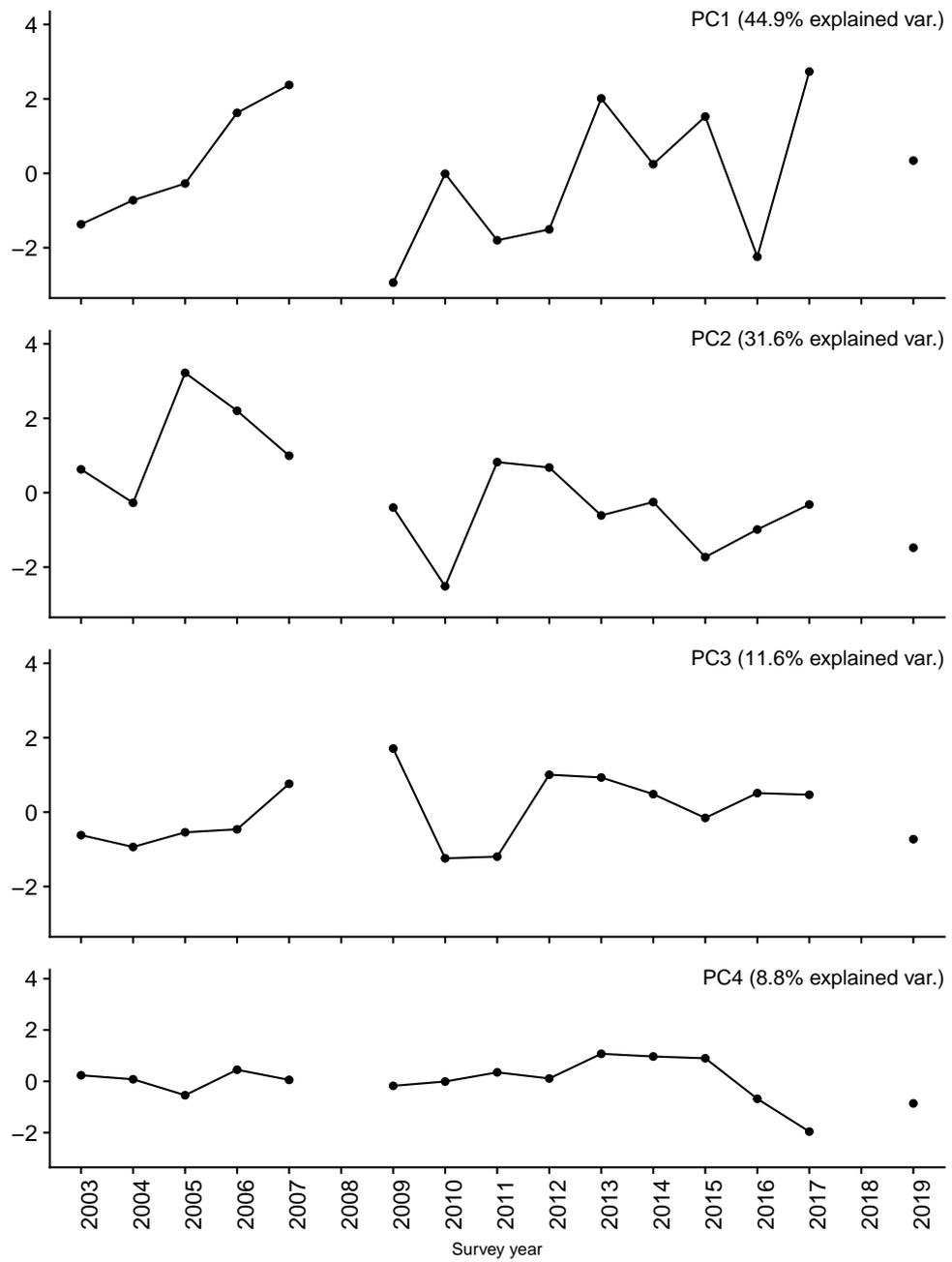
Figure 4.3: The first four principal components of Western Core Box Echo-metrics by survey year.
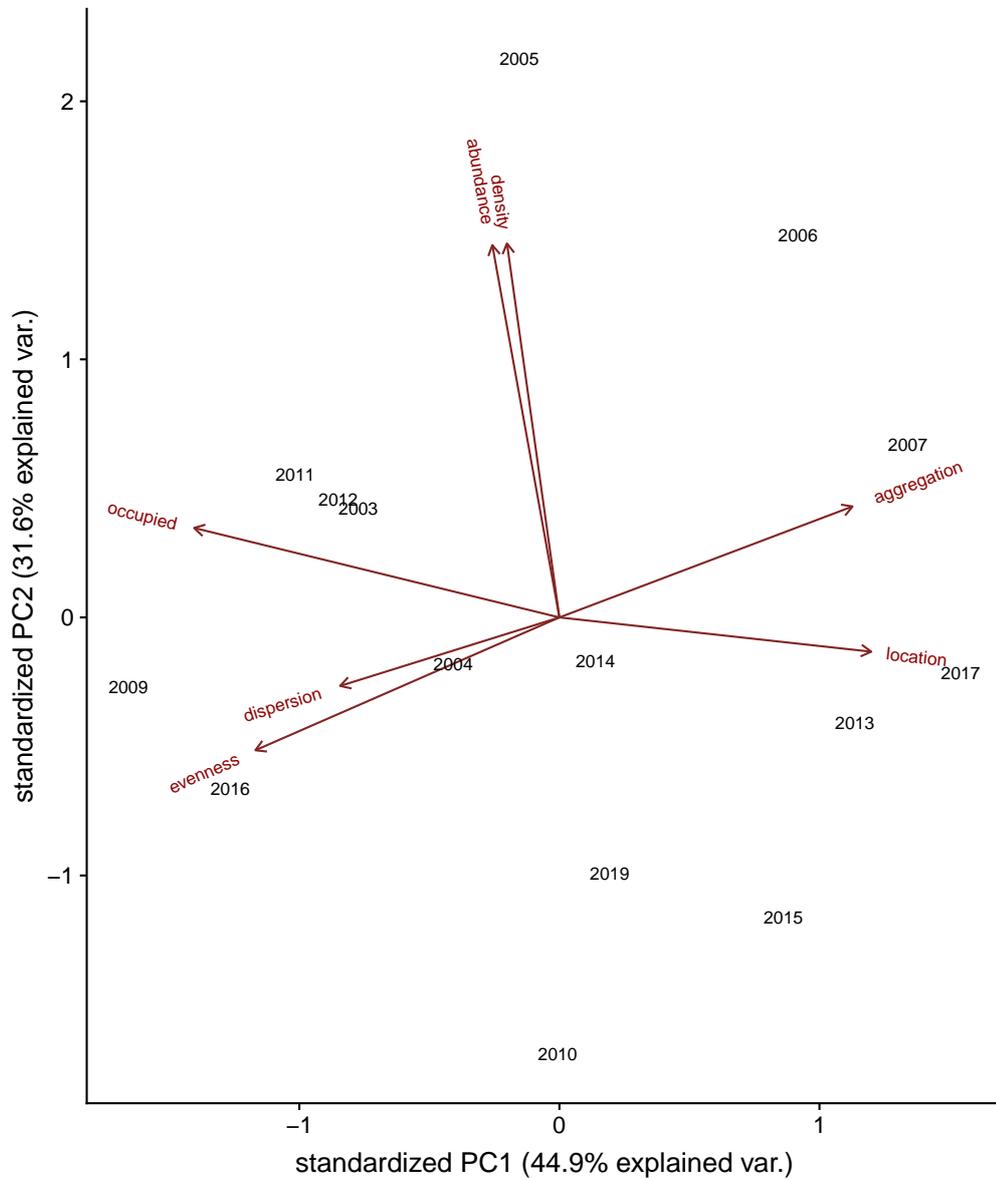
Figure 4.4: Western Core Box interannual variability shown in the first two dimensions of principal component space. The PCA uses density, abundance, location, dispersion, occupied, evenness and aggregation from Urmy et al. (2012).

4.3.2 Comparison with krill metrics

Density and *abundance* are strongly positively correlated with krill density (*KLD*) and median krill (*KLM*), and negatively correlated with smaller krill (*KL40*) (Tables 4.5 and 4.6, Figure 4.5).

Table 4.5: Pearson correlation (r) between Echometrics and other annual indices. Statistically significant results are shown in bold ($p < 0.05$). Day is the survey date relative to Jan 1. Krill metrics are krill density (KLD), median krill length (KLM) and smaller krill (KL40). Local variables are sea surface temperature (SST), chlorophyll (CHL) and mixed layer depth (MLD). Climatic variables are Southern Annular Mode (SAM), El Niño 3.4 region temperature anomaly (ENSO), September sea ice extent (SII), August sea surface temperature (SST') and peak chlorophyll (CHL'). PC1, PC2 and PC3 are the first three principal components of the Echometrics.

	Timing		Krill			Local variables			Climatic variables				
	year	day	KLD	KLM	KL40	SST	CHL	MLD	SAM	ENSO	SII	SST'	CHL'
density	**-0.62**	0.39	**0.83**	**0.60**	**-0.54**	**0.57**	0.09	-0.29	-0.30	-0.42	0.01	-0.37	0.10
abundance	**-0.63**	0.40	**0.83**	**0.62**	**-0.57**	**0.57**	0.14	-0.32	-0.28	-0.39	-0.02	-0.35	0.13
location	0.02	-0.33	-0.03	-0.41	0.31	-0.41	**-0.70**	0.10	-0.21	-0.08	**0.68**	0.18	**-0.56**
dispersion	-0.19	0.40	-0.13	-0.16	0.14	0.31	0.19	**-0.53**	0.21	0.09	-0.27	0.09	0.00
occupied	-0.35	0.41	0.09	**0.56**	**-0.54**	**0.54**	**0.59**	-0.20	0.27	-0.12	-0.41	-0.01	**0.65**
evenness	0.16	-0.00	-0.33	0.21	-0.28	0.02	**0.59**	0.23	0.29	-0.07	-0.26	0.31	**0.76**
aggregation	0.09	0.01	0.14	-0.41	0.51	0.01	**-0.60**	0.10	-0.38	-0.08	-0.05	-0.50	**-0.62**
PC1	0.19	-0.32	0.03	-0.46	0.47	-0.38	**-0.70**	0.18	-0.31	0.04	0.40	-0.13	**-0.70**
PC2	**-0.59**	0.37	**0.81**	**0.54**	-0.46	**0.55**	0.00	-0.27	-0.33	-0.37	-0.02	-0.45	-0.01
PC3	0.24	-0.34	-0.05	0.35	-0.35	-0.23	0.23	**0.61**	-0.01	-0.12	0.07	0.09	0.50
year	**1.00**	**-0.61**	-0.01	-0.28	0.25	-0.44	-0.01	0.17	-0.08	0.14	-0.03	-0.05	-0.14
day	**-0.61**	**1.00**	0.40	0.06	0.01	**0.81**	0.16	-0.42	-0.01	-0.16	**-0.64**	**-0.55**	0.11
KLD	-0.01	0.40	**1.00**	0.49	-0.44	0.46	0.19	-0.37	-0.32	0.03	-0.22	-0.47	0.12
KLM	-0.28	0.06	0.49	**1.00**	**-0.96**	0.35	**0.52**	0.04	0.09	-0.20	-0.10	0.13	**0.57**
KL40	0.25	0.01	-0.44	**-0.96**	**1.00**	-0.37	-0.50	-0.03	-0.07	0.26	0.06	-0.29	**-0.61**

There is a modest correlation between *occupied* and median krill length (*KLM*), and *occupied* and smaller krill (*KL40*), suggesting higher occupation with larger animals (Figure 4.6), and therefore, that larger animals occupy more space.

Table 4.6: Spearman's rank correlation (r_s) between Echometrics and other annual indices. Statistically significant results are shown in bold ($p < 0.05$). Day is the survey date relative to Jan 1. Krill metrics are krill density (KLD), median krill length (KLM) and smaller krill (KL40). Local variables are sea surface temperature (SST), chlorophyll (CHL) and mixed layer depth (MLD). Climatic variables are Southern Annular Mode (SAM), El Niño 3.4 region temperature anomaly (ENSO), September sea ice extent (SII), August sea surface temperature (SST') and peak chlorophyll (CHL'). PC1, PC2 and PC3 are the first three principal components of the Echometrics.

	Timing		Krill			Local variables			Climatic variables				
	year	day	KLD	KLM	KL40	SST	CHL	MLD	SAM	ENSO	SII	SST'	CHL'
density	**-0.62**	0.43	**0.79**	**0.57**	-0.50	**0.60**	0.37	-0.32	-0.26	-0.49	-0.03	-0.43	0.18
abundance	**-0.59**	0.43	**0.80**	**0.56**	-0.49	**0.59**	0.42	-0.44	-0.23	-0.42	-0.05	-0.37	0.20
location	0.04	-0.46	-0.13	-0.42	0.36	-0.50	**-0.64**	0.30	-0.15	0.11	**0.65**	0.13	-0.52
dispersion	-0.21	0.39	-0.16	-0.15	0.17	0.32	0.23	-0.49	0.11	0.19	-0.28	0.09	0.16
occupied	-0.35	0.45	0.22	**0.57**	-0.55	**0.57**	**0.62**	-0.27	0.12	-0.31	-0.37	-0.04	**0.60**
evenness	0.16	-0.01	-0.27	0.11	-0.19	0.07	0.42	0.04	0.15	-0.11	-0.28	0.36	**0.57**
aggregation	0.06	-0.08	0.18	-0.40	0.46	-0.11	**-0.61**	-0.02	-0.17	0.18	0.21	-0.32	**-0.66**
PC1	0.23	-0.32	0.03	-0.49	0.50	-0.40	**-0.71**	0.23	-0.16	0.13	0.37	-0.15	**-0.68**
PC2	**-0.58**	0.41	**0.76**	0.40	-0.31	**0.54**	0.15	-0.39	-0.23	-0.38	0.01	-0.45	-0.08
PC3	0.22	-0.35	0.21	0.43	-0.47	-0.23	0.24	0.41	-0.02	-0.21	0.13	0.11	0.30
year	**1.00**	**-0.57**	0.05	-0.27	0.17	-0.36	-0.19	0.13	-0.05	0.17	-0.04	-0.10	-0.04
day	**-0.57**	**1.0**	0.32	0.16	0.01	**0.75**	0.39	-0.30	0.26	-0.19	**-0.65**	**-0.56**	0.06
KLD	0.05	0.32	**1.00**	0.49	-0.42	0.43	0.45	-0.46	-0.33	0.12	-0.11	-0.46	0.28
KLM	-0.27	0.16	0.49	**1.00**	**-0.96**	0.35	**0.70**	-0.09	0.06	-0.34	-0.11	0.01	**0.61**
KL40	0.17	0.01	-0.42	**-0.96**	**1.00**	-0.34	**-0.67**	0.06	-0.03	0.38	0.09	-0.19	**-0.68**
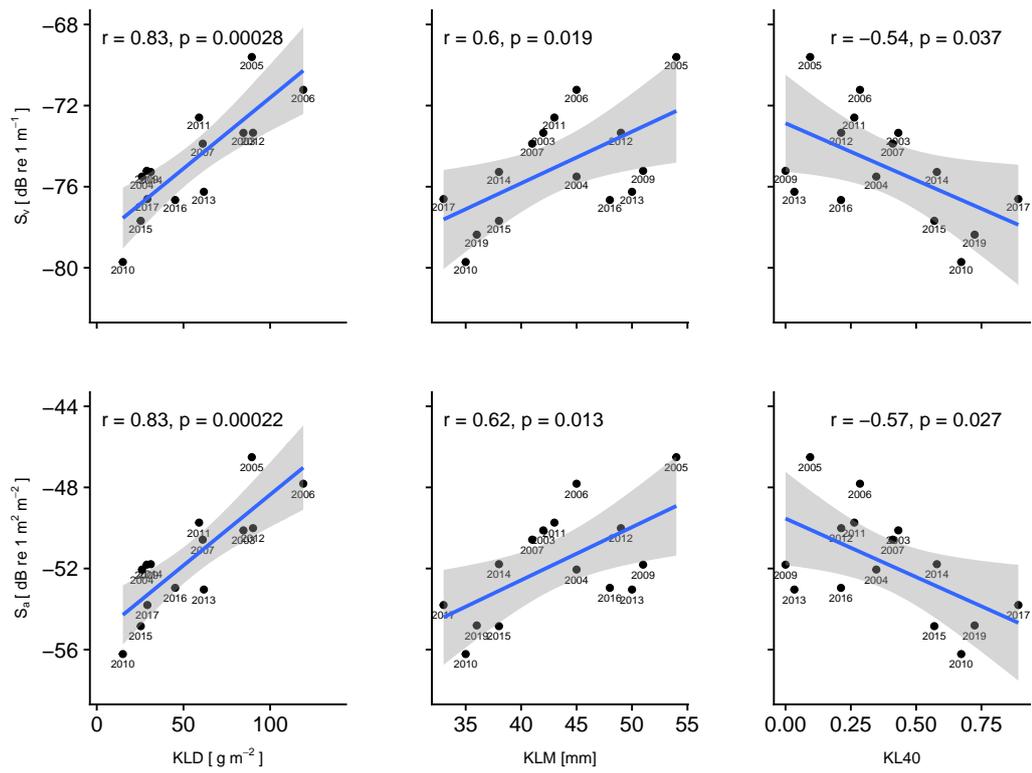
Figure 4.5: Density (S_v, top) and abundance (S_a, bottom) by krill density (KLD), median krill length (KLM) and smaller krill (KL40).
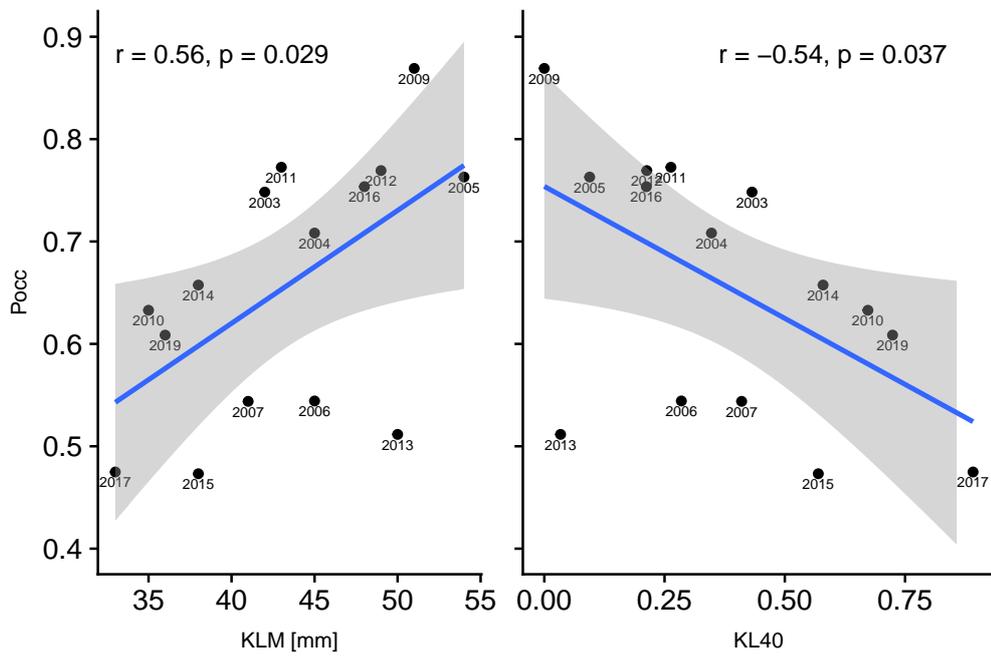
Figure 4.6: Occupied by median krill length (KLM) and occupied by smaller krill (KL40).

4.3.3 Comparison with local, environmental variables

Density, *abundance* and *occupied* show modest correlation with sea surface temperature (Tables 4.5 and 4.6, Figure 4.7). *Location* is strongly correlated with chlorophyll (*CHL*), whilst *occupied*, *evenness*, *aggregation* show a modest correlation (Tables 4.5 and 4.6). Backscatter is shallower, less aggregated, more even and occupies more of the water column with increased chlorophyll (Figure 4.8). *Dispersion* shows modest correlation with mixed layer depth (*MLD*); backscatter is more dispersed when the mixed layer is deeper (Figure 4.9).
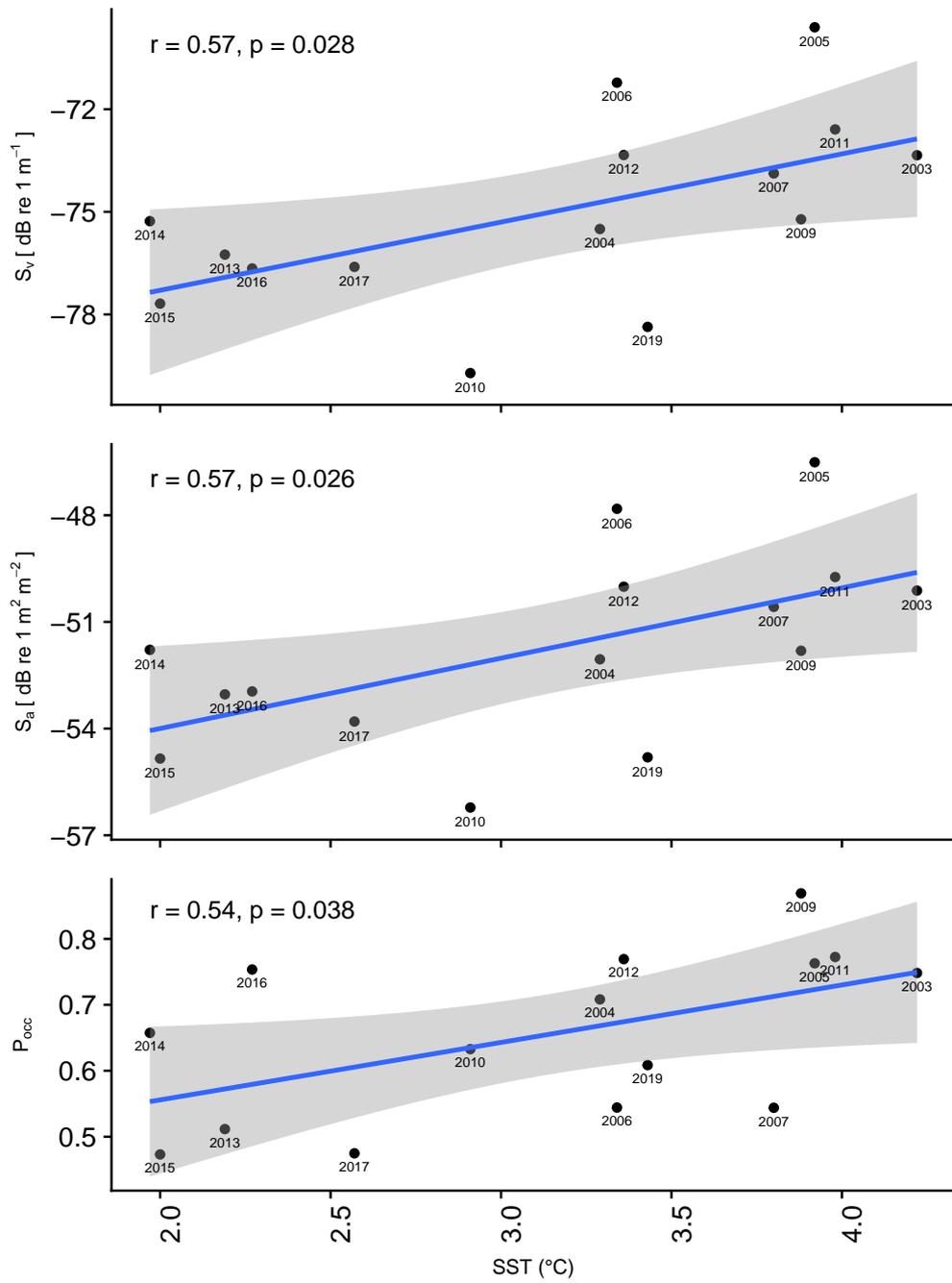
Figure 4.7: Density (S_v), abundance (S_a) and occupied (P_{occ}) by in situ, cotemporal sea surface temperature (SST).
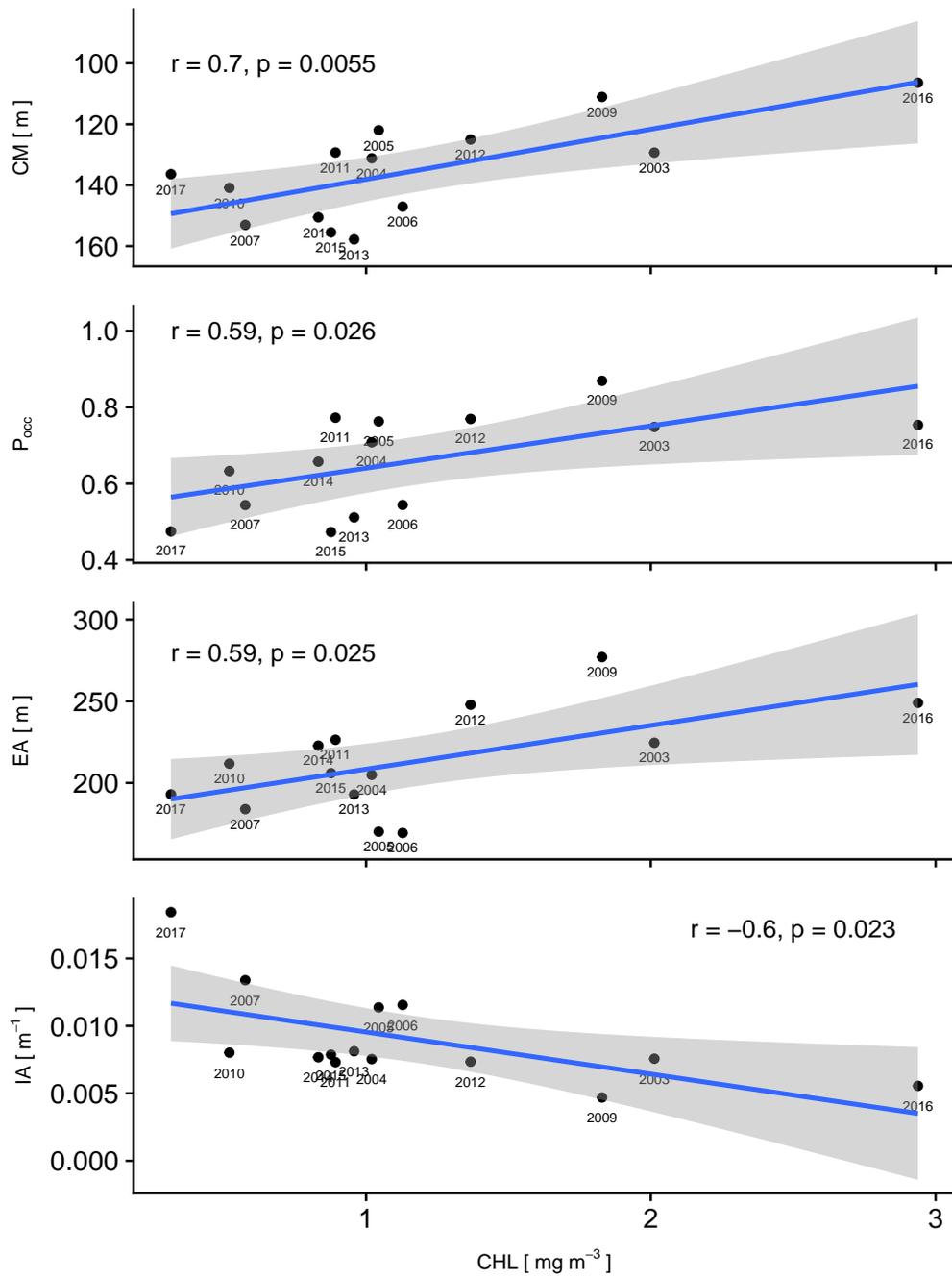
Figure 4.8: From top, location (CM), occupied (P_{occ}), evenness (EA) and aggregation (IA) by in situ, cotemporal chlorophyll (CHL).
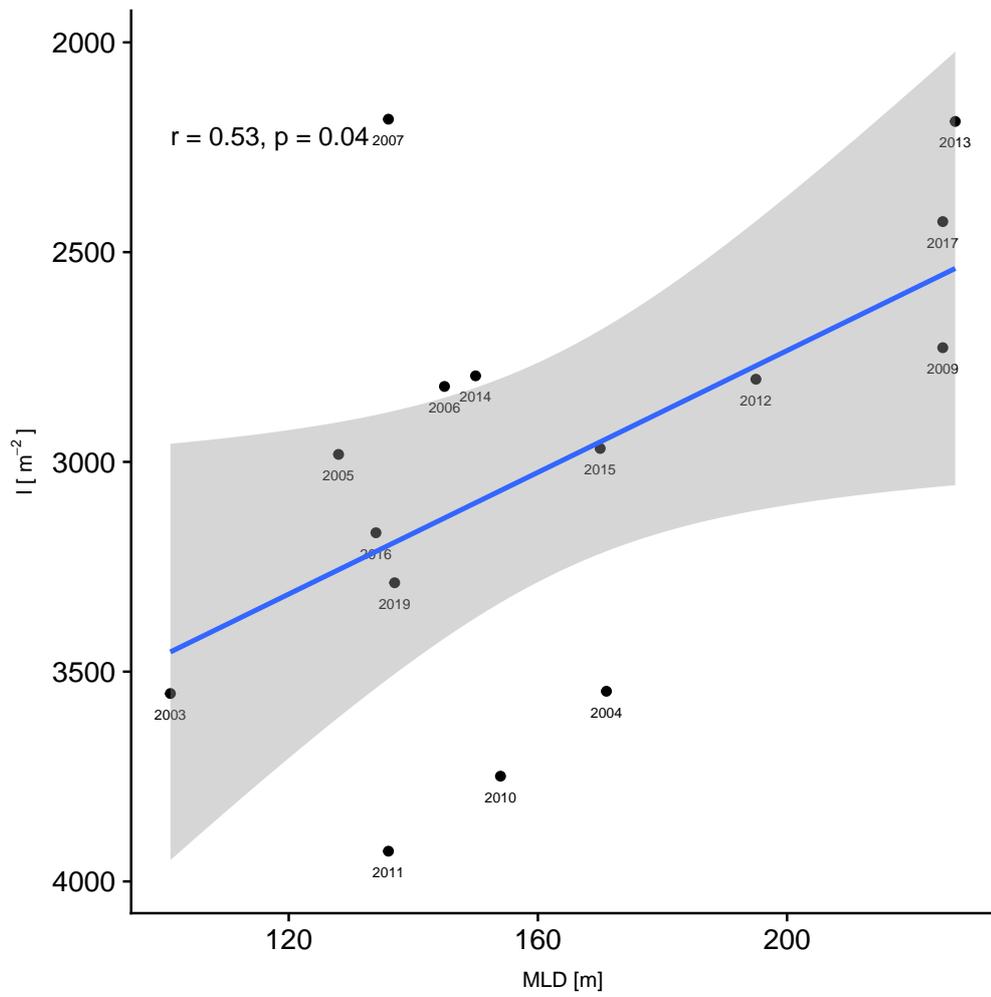
Figure 4.9: Dispersion (I) by in situ, cotemporal mixed layer depth (MLD).

4.3.4 Comparison with larger scale, climatic variables

None of the Echometrics show significant correlation with either SAM, ENSO or August SST. There is a correlation between krill density and August SST between 2003 and 2013 ($r = -0.63$, $p < 0.01$) consistent with Fielding *et al.* (2014). The correlation weakens when later years are considered ($r = -0.47$, $p < 0.05$), however this appears be driven by 2017 which was a particularly cold year, with low krill density (Figure 4.10).
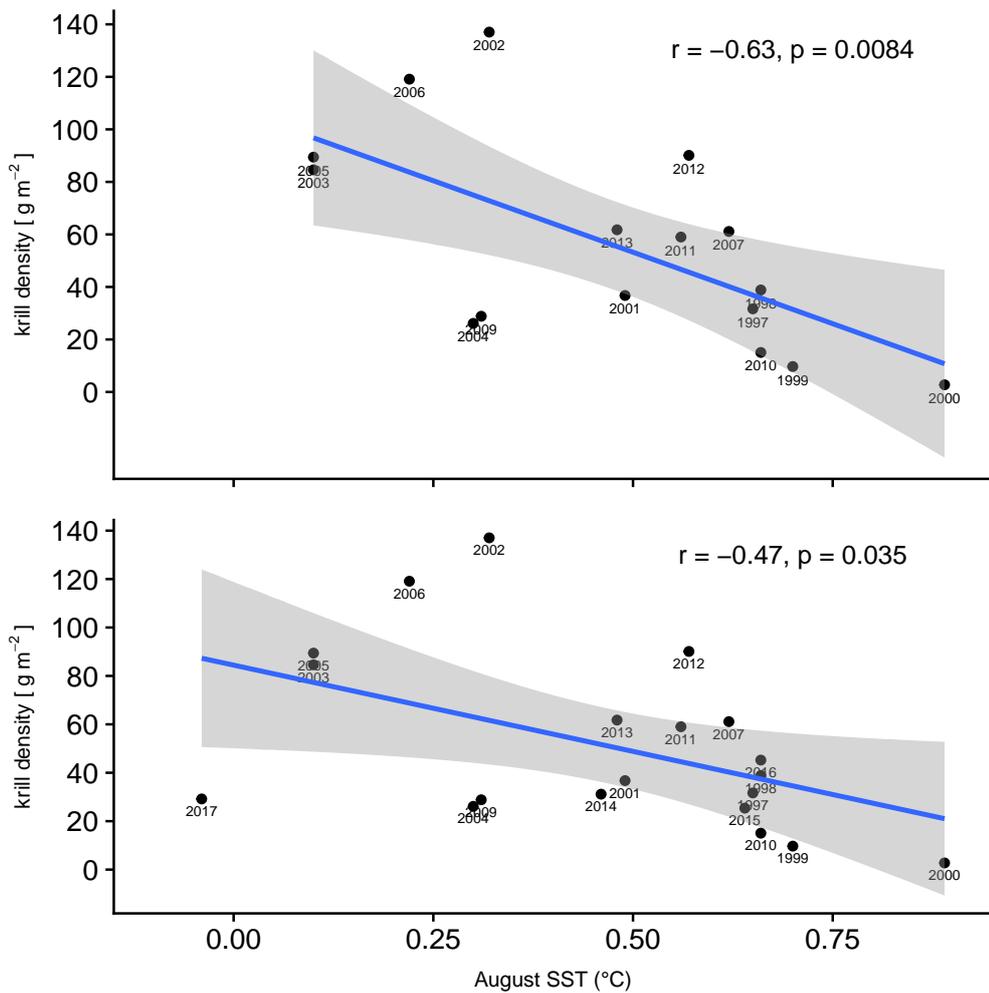
Figure 4.10: Krill density by August SST. The top graph uses data from 2003 to 2013, the bottom from 2003 to 2019

Location shows a modest correlation with September sea ice extent (*SII*);

backscatter is deeper following high sea ice extent (Figure 4.11). *Evenness* shows a strong correlation with peak chlorophyll (*CHL'*); *location, occupied* and *aggregation* show modest correlation (Figure 4.12), but these correlations are driven by unusually high peak chlorophyll in 2009, without which the correlations are not significant.
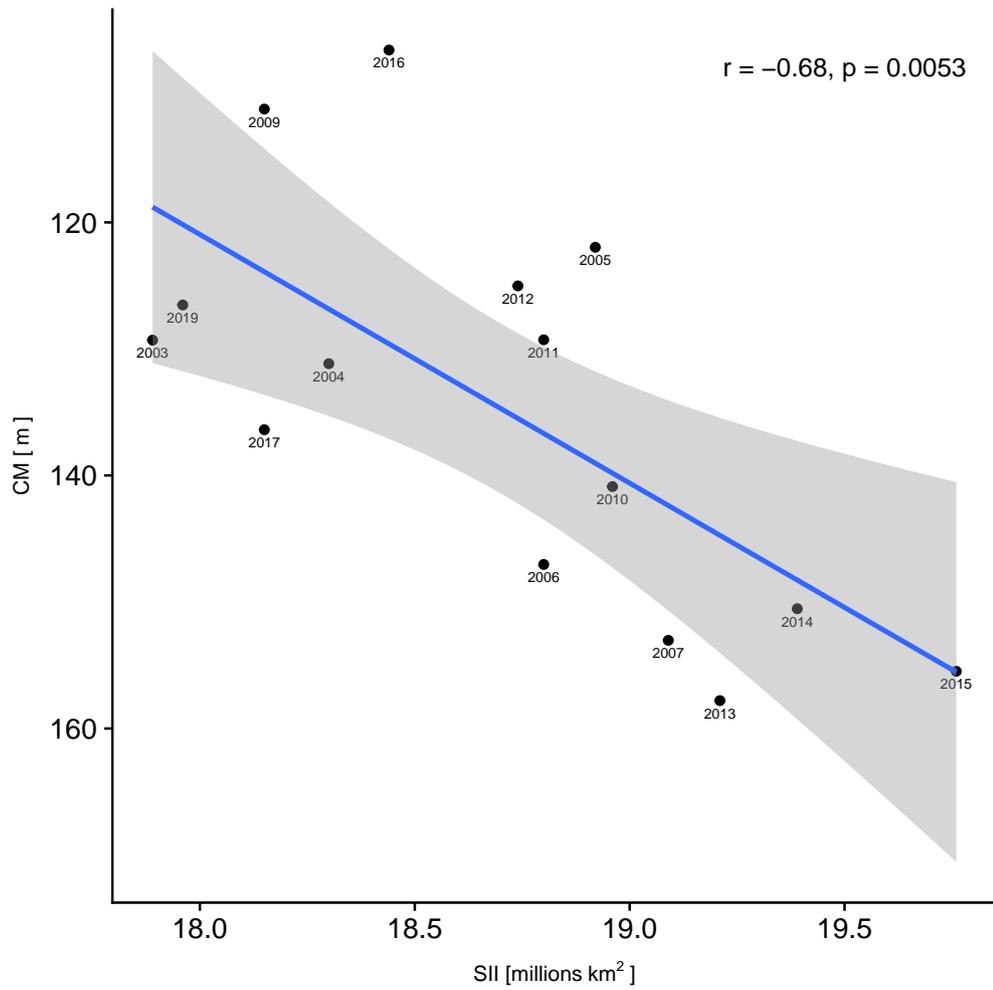
Figure 4.11: Location (CM) by September sea ice extent (SII).
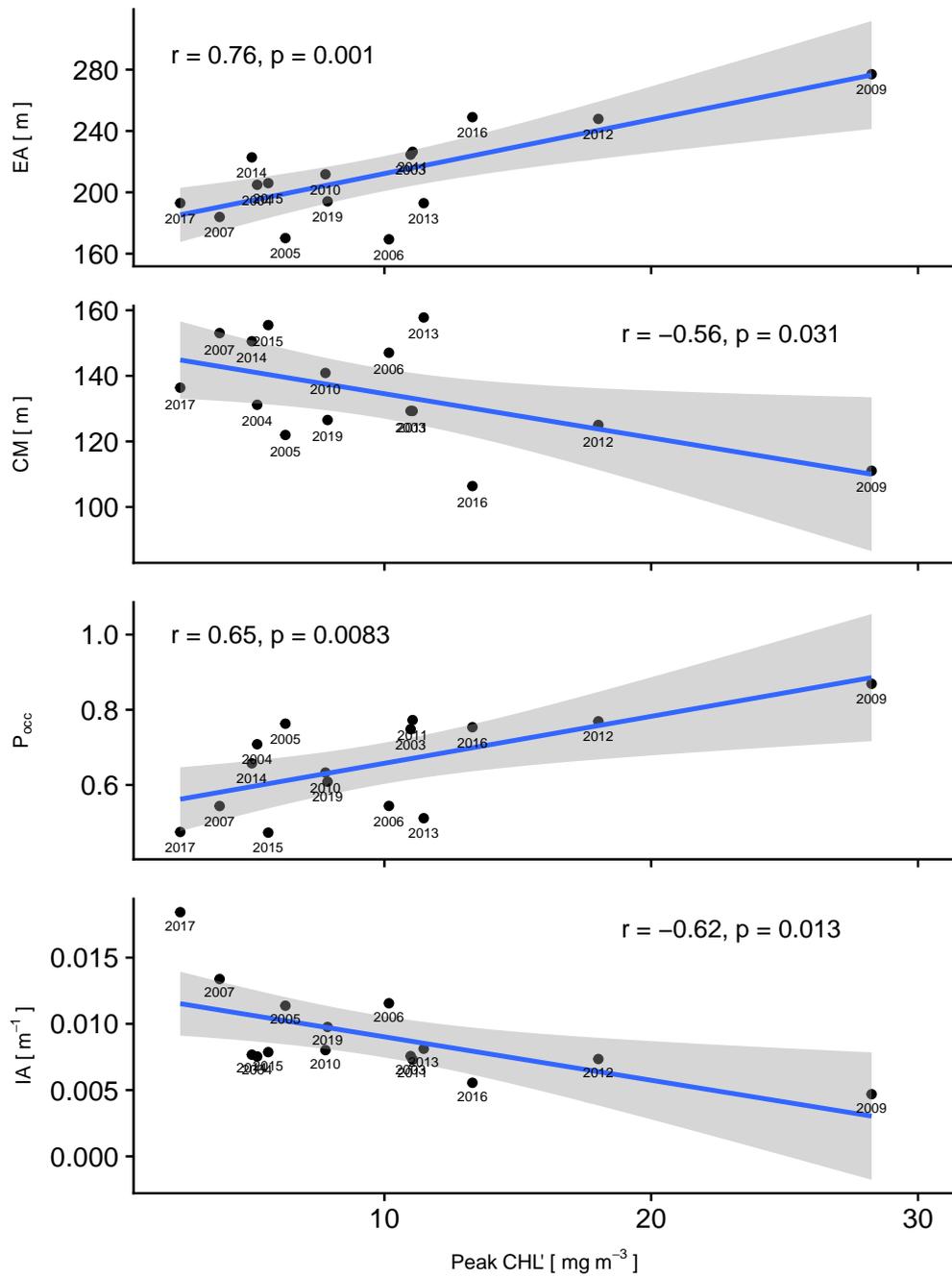
Figure 4.12: Evenness (EA), location (CM), occupied (P_{occ}) and aggregation (IA) by peak chlorophyll.

4.3.5 Impact of survey parameters

There is a modest negative correlation between the survey year (*year*) and the survey date (*day*), indicating that surveys have typically occurred earlier in the season during recent years (Figure 4.13). Although there is only weak correlation between survey date and *abundance* ($r = 0.41$) (Figure 4.14), a comparison of the distribution of *abundance* in early and late season shows as much as $5\,\mathrm{dB}$ difference between early and late season surveys (Figure 4.15a). The difference in the *abundance* distribution from surveys before 2011 when compared to surveys after 2011 is $\approx 2\,\mathrm{dB}$ (Figure 4.15b).
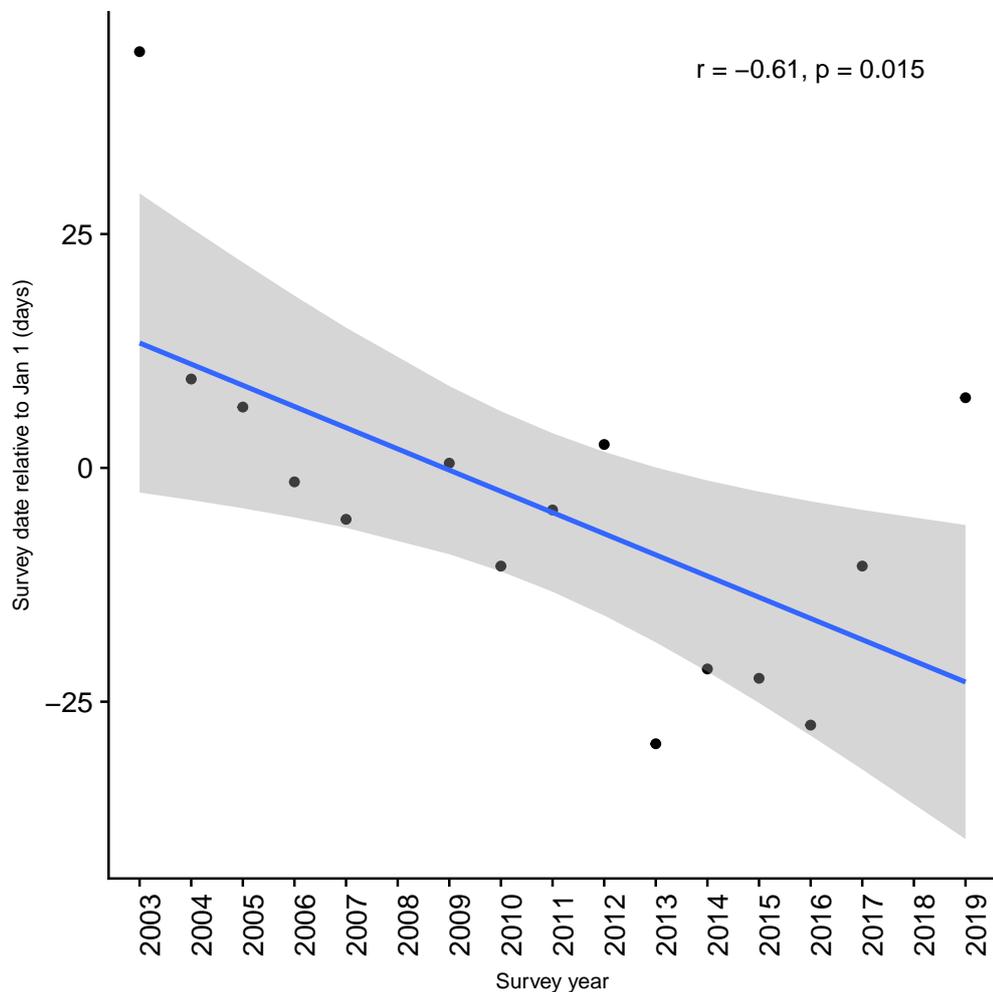
Figure 4.13: Western Core Box survey date by survey year.
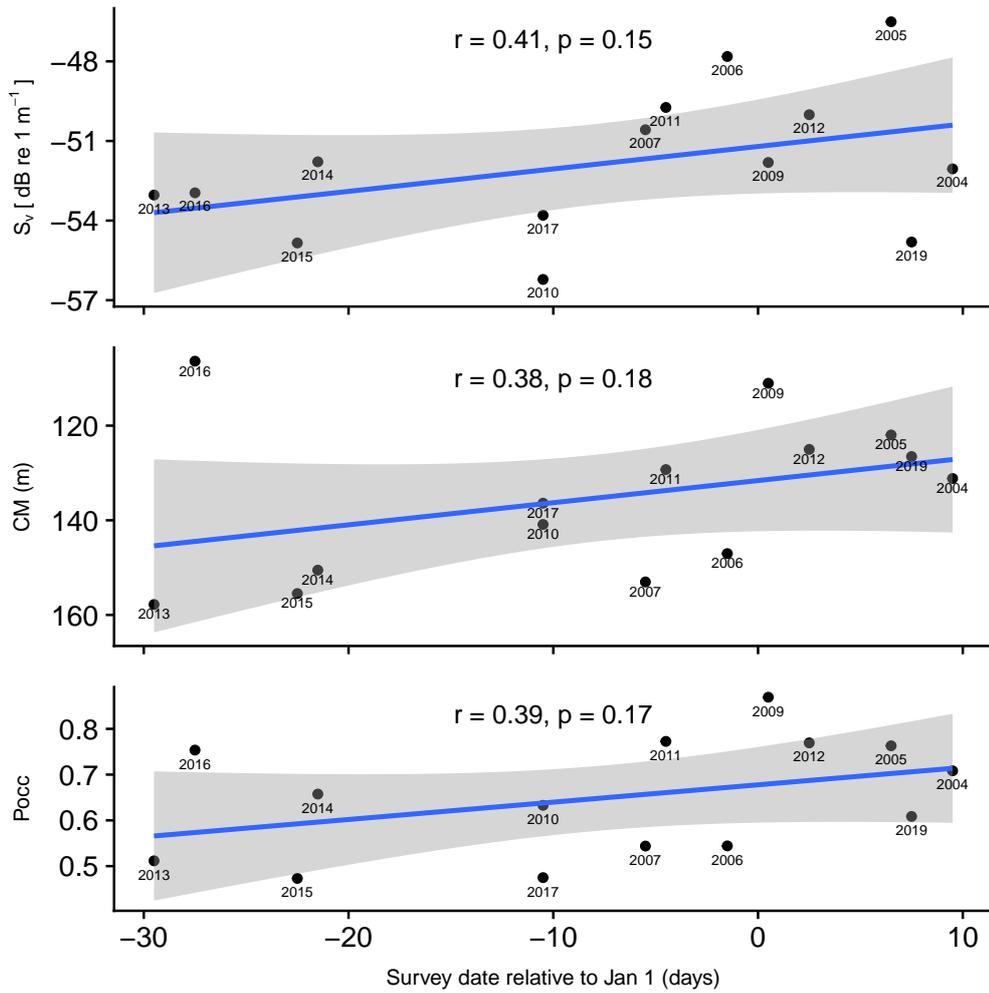
Figure 4.14: Abundance (S_a), location (CM) and occupied (P_{occ}) by survey date.

Whether transects were sailed in a northerly or southerly direction or in the morning or the afternoon appears to have little effect on the *abundance* distribution (Figure 4.15c and d).
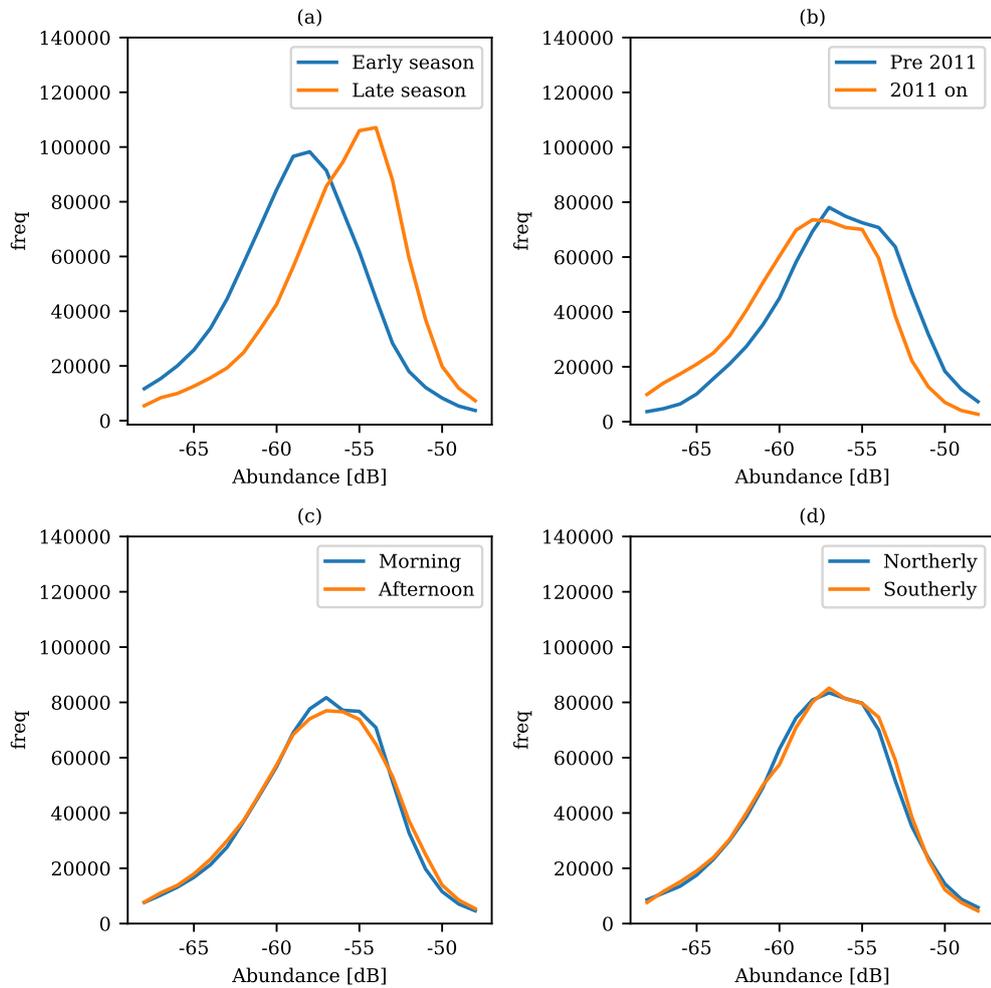
Figure 4.15: Effect of survey parameters on abundance. (a) Surveys conducted in early or late season, (b) Surveys before and after 2011, (c) Transects conducted in morning or afternoon, and (d) Transects sailed in a northerly or southerly direction.

4.3.6 Echometric distributions

In earlier Figures, we used the mean as a measure of central tendency for each of the Echometrics. The full distributions are shown as violin plots below (Figures 4.16 , 4.17 , 4.18 , 4.19 , 4.20 , 4.21 and 4.22).
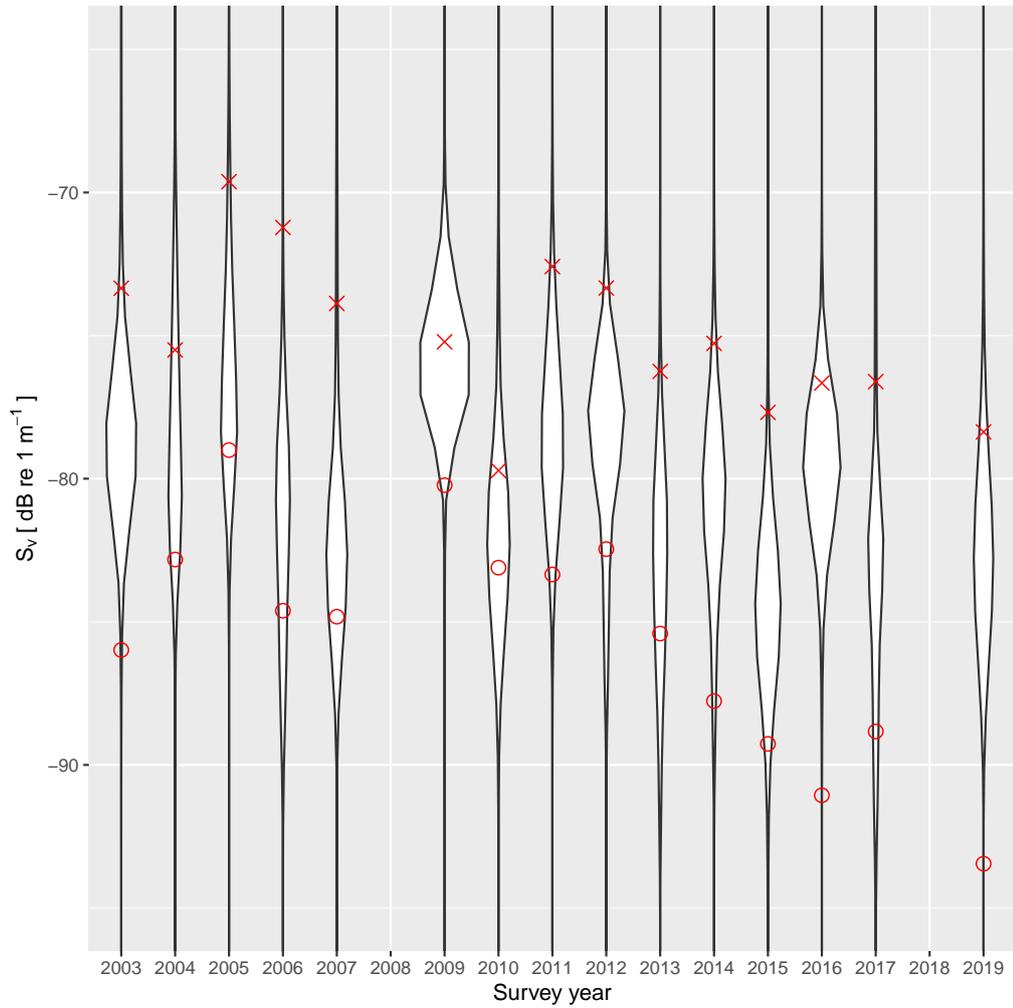
Figure 4.16: Echometrics: density by survey year (o marks the mean value, and × the mean computed in the linear domain).
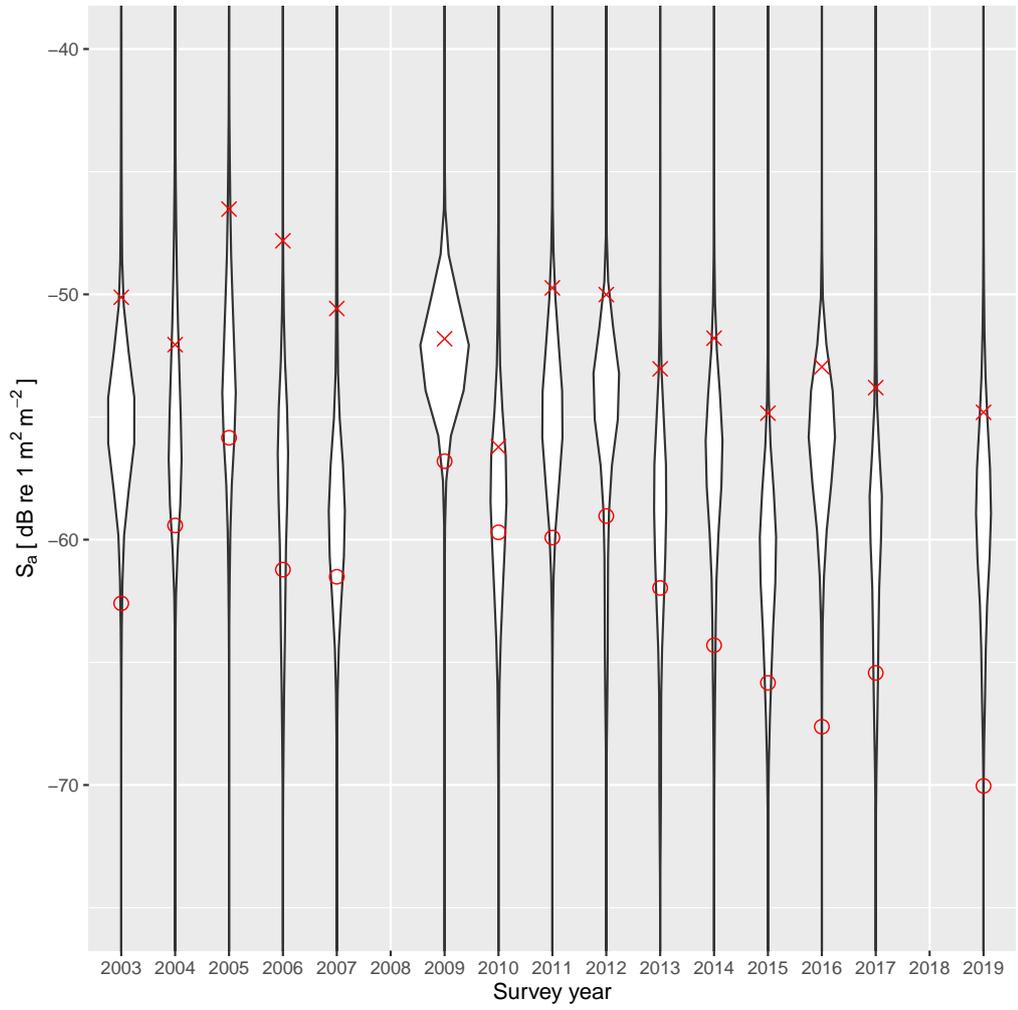
Figure 4.17: Echometrics: abundance by survey year (o marks the mean value, and × the mean computed in the linear domain).
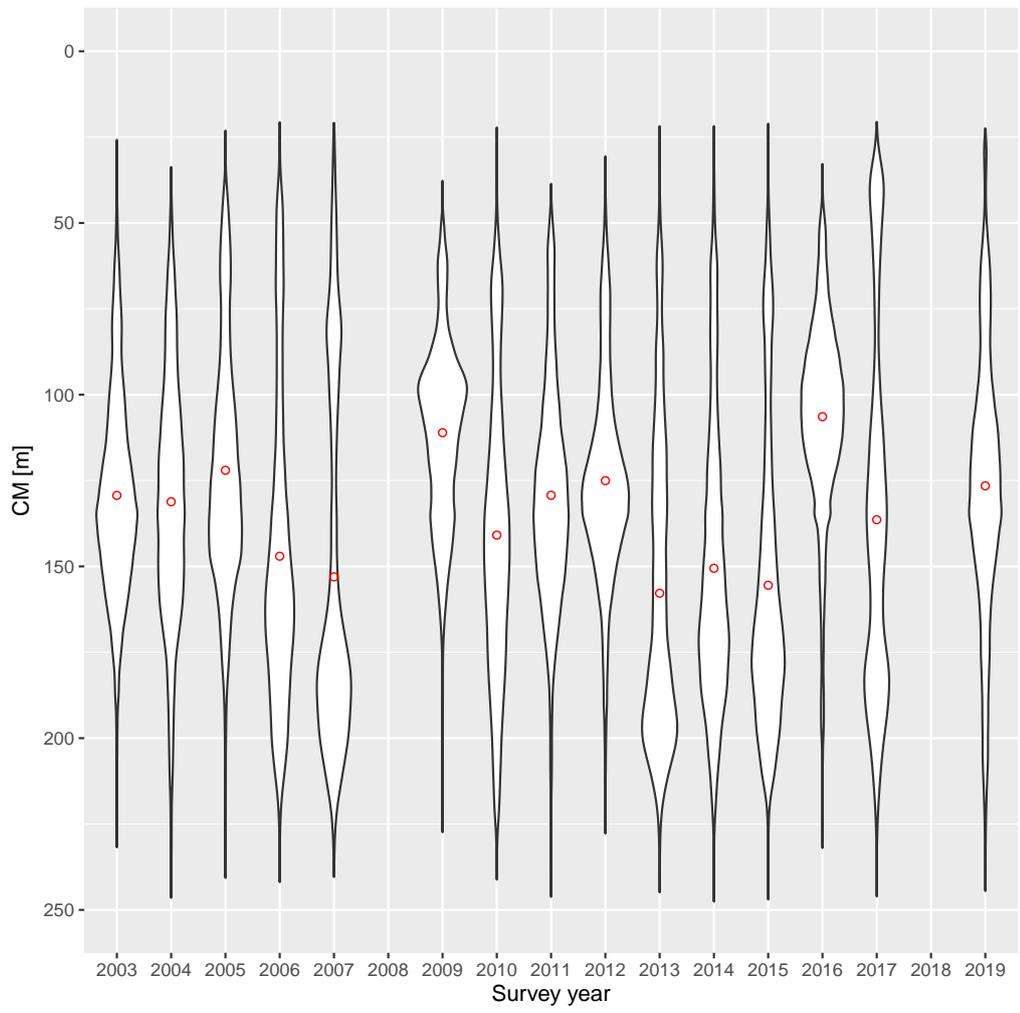
Figure 4.18: Echometrics: location by survey year (o marks the mean).
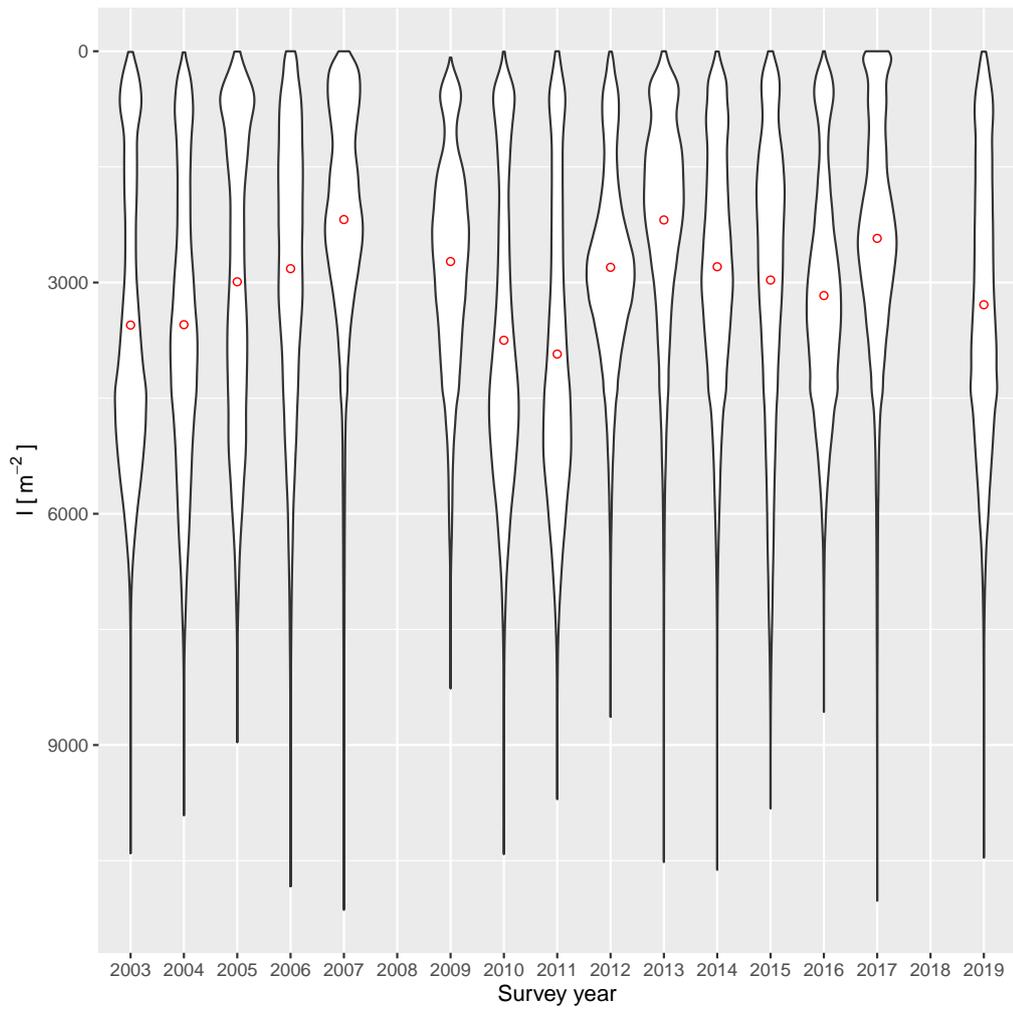
Figure 4.19: Echometrics: dispersion by survey year (o marks the mean).
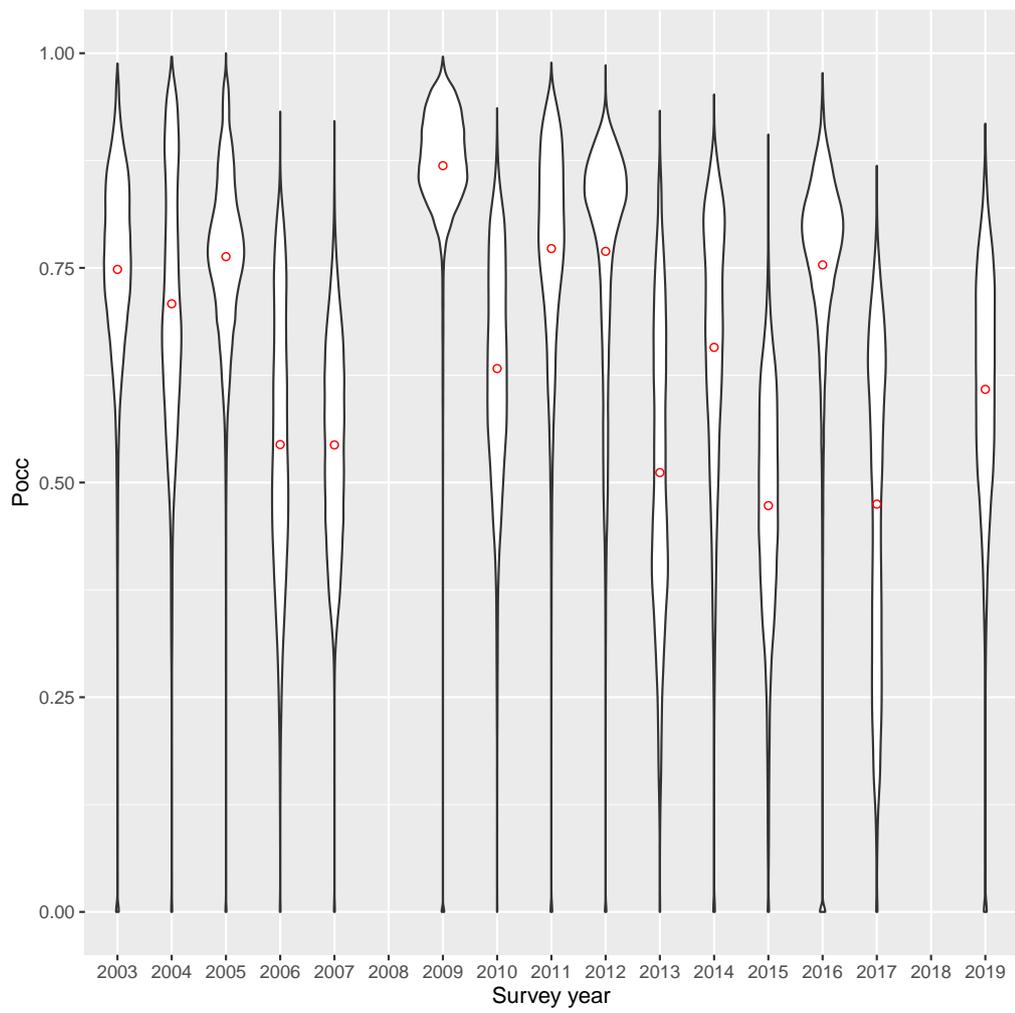
Figure 4.20: Echometrics: occupied by survey year (o marks the mean).
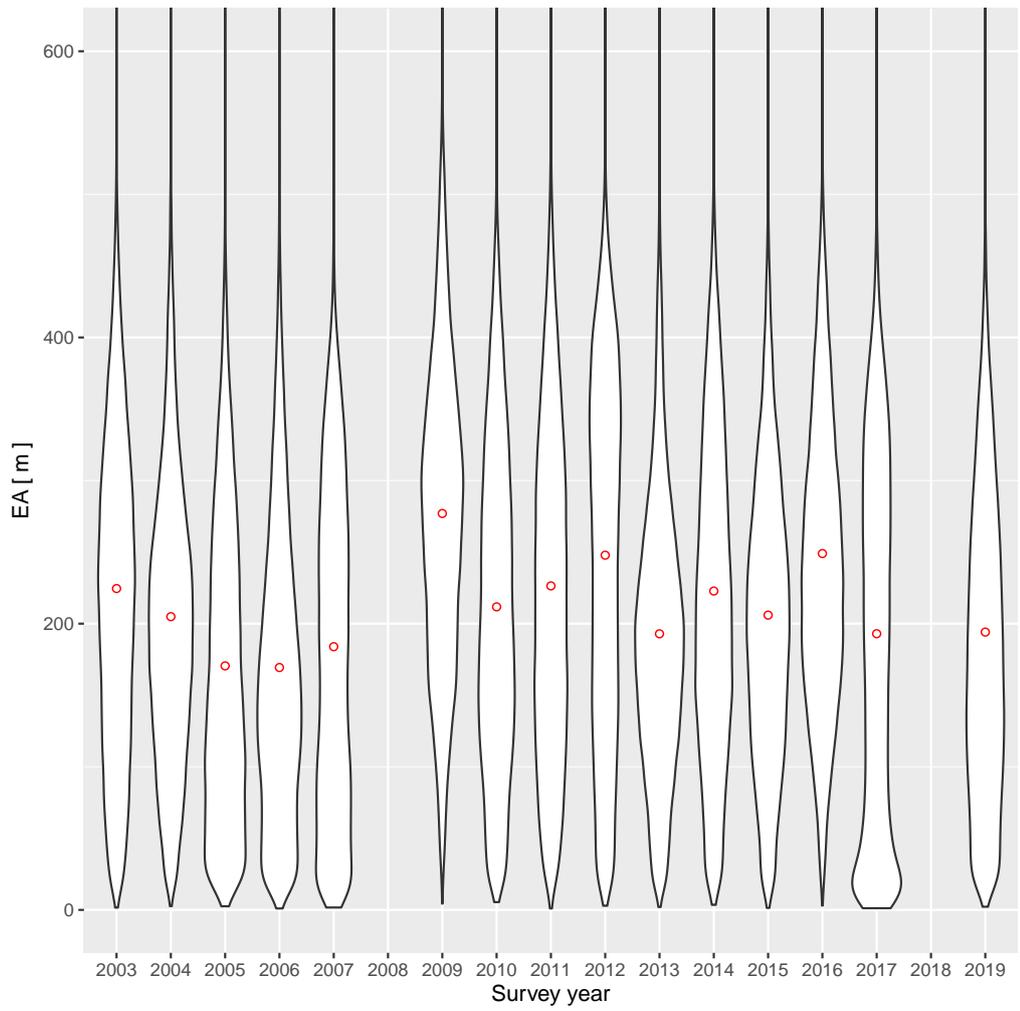
Figure 4.21: Echometrics: evenness by survey year (o marks the mean).
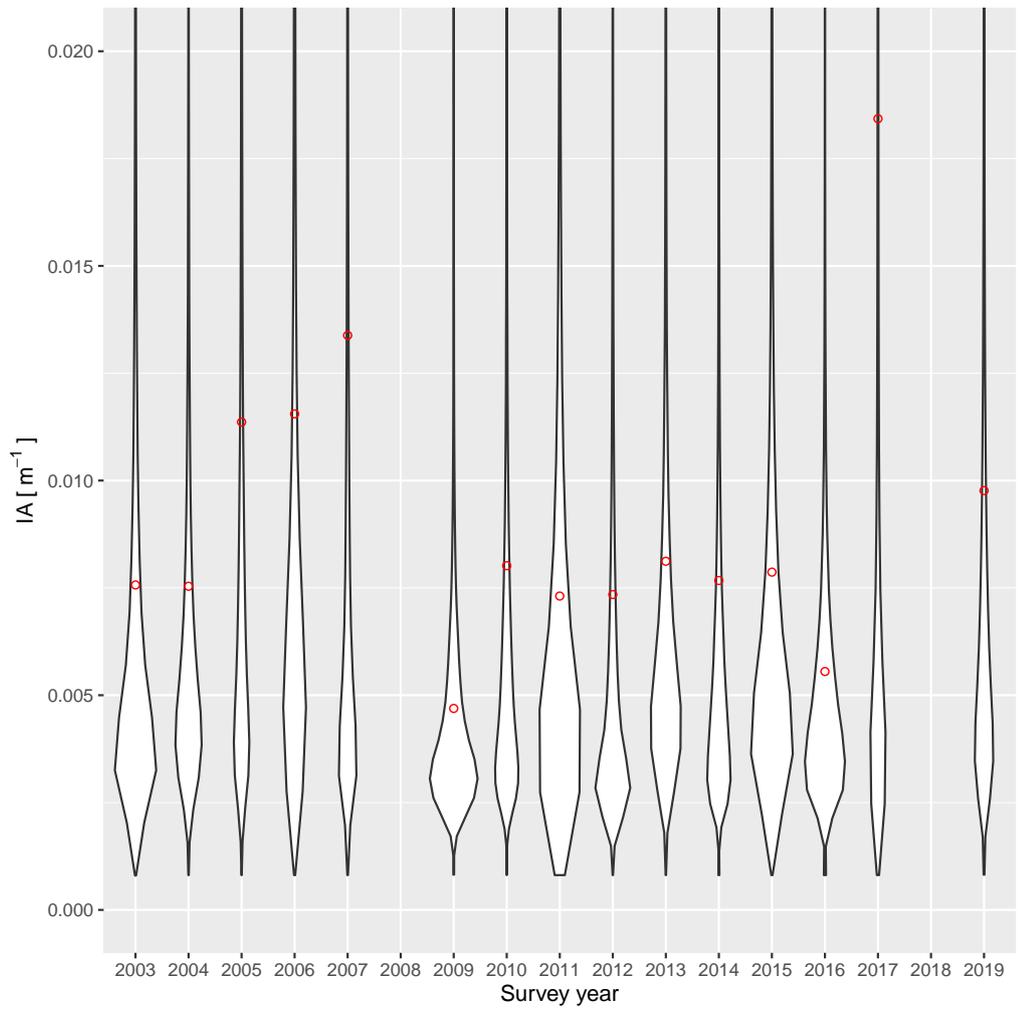
Figure 4.22: Echometrics: aggregation by survey year (o marks the mean).

4.4 Discussion

4.4.1 Interannual variability

Our results suggest a decrease in *density* and *abundance* between 2003 and 2019 (Figure 4.2), however this could be an alias of survey timing (discussed further in Section 4.4.5). *Density* and *abundance* are measures of acoustic backscatter from the water column which is a proxy for biology. Antarctic krill is considered to be the dominant zooplankton species in the Southern Ocean, South Georgia pelagic ecosystem (Murphy *et al.*, 2016). Atkinson *et al.* (2004) reported a decline in krill stocks since the 1970s, and our results may provide evidence of a continuing trend. Some models predict further decline in Antarctic krill in the North Scotia Sea this century due to climate change (Klein *et al.*, 2018).

The WCB time series is still too short to accurately discern other patterns of interannual variability (Figure 4.1). We might reasonably expect oscillation in the data, driven by multi-year climatic effects such as SAM or ENSO. *Dispersion* and *location* may indicate a multi-year cycle, but there is insufficient data to confidently resolve any such patterns.

4.4.2 Comparison with krill metrics

Density and *abundance* are strongly correlated with krill density (Figure 4.5), but are much easier to compute. Krill density requires net haul data to be combined with acoustic data, and takes a considerable amount of effort to collect. Computation of *density* and *abundance*, like the computation of krill density (Madureira, Everson and Murphy, 1993; Fielding *et al.*, 2014), still requires that acoustic data be preprocessed to improve the signal to noise ratio (this is further discussed in Section 4.6.2). There are years where the correlation is weaker (e.g. 2004 and 2009), but even so, these results suggest that *density* and *abundance* could be used as reasonable and parsimonious approximations of krill density.

4.4.3 Comparison with local, environmental variables

When chlorophyll is high, backscatter is closer to the surface (lower *location*), less aggregated, more even and occupies more of the water column (Figure 4.8). Chlorophyll is often used as a proxy for phytoplankton which grow near the surface using light for photosynthesis. More phytoplankton means higher food availability for zooplankton (Folt and Burns, 1999) and this could explain increased backscatter towards the surface.

Relating krill density to environmental correlates remains a key goal (Whitehouse *et al.*, 2008; Santora *et al.*, 2012; Silk *et al.*, 2016; Davis *et al.*, 2017), as we seek to understand the effect of climate change on krill distribution (Flores *et al.*, 2012). A positive relationship between chlorophyll-a concentration and krill density has been reported previously (Whitehouse *et al.*, 2008; Silk *et al.*, 2016). We also found a weak positive relationship of krill with SST, however we must remember that krill are a stenothermic organism (Wiedenmann, Cresswell and Mangel, 2008) and South Georgia is at the northern limit of its distribution range (Hill, Phillips and Atkinson, 2013).

Location, *dispersion*, *occupied*, *evenness* and *aggregation* all measure aspects of the vertical backscatter distribution. The correlation between *location* and chlorophyll reinforces the observation that krill distribution is influenced by chlorophyll, with "krill" moving closer to the surface when greater productivity is observed. We also observed a weak association between mixed layer depth and dispersion, which would indicate that a shallowing of the mixed layer resulted in acoustic backscatter being located higher in the water column. These features may be related. The phytoplankton bloom at South Georgia is fuelled by iron replete conditions, shallower mixed layers and slightly elevated temperatures (Korb *et al.*, 2008).

This study highlights that Echometrics can be used to provide both measures of abundance and distribution that are correlated with environmental parameters. Whilst biomass is a key driver in determining the management of the Antarctic krill fishery in terms of quantity, the ability to predict "hotspots" in the distribution of organisms is pertinent to predator prey

interactions (Murphy *et al.*, 2007; Davis *et al.*, 2017)

4.4.4 Comparison with larger scale, climatic variables

We found no significant correlation between Echometrics and SAM or ENSO. Although correlation between krill density and August Sea Surface temperature is weaker than in the earlier study by Fielding *et al.* (2014), this could be caused by 2017 which had exceptionally low SST, and the relation may still hold (Figure 4.10). Finding climatically driven trends in biological data is complex and requires long time series. Analyses of primary productivity data suggests that a time series of more than forty years is required for trend detection and resolution of anthropogenic influence in the Southern Ocean (Henson, Beaulieu and Lampitt, 2016). This would indicate that another twenty years of data are required in the Western Core Box.

Acoustic backscatter is deeper (has a higher *location*) following high sea ice extent in the preceding austral winter (Figure 4.11). Reduced ocean mixing and increased stratification are associated with higher sea ice extent (Kjellsson *et al.*, 2015), however we found only weak correlation between *location* and mixed layer depth ($r = 0.1$). The krill life cycle is known to depend on sea ice, with under-ice algae being an important winter food source, and some analyses suggesting a decline in krill biomass linked to sea ice reduction (Atkinson *et al.*, 2019). However, we found no direct correlation between *density* and *abundance* compared to sea ice extent. It is hard to understand exactly why the winter sea ice extent would have a summer effect on *location* in the South Georgia region, where no sea ice itself exists and this relationship may be a type I error.

4.4.5 Impact of survey parameters

The survey timing may have caused sampling bias and may account for the apparent decrease in *density* and *abundance* seen since 2003. The Western Core Box is known to exhibit considerable intra-annual variability, with low krill biomass in early season and high krill biomass in mid-season having

been observed using mooring data and ship based surveys (Saunders *et al.*, 2007; Reid *et al.*, 2010). There has been logistics pressure to conduct Western Core Box surveys earlier in the season, and this trend is confirmed in Figure 4.13. The relationship between *density* and *abundance* and sea surface temperature may also be an alias of survey timing, with sea surface temperature typically cooler in early season and warmer in later season.

The influence of survey timing on biomass estimates has been reported previously, for example by Greenstreet *et al.* (2006). In their case they were able to adjust their sand eel survey estimate by applying a correction based on timing of the survey with respect to the spring bloom. In our case, we know that the population of krill at South Georgia is not linked to the spring bloom or local production, but results from recruitment from the Peninsula (Murphy *et al.*, 2007, 2012). This makes it difficult to determine a correction. Greater knowledge of the intra-annual variability of krill at South Georgia from moorings or autonomous vehicle would provide greater confidence in these large-scale estimates.

4.4.6 Echometrics

Fisheries acoustic surveys often focus on deriving biomass estimates of a single species (e.g. krill). However, the change in an ecosystem could be reflected not just in biomass, but in the distribution and behaviour of all animals. Our principal component analysis suggests that more variability is explained by dimensions that are orthogonal to *density* and *abundance* (Figure 4.4). *Location* and *aggregation* are more closely aligned with the first principal component and may therefore be better descriptors of ecosystem variability.

The Global Ocean Observing System (GOOS) provides a framework for measuring a wide range of variables but acoustic measurements are not yet included in a coordinated way (Lindstrom *et al.*, 2012). If acoustic data processing methods could be standardised, then Echometrics could enable a systematised methodology for examining and comparing acoustic data.

Density and *abundance* are highly correlated ($r = 0.995$) and provide similar results across all comparisons in this study. For brevity, future studies may choose to report either one of these Echometrics but not both. *Evenness* is the reciprocal of *aggregation*, and this redundancy could also be removed.

The *location* Echometric may be invariant to instrument type and provide a way to compare different acoustic data sets, since *Location* is not dependent on an absolute measure or threshold of backscattering strength, and should be resilient to calibration drift and differences between instruments. *Density* and *abundance* are highly dependent on instrument calibration, and differences between instruments can make it hard to compare survey results (De Robertis *et al.*, 2019). The *dispersion* measure decreases as dispersion increases and this can be confusing. We suggest inverting the *dispersion* measure or renaming *dispersion* to *convocation* in future studies.

The Western Core Box survey was designed primarily to study Antarctic krill, which are typically located in the top $250\,\mathrm{m}$ of the water column (Quetin and Ross, 1991). We used $120\,\mathrm{kHz}$ which is the most suitable frequency for their detection (Madureira, Everson and Murphy, 1993). However, $38\,\mathrm{kHz}$ data are also collected, have a range in excess of $500\,\mathrm{m}$, and may provide ecosystem information on larger organisms. Echometrics were designed to summarise fisheries acoustic backscatter data without regard to taxa (Urmy, Horne and Barbee, 2012). Here, we show that *density* and *abundance* correlate with estimates of krill density, suggesting that krill dominate the acoustic backscatter in this study area. Since single frequency ($120\,\mathrm{kHz}$) *density* and *abundance* are more straightforward to compute than multi-frequency detection (e.g. Madureira, Everson and Murphy, 1993; Conti and Demer, 2006), they may be more suitable for onboard processing on marine autonomous vehicles.

4.5 Conclusions

The Southern Ocean has experienced collapses of marine species following exploitation, including seals in the 19th century and whales in the middle of

the 20th century (Constable *et al.*, 2014). The ecosystem now faces pressure due to climate change. Ecosystems management is complex, with challenges including: defining long term, ecosystem related objectives; determining meaningful reference values and indicators for desirable or undesirable states of the ecosystem; and developing appropriate data collection, analytical tools and models (Cury *et al.*, 2005). Nature may not be predictable, but it is not totally unpredictable either. We have shown that Echometrics may be descriptive indicators of future ecosystem change at South Georgia.

We used Echometrics to show variability in an Antarctic marine ecosystem. That variability correlated well with traditional krill biomass surveys and showed some correlation with local, environmental variables (e.g. chlorophyll). We suggest that Echometrics could be suitable essential ocean variables (Constable *et al.*, 2016) and could be used as a proxy for measuring the pelagic realm as part of the Global Ocean Observing System.

4.6   Supplementary material

4.6.1   Echometric data

Table 4.7 shows Echometrics computed by survey. Uncertainty is quoted as the standard error of the mean across intra-annual transects (the standard error of the mean in the linear domain was used for decibel values).

Table 4.7: The Western Core Box 120 kHz Echometrics time series.

Year	n	Abundance	Density	Location	Dispersion	Occupied	Evenness	Aggregation
2003	149076	-50.12 ±0.08	-73.35 ±0.08	129.31 ±0.07	3552.14 ±4.75	0.748 ±0.0003	224.56 ±0.35	0.008 ±0.0000
2004	124176	-52.05 ±0.04	-75.50 ±0.04	131.17 ±0.10	3546.70 ±5.19	0.708 ±0.0004	204.92 ±0.34	0.008 ±0.0000
2005	74370	-46.51 ±0.12	-69.60 ±0.12	121.97 ±0.13	2982.12 ±7.02	0.763 ±0.0004	170.15 ±0.42	0.011 ±0.0001
2006	127692	-47.82 ±0.35	-71.22 ±0.42	147.03 ±0.12	2820.14 ±4.94	0.544 ±0.0004	169.37 ±0.32	0.012 ±0.0000
2007	89142	-50.58 ±0.15	-73.88 ±0.14	153.03 ±0.17	2183.10 ±5.07	0.544 ±0.0004	183.93 ±0.42	0.013 ±0.0001
2009	128428	-51.81 ±0.01	-75.22 ±0.01	111.05 ±0.07	2727.78 ±3.75	0.869 ±0.0002	277.01 ±0.34	0.005 ±0.0000
2010	116818	-56.22 ±0.07	-79.71 ±0.06	140.88 ±0.12	3749.17 ±5.52	0.633 ±0.0004	211.76 ±0.33	0.008 ±0.0000
2011	127624	-49.74 ±0.16	-72.59 ±0.14	129.28 ±0.09	3927.92 ±5.34	0.773 ±0.0004	226.40 ±0.38	0.007 ±0.0000
2012	182800	-50.01 ±0.13	-73.34 ±0.15	125.02 ±0.07	2802.96 ±2.92	0.769 ±0.0003	247.86 ±0.32	0.007 ±0.0000
2013	131090	-53.04 ±0.18	-76.25 ±0.18	157.79 ±0.12	2188.49 ±3.73	0.512 ±0.0005	192.94 ±0.28	0.008 ±0.0000
2014	125254	-51.79 ±0.13	-75.27 ±0.15	150.54 ±0.11	2794.85 ±4.30	0.657 ±0.0004	222.81 ±0.39	0.008 ±0.0000
2015	130786	-54.84 ±0.16	-77.68 ±0.17	155.48 ±0.12	2967.97 ±5.05	0.473 ±0.0004	205.98 ±0.31	0.008 ±0.0000
2016	125982	-52.95 ±0.78	-76.66 ±0.72	106.38 ±0.08	3168.91 ±4.14	0.754 ±0.0004	249.01 ±0.40	0.006 ±0.0000
2017	139930	-53.80 ±0.07	-76.61 ±0.06	136.39 ±0.14	2427.19 ±4.03	0.475 ±0.0005	192.99 ±0.39	0.018 ±0.0001
2019	136160	-54.81 ±0.08	-78.36 ±0.07	126.53 ±0.10	3288.09 ±4.70	0.609 ±0.0004	194.13 ±0.39	0.010 ±0.0000

4.6.2   Noise and unwanted signal

To assess the impact of noise removal algorithms, acoustic processing steps were repeated with each noise removal step disabled in turn (a so-called One-Factor-At-a-Time (OAT) analysis, Razavi and Gupta, 2015). The fraction of data removed from the top 250 m depth as a result of each strategy was recorded per transect, as was the impact on mean S_v for that transect.

Removal of noise and unwanted signal is an essential preprocessing step, without which the signal to noise ratio would be unacceptably low and *density* and *abundance* would be unusable. Surface noise, seabed, aliased seabed and impulse noise removal have a large effect on S_v ($\Delta\mu S_{v38} > 40$ dB, Table 4.8). Transient noise, background noise and attenuated signal have a comparatively small effect ($\Delta\mu S_v < 1$ dB).

Noise and unwanted signal account for 27% of 38 kHz and 20% of 120 kHz data. Removal of this noise and unwanted signal reduces data size with

Table 4.8: Fraction of 38 kHz and 120 kHz data removed from the top 250 m of the water column by noise removal process. $\Delta\mu S_{v38}$ and $\Delta\mu S_{v120}$ are the corresponding change in mean volume backscattering strength.

Noise	38 kHz	120 kHz	$\Delta\mu S_{v38}$	$\Delta\mu S_{v120}$
Attenuated signal	0.046 ±0.004	0.006 ±0.001	0.02 ±0.01	0.01 ±0.00
Aliased seabed	0.021 ±0.002		45.25 ±0.75	
Background noise			0.01 ±0.00	0.40 ±0.15
Impulse noise	0.018 ±0.001	0.008 ±0.001	40.30 ±10.33	32.06 ±11.53
Seabed	0.098 ±0.003	0.099 ±0.003	45.25 ±0.75	35.54 ±0.58
Surface noise	0.080 ±0.000	0.080 ±0.000	69.19 ±0.70	76.91 ±0.68
Transient noise	0.005 ±0.002	0.003 ±0.001	0.11 ±0.06	0.03 ±0.01

a compression ratio of 1.37. Approximately 10% of 38 kHz samples are reflections from the seabed (Table 4.8). Failure to remove seabed causes substantial bias in backscatter estimates (S_v) ($\Delta\mu S_{v38} = 45$ dB , $\Delta\mu S_{v120} = 36$ dB), but seabed removal features are common in fisheries acoustic software (e.g. Echoview). Aliased seabed is present in 38 kHz data ($\approx 2\%$, $\Delta\mu S_{v38} = 45$ dB). Whilst aliased seabed reflections can be avoided in some surveys (e.g. using the methods of Renfree and Demer, 2016), unsupervised removal remains a key unresolved problem for automated acoustic data processing, which is therefore the problem we study next.

Chapter 5

Detecting aliased seabed echoes in fisheries acoustic data

"An algorithm must be seen to be believed."

Donald Knuth, Vol. I, Fundamental Algorithms (1968)

Acoustic data must be preprocessed to improve the signal to noise ratio before indices such as Echometrics can be computed (Section 4.6.2). Unsupervised algorithms exist for many forms of noise and corruption (e.g. impulse noise, background noise and seabed detection), but aliased seabed detection and removal is currently undertaken manually, a laborious task and a critical block to autonomous operation on MAVs. In this chapter we develop algorithms for aliased seabed detection.

Some of this material has previously been published as a preprint (R. Blackwell *et al.*, 2019).

5.1 Introduction

Echosounders are routinely used in fisheries acoustics to survey marine ecosystems (Simmonds and MacLennan, 2005). Sound pulses ("pings' ') are transmitted towards a target and the intensity (Volume backscatter, S_v) is measured, integrated and recorded. Signals in acoustic data come from a combination of biotic targets (e.g. fish), abiotic targets (e.g. seabed, gas fluxes) and noise. Therefore, reflections from biological targets may be obscured by various types of acoustic noise, corruption or attenuation. Figure 5.1a shows an example echogram where the horizontal stripe of high S_v is caused by reflections from zooplankton. The curve of high S_v below is not the seabed, but an alias caused by seabed reverberations from preceding pings coinciding with the current ping reception.

Failure to detect and remove unwanted signal prior to biological target detection could result in poor estimates of animal abundance or biomass (MacLennan *et al.*, 2004). Algorithms exist for the detection of many of these corruptions: impulsive noise spikes (Anderson, Brierley and Armstrong, 2005); attenuated signal (Ryan *et al.*, 2015); transient noise (persisting for multiple pings) (Ryan *et al.*, 2015); and background noise (relatively constant for extended periods) (De Robertis and Higginbottom, 2007). However, aliased seabed is typically either avoided or removed manually, a notoriously laborious task. Aliased seabed and biology can have a similar appearance in echograms (e.g. Figure 5.1a), and when they cross it can be difficult to precisely determine the boundary. Aliased seabed detection is therefore subjective and a much harder problem than true seabed detection.

Although aliased seabed can occur at any frequency, it is common in lower frequency data (e.g. 18 kHz, 38 kHz) when using a fixed, short transmit pulse interval (I_T) and crossing the continental shelf. Acoustic signals are attenuated by absorption with range (R) as a function of frequency, temperature and seawater chemical composition (Moll, Ainslie and Vossen, 2009), limiting echosounder range (R_{max}). Typical maximum seabed detection depths by frequency are shown in Table 5.2. If the ping interval I_T is short
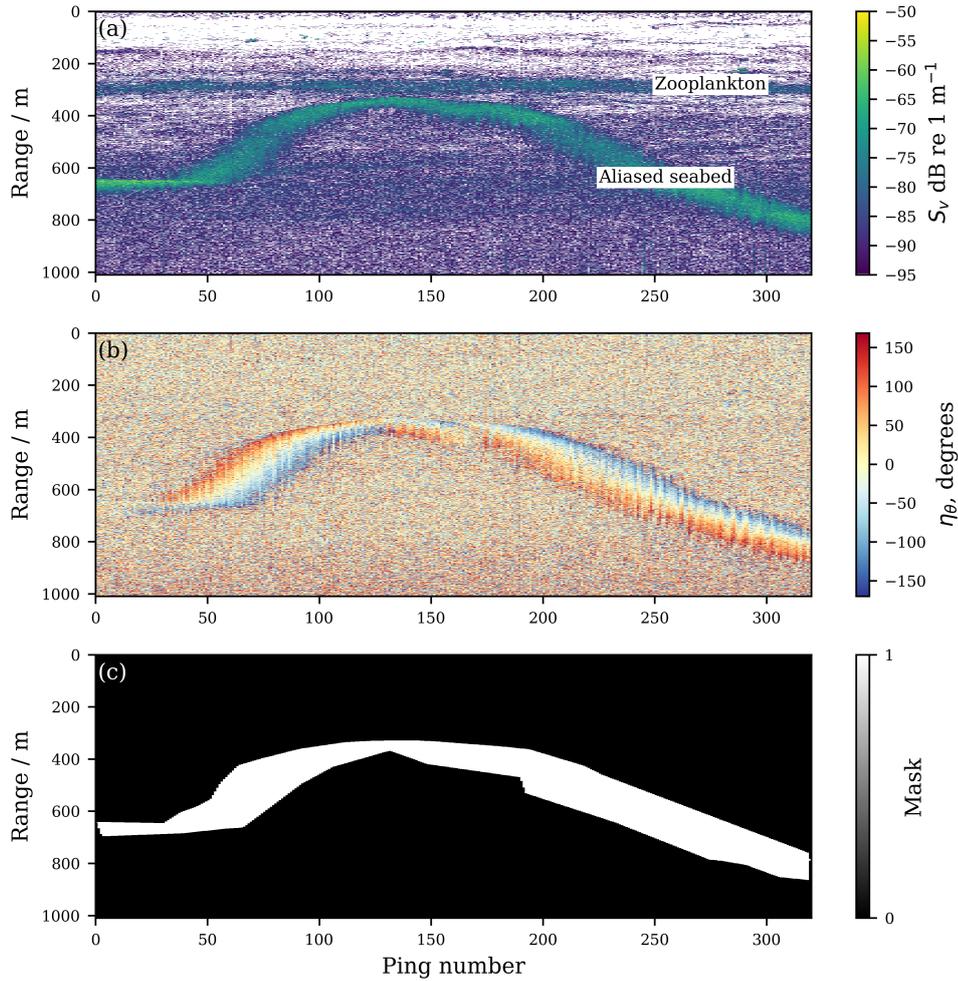
Figure 5.1: Aliased seabed echoes seen in a section of $38\,\mathrm{kHz}$ acoustic data with (a) volume backscatter (S_v), (b) along-ship split beam angle (η_θ) and (c) a typical, hand-drawn aliased seabed removal mask. The horizontal axis shows pings with interval (I_T) of $2\,\mathrm{s}$, nominal speed $10\,\mathrm{kts}$ and an extent of about $3.3\,\mathrm{km}$. Data recorded using a Simrad EK60 scientific echosounder onboard RRS James Clark Ross, cruise JR280.

with respect to the time taken for a reflection to occur from a seabed beyond the logging range R_L, as described in (5.1), then aliasing can occur with reflections from preceding pings coinciding with echoes from the current ping. However, practical use of (5.1) for prediction requires detailed bathymetry data that are rarely available with sufficient spatial accuracy

Table 5.1: Terms, symbols and units.

Term	Symbol	Unit	Description
Range	R	m	Distance from transducer.
Maximum seabed detection range	R_{max}	m	Maximum seabed detection range as a consequence of absorption and loss.
Data logging range	R_L	m	Range to which data are logged.
Seabed range	R_S	m	Distance from the transducer to the seabed.
Aliased seabed range	$R_{\mathcal{A}}$	m	Range to aliased seabed.
Transmit pulse interval	I_T	s	Time between consecutive pulse transmissions.
Sound speed	c	ms^{-1}	Speed of sound in seawater (approximately $1500ms^{-1}$
Modulo function	mod		$mod(a,m)$ returns the remainder after division of a by m , where a is the dividend and m is the divisor.
Volume backscattering strength	S_v	dB re 1 m^{-1}	
Along-ship split-beam angle	η_θ	Signed octet	-128 to 127, corresponding to -180 to 180 degrees between fore and aft transducer segments.
Athwart-ship split-beam angle	η_ϕ	Signed octet	-128 to 127, corresponding to -180 to 180 degrees between port and starboard transducer segments.
Feature matrix	X		Feature matrix used as input to machine learning algorithms.
Labels	L		Matrix of class labels (e.g. aliased seabed, biology, other) for echogram elements.
Bayes error	ϵ		The Bayes error (the minimum error possible).
S_v threshold	T	dB re $1m^{-1}$	Threshold used when selecting volume backscatter data.
η_θ threshold	T_θ		Threshold used when selecting squared along-ship split-beam angle data.
η_ϕ threshold	T_ϕ		Threshold used when selecting squared athwart-ship split-beam angle data.
Aliased seabed pixels	$\mathcal{A}$		The set of aliased seabed pixels.
Biology pixels	$\mathcal{B}$		The set of biology candidate pixels.
Other pixels	$\mathcal{O}$		The set of pixels considered to be confidently outside $\mathcal{A}$ and $\mathcal{B}$ having excluded bottom.

and resolution (e.g. Global Bathymetric Chart of the Oceans (Hall, 2006) $\approx$ 1000 m resolution, South Georgia Bathymetry Database (Hogg *et al.*, 2016) $\approx$ 100 m resolution) compared to the scale of the acoustic data (e.g. 10 m). Renfree and Demer (2016) present the strategy for avoiding aliased seabed, by dynamically optimising I_T and the data logging range (R_L). However, changing parameters mid-survey causes changes in spatial resolution complicating subsequent data analyses. In addition, the background noise removal method implemented by De Robertis and Higginbottom (2007) requires a large R_L to determine the noise level, thus constraining the adjustment

Table 5.2: Maximum seabed detection range (R_{max}), using typical transducer settings, according to the Simrad EK60 reference manual.

Frequency (kHz)	R_{max} (m)
18	7000
38	2800
70	1100
120	850
200	550

demanded by Renfree and Demer.

$$R_{\mathcal{A}} = \frac{\mathrm{mod}(2R_S,\ c\ I_T)}{2}, \quad \text{where} \quad R_L < R_S < R_{max} \tag{5.1}$$

We note that "false bottom" and "shadow bottom" are broad, colloquial terms used to describe a variety of different phenomena and we henceforth use the term "aliased seabed" to mean the precise conditions described in (5.1). We are explicitly not concerned with the following effects:

1. dense fish aggregations causing a false detection of the seabed (Foote *et al.*, 1991);

2. secondary echoes caused by reverberation from the current ping. (Note that secondary echoes appear below the true bottom in echograms and are therefore already excluded by bottom detection algorithms);

3. secondary echoes from transducer sidelobes (Clarke, 2006).

Modern echosounders use split-beam transducers, which are divided into four quadrants allowing target direction to be determined by comparing the signal received at each quadrant (Simmonds and MacLennan, 2005). In addition to recording amplitude, they also record the split-beam angle (SBA). The along-ship angle (η_θ) is the phase difference between the fore and aft transducer halves, and the athwart-ship angle (η_ϕ) is determined from the starboard and port halves. Reflection and scattering from a deep

seabed occur over a large area due to beam spreading, causing variance in wave arrival times. A rising seabed is detected at the fore quadrants of the split-beam transducer before the aft quadrants and vice-versa for a falling seabed. These effects, caused by the seabed geometry, are particularly visible in η_θ data and appear to differentiate aliased seabed from biological reflections (Figure 5.1b). MacLennan *et al.* (2004) show that SBA reflections from fish aggregations are not necessarily an accurate indication of target direction whilst reflections from the seabed correlate well to seabed slope. Bourguignon *et al.* (2009) show that seabed detection with a Simrad ME70 using SBA and amplitude together is more effective than using amplitude alone. This would suggest that SBA is an additional discriminatory variable.

An echogram is a matrix, or image, of signal values indexed by depth or range and along-track distance. We denote the volume backscatter as $S_v(j,k)$ where j is the range index and k the along-track distance index. The echogram can also be indexed one-dimensionally as $S_v(i)$ where i varies across all combinations of j and k. $\eta_\theta(i)$ and $\eta_\phi(i)$ are similar and represent SBA. Elements, or pixels, in an echogram can be labelled as belonging to a known class (e.g. aliased seabed). We denote the label for $S_v(i)$, $\eta_\theta(i)$ and $\eta_\phi(i)$ as $L(i)$.

A classifier is a function that predicts labels from features (in our case S_v, η_θ and η_ϕ). Some classifiers are expressed algorithmically, others are the result of machine learning. Given a training dataset with feature vectors X, and corresponding classification labels L, then a learning algorithm is a function f that returns a hypothesis function h. h can be used to predict labels $\widehat{L}$ from arbitrary feature vectors X' as in (5.2). The selection of a suitable, discriminating feature vector is known as feature extraction. The adjustment of the classifier parameters is machine learning.

$$ h = f(X, L), \quad \widehat{L} = h(X'). \tag{5.2} $$

There is a huge literature devoted to machine learning and many different

kinds of machine learning algorithms. A perceptron is a simple model of a biological neuron (Rosenblatt, 1958) that makes classification predictions based on learned linear decision boundaries. It is useful for determining whether a problem is linearly separable. The k-nearest-neighbour (kNN) is one of the simplest non-linear machine learning algorithms. It treats all training data as points in n-dimensional feature space and makes a classification prediction for a new datum p, by assessing the k nearest examples to p (Cover and Hart, 1967). Notwithstanding its simplicity, it has the useful asymptotic property that as $k \to \infty$ the probability of error cannot be more than twice the Bayes probability of error (the minimum error possible). As such, it provides a benchmark with which to compare the performance of other classifiers that may have no known bounds on optimality. Random forests are an ensemble learning method that combine multiple decision trees based on random selections from the data (Breiman, 2001). They often create accurate classifiers that do not over-fit the data. Artificial neural networks, such as the multilayer perceptron (MLP), use layers of neurons between input and output (Rumelhart, Hinton and Williams, 1986). Neurons fire according to an activation function and associated weights. Neural networks are capable of learning non-linear models by iterative adjustment of weights during training, a process known as backpropagation.

Machine learning has been used in fisheries acoustics for species identification, for example Simmonds, Armstrong and Copland (1996), Haralabous and Georgakarakos (1996) Woodd-Walker, Kingston and Gallienne (2001) use neural networks and Fernandes (2009), Fallon, Fielding and Fernandes (2016) use tree-based methods. The general approach has been to identify target schools, extract features based on school morphology and acoustic response, and then apply a classifier. Recent advances now allow machine learning to be applied directly to echogram pixels, removing the need for feature extraction, and potentially increasing accuracy. Deep learning models are composed of multiple processing layers (LeCun, Bengio and Hinton, 2015) and take advantage of modern high-performance computers to train deeper and more complex networks. Deep convolutional neural

networks (CNN), inspired by animal visual systems, have brought about breakthroughs in many fields including image processing. As an example, the MNIST problem[1], which requires classification of handwritten digits, has become a de facto standard test case and benchmark for machine learning classifiers. CNNs currently account for the best performing solutions because of their ability to find structure in high dimensional space without the need for preprocessing or explicit feature extraction.

The evaluation of machine learning algorithms can be highly inaccurate if the same data are used for training and test purposes (Flexer, 1996). Models become over-fitted for a particular dataset in such a way that they cannot generalise for new, unseen data. This can be avoided using cross validation where the data are partitioned into n folds so that n subsets of $n-1$ folds can each be used for training, with one fold for testing. For example, in a ten-fold cross validation, there are ten combinations of nine training and one test partition. By running the learning algorithm separately on these ten combinations, results can be aggregated and quoted in terms of a mean and standard error.

Conventionally, machine learning is associated with automation of difficult problems. However, less discussed aspects are the use of machine learning algorithms as part of exploratory data analysis (Tukey, 1962) and as a benchmark with which to evaluate the performance of conventional algorithms. We are not only interested in presenting an algorithmic solution to the stated problem, we are interested in showing a methodology for designing such algorithms. We assemble a training dataset of aliased seabed examples and counterexamples and use it to train linear perceptron, kNN, Random forest, MLP and CNN machine learning classifiers. We evaluate and compare classifiers and use our results to inform the design of a simpler algorithm that can be applied without prior learning.

---

[1]See http://yann.lecun.com/exdb/mnist/

5.2 Materials and methods

Data were acquired from an annual ship-based survey (the "Western Core Box''') conducted off the North West coast of South Georgia by the British Antarctic Survey (Fielding *et al.*, 2014, Section 1.2). Each survey consisted of eight 80 km transects run in daylight hours, alternately in on and off shelf directions at a nominal speed of 10 knots with a fixed ping rate, $I_T = 2\,\text{s}$ (Figure 1.2). Acoustic data were captured using a Simrad EK60 scientific echosounder (38, 120 and 200 kHz). Power settings varied between years but were consistent within year. Seabed depth (R_S) varied from a few tens of metres to more than 3000 m causing large regions of aliased seabed in echograms. 30 example transects were randomly selected from the 2009 to 2013 surveys.

In this dataset, aliased seabed appears in the 38 kHz data, and although other frequencies are available, this may not always be the case for other surveys and especially where ships of opportunity (e.g. fishing vessels) are employed. We therefore chose to consider only 38 kHz data. Power and angle data were converted to echograms of S_v, η_θ, and η_ϕ using EchoJulia[2]. Echosounder calibration corrections were determined using standard sphere techniques (Demer *et al.*, 2015) and applied during conversion. The first 10 m of range were excluded, to ensure far field operation and avoid transducer ringing effects (Simmonds and MacLennan, 2005). The seabed and below were removed using a maximum S_v bottom pick followed by manual inspection and correction where necessary.

Areas of aliased seabed were identified using human echogram image interpretation of S_v data and corresponding masks were hand-drawn. Otsu's method (Otsu, 1979) was used to refine the boundaries of the hand-drawn regions whereby a greyscale image with a bimodal histogram is converted to a binary image using an optimal threshold. The pixels in the hand-drawn region which were not in the refined region were deliberately excluded from further analysis because of their potentially uncertain classification. We

---

[2]https://echojulia.github.io/

used integers to label the data, with $L(i) = 2$, chosen arbitrarily, to denote aliased seabed. Therefore, the set of aliased seabed pixels is given by $\mathcal{A} = \{i \mid L(i) = 2\}\forall_i$.

Discrimination of aliased seabed pixels ($\mathcal{A}$) from other ($\mathcal{O}$) is a two-class problem, but when aliased seabed overlaps biology, we must also preserve as much uncorrupted biology from the echogram as possible. We therefore considered an additional class, biology candidate ($\mathcal{B}$) so that misclassification could be measured. In our data, Antarctic krill are a key biological target (Fielding *et al.*, 2014), and previous studies have identified aggregations using the SHAPES school detection algorithm (Barange, 1994; Coetzee, 2000) using 120 kHz acoustic data. We employed the same technique using Echoview® to identify $\mathcal{B}$, parameterised after Fielding *et al.* (2012). Within Fielding *et al.* (2012) a 120 kHz - 38 kHz dB window technique was further applied to identify whether a school was likely to be fish or krill. In our case we accepted all aggregations as biological. Areas of $\mathcal{O}$ were determined as being outside both the original hand-drawn aliased seabed regions. We used $L(i) = 1$ to denote biology, and $L(i) = 0$ to denote "other". Thus, $\mathcal{B} = \{i \mid L(i) = 1\}\forall_i$ and $\mathcal{O} = \{i \mid L(i) = 0\}\forall_i$.

Stratified, random sampling was applied to the 30 transects to select 5000 examples of each of the three classes $\mathcal{A}$, $\mathcal{B}$ and $\mathcal{O}$ from each transect giving a total of 450,000 pixel exemplars. The 30 transects were partitioned into ten sets, each with three transects. These ten sets formed the ten folds used for training and testing with cross fold validation. The features available for each pixel were 38 kHz S_v, η_θ, η_ϕ and R. R was discarded as being biased because schools detection (and thus $\mathcal{B}$) was limited to the top 250 m of the water column. All feature data were normalised by removing the mean and scaling to unit variance when used as input to machine learning algorithms. Regions of $\mathcal{A}$ and $\mathcal{B}$ typically span more than one pixel, so we also considered a window around each pixel. An $n \times n$ window w was indexed as $w(\lceil\frac{1-n}{2}\rceil : \lfloor\frac{n}{2}\rfloor, \lceil\frac{1-n}{2}\rceil : \lfloor\frac{n}{2}\rfloor)$, with $w(0,0)$ being the central pixel.

A principal component analysis (PCA) was applied to determine feature

vectors explaining most of the variance in the data (Pearson, 1901). The most important principal components were then used as input to a kNN. The perceptron, kNN, random forest and MLP were implemented using scikit-learn (Pedregosa *et al.*, 2011) with default settings unless otherwise specified. The MLP used two hidden layers of 15 and 7 neurons respectively. These sizes were chosen based on 15 inputs (the 15 principal components) and a desire to constrain the output to three classes. A default configuration using rectified linear unit activation (Nair and Hinton, 2010) and an Adam solver (Kingma and Ba, 2014) was employed. A CNN was implemented using Keras (Chollet and others, 2015) and Tensorflow (Abadi *et al.*, 2016). CNNs offer a wide variety of architecture and configuration options, and so we chose a design which is typical of demonstration solutions to the MNIST problem (Figure 5.2).The front end uses convolutional layers and a max pooling layer for feature extraction. The flatten layer reduces dimensionality and passes features on to the classifier. A fully connected layer ensures that all features are weighted. A softmax activation layer reduces the output to three nodes, each providing a probability for an output class. Dropout layers help to avoid over-fitting. Three channels were used as input (normalised S_v, η_θ and η_ϕ). We used 12 training epochs per fold.

Classifier performance was evaluated using cross-fold validation, comparing outputs $\widehat{\mathcal{A}}$, $\widehat{\mathcal{B}}$ and $\widehat{\mathcal{O}}$ with ground truth $\mathcal{A}$, $\mathcal{B}$ and $\mathcal{O}$. The probability of accurate aliased seabed detection is

$$P(\mathcal{A} \mid \widehat{\mathcal{A}}) = \frac{N([\mathcal{A}_i] = [\widehat{\mathcal{A}_i}])}{N([\widehat{\mathcal{A}_i}])} \forall_i \tag{5.3}$$

The probability of reliable aliased seabed detection is

$$P(\widehat{\mathcal{A}} \mid \mathcal{A}) = \frac{N([\mathcal{A}_i] = [\widehat{\mathcal{A}_i}])}{N([\mathcal{A}_i])} \forall_i \tag{5.4}$$

The probability that biology is misclassified as aliased seabed is

```
num_classes = 3

model = models.Sequential()

model.add(layers.Conv2D(32, kernel_size=(3, 3),
            activation="relu",
            input_shape=(28,28,3)))
model.add(layers.Conv2D(64, (3, 3), activation="relu"))
model.add(layers.MaxPooling2D(pool_size=(2, 2)))
model.add(layers.Dropout(0.25))
model.add(layers.Flatten())
model.add(layers.Dense(128, activation="relu"))
model.add(layers.Dropout(0.5))
model.add(layers.Dense(num_classes, activation="softmax"))

model.compile(loss="sparse_categorical_crossentropy",
        optimizer="Adadelta",
        metrics=["accuracy"])
```

Figure 5.2: Keras snippet describing the CNN model architecture and configuration.

$$P(\mathcal{B} \mid \widehat{\mathcal{A}}) = \frac{N([\mathcal{B}_i] = [\widehat{\mathcal{A}_i}])}{N([\widehat{\mathcal{A}_i}])} \forall_i \tag{5.5}$$

5.3 Results

Aliased seabed ($\mathcal{A}$), biology ($\mathcal{B}$) and other ($\mathcal{O}$) cannot be separated by simply thresholding the distributions of S_v, η_θ or η_ϕ because there is too much overlap (Figure 5.3a, b and c). The overlapping coefficients (Inman and Bradley Jr, 1989) for $\mathcal{A}$ and $\mathcal{B}$ are 0.81, 0.86 and 0.86 for S_v, η_θ and η_ϕ respectively. To determine window sizes, a sensitivity analysis of spatial averaging, using the mean of an $n \times n$ window around each pixel and varying n to maximise the chi-squared distance between the distributions of $\mathcal{A}$ and $\mathcal{O}$, gives $n = 9$ for S_v, $n = 28$ for η_θ and $n = 52$ for η_ϕ. There is still considerable overlap ($\mathcal{A}$, $\mathcal{B}$ is 0.68, 0.21 and 0.39 respectively) (Figure 5.3c, d and e). As an aside, we note that there are spikes in the SBA distributions at signed octet values -96, -32, 32 and 96 (Figure 5.3b and 5.3c). These

appear to be an artefact of the Simrad EK60 instrument and we are unable to provide an explanation for them[3].

The mean is one possible statistical summary of an $n \times n$ window (as used above), but given a set of $n \times n$ windows, the first principal component explains the most variance in the set. We therefore conduct a PCA across all three variables with window size $n = 28$ (Figure 5.4). There is still considerable overlap when considering the first and second components (Figure 5.4 columns one and two). Principal components beyond about dimensionality 15 show only minimal explained variance (Figure 5.4 column 3). Cumulative explained variance shows only a slow convergence to 100 percent (Figure 5.4 column 4). The principal components do not allow linear separability.
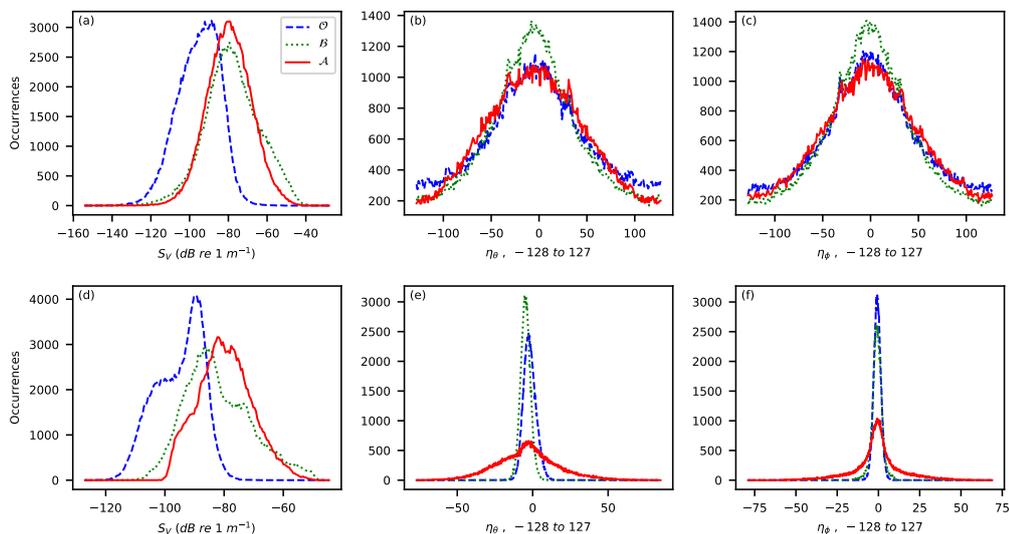
Figure 5.3: Histograms of S_v, η_θ and η_ϕ for pixels in three classes: aliased seabed ($\mathcal{A}$), biology candidate ($\mathcal{B}$), and other ($\mathcal{O}$), using all 450,000 pixel exemplars. The first row considers individual pixels. The second row uses the mean over a surrounding $n \times n$ window. Window sizes are $n = 9$ for S_v, $n = 28$ for η_θ and $n = 52$ for η_ϕ.

Having shown that simple statistics are insufficient to separate the classes,

---

[3]We have seen these spikes in all Simrad EK60 data that we have examined, including those from three separate research vessels. Simrad have acknowledged this as a instrument defect. Supplementary information is provided in Appendix F
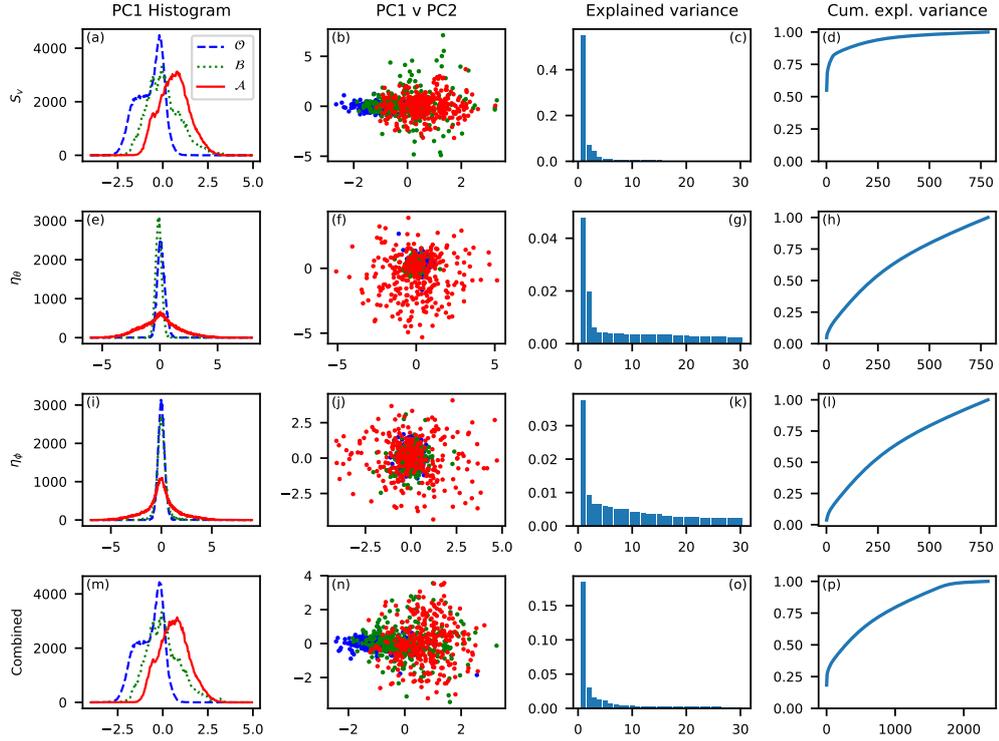
Figure 5.4: Principal component analysis of 450,000 samples using 28×28 windows over 38 kHz data. Column one plots the histograms of aliased seabed ($\mathcal{A}$), biology candidate ($\mathcal{B}$), and other ($\mathcal{O}$) of the first principal component of S_v, η_θ, η_ϕ and the combined data. Column two compares the first and second principal components. Column three shows the explained variance of the first 30 components. Column four shows the cumulative variance explained by dimension.

we train a kNN using the first 15 principal components of each sample (Table 5.3). The overall accuracy of 0.84 ± 0.003 is calculated by dividing the trace of the confusion matrix by the sum of its elements. The probability that predicted aliased seabed is indeed aliased seabed ($P(\mathcal{A} \mid \widehat{\mathcal{A}}) = 0.98 \pm 0.001$) and the probability that aliased seabed is identified by the algorithm ($P(\widehat{\mathcal{A}} \mid \mathcal{A}) = 0.80 \pm 0.007$) are high; while the probability that biology candidates are misclassified as aliased seabed is low ($P(\mathcal{B} \mid \widehat{\mathcal{A}}) = 0.01 \pm 0.001$). We use the same evaluation procedure for all classifiers and compare performance using these four measures (Table 5.4). We run kNN using S_v

Table 5.3: Matrices showing results of the kNN classifier with $k = 35$ (determined by searching $0 < k < 100$ for odd k), for the three classes aliased seabed ($\mathcal{A}$), biology candidate ($\mathcal{B}$) and other ($\mathcal{O}$). The first table is a confusion matrix, the second an accuracy matrix showing $P(y \mid \hat{y})$ and the third a reliability matrix showing $P(\hat{y} \mid y)$.

		Predicted		
		$\mathcal{O}$	$\mathcal{B}$	$\mathcal{A}$
Actual	$\mathcal{O}$	13972.57 ± 24.987	967.24 ± 22.904	60.19 ± 2.409
	$\mathcal{B}$	2996.42 ± 145.906	11839.04 ± 137.546	164.53 ± 15.816
	$\mathcal{A}$	1996.71 ± 109.020	976.81 ± 31.094	12026.48 ± 110.610

		Predicted		
		$\mathcal{O}$	$\mathcal{B}$	$\mathcal{A}$
Actual	$\mathcal{O}$	0.74 ± 0.007	0.07 ± 0.001	0.00 ± 0.000
	$\mathcal{B}$	0.15 ± 0.006	0.86 ± 0.002	0.01 ± 0.001
	$\mathcal{A}$	0.10 ± 0.005	0.07 ± 0.002	0.98 ± 0.001

		Predicted		
		$\mathcal{O}$	$\mathcal{B}$	$\mathcal{A}$
Actual	$\mathcal{O}$	0.93 ± 0.002	0.06 ± 0.002	0.00 ± 0.000
	$\mathcal{B}$	0.20 ± 0.010	0.79 ± 0.009	0.01 ± 0.001
	$\mathcal{A}$	0.13 ± 0.007	0.07 ± 0.002	0.80 ± 0.007

without SBA and kNN using η_θ without S_v and find that neither result is as good as for the combined data.

As a final check for linear separability, we run a linear perceptron, which does not have good performance ($P(\mathcal{A} \mid \widehat{\mathcal{A}}) = 0.61 \pm 0.014$, $P(\widehat{\mathcal{A}} \mid \mathcal{A}) = 0.62 \pm 0.053$ and $P(\mathcal{B} \mid \widehat{\mathcal{A}}) = 0.23 \pm 0.018$). Our principal conclusion at this point is that even though the classes are not easily linearly separable, all hope is not lost - a simple non-linear classifier gives promising results.

Although the kNN has attractive asymptotic properties, those are only manifest with large quantities of data. However, since $k = 35$ gives the highest kNN accuracy for $0 < k < 100$, and the trend appears to be reducing accuracy with increasing k (Figure 5.5).

We can make a crude estimate of the Bayes error of $0.08 \leq \epsilon \leq 0.16$ and hence expect the best possible overall accuracy to be between 0.84 and 0.92. The computation of N-dimensional distances and subsequent

Table 5.4: Summary of classifier performance comparing aliased seabed detection accuracy (5.3), reliability (5.4) and misclassification of biology (5.5). The mean and standard error of probabilities are computed over ten folds (450,000 pixels).

Method	Accuracy $P(\mathcal{A} \mid \widehat{\mathcal{A}})$	Reliability $P(\widehat{\mathcal{A}} \mid \mathcal{A})$	Misclassification $P(\mathcal{B} \mid \widehat{\mathcal{A}})$	Overall accuracy
Linear perceptron	0.61 ± 0.014	0.62 ± 0.053	0.23 ± 0.018	0.62 ± 0.009
kNN S_v	0.77 ± 0.027	0.74 ± 0.050	0.19 ± 0.027	0.75 ± 0.016
kNN η_θ	0.99 ± 0.002	0.58 ± 0.026	0.01 ± 0.002	0.60 ± 0.008
kNN S_v, η_θ and η_ϕ	0.98 ± 0.001	0.80 ± 0.007	0.01 ± 0.001	0.84 ± 0.003
Random forest	0.93 ± 0.010	0.86 ± 0.019	0.04 ± 0.007	0.85 ± 0.007
MLP	0.95 ± 0.007	0.87 ± 0.020	0.03 ± 0.005	0.87 ± 0.006
CNN	0.96 ± 0.019	0.89 ± 0.022	0.02 ± 0.010	0.90 ± 0.007
Algorithm	0.96 ± 0.010	0.77 ± 0.021	0.02 ± 0.009	
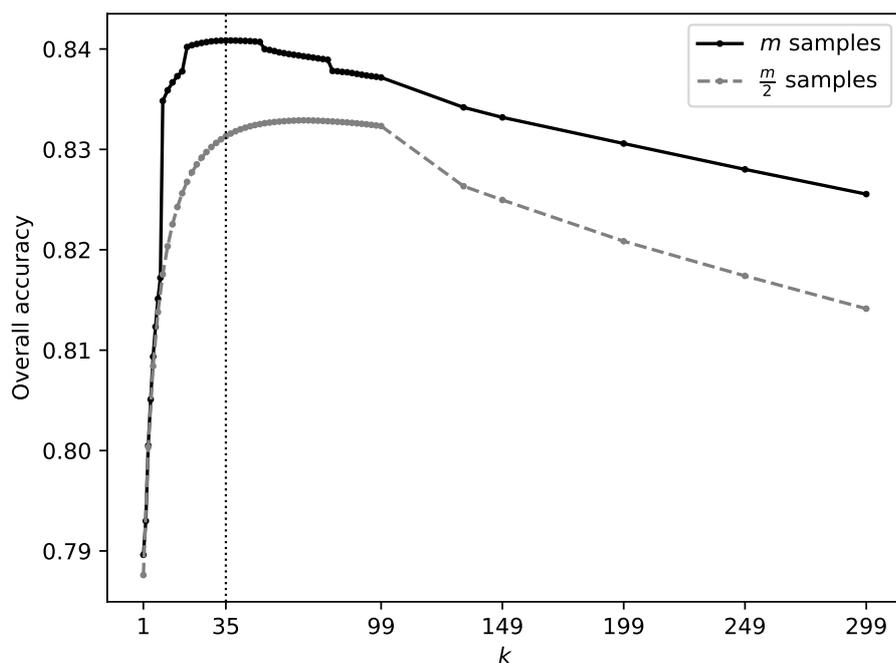
Figure 5.5: Overall accuracy, for the kNN by k. Note the turning point at $k = 35$ and declining accuracy with increasing k thereafter. m is the total number of samples. For comparison, we also show the curve calculated with $\frac{m}{2}$ samples. As $m \to \infty$, accuracy declines more slowly with increasing k owing to the k nearest neighbours being closer in n-dimensional space.

sorting can make kNN very computationally expensive at run time, so we now consider more efficient classifiers. Random forest and MLP applied to the first 15 principal components show small improvements in overall accuracy compared to kNN but demonstrate that classification is practical with acceptable performance (Table 5.4). The CNN is capable of using the whole window (28×28) as input rather than just the principal components. With an overall accuracy of 0.90, approaching the upper bound of our Bayes accuracy estimate (0.92), the CNN is the best performing classifier.

Up to this point we have been considering the operation of machine learning algorithms which are created automatically from the training data. However, as is common with machine learning algorithms, there is no easily accessible explanation of why they perform well or poorly. To explore this, we consider example windows from $\mathcal{A}$, $\mathcal{B}$ and $\mathcal{O}$ and compare their projections into principal components (Figure 5.6). Principal components 1 to 15 for the combined feature vector $[S_v, \eta_\theta, \eta_\phi]$ are used to reconstruct the images. The effect is to smooth the images. The $\mathcal{A}$ example has a strong response in both S_v and η_θ, $\mathcal{B}$ has a strong response in S_v but not in η_θ and $\mathcal{O}$, no response in either. Whilst the presence or absence of signal in either η_θ or η_ϕ would seem to differentiate $\mathcal{A}$ from $\mathcal{O}$, we know that the angular data are noisy (Figure 5.4) and, taken alone, are insufficient to give good machine learning results (Table 5.4). This leads to the intriguing possibility that we might find areas of strong S_v and only consider them to be aliased seabed if there is a correspondingly strong signal in either η_θ or η_ϕ.

The patterns seen in η_θ and η_ϕ are difficult to segment because of noise. Pixel values vary between -128 and 127 and so we take the mean-squared over a moving window to smooth the image and accentuate coherent signal (window sizes determined using the earlier chi-squared distance analysis). Whilst these pixels fall within the aliased seabed regions, only a small percentage of area is identified. However, we can take these pixels and then examine the surrounding region in S_v. Hence, we derive a five-step algorithm:
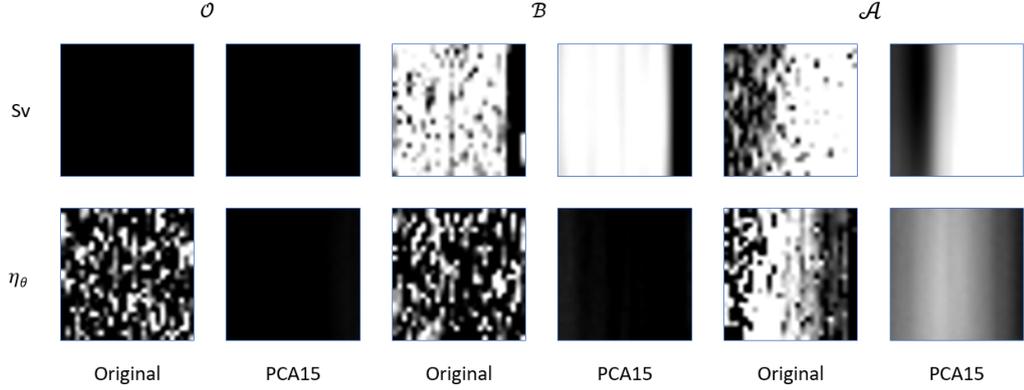
Figure 5.6: 28×28 images of volume backscatter S_v and along-ship angle η_θ for each of the three classes: other ($\mathcal{O}$), biology candidate ($\mathcal{B}$), and aliased seabed ($\mathcal{A}$). Also shown are the reprojections of each image from the first 15 principal components.

1. Find the mean squared of a 28×28 moving window over η_θ and select cells $> T_\theta$ to produce a mask m_1;

2. Find the mean squared of a 52×52 moving window over η_ϕ and select cells $> T_\phi$ to produce a mask m_2;

3. Combine the masks $m = m_1 \vee m_2$ (where $\vee$ is the logical or operator);

4. Select pixels from S_v using the mask, m and determine the median S_v value of the selection to use as a threshold T;

5. Select regions from S_v where $S_v > T$ and which intersect m. The resulting mask is the union of the selected regions and m.

The final mask is a grid indicating those pixels that have been classified as aliased seabed. It can be used to label aliased seabed pixels in the original echogram or to replace them, using a suitable token (e.g. -999) indicating "no data" or "missing value".

We would like to maximise the algorithm's accuracy and reliability, but the choice of T_θ and T_ϕ is a compromise, (on the one hand, choosing many pixels in an echogram gives high reliability and poor accuracy, on the other hand, choosing only few aliased seabed pixels gives high accuracy and poor

reliability). We generally prioritise accuracy over reliability to avoid misclassification of biology. Using the mean squared distributions of η_θ and η_ϕ from our test data, we select values for each percentile and plot $P(\mathcal{A} \mid \widehat{\mathcal{A}})$, $P(\widehat{\mathcal{A}} \mid \mathcal{A})$ and $P(\mathcal{B} \mid \widehat{\mathcal{A}})$. We find that the 80th percentile values $T_\theta = 702$ and $T_\phi = 282$ give similar accuracy and misclassification results to the CNN at the expense of some reduction in reliability. The results from the CNN and this final algorithm are compared in Figure 5.7 and Table 5.4. The hand-drawn aliased seabed has an area of 213470 pixels. Otsu's method reduces this to 125599 pixels and the final mask from the algorithm is 178399 pixels.

5.4 Discussion

Aliased seabed is typically removed by manual scrutinization of echograms and we use this technique, along with biological data determined using the SHAPES algorithm (Barange, 1994; Coetzee, 2000), to assemble samples with which to explore automated discrimination methods. We are unable to discriminate aliased seabed from biology using simple thresholding of either volume backscatter or split-beam angle at a single pixel level or with spatially averaged data. Instead we apply machine learning algorithms using both volume backscatter and split-beam angle and show that non-linear classifiers can accurately identify aliased seabed. A CNN gives the best aliased seabed detection performance (accuracy 0.96, reliability 0.89). Aliased seabed removal is usually undertaken prior to biology detection methods and so minimising misclassification of biology is important (the CNN misclassification is 0.02). Other deep learning architectures and hyperparameter tuning could yield accuracy improvement, but we show that the CNN described is already performing close to our estimate of the Bayes error which we determine using a kNN. When the classifiers are run on volume backscatter alone or split-beam angle alone, we find that they do not achieve the same performance as when using the combined data.

Our manually drawn regions of aliased seabed tend to be larger than strictly

necessary because of the difficulty and labour in tracing irregular shapes (the hand-drawn mask in Figure 5.1, is about 20% larger than the final mask in Figure 5.7). We crudely refine the region boundaries using Otsu's method, commonly used in image processing, and this technique could be applied more widely during scrutinization of echograms. Even so, the boundary between overlapping aliased seabed and biology may be impossible to determine and our "ground truth'' is subjective. This may explain the reliability of our aliased seabed detection algorithms being lower than their accuracy (Table 5.4). Speckle is seen in some aliased seabed detections (Figure 5.7c), also reducing the reliability scores. This can be removed using a hole filling image processing algorithm (e.g. morphological reconstruction (Soille, 2013), as used by MATLAB imfill). Visual inspection of echograms shows that our automated results find several instances of aliased seabed that had not been identified in the ground truth dataset. On further inspection these appear to be genuine and, in some cases, are fainter aliases caused by the echoes from antepenultimate pings. More precise delineation of aliased seabed will improve survey accuracy and reduce misclassification of biology.

We have some reservations about the use of machine leaning algorithms which are usually applied in a "black box manner'', with no information provided about what exactly makes them arrive at their predictions (Samek, Wiegand and Müller, 2017). Whilst human operators can reason about previously unseen inputs, there is no way to be confident that a machine learning algorithm will interpolate or extrapolate in a reasonable manner for data that are significantly different to training samples (Lake *et al.*, 2017), (in our case, we consider data from five survey years). Machine learning algorithms can be complex to implement in simple scripting languages such as those provided by commercial hydroacoustic processing software. The computational demands can be beyond the limits of small, low power processors which are common in marine autonomous vehicles and embedded systems. Classical algorithms have the advantage of being more transparent, understandable and debuggable.

There is a strong, legitimate desire for algorithms based on physical princi-

ples, but also a need to show that such algorithms are accurate and reliable. We use machine learning to explore the performance that can be expected, and to estimate an upper bound on optimality so that new algorithms can be evaluated. Furthermore, we show that machine learning and exploratory data analysis can inform algorithm design (e.g. in our case, varying feature extraction shows the importance of using both S_v and split-beam data; physical principles are confirmed by seeing reprojections of the PCA; window sizes are determined by chi-squared distance; and thresholds by comparison with CNN performance). Machine learned algorithms can be run over large datasets to find additional example cases that can be studied to gain more insight into a particular phenomenon. Whilst it is easy to dismiss machine learning methods, we show their utility as a methodology for algorithm development.

Our final algorithm is simple to implement and efficient in terms of computational resources. The windowing operations can be implemented using two-dimensional convolution which is fast on modern hardware (the example in Figure 5.7 takes about 0.43 s on a 2016 Intel Skylake i7 processor). Whilst the algorithm does not rely on other noise removal strategies beyond true seabed removal, its performance can reduce if the data include impulse noise, transient noise or attenuated signal. In these cases, the methods described by Anderson, Brierley and Armstrong (2005) and Ryan *et al.* (2015), combined with interpolation (e.g. median filtering) to replace the noise, are an effective preprocessing step. If using background noise removal (e.g. De Robertis and Higginbottom, 2007), we recommend implementing this after aliased seabed detection. Aliased seabed is an additive backscatter corruption, so the algorithm assumes that the area surrounding an alias is likely to have a lower backscatter than the alias. The backscatter threshold (T) is determined dynamically, making the algorithm less sensitive to calibration correction accuracy. The median is used to determine backscatter threshold (T), being less susceptible to outliers than the mean. Whilst the algorithm is not machine-learned, the accuracy of aliased seabed detection and misclassification of biology are comparable to the best performing machine learning

algorithm (the CNN), albeit with reduced reliability (Table 5.4).

We want our method to be independent of ping interval (I_T) and logging range (R_L), and so we choose to use a single frequency. We are also interested in using data from ships of opportunity (e.g. fishing vessels) which may only have a single frequency. However, if multi-frequency data are available then, depending on maximum range (R_{max}) and seabed depth (R_S), other frequencies can be used to further validate aliased seabed. (E.g. if an aliased seabed candidate was observed at 500 m in 38 kHz data, with ping interval $I_T = 2s$ then, using (5.1), seabed depth $R_S = 2000$ m. If a corresponding signal was seen in 70 kHz data, then the maximum range (R_{max}) would be insufficient to reach the seabed, and so the signal must have another cause). Lower frequency data could allow R_S to be detected automatically and allow the methods of Renfree and Demer (2016) to be used as part of a hybrid approach. A consequence of (5.1) is that $R_S \not< R_L$ and so aliased seabed cannot occur in a ping where the true seabed has already been detected.

Using split-beam angle in addition to volume backscatter is known to improve bottom detection (MacLennan *et al.*, 2004; Bourguignon *et al.*, 2009). Large coherent patterns in SBA are a strong indication of reflections from the seabed, but not biology. We extend this observation to aliased seabed and use it to create an automated algorithm providing consistent, repeatable results. We have tested the algorithm with Simrad EK60 data, which uses a four quadrant, split-beam configuration. Some new transducers use a three-sector design, however we expect the principles to be transferable. The split-beam angle threshold values, T_θ and T_ϕ, and the convolution window sizes presented here, are determined from data collected around South Georgia, where the seabed substrate consists of fine-grained sediments and clays and there is rapid change in bathymetry (Hogg *et al.*, 2016). Although we designed the algorithm for aliased seabed detection, *mutatis mutandis*, it may also have applications as a bottom detector.

Ocean observing systems using acoustic sensors on ships of opportunity

(e.g. fishing vessels, Kloser *et al.*, 2009) and marine autonomous vehicles (Guihen *et al.*, 2014) are becoming more common, leading to increased data volumes. New broadband acoustic systems collect even more data. Manual processing has already become "overwhelming'' and large-scale automated analysis is challenging (Wall, Jech and McLean, 2016). The methods described are a first step towards automated, unsupervised aliased seabed detection and removal,

5.5 Future work

Deep learning in image processing is known to be more effective when using larger quantities of labelled training data (Sun *et al.*, 2017). The pedagogical ImageNet database contains one million images, but this study used only thirty available labelled transects. A larger set of labelled training data should be assembled if we are to further improve accuracy and reliability.

Seabed aliases are large scale features and human detection is based on shape, size and proximity to the true seabed. A CNN with a multi-scale retina may allow this additional context to be represented, and may improve accuracy and reliability.

Transferability of these algorithms to other vessels and other ocean areas has not yet been demonstrated. This study used training data from a single vessel, but future training data should include representative examples from other vessels and ocean areas.

5.6 Next steps

Having shown how machine learning can be used to automate processes previously thought to require human intervention, in the next chapter we construct a fully autonomous acoustic data processing system.
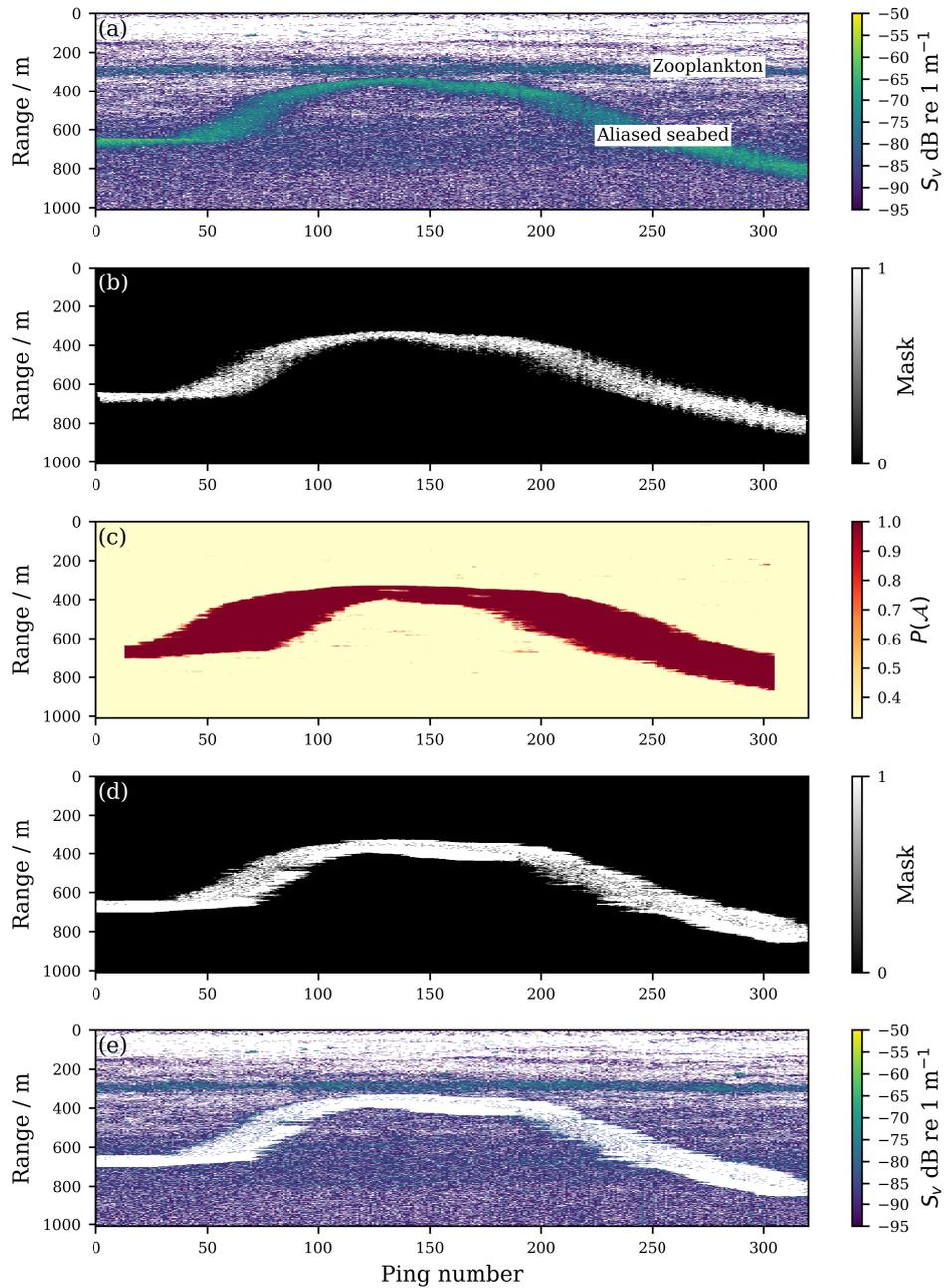
Figure 5.7: Detection and removal of aliased seabed. (a) is the original echogram, (b) "ground truth" created by applying Otsu's algorithm to the hand-drawn mask, (c) aliased seabed probability determined by the CNN, (d) aliased seabed determined using the algorithm, and (e) the echogram with aliased seabed, from the algorithm, removed.

111

Chapter 6

RAPIDKRILL: Real-time reporting of fisheries acoustic data

> "Scientists investigate that which already is; engineers create
> that which has never been."
>
> Albert Einstein

In this chapter, we build a proof of concept autonomous, unsupervised, real-time reporting system (RAPIDKRILL), that is intended initially for fishing vessels. We explore requirements for hardware and software components and present a system design that is informed by earlier chapters.

Robert Blackwell came up with the original concept for a small, low cost add-on to an echosounder that would summarise acoustic data in real time, undertook systems integration and helped assemble the RAPIDKRILL demonstrator. He contributed to the design and development of Echopy[1] and RAPIDKRILL[2] software. The RAPIDKRILL prototype system was demonstrated at the Working Group for Fisheries Acoustics Science and Technology (WGFAST) 2019 in Galway, Ireland.

---

[1] https://github.com/bas-acoustics/echopy, accessed April 2020.
[2] https://www.bas.ac.uk/project/rapidkrill, accessed April 2020.

EchoJulia[3] was developed by Robert Blackwell and was presented at the Julia Conference 2018 in London.

6.1   Introduction

Dynamic ocean management uses near real-time data to manage changes rapidly in space and time in response to the shifting nature of the ocean and its users (Maxwell *et al.*, 2015). Ocean resource managers must balance marine resource protection with sustainable use (e.g. fishing), but marine habitats can change rapidly. Advances in data collection and sharing, particularly in remote sensing, are enabling reactive and adaptive management strategies where changes can be implemented quickly in response to changing conditions.

The Commission for the Conservation of Antarctic Marine Living Resources (CCAMLR) uses a precautionary ecosystem management approach (Kock, 2000) with fixed catch limits applied to the Antarctic krill fishery. CCAMLR would like to develop a more timely, dynamic feedback management approach but there are high levels of spatial and temporal variability leading to uncertainty in the structure and operation of the ecosystem (Hill, Phillips and Atkinson, 2013). Data are collected by national science and scientific observer programmes, but these data can take substantial time and effort to process, delaying management reports.

Marine Autonomous Vehicles (MAVs) are increasingly being used to survey marine ecosystems with additional spatial and temporal resolution (Testor *et al.*, 2019). One of the appeals of MAVs is directing them to regions of interest and receiving data in real-time (e.g. Klinck *et al.*, 2012 use Seagliders to receive near real-time information about beaked whales). A wide range of sensors and instruments can be deployed (e.g. to measure temperature, salinity and turbulence) with data being relayed to ground stations via satellite communication networks. MAVs carrying active acoustic sensors (echosounders) are used for ecosystem research but high data volumes

---

[3]https://echojulia.github.io, accessed April 2020.

present challenges for data communication (Guihen *et al.*, 2014). Sensors currently store data locally for retrieval and analysis once the vehicle is recovered, delaying publication of results.

Acoustically derived summary metrics such as Nautical Area Scattering Coefficient (NASC), backscatter density, abundance and distribution have been shown to be useful ecosystem descriptors (Urmy, Horne and Barbee, 2012, Chapter 4), but to transmit these in real-time requires that they first be computed onboard the vehicle. This computation requires a computer, running unsupervised acoustic processing software, to be attached to the echosounder (Benoit-Bird *et al.*, 2018). MAVs are typically power, size and weight constrained, and we would like to minimise battery consumption, size and weight of the instrument payload.

Acoustic data processing is usually undertaken by experts using interactive, desktop software. Echoview® (Echoview Software Pty Ltd) and LSSS (Korneliussen *et al.*, 2016) are commonly used, but neither are designed to run autonomously in embedded, unsupervised environments. That has not stopped scientists from trying (e.g. Benoit-Bird *et al.*, 2018)!

Embedded software systems, such as those deployed in scientific instruments, are usually written in low level languages such as C, C++ or assembly language. Most scientists are more familiar with high level, high productivity, scientific and statistics languages (including MATLAB, Python and R). This leads to the so-called *two-language problem*, where scientific software is often written by a scientist in a high-level language and then reimplemented by a software engineer in a low level language such as C, C++ or FORTRAN, for speed and resource efficiency. Julia is a high-level, high-performance dynamic programming language for numerical computing, initially developed at MIT, that claims to solve the two-language problem (Bezanson *et al.*, 2017).

The Python programming language has become a popular tool for scientific computing and statistics (McKinney, 2010), and libraries are starting to

emerge for fisheries acoustics (e.g. Echopype[4]; PyEcholab[5]). Python is accessible and convenient for a broad audience, including scientific researchers, and can be used to write programs which automate repetitive analysis tasks. There is growing interest in the use of Python for fisheries acoustic data processing (ICES, 2018).

Intel based PC computer systems running the Microsoft Windows operating system have typically been used for echosounder applications (e.g. Benoit-Bird *et al.*, 2018). These systems can be large, expensive and have high power consumption, making their use challenging in MAVs. Low cost, system-on-chip computers such as the Raspberry Pi[6] are increasingly being used for so-called Internet-of-things (IOT) applications, where devices with sensors and actuators are connected to the Internet (Upton and Halfacree, 2014; Vujović and Maksimović, 2015). These devices typically use the Linux operating system which is highly customisable and runs a wide variety of software.

Satellite communication has a reputation for being expensive, but protocols such as Iridium Short Burst Data (SBD) allow transmission of small, low cost messages (Lysogor, Voskov and Efremov, 2018). Mobile originated messages of up to 340 bytes in length can be sent for less than £0.15. Low cost development kits such as the Rock Seven RockBlock[7] are readily available.

In this chapter, we survey existing fisheries acoustic software tools and develop new, open-source software libraries for fisheries acoustic data processing. We test the performance of sample programs and demonstrate a prototype, unsupervised system running on a small system-on-chip computer (a Raspberry Pi) that could be deployed in unsupervised, autonomous settings.

---

[4]https://echopype.readthedocs.io/en/latest/, accessed April 2020.
[5]https://github.com/CI-CMG/pyEcholab, accessed April 2020.
[6]Raspberry Pi Foundation, https://www.raspberrypi.org, accessed April 2020.
[7]https://www.rock7.com/products-rockblock, accessed April 2020.

6.2 Materials and methods

6.2.1 Software

We looked at existing acoustic data processing software, as well as software development systems as part of a "buy or build" assessment. Our initial software requirements are shown in Table 6.1.

Table 6.1: Requirements for real-time acoustic data processing.

Requirement	Notes
Open	Able to use and modify software without undue cost or restriction.
Fast	Computation must keep pace with data availability.
Efficient	Having low computational resource requirements in terms of memory, processor and storage.
Capable	Having the facility for active acoustic data processing.
Extensible	Allowing experimentation with different acoustic processing algorithms.
Portable	Run on a wide variety of hardware platforms.
Documented	Understandable and customisable.
Low cost	Low runtime cost to allow widespread deployment.

We compiled a list of fisheries acoustic software tools from the literature, word-of-mouth and web-based searches, noting their characteristics and licensing terms. One hundred journal papers matching the search term "fisheries echogram", published after 2009 in the ICES Journal of Marine Science, were examined (Appendix H). A paper was attributed to a software tool if that software tool occurred at least once in the paper. If a paper contained more than one software tool, it was attributed to all software tools present.

None of the fisheries acoustic software tools met our exact requirements, and so we decided to develop custom software. The RAPIDKRILL project is a collaborative effort involving a team of scientists, and the consensus was to use Python for the prototype, primarily due to existing skills and interest in Python amongst the fisheries acoustics community. Even so, we wanted to compare the performance of Python based programs with equivalent Julia based implementations. Two simple programs were implemented to

116

read Simrad EK60 RAW files and calculate mean volume backscattering coefficient, first using Python 3.7.5 and PyEcholab and second using Julia 1.3.1 and SimradEK60.jl. We tested the Julia software using both 32 bit and 64 bit arithmetic. Execution times were recorded running on an Intel(R) Core(TM) i5-8400 CPU @ 2.80GHz (2018) system using the Linux time command[8].

The Python prototype reads EK60 data, and corrects for noise before calculating and transmitting summary statistics. Although we demonstrated sufficient accuracy and precision using 32 bit arithmetic (Chapter 2), the prototype was forced to use 64 bit arithmetic because of the dependency on PyEchoLab software. The noise removal strategy was informed by the experiments in Chapter 4 and the sensitivity of results to noise reported in Section 4.6.2: Impulse Noise (IN), defined as noise "spikes" of less than one ping in duration, was identified with a two-sided comparison method using a resolution of 5 m vertical bins and a 10 dB threshold (Ryan *et al.*, 2015). Attenuated Signal (AS), defined as signal of lower amplitude due to bubbles, was identified by comparing the deviation of each ping from S_v data within the 100 to 200 m range, using a 30 ping average and -6 dB threshold (Ryan *et al.*, 2015). Samples detected as noise were regarded as "empty water" and replaced with -999 dB which is approximately 0 in the linear domain. The impact of seabed reflections was mitigated by only operating with offshore, deep water samples (selected based on bathymetry). The risk of aliased seabed (ASB) was mitigated by using 120 kHz data which is less prone to ASB (Chapter 5).The RAPIDKRILL project is concerned with measuring Antarctic krill abundance, and in Chapter 4 we showed that volume backscattering strength (S_v) is a reasonable proxy for krill density. We therefore used the SHAPES algorithm (Barange, 1994; Coetzee, 2000) to segment areas of echograms most likely to be krill and summarised these using nautical area scattering coefficient (NASC) derived from S_v (6.1), where T is mean thickness of the domain being integrated. Summary

---

[8]The Linux time command manual page, https://linux.die.net/man/1/time, accessed April 2020.

results were transmitted to shore based systems via email (if a TCP/IP network was present) or using the Iridium Short Burst Data (SBD) service. All echosounder data were recorded on an attached disk drive connected via Universal Serial Bus (USB).

$$\text{NASC} = 4\pi \times 1852^2 \times 10^{\frac{S_v}{10}} \times T \tag{6.1}$$

Unit testing, where components are tested individually (Runeson, 2006), and integration testing, where components are combined and tested as a group (Leung and White, 1990), were used to help ensure correct operation of the software as the project progressed. All tests used data recorded in the Southern Ocean as part of the British Antarctic Survey Ecosystems programme (Cruises JR230[9] and DY098).

6.2.2 Hardware

Our objective was to assemble a bench-based prototype system with a computer connected to an echosounder that could be used for development, testing and experimentation. Our initial computer system requirements are shown in Table 6.2.

The power consumption (in Watts) of a Raspberry Pi Model 3 B+ was compared with an Intel Core i5 based laptop using an Energenie 429.856UK power meter. The systems were measured under low CPU load (in an idle state) and under high CPU load (using the stress –cpu 4 command under Linux).

A Raspberry Pi Model 3 B+ computer running the Linux operating system was selected to build the prototype. A RockBLOCK Iridium SBD transceiver and antenna was used to experiment with satellite communication and networking.

---

[9]https://github.com/bas-acoustics/krill-ball, accessed April 2020.

Table 6.2: Requirements for a computer to be connected to an echosounder for real-time acoustic data processing.

Requirement	Notes
Low power	Able to run on battery power for a number of days.
Small	Capable of being deployed within an autonomous vehicle.
Open	Able to run custom operating systems and software without additional fees.
Capable	Having sufficient computational resources for acoustic processing.
Headless	Able to run without a display and without operator intervention.
Extensible	Able to add custom hardware and sensors.
Documented	Understandable and customisable.
Low cost	Affordable for multiple deployments.

6.2.3 Echosounder integration

Simrad provide a data subscription facility using extensible markup language (Simrad, 2012). After experimentation, we found that the data available are only a subset of those provided in the underlying Simrad RAW files. We considered intercepting and reverse engineering the echosounder's communication (which uses the User Datagram Protocol[10]), but were discouraged from so doing by license terms.

Instead, we chose a simple file sharing mechanism where the Raspberry Pi exposed part of its file system using the Server Message Block (SMB) protocol[11] to which the echosounder could write. Data files were then detected using a simple polling mechanism and processed on arrival.

Using echosounders in an office environment is inconvenient and so we used Simrad ER60 software running on a PC, in place of a Simrad EK60 echosounder, to "replay" real data recorded on earlier ship-based surveys.

---

[10]Internet Standard RFC768, J. Postel, https://tools.ietf.org/html/rfc768, accessed April 2020.

[11]The Server Message Block (SMB Protocol) https://msdn.microsoft.com/en-us/library/cc246482.aspx, accessed April 2020.

6.2.4 Communication network

We tested two forms of data network from the Raspberry Pi: Iridium SBD (using a Rock Seven RockBlock transponder) and email (simulating a ship's broadband satellite connection). For SBD we used the MessagePack protocol[12] to compress data. For email, we sent comma separated value (CSV) files using SendGrid[13].

6.2.5 Prototype

The prototype system consists of a Raspberry Pi computer connected to a Simrad ER60 PC (in place of an echosounder). Acoustic data files are processed, with summary metrics displayed on the screen and relayed to a land station via email or SBD (Figure 6.1). The bill of materials for the prototype is shown in Table 6.3.

Table 6.3: RAPIDKRILL bill of materials. Prices in GBP exclude VAT and are correct as of January 2020. Iridium SBD messages are less than £0.05 when purchased in bulk.

Item	Quantity	Unit Price	Total
Raspberry Pi 3 Model B+	1	28.39	28.39
32GB Micro SD card	1	8.43	8.43
Raspberry Pi power supply	1	6.45	6.45
Raspberry Pi 7-inch touchscreen	1	48.75	48.75
Edimax USB3 to Ethernet adapter	2	18.97	37.94
CAT 6 RJ45 2m cable	2	4.96	9.92
Rock Seven RockBlock 9602 Iridium SBD transceiver	1	175.00	175.00
FTDI/USB cable	1	19.00	19.00
Iridium SBD messages	200	0.11	22.00
Total			£355.88

6.3 Results

Of the 100 journal papers analysed, Echoview was used for analysis in 48 papers, LSSS in 11 and MOVIES in 4. Table 6.4 contains a list of all

---

[12]https://msgpack.org, accessed April 2020.
[13]https://sendgrid.com, accessed April 2020.
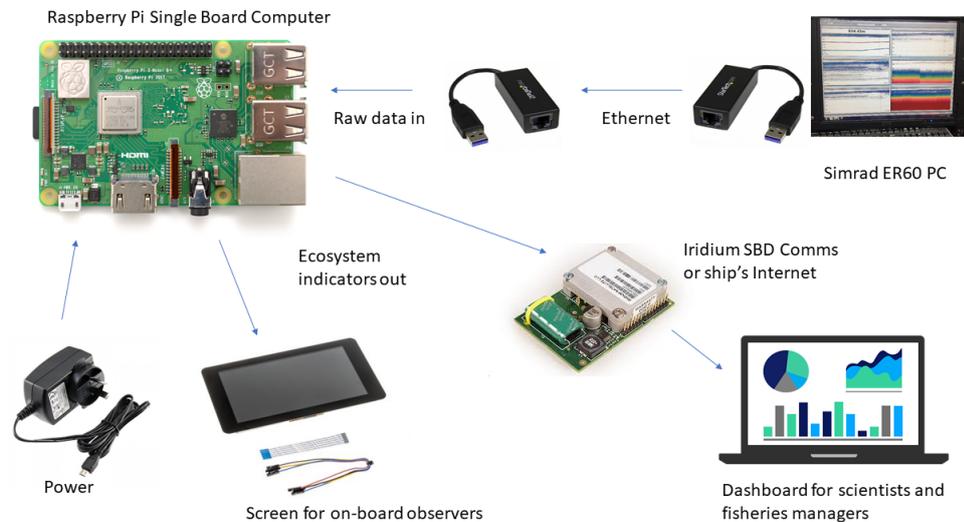
Figure 6.1: RAPIDKRILL Vessel Data and analysis System which reads data from a Simrad EK60 echosounder, logs it to a memory card and sends summary ecosystem indicators via an Iridium Short Burst Data satellite communication system or ship's Internet to scientists and fisheries managers.

echosounder processing software compiled during our research.

Of our programs calculating mean volume backscattering strength (S_v), the Julia program using 32 bit floating point arithmetic was fastest, and the Python program slowest (Table 6.5). The Python program took more than four times the real (elapsed) time to run. The Raspberry Pi computer used 20% of the power used by the PC when idling, and 17% at full load (Table 6.6).

A RAPIDKRILL prototype system was demonstrated at the Working Group for Fisheries Acoustics Science and Technology (WGFAST) 2019 in Galway, Ireland[14], summarising Simrad EK60 data as binned Nautical Area Scattering Coefficient (NASC).

[14]A video is available at https://www.youtube.com/watch?v=_PAiWBJLqWo

Table 6.4: List of fisheries acoustic data processing tools.

Software	License	Language	Notes
BEI	Commercial?	C	Described in Knudsen (1990). Superseded by LSSS.
echogram	Unspecified	R	Echogram Visualisation and Analysis (https://github.com/hvillalo/echogram).
Echopype	Apache	Python?	Enhancing the interoperability and scalability in analyzing ocean sonar data (https://github.com/OSOceanAcoustics/echopype).
Echoview	Commercial	C++?	Hydroacoustic visualization and analysis software (https://www.echoview.com).
EchoviewR	GNU GPL	R	A free interface between Echoview and R using COM scripting (https://github.com/AustralianAntarcticDivision/EchoviewR).
ESP3	MIT	MATLAB	Acoustic data processing software (https://bitbucket.org/yladroit/esp3)
Hermes	Closed source		Hydroacoustics Efficient Recording Module for EchoSounders (https://bit.ly/39Rh2c4)
LSSS	Commercial	Java?	Large Scale Survey System (https://www.marec.no
Matecho	?	MATLAB	Integrated and supervised Matlab processing chain (https://bit.ly/2SHRQPm).
MOVIES	-	-	Acoustic processing software described in Weill et al. (1993).
MOVIES3D	Closed source		Display echosounder data in a 3D environment described in Trenkel et al. (2009) (https://bit.ly/39Rh2c4)
PyEcholab	Unknown	Python	Toolkit for reading, processing, plotting and exporting fisheries acoustic echosounder data (https://github.com/CI-CMG/pyEcholab).
readHAC	Unspecified	R	Read acoustic HAC format files (https://github.com/kaskr/HAC).
SonarX	Commercial	?	Post processing tools(http://folk.uio.no/hbalk/sonar4_5/index.htm).
EchoJulia	MIT	Julia	Hydroacoustic data processing software in Julia (https://github.com/EchoJulia)
Echopy	MIT	Python	Fisheries acoustic data processing in Python (https://github.com/bas-acoustics/echopy).

Table 6.5: Performance of Python and Julia programs used to calculate mean volume backscattering coefficient.

Program	Real (m:ss)	User (s)	Sys (s)	Mem (KB)
Python	11:59.51	1756.16	34.97	351376
Julia (64 bit floating point)	2:46.04	100.19	13.87	349728
Julia (32 bit floating point)	2:27.42	88.12	12.34	292264

Table 6.6: Power consumption (in Watts) of a Raspberry Pi 3 B+ and an Intel Core i5 laptop during idle and under high processor load.

Computer	State	Power
Raspberry Pi Model 3B+	Idle	3
Raspberry Pi Model 3B+	Load	6
PC	Idle	11
PC	Load	34

6.4 Discussion

There are already a variety of tools and software libraries for fisheries acoustic data processing (Table 6.4). The Bergen Echo Integrator (BEI, Foote *et al.*, 1991) and MOVIES (Weill, Scalabrin and Diner, 1993) were amongst the earliest general-purpose systems, but Echoview and LSSS are amongst the most popular systems used today. Some recent systems are designed to allow custom software to be written: *readHAC* and *echogram* (Villalobos, 2017) use the R programming language; *EchoviewR* provides a bridge between R and Echoview software (Harrison *et al.*, 2015); *Matecho* and *ESP3* are implemented using MATLAB; *PyEcholab* and *Echopype* use Python.

Neither Echoview nor LSSS use open source software licences. Fisheries scientists rely on the accuracy and reliability of results from Echoview and LSSS, and whilst their methods are well documented, the source code for their implementation cannot be inspected or easily subjected to the scientific process. The software cannot be customised without recourse to the original developers. The open source software systems listed in Table 6.4 can be inspected and freely modified. However open source software may not be as mature, well supported, or maintained. Scientific open source software is often created by individuals and research groups and may not have the same range of features, or be tested to the same degree as commercial software.

None of these systems completely met our requirements and so we decided to build new software for RAPIDKRILL. We also wanted to experiment with image processing techniques (Chapters 2 and 3). Our research group already had experience with the Python programming language, and so we initially chose to use PyEcholab to read acoustic data and develop a new library, Echopy, for acoustic data processing. Echopy now includes a range of methods for noise removal and summarisation. Echopy may also have applications in so-called "Big Data" (Mayer-Schönberger and Cukier, 2013) processing of historic and very large archived acoustic data sets.

Software development is time consuming and can be expensive. The bill of materials (Table 6.3) does not include the software that was developed

by scientists during the project. We estimate that the true cost of software development, if undertaken by a commercial organisation would be in excess of £100k.

Although early versions of the software functioned correctly, we had to carefully program RAPIDKRILL to ensure that it was fast and efficient enough to run on a Raspberry Pi. Performance analysis prompted us to optimise code. We also considered alternative software development systems, and found that a Julia program used to calculate mean volume backscattering coefficient, was four times faster than the equivalent Python code. Julia has been designed to exploit type inference in its compiler, often allowing more efficient code generation than with traditional dynamically typed languages (Bezanson *et al.*, 2017). Poor performance in embedded software on marine autonomous vehicles could waste battery power. Julia is interoperable with other programming environments and can call C, C++, Python or R code directly. Future versions of RAPIDKRILL could use Julia for performance critical code, without necessarily reimplementing the whole software system.

According to the Technology Readiness Level scale (Mankins, 1995), the RAPIDKRILL demonstration system is at TRL 4 (Component and/or Breadboard Laboratory Validated). Whilst the system is not mature enough for deployment, it has proved useful for experimentation and exploration of the challenges posed by autonomous, unsupervised fisheries acoustic data processing.

The Raspberry Pi computer is physically smaller and consumes less electrical power than a PC based system. Whilst a PC has more computational capacity, the Raspberry Pi was able to keep pace with the echosounder, delivering summary information in near real-time. Benoit-Bird *et al.* (2018) report a doubling of power consumption by adding a Windows PC to a Simrad echosounder on a Slocum glider. Our results show that a small system-on-chip computer could reduce these power requirements compared to a PC. Embedded systems technology is developing rapidly with further

reductions in power expected. The software could also be further optimised to reduce power consumption (for example, by converting more of the code to the Julia programming language).

Connecting the computer with the echosounder was the most troublesome part of the project and still has reliability issues. We tried using the Simrad provided subscription method but found this only provided a subset of the required data. We considered intercepting and reverse engineering the user datagram protocol packets, but this would have contravened licensing terms. We eventually used a rudimentary file sharing and polling mechanism, but this is fragile and prone to stop working if there is a network interruption. A more reliable system will be required as we develop the system further. Discussions with Simrad suggest that better publish and subscribe mechanisms are likely to be made available in future echosounder software versions.

RAPIDKRILL shows that bench-based prototype marine science systems can be developed quickly and cheaply to allow experimentation. Low cost, system-on-chip computers and satellite communication devices are readily available and straightforward to integrate. RAPIDKRILL has allowed us to test the principles of operation of an automated, unsupervised active acoustic processing system without the costs associated with marinisation and deployment. We hope that with additional investment, the system can be further developed. Initial deployments are expected to be onboard research vessels and fishing vessels. The system could be extended for use with a wide variety of marine autonomous vehicles.

Chapter 7

Conclusions and future work

> "If I have not seen as far as others, it is because giants were standing on my shoulders."
>
> Hal Abelson

In Chapter 2, we showed that generic data compression programs (e.g ZIP) are insufficient to allow transmission of raw acoustic data using current maritime communication technology. Echosounders generate very large amounts of data. General purpose compression algorithms deliver compression ratios of < 3, which is helpful for data storage onboard a ship where disk space can be at a premium. However, ratios numbered in hundreds or more are required to even consider lossless acoustic data transmission using low bandwidth networks. Satellite communication is often the only practical method for relaying data from remote areas such as the South Atlantic. New low earth orbit broadband satellite systems are being deployed (e.g. Iridium NEXT[1]; STARLINK[2]), but these are unlikely to solve the problems posed by marine autonomous vehicles. STARLINK is likely to be targeted at urban areas only, and both systems require stable antenna systems which are difficult to achieve at sea on small vehicles.

Some fisheries acoustic applications store samples as 64 bit floating point

---

[1] https://www.iridiumnext.com/, accessed April 2020.
[2] https://www.starlink.com/, accessed April 2020.

numbers, but 32 bit floating point numbers halve the data size (Section 2.3). Reduced numeric precision is a form of lossy compression, but our results show that 32 bit floating point arithmetic is adequate when working with data from Simrad EK60 echosounders.

Acoustic data can be converted to echogram images, and these can use image compression to reduce data size (Chapter 2). Some image file formats use compression techniques that exploit the nature of images and human perception. However, echogram quantisation (the conversion of backscatter values into a discrete set of colours) is itself a form of lossy compression. It is therefore important to optimise echogram colour maps for human perception. In Chapter 3 we found that quantitative echograms should use colour maps which are colourful (have a perceived variety and intensity of colours), sequential (have monotonic lightness), and perceptually uniform (have consistency of perceived colour contrast over their range). Whilst all the traditional fisheries acoustic colour maps tested are colourful, none is sequential or perceptually uniform. Modern colour maps (e.g. Viridis) have been specifically designed for colour contrast consistency, accessibility for viewers with red-green colour-blindness, and legibility when printed in monochrome. Fisheries acousticians rely on echograms for visualisation of acoustic data, but these are often perceptually suboptimal. Our paper, *Colour maps for fisheries acoustic echograms* (R. E. Blackwell *et al.*, 2019) has gone some way to addressing this problem, with software, training and practice all now beginning to change.

Simple echograms are useful for presenting single frequency acoustic data, but we often want to compare multi-frequency data. In these cases, it is common to present echograms side-by-side. It would be more convenient if we could take a data fusion approach, mapping multiple signals into a combined pseudo-coloured composite image. Colour composite echograms have been used to combine multi-frequency fisheries acoustic data (e.g. Cochrane *et al.*, 1991; Jech and Michaels, 2006; Ross, Keister and Lara-Lopez, 2013), but previous work does not consider perceptual uniformity. Based on the work in Chapter 3, we have started to extend the method into two and

three dimensions by finding large squares and cubes in CIELAB space (see Appendix C). These squares and cubes can then be used as colour spaces to plot two- and three-dimensional data respectively. Early results have been used to visualise krill swarms (e.g. Figure 7.1), but additional work is required to refine and evaluate this approach. A further problem with current echograms is that, whilst we treat them as images, they are not geometrically accurate or drawn to scale. We suggest that echogram visualisation is a topic worthy of further research.
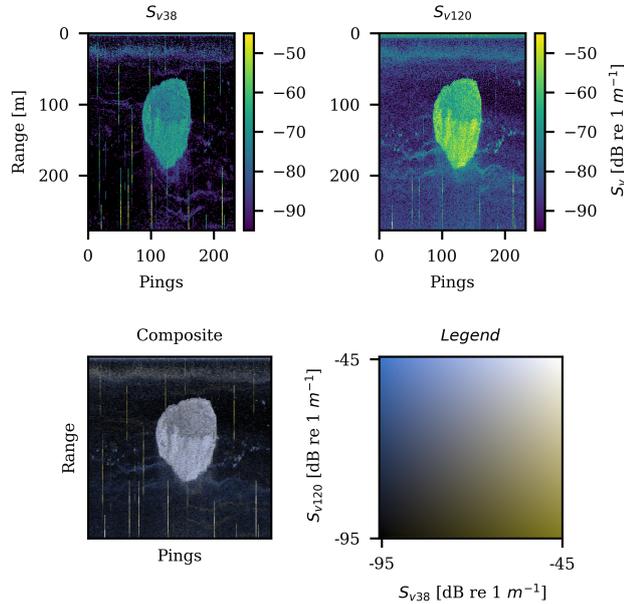
Figure 7.1: 38 and 120 kHz echograms shown side by side (top) and combined as a colour composite echogram and legend (bottom).

Having shown that generic compression and image compression algorithms do not provide sufficient compression ratios for acoustic data transmission, Chapter 4 considered summarisation of fisheries acoustic data from the Western Core Box (a survey originally designed to study Antarctic krill at South Georgia). If ground truth had already been available, then we could have simply machine-learned a compressor, but without ground truth, it is difficult to know which aspects of acoustic data are important. Therefore, we assessed correlation between Echometrics and independent environmen-

tal indices, reasoning that those Echometrics that show strongest correlation are more descriptive. There is a strong correlation between *abundance* and traditional krill density metrics ($r = 0.83$, $p < 0.01$), suggesting that it may be a useful and parsimonious proxy. *Location*, a measure of the centre of mass of acoustic backscatter, correlates with chlorophyll ($r = -0.7$, $p < 0.01$) and may therefore help to describe patchiness and predator/prey interactions. Active acoustics are usually used for species specific abundance surveys, but our results show that Echometrics can be more easily computed and provide concise, useful, generic ecosystem descriptors. Indeed, more variability in WCB acoustic data is explained by measures of distribution such as *location* (centre of mass of acoustic backscatter) than *abundance*. Given that distribution and patchiness of animals is of scientific interest (e.g. Tarling *et al.*, 2009), it is perhaps surprising that these metrics are not more widely used.

Variation in survey timing of the Western Core Box (the survey has typically been earlier in recent years), as well as a lack of data makes interannual comparison difficult. The ecosystem is dominated by Antarctic krill and the local population sees an increase due to transport of animals from the Antarctic Peninsula (Murphy *et al.*, 2007, 2012). Mooring data provides some insight into the timing of krill arrival (Saunders *et al.*, 2007), but increased spatial and temporal sampling are required to fully understand the interannual and intra-annual population variability.

When we calculated the Echometrics, we also demonstrated how important it is to remove noise during processing of backscatter (Section 4.6.2). Acoustic data processing is typically undertaken by experts using graphical tools. Tasks such as the detection and removal of seabed reflections are particularly challenging to automate, but we use machine learning classifiers to show how unsupervised methods are becoming possible. Aliased seabed is a corruption caused by acoustic reflections from the seabed. Aliased seabed detection and removal is an example of an acoustic processing step that is currently undertaken manually. In Chapter 5, we used machine learning techniques and a conventional algorithm to detect aliased seabed in single

frequency, split-beam echosounder data without the need for bathymetry.

In Chapter 3, we considered echograms optimised for human perception, but we need to stop relying on echogram interpretation and realise the potential of computational approaches. Manual scrutinisation of echograms is subjective and confounds reproducible results. Different fisheries acousticians will make different judgements regarding echogram segmentation and classification. As the data increase in resolution and complexity, the human vision system may not be able to discern nuances in the data. Studies of apophenia in psychology demonstrate that humans see patterns when there are none (Steyerl, 2016). In the future, machine learning approaches are likely to be more consistent and effective than human scrutinisation.

Traditional, manual echogram scrutinisation is laborious and impractical for large scale data analysis. Automated methods can be used to reduce workload and ultimately replace human input, but challenges remain. The aliased seabed detector that we developed has proven to be useful however, the very low signal to noise ratio in unprocessed acoustic data makes accurate and reliable seabed reflection removal essential (Chapter 4.6.2). Consequently, we still manually check results. Larger labelled data sets are required from more vessels, more instruments and more ocean areas before such algorithms can be fully machine-learned, automated and trusted. These datasets are only just becoming available (e.g. Brautaset *et al.*, 2020).

Machine learning can be used for acoustic data classification, but fisheries acousticians tend to be wary of black box approaches, preferring explainable algorithms (Chapter 5). The use of machine learning in fisheries acoustics has hitherto been confined to data that have been preprocessed (for example to classify species type, e.g. Fallon, Fielding and Fernandes, 2016; Robotham *et al.*, 2010). However, the success of deep neural networks (DNN) and convolutional neural networks (CNN) in domains including image processing suggest that machine learning could be exploited further to classify raw, unprocessed acoustic data.

A key problem for the application of machine learning to fisheries acoustic

data is the lack of large, labelled data sets that can be used for training and evaluation. Whilst large acoustic data sets are now being assembled (Wall, Jech and McLean, 2016), classification for labelling is still a manual, subjective process. One of the most troublesome problems for fisheries acoustic surveys is still the acquisition of ground truth data (McClatchie *et al.*, 2000).

Split-beam angle data are often discarded during fisheries acoustic data processing. Whilst Simrad EK60 split-beam angle data are noisy, the results in Chapter 5 demonstrate their utility for detecting aliased seabed. Classification improved when split-beam angle data was included in our training data. Machine learning algorithms can often perform well in the presence of noise, and these results suggest that split-beam angle data contain additional discriminatory information.

When removing noise from echograms for biomass estimates, a replacement value of -999 dB is commonly used as a precautionary measure to represent "empty water", but this value never occurs in raw data. The calibrated acoustic data examined in this thesis never contain samples less than -247 dB prior to noise removal. The most commonly occurring S_v value is -85 dB ($p = 0.03$) in 38 kHz data and -79 dB ($p = 0.02$) in 120 kHz data. It would be interesting to repeat the analysis replacing noise using a maximum likelihood estimate instead of -999 dB, thus better preserving the statistical distribution of the data.

Whilst standard methods exist for acoustic data preprocessing (e.g. for CCAMLR surveys, Watkins *et al.*, 2004), results are often dependent on choices made by the researcher and the particular software employed. It is true that different surveys demand different treatment of data, but these differences make it hard to compare processed data sets, and standard products would be helpful. In other disciplines such as satellite remote sensing, researchers typically work with data that is supplied ortho-corrected, calibration corrected and converted to convenient data formats, not the raw data from the instrument (e.g. see the European Space Agency Sentinel-

1 SAR Technical documentation[3]). A similar approach could be used in fisheries acoustics.

Many fisheries acoustic data processing algorithms have analogues in image processing (e.g. transient noise removal is a median filter). This thesis borrowed liberally from image processing practice (e.g. the use of interactive graphics software to inspect echograms, and the application of Otsu's method (Otsu, 1979) to improve image segmentation). There is a huge literature in image processing and more opportunities to repurpose algorithms, software and techniques for fisheries acoustics.

The RAPIDKRILL system demonstrates that acoustic data can be summarised and transmitted to land stations in real-time for scientific reporting purposes (Chapter 6). The current system is a bench-based proof of concept (TRL 4) that allows rapid experimentation and proves principles, but reliability and production engineering are required before it can be deployed onboard fishing vessels or marine autonomous vehicles.

Whilst PCs are typically used to control echosounders, we have shown that system-on-chip computers could be smaller, cheaper, lower-powered alternatives (Chapter 6). The RAPIDKRILL system used a Raspberry Pi computer which is much smaller than a PC ($85\,\mathrm{mm} \times 56\,\mathrm{mm} \times 17\,\mathrm{mm}$) and uses less than 20% of the electrical power. Unfortunately, integration is still hampered by restrictive license terms, with some vendors requiring Windows PCs using proprietary, closed-source software.

For RAPIDKRILL, we selected a Raspberry Pi computer for expediency, low cost, familiarity and wide availability, however other computers with different specifications could also be considered. Many acoustic data processing algorithms operate on matrices and could be parallelised using Graphics Processing Units (GPU). Field Programmable Gate Arrays (FPGA) could be used for specialised operations. In the future, it may be possible to work with echosounder manufacturers to embed computational capacity within

---

[3]Sentinel-1 SAR Technical Guide https://sentinel.esa.int/web/sentinel/technical-guides/sentinel-1-sar, accessed April 2020.

the echosounder instrument itself.

The Python programming language has become popular for data science and there is much interest in building Python software for acoustic data processing (as evidenced by discussion groups at conferences such as ICES, 2018 and the development of libraries such as Echopype and Pyecholab). However, in Chapter 6 we showed that the Julia programming language can generate faster, more efficient code and may be more suitable for developing embedded scientific applications.

Big data analysis has been recognised as an opportunity for marine science (Bakker *et al.*, 2020). Unsupervised data processing algorithms could enable large scale processing of fisheries acoustic data sets. Large quantities of acoustic data exist but standard file and metadata formats (e.g. McQuinn *et al.*, 2005; ICES, 2013; Macaulay and Peña, 2018) have not yet been widely adopted, and not all data are readily available online (Wall, Jech and McLean, 2016). Many of the computations in fisheries acoustics are inherently parallel, with data being partitioned independently by pings, transects or statistical bins. In other disciplines, high performance cloud computing infrastructure has allowed researchers to undertake massively parallel, resource intensive computations without having to invest in hardware (Lee *et al.*, 2012). Graphics Processing Units (GPU) such as those provided by Nvidia allow massive parallelisation of 32 bit operations (Fung and Mann, 2005). Neither cloud computing nor GPU computing has yet been widely exploited for fisheries acoustic data processing and is a future research opportunity.

Marine autonomous vehicles offer the promise of wider spatial and temporal sampling and are being considered for future Western Core Box surveys. Autonomous surface vehicles such as the Saildrone can be equipped with scientific echosounders (e.g. Mordy *et al.*, 2017), and a derivative of RAPID-KRILL (Chapter 6) could be used to transmit summary data via a satellite link. With miniaturisation and marinisation, the technology could also be deployed on autonomous underwater vehicles.

This thesis began with the question: "Can we find acoustic data compression and summarisation algorithms that could be deployed alongside echosounders on marine autonomous vehicles, to deliver real-time ecosystem indicators?". It ends with an innovative hardware and software system (RAPIDKRILL) that processes echosounder data in real-time and relays summary metrics via a low-cost Iridium satellite link. Whilst the system is currently only a prototype, it demonstrates how real-time acoustic data summaries could make a practical contribution to marine ecosystems monitoring and management.

Appendix A

The sonar equation for Simrad EK60 data

In this thesis, volume backscattering coefficient (S_v; dB re 1 m^{-1}) was calculated using (A.1), with symbols defined in Table A.1. This equation is a derivation of the SONAR equation (Urick, 1967) arranged specifically for Simrad EK60[1] power measurements.

$$S_v(R, P_r) = P_r + 20 \log_{10} R + 2\alpha r - 10 \log_{10} \frac{P_t G_0^2 \lambda^2}{16\pi^2} - 10 \log_{10} \frac{c\tau\psi}{2} - 2s_{ac}$$

$$\text{(A.1)}$$

---

[1]Ex60 Power, Power to Sv and TS, Echoview Help file 10.0.38 for Echoview 10.0.257, https://tinyurl.com/y28sn3lg, accessed September 2019.

Table A.1: Symbols, terms and units.

Symbol	Description	Units
r	Range	m
R	Corrected range	m
P_r	Received power	dB re 1 W
P_t	Transmitted power	W
α	Absorption coefficient	dB/m
G_0	Transducer peak gain	Non-dimensional
λ	Wavelength ($\lambda = \frac{c}{f}$)	m
f	Frequency	Hz
c	Sound speed	ms^{-1}
τ	Transmit pulse duration	s
ψ	Equivalent Two-way beam angle	Steradians
S_{ac}	Correction factor, determined during calibration	dB re $1m^{-1}$
S_v	Volume backscaterring strength	dB re $1m^{-1}$

Appendix B

Western Core Box calibration corrections

Calibration corrections (S_{ac}) were determined annually using standard sphere techniques (Demer *et al.*, 2015). Sound speed (c) and absorption (α) were determined from cruise CTD stations undertaken during each cruise (Francois and Garrison, 1982), averaged over the top 250 m of the water column. The calibration corrections used for Western Core Box data are listed in Table B.1.

Table B.1: Western Core Box survey calibration correction parameters for 38 and 120 kHz data by year. c is the speed of sound in seawater, α is the absorption coefficient, G_0 is the transducer gain and S_{ac} the calibration correction.

Season	Cruise	c	α_{38}	$G_{0_{38}}$	$S_{ac_{38}}$	α_{120}	$G_{0_{120}}$	$S_{ac_{120}}$
2003	JR82	1456	0.0104	24.19	-0.07	0.02793	22.43	-0.42
2003	JR82	1456	0.0104	24.19	-0.07	0.02793	22.43	-0.42
2004	JR96	1461	0.01012	24.18	-0.61	0.02648	21.25	-0.42
2005	JR116	1460	0.01014	24.14	-0.58	0.02665	20.23	-0.45
2006	JR140	1461	0.01017	24.24	-0.64	0.02683	21.31	-0.38
2007	JR162	1462	0.01014	24.07	-0.63	0.02683	21.31	-0.4
2009	JR188	1462	0.01014	23.89	-0.6	0.02683	22.16	-0.39
2010	JR228	1462	0.01014	26	-0.52	0.02683	21.7	-0.43
2011	JR245	1459	0.010396	25.62	-0.51	0.02868	22.09	-0.4
2012	JR260	1456.04	0.01043	25.51	-0.52	0.027516	22.15	-0.41
2013	JR280	1462	0.010072	25.71	-0.51	0.028156	22.17	-0.42
2014	JR291	1453.57	0.010435	25.53	-0.49	0.027352	21.79	-0.45
2015	JR304	1452.94	0.010425	25.65	-0.54	0.027207	23.29	-0.45
2016	JR15002	1452	0.010416	25.66	-0.55	0.026998	23.38	-0.29
2017	JR16003	1451.38	0.010390	25.72	-0.52	0.026844	23.72	-0.27
2018	JR17002	1455.79	0.010456	25.66	-0.52	0.027872	23.4	-0.24
2019	DY098	1455.32	0.010461	25.94	-0.64	0.027767	27.07	-0.41

Appendix C

Colour composite echograms

C.1   Introduction

In this appendix, we outline a method for finding two- and three-dimensional perceptually uniform colour spaces where all constituent colours are contained within the sRGB colour gamut. These colour spaces can be used to construct colour composite echograms combining multi-frequency acoustic data such as that shown in Figure 7.1. This work builds on the methods in Chapter 3 and is an intriguing future research direction.

C.2   Method

An echogram is a matrix of signal values indexed by depth or range and along-track distance. When combining echograms, we require that they share common axes and if necessary, we reproject, resample or interpolate data to achieve this. We denote the combined multi-dimensional echogram data as $X(i, j, k)$, where i is the range index, j the along-track distance index and k the individual echogram index. We map $X(i, j, k)$ to pixels $c(i, j)$ to form a digital image.

If our multi-dimensional echogram has three dimensions ($k = \{1, 2, 3\}$) then we could treat CIELAB as a vector space, and naively map each k in to L^*,

a^* and b^* respectively to find colours whose distances in CIELAB space are proportional to distances in measurement space. Unfortunately, not all combinations of L^*, a^* and b^* can be displayed or printed and so extreme values become saturated. In order to determine the colour gamut (the full range of colours available on a device), we generated all combinations of 24-bit sRGB colours ($r \in \{0, 1, ..255\}$, $g \in \{0, 1, ..255\}$, $b \in \{0, 1, ..255\}$) and converted them to CIELAB using the PerceptualColourMaps.jl software library[1] (Figure C.1).
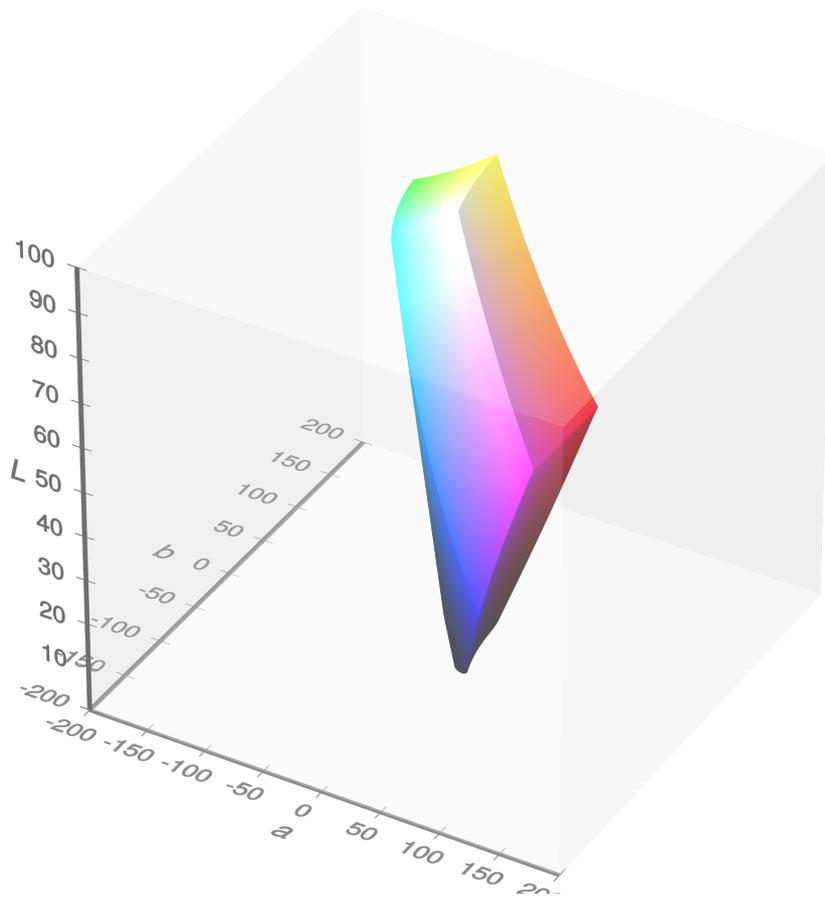
Figure C.1: The sRGB colour gamut plotted in CIELAB space under D65 illumination (courtesy Michael Horvath, Christoph Lipka, CC BY-SA https://creativecommons.org/licenses/by-sa/4.0).

---

[1]https://github.com/peterkovesi/PerceptualColourMaps.jl, accessed April 2020.

To stay within the colour gamut we must transform coordinates into a subspace within CIELAB. In three-dimensional geometry, coordinate transformations can be expressed as a matrix. Applying this to CIELAB space, we have scaling (C.1), rotation around the a^* axis (C.2), rotation around the b^* axis (C.3), rotation around the L^* axis (C.4) and finally, translation (C.5). We would like to find large cuboids within the gamut and map X(i,j,k) into that cuboid's vector space. If each of the three dimensions in k is of equal perceptual importance, then we need to find a cube. For two dimensional echograms ($k = \{1, 2\}$), we must find a rectangle whose edges all lie within the gamut. If each of the two dimensions in k is of equal perceptual importance, then we need to find a square.

$$S = \begin{pmatrix} sx & 0 & 0 & 0 \\ 0 & sy & 0 & 0 \\ 0 & 0 & sz & 0 \\ 0 & 0 & 0 & 1 \end{pmatrix} \tag{C.1}$$

$$R_x = \begin{pmatrix} 1 & 0 & 0 & 0 \\ 0 & \cos\theta_x & -\sin\theta_x & 0 \\ 0 & \sin\theta_x & \cos\theta_x & 0 \\ 0 & 0 & 0 & 1 \end{pmatrix} \tag{C.2}$$

$$R_y = \begin{pmatrix} \cos\theta_y & 0 & \sin\theta_y & 0 \\ 0 & 1 & 0 & 0 \\ -\sin\theta_y & 0 & \cos\theta_y & 0 \\ 0 & 0 & 0 & 1 \end{pmatrix} \tag{C.3}$$

$$R_z = \begin{pmatrix} \cos\theta_z & -\sin\theta_z & 0 & 0 \\ \sin\theta_z & \cos\theta_z & 0 & 0 \\ 0 & 0 & 1 & 0 \\ 0 & 0 & 0 & 1 \end{pmatrix} \tag{C.4}$$

$$
T = \begin{pmatrix} 1 & 0 & 0 & tx \\ 0 & 1 & 0 & ty \\ 0 & 0 & 1 & tz \\ 0 & 0 & 0 & 1 \end{pmatrix}
\tag{C.5}
$$

$$
M = T \cdot R_x \cdot R_y \cdot R_z \cdot S
\tag{C.6}
$$

Where only one dimension of k relates to intensity, the cuboid, cube, rectangle or square can be aligned with one axis parallel to L^*. Where all dimensions in k include an intensity component, we require that the diagonal of the square or rectangle aligns with L^*.

We search for rectangles and squares with the largest areas and cuboids and cubes with the largest volumes. We generate candidate geometries in CIELAB space and test whether they fall within the gamut. To make the computation tractable, we limit L^*, a^* and b^* to integer values.

C.3 Results

The sRGB colour gamut extent measured in CIELAB space was found to be $0 < L* < 100.00$, $-86.18 < a* < 98.23$ and $-107.86 < b* < 94.48$. Thus a naive transformation from $X(i, j, k)$ into L^*, a^* and b^* is given by $tx = 0$, $ty = 0$, $tz = 0$, $\theta_x = 0$, $\theta_y = 0$, $\theta_z = 0$, $sx = 100$, $sy = 98$ and $sz = 94$.

The largest square whose diagonal aligns with the grey line was found to be described by $tx = 0$, $ty = 0$, $tz = 0$, $\theta_x = 280$, $\theta_y = 0$, $\theta_z = -45$, $sx = 71$, $sy = 71$ and $sz = 0$. This can be used to construct two-dimensional echograms where each dimension contributes equally to luminance.

The largest cube whose diagonal aligns with the grey line was found to be described by $tx = 16$, $ty = 0$, $tz = 0$, $\theta_x = 305$, $\theta_y = 35$, $\theta_z = -45$, $sx = 49$, $sy = 49$ and $sz = 49$. This can be used to construct three-dimensional echograms where each dimension contributes equally to luminance.

Appendix D

Western Core Box supplementary data

Table D.1 lists the Western Core Box survey transects used in our analyses.

Table D.1: List of Western Core Box survey transects with begin and end times in Universal Time (UTC).

Year	Transect	Begin	End
2003	2003wcbjr82_1_1	2003-02-13T08:10:00	2003-02-13T12:53:00
2003	2003wcbjr82_1_2	2003-02-13T14:07:00	2003-02-13T18:25:00
2003	2003wcbjr82_2_1	2003-02-14T08:05:00	2003-02-14T12:27:00
2003	2003wcbjr82_2_2	2003-02-14T13:39:00	2003-02-14T18:10:00
2003	2003wcbjr82_3_1	2003-02-15T08:09:00	2003-02-15T11:42:00
2003	2003wcbjr82_4_1	2003-02-16T08:11:00	2003-02-16T10:52:00
2003	2003wcbjr82_4_2	2003-02-16T11:30:00	2003-02-16T14:01:00
2004	2004wcbjr96_1_1	2004-01-08T16:45:00	2004-01-08T21:04:00
2004	2004wcbjr96_1_2	2004-01-08T09:10:00	2004-01-08T13:51:00
2004	2004wcbjr96_2_1	2004-01-09T10:00:00	2004-01-09T14:28:00
2004	2004wcbjr96_2_2	2004-01-09T16:17:00	2004-01-09T20:32:00
2004	2004wcbjr96_4_2	2004-01-12T18:38:00	2004-01-12T21:54:00
2004	2004wcbjr96_3_1	2004-01-16T07:00:00	2004-01-16T11:24:00

2004	2004wcbjr96_3_2	2004-01-16T12:40:00	2004-01-16T16:53:00
2004	2004wcbjr96_4_1	2004-01-16T17:18:00	2004-01-16T22:14:00
2005	2005wcbjr116_1_1	2005-01-06T11:20:00	2005-01-06T15:44:00
2005	2005wcbjr116_1_2	2005-01-06T17:02:00	2005-01-06T19:40:00
2005	2005wcbjr116_2_1	2005-01-07T08:30:00	2005-01-07T12:59:00
2005	2005wcbjr116_2_2	2005-01-07T14:09:00	2005-01-07T18:42:00
2005	2005wcbjr116_3_1	2005-01-08T19:02:00	2005-01-08T23:24:00
2005	2005wcbjr116_3_2	2005-01-10T06:45:00	2005-01-10T11:05:00
2005	2005wcbjr116_4_1	2005-01-10T11:57:00	2005-01-10T16:22:00
2005	2005wcbjr116_4_2	2005-01-10T17:09:00	2005-01-10T21:06:00
2006	2006wcbjr140_1_1	2005-12-29T08:56:00	2005-12-29T13:35:00
2006	2006wcbjr140_1_2	2005-12-29T14:49:00	2005-12-29T19:08:00
2006	2006wcbjr140_2_1	2005-12-30T09:10:00	2005-12-30T13:42:00
2006	2006wcbjr140_2_2	2005-12-30T15:23:00	2005-12-30T19:45:00
2006	2006wcbjr140_3_1	2005-12-31T09:00:00	2005-12-31T13:26:00
2006	2006wcbjr140_3_2	2005-12-31T14:47:00	2005-12-31T19:10:00
2006	2006wcbjr140_4_1	2006-01-01T09:18:00	2006-01-01T13:49:00
2006	2006wcbjr140_4_2	2006-01-01T14:27:00	2006-01-01T18:46:00
2007	2007wcbjr162_1_1	2006-12-25T07:00:00	2006-12-25T11:23:00
2007	2007wcbjr162_2_2	2006-12-26T17:56:00	2006-12-26T21:45:00
2007	2007wcbjr162_3_1	2006-12-27T07:00:00	2006-12-27T11:21:00
2007	2007wcbjr162_3_2	2006-12-27T12:30:00	2006-12-27T16:47:00
2007	2007wcbjr162_4_1	2006-12-27T17:24:00	2006-12-27T21:44:00
2007	2007wcbjr162_4_2	2006-12-28T07:00:00	2006-12-28T11:20:00
2009	2009wcbjr188_1_1	2008-12-31T09:05:00	2008-12-31T13:46:00
2009	2009wcbjr188_1_2	2008-12-31T14:55:00	2008-12-31T19:15:00
2009	2009wcbjr188_2_1	2009-01-01T09:03:00	2009-01-01T13:41:00
2009	2009wcbjr188_2_2	2009-01-01T14:59:00	2009-01-01T19:30:00
2009	2009wcbjr188_3_1	2009-01-02T09:00:00	2009-01-02T13:45:00
2009	2009wcbjr188_3_2	2009-01-02T14:45:00	2009-01-02T19:06:00
2009	2009wcbjr188_4_1	2009-01-03T06:30:00	2009-01-03T10:25:00
2009	2009wcbjr188_4_2	2009-01-03T11:01:00	2009-01-03T15:43:00
2010	2010wcbjr228_1_1	2009-12-20T08:00:00	2009-12-20T12:37:00

2010	2010wcbjr228_1_2	2009-12-20T13:42:00	2009-12-20T17:59:00
2010	2010wcbjr228_2_1	2009-12-21T07:58:00	2009-12-21T12:38:00
2010	2010wcbjr228_2_2	2009-12-21T13:45:00	2009-12-21T18:02:00
2010	2010wcbjr228_3_1	2009-12-22T07:46:00	2009-12-22T12:17:00
2010	2010wcbjr228_3_2	2009-12-22T13:21:00	2009-12-22T17:47:00
2010	2010wcbjr228_4_1	2009-12-23T07:40:00	2009-12-23T12:13:00
2010	2010wcbjr228_4_2	2009-12-23T12:59:00	2009-12-23T17:38:00
2011	2011wcbjr245_1_1	2010-12-26T08:58:00	2010-12-26T13:30:00
2011	2011wcbjr245_1_2	2010-12-26T14:40:00	2010-12-26T19:00:00
2011	2011wcbjr245_2_1	2010-12-27T09:26:00	2010-12-27T13:56:00
2011	2011wcbjr245_2_2	2010-12-27T15:17:00	2010-12-27T19:42:00
2011	2011wcbjr245_3_1	2010-12-28T09:05:00	2010-12-28T13:34:00
2011	2011wcbjr245_3_2	2010-12-28T14:41:00	2010-12-28T18:55:00
2011	2011wcbjr245_4_1	2010-12-30T09:00:00	2010-12-30T13:35:00
2011	2011wcbjr245_4_2	2010-12-30T14:50:00	2010-12-30T19:24:00
2012	2012wcbjr260_1_1	2012-01-02T09:00:00	2012-01-02T13:45:00
2012	2012wcbjr260_1_2	2012-01-02T14:54:00	2012-01-02T19:12:00
2012	2012wcbjr260_2_1	2012-01-03T09:00:00	2012-01-03T13:41:00
2012	2012wcbjr260_2_2	2012-01-03T14:42:00	2012-01-03T19:03:00
2012	2012wcbjr260_3_1	2012-01-04T09:00:00	2012-01-04T13:36:00
2012	2012wcbjr260_3_2	2012-01-04T14:48:00	2012-01-04T19:07:00
2012	2012wcbjr260_4_1	2012-01-05T09:00:00	2012-01-05T13:40:00
2012	2012wcbjr260_4_2	2012-01-05T14:17:00	2012-01-05T18:57:00
2013	2013wcbjr280_1_1	2012-12-01T09:01:00	2012-12-01T13:44:00
2013	2013wcbjr280_1_2	2012-12-01T14:57:00	2012-12-01T19:17:00
2013	2013wcbjr280_2_1	2012-12-02T09:00:00	2012-12-02T13:46:00
2013	2013wcbjr280_2_2	2012-12-02T14:54:00	2012-12-02T19:17:00
2013	2013wcbjr280_3_1	2012-12-03T09:00:00	2012-12-03T13:43:00
2013	2013wcbjr280_3_2	2012-12-03T15:00:00	2012-12-03T19:19:00
2013	2013wcbjr280_4_1	2012-12-04T09:30:00	2012-12-04T14:09:00
2013	2013wcbjr280_4_2	2012-12-04T14:49:00	2012-12-04T19:24:00
2014	2014wcbjr291_1_1	2013-12-09T08:00:00	2013-12-09T12:31:00
2014	2014wcbjr291_1_2	2013-12-09T13:40:00	2013-12-09T18:00:00

2014	2014wcbjr291_2_1	2013-12-10T08:00:00	2013-12-10T12:29:00
2014	2014wcbjr291_2_2	2013-12-10T13:40:00	2013-12-10T18:00:00
2014	2014wcbjr291_3_1	2013-12-11T08:30:00	2013-12-11T13:02:00
2014	2014wcbjr291_3_2	2013-12-11T14:03:00	2013-12-11T18:28:00
2014	2014wcbjr291_4_1	2013-12-12T08:05:00	2013-12-12T12:42:00
2014	2014wcbjr291_4_2	2013-12-12T13:13:00	2013-12-12T17:45:00
2015	2015wcbjr304_1_1	2014-12-08T09:06:00	2014-12-08T13:49:00
2015	2015wcbjr304_1_2	2014-12-08T15:00:00	2014-12-08T19:21:00
2015	2015wcbjr304_2_1	2014-12-09T09:41:00	2014-12-09T14:28:00
2015	2015wcbjr304_2_2	2014-12-09T15:32:00	2014-12-09T19:58:00
2015	2015wcbjr304_3_1	2014-12-10T09:00:00	2014-12-10T13:36:00
2015	2015wcbjr304_3_2	2014-12-10T14:37:00	2014-12-10T18:46:00
2015	2015wcbjr304_4_1	2014-12-11T09:00:00	2014-12-11T13:37:00
2015	2015wcbjr304_4_2	2014-12-11T14:12:00	2014-12-11T18:56:00
2016	2016wcbjr15002_1_1	2015-12-03T09:07:00	2015-12-03T13:30:00
2016	2016wcbjr15002_1_2	2015-12-03T14:45:00	2015-12-03T19:04:00
2016	2016wcbjr15002_2_1	2015-12-04T09:30:00	2015-12-04T14:07:00
2016	2016wcbjr15002_2_2	2015-12-04T15:10:00	2015-12-04T19:30:00
2016	2016wcbjr15002_3_1	2015-12-05T09:06:00	2015-12-05T13:30:00
2016	2016wcbjr15002_3_2	2015-12-05T15:08:00	2015-12-05T19:12:00
2016	2016wcbjr15002_4_1	2015-12-06T09:10:00	2015-12-06T13:40:00
2016	2016wcbjr15002_4_2	2015-12-06T14:25:00	2015-12-06T18:59:00
2017	2017wcbjr16003_1_1	2016-12-20T09:00:00	2016-12-20T13:41:00
2017	2017wcbjr16003_1_2	2016-12-20T14:42:00	2016-12-20T19:00:00
2017	2017wcbjr16003_2_1	2016-12-21T09:00:00	2016-12-21T13:44:00
2017	2017wcbjr16003_2_2	2016-12-21T14:44:00	2016-12-21T19:02:00
2017	2017wcbjr16003_3_1	2016-12-22T09:00:00	2016-12-22T15:56:00
2017	2017wcbjr16003_3_2	2016-12-22T17:05:00	2016-12-22T21:30:00
2017	2017wcbjr16003_4_1	2016-12-23T08:00:00	2016-12-23T13:24:00
2017	2017wcbjr16003_4_2	2016-12-23T14:09:00	2016-12-23T18:43:00
2018	2018wcbjr17002_1_1	2018-01-08T09:30:00	2018-01-08T14:06:00
2018	2018wcbjr17002_1_2	2018-01-08T15:15:00	2018-01-08T19:37:00
2018	2018wcbjr17002_2_1	2018-01-09T09:08:00	2018-01-09T13:36:00

2018	2018wcbjr17002_2_2	2018-01-09T14:45:00	2018-01-09T19:21:00
2018	2018wcbjr17002_3_1	2018-01-10T09:00:00	2018-01-10T13:28:00
2018	2018wcbjr17002_3_2	2018-01-10T14:48:00	2018-01-10T19:08:00
2018	2018wcbjr17002_4_1	2018-01-11T09:00:00	2018-01-11T13:27:00
2018	2018wcbjr17002_4_2	2018-01-11T14:08:00	2018-01-11T18:38:00
2019	2019wcbdy098_1_1	2019-01-07T09:06:00	2019-01-07T13:47:00
2019	2019wcbdy098_1_2	2019-01-07T15:13:00	2019-01-07T21:17:00
2019	2019wcbdy098_2_1	2019-01-08T09:07:38	2019-01-08T12:34:00
2019	2019wcbdy098_2_2	2019-01-08T13:45:00	2019-01-08T18:31:00
2019	2019wcbdy098_3_1	2019-01-09T09:35:00	2019-01-09T14:55:00
2019	2019wcbdy098_3_2	2019-01-09T16:13:00	2019-01-09T20:30:00
2019	2019wcbdy098_4_1	2019-01-10T08:55:00	2019-01-10T14:01:00
2019	2019wcbdy098_4_2	2019-01-10T14:39:00	2019-01-10T19:34:00

Appendix E

Western Core Box spatial analysis

A key output from chapter 4 is a database of Echometrics by ping. The data also include Global Positioning System (GPS) coordinates and bathymetry (using data from Hogg *et al.*, 2016) enabling various kinds of geospatial analysis outside the scope of this thesis. As an example, Figure E.1 considers the spatial distribution of *abundance* for all surveys, throughout the Western Core Box survey area.

Regions of high *abundance* tend to occur on the shelf and in those transects closest to land (Figure E.2). These results are consistent with Silk *et al.* (2016) who note that the krill fishery is currently concentrated in shelf areas, where high densities of krill are most predictable. The map appears to show *abundance* concentrations over gullies and areas of rapid change in bathymetry (Figure E.1).
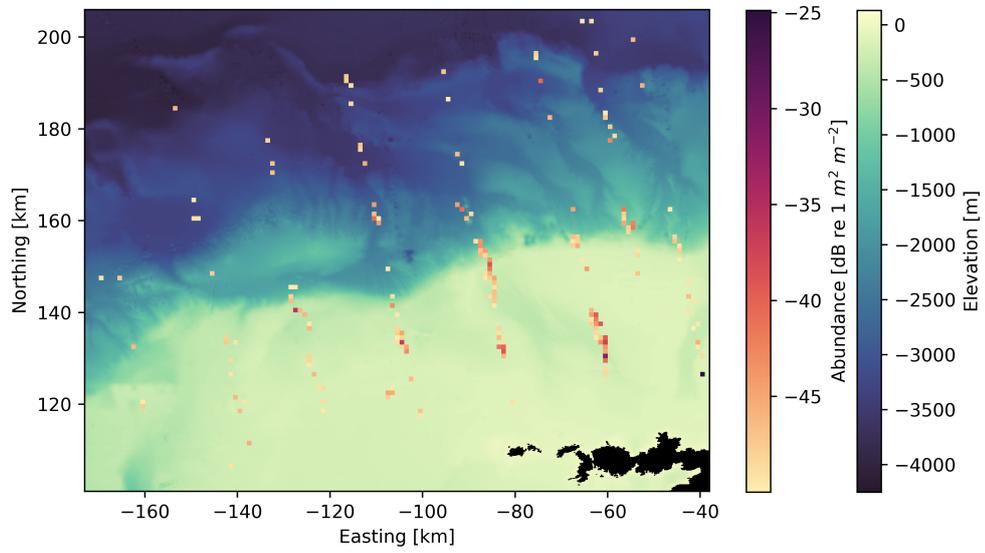
Figure E.1: Abundance along transect lines. Regions of high abundance are shown on a $1\,\text{km}^2$ grid over SGBD baythmetry using a South Georgia Lambert projection.
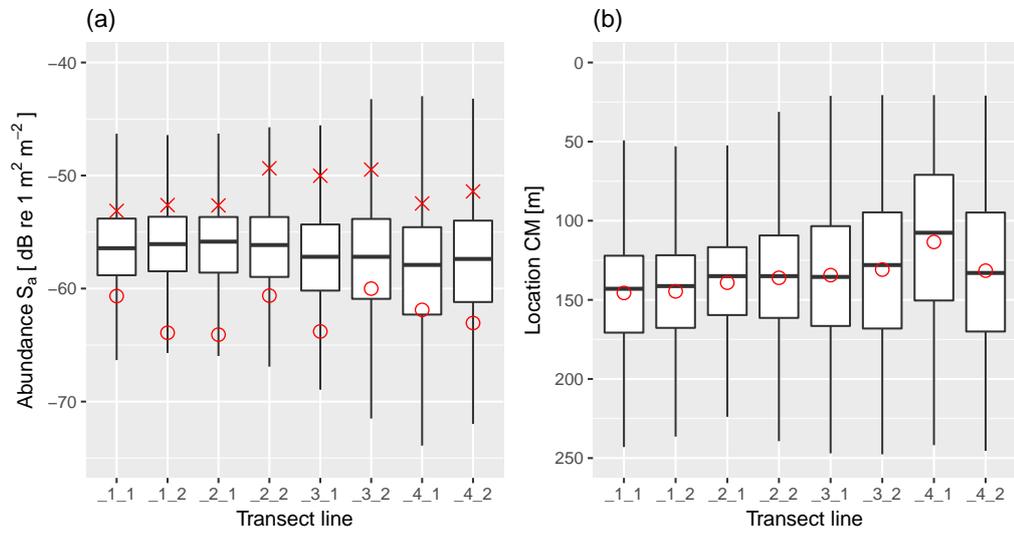
Figure E.2: Comparison of transect lines, using (a) abundance and (b) location. The boxes show the first quartile, median and third quartile. o marks the mean. × marks the mean computed in the linear domain.

Appendix F

Simrad EK60 split-beam angle anomalies

During our analysis of Simrad EK60 echosounder data, we repeatedly saw peaks in the histograms of split-beam angle at data values -96, -32, 32 and 96 (measurements in raw, signed 8 bit integers), see Figure F.1. These appeared to be randomly distributed spatially. We saw the same effect in both along-ship and athwart-ship data for 38 kHz and 120 kHz.

We looked at data from three different EK60 instruments on three different research vessels, and the effect was seen in all three. We did not observe the effect in Simrad EK80 data.

We raised the issue with Simrad and they acknowledged the problem. It seems suspicious that these values are 64 apart given the 8-bit integer representation and a bug in the analogue to digital conversion is suspected.

Future researchers should also be aware that there is a recently discovered non-linearity in the Simrad EK60 instrument documented by De Robertis *et al.* (2019).
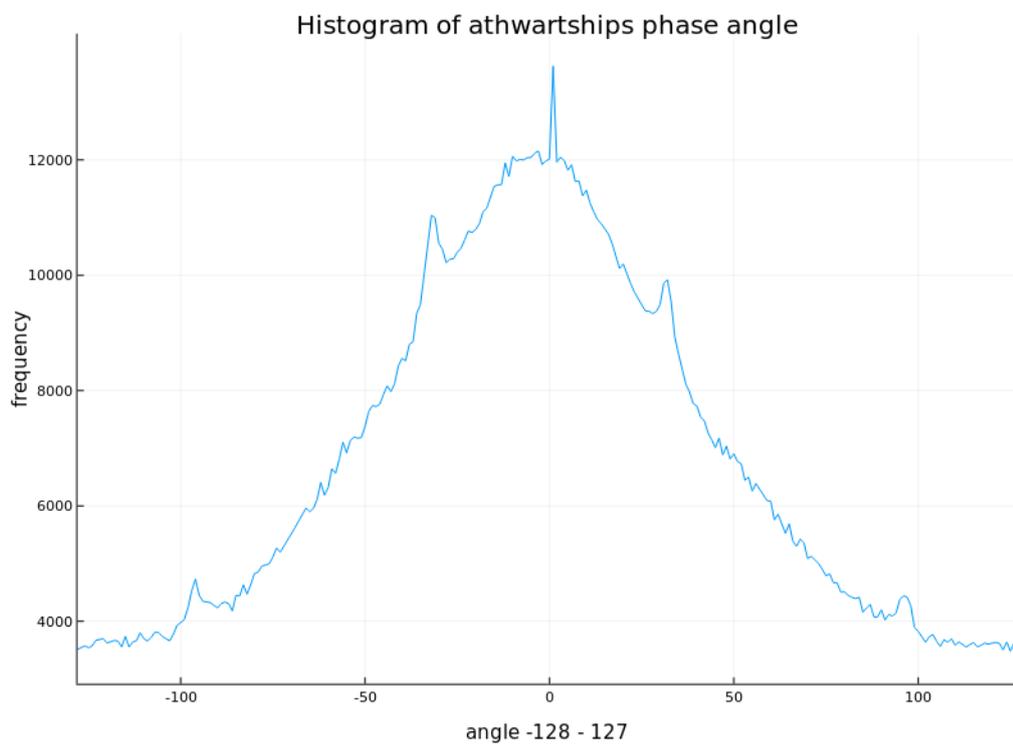
Figure F.1: Histogram of athwartship angle data, 38 kHz, RRS James Clark Ross.

Appendix G

The impact of averaging fisheries acoustic data

G.1 Introduction

Data binning (sometimes called bucketing) partitions an ordered set of samples $X = \{x_1, x_2, ..., x_n\}$ into k bins and presents a summary statistic for each bin $Y = \{\bar{y}_1, \bar{y}_2, ...\bar{y}_k\}$. Data binning is used extensively in fisheries acoustic data processing, for at least four reasons:

1. It reduces the resolution and size of the data ($k < n$), making it easier to store on disk and faster to load and process;

2. It can reduce the effect of noise extrema by smoothing the data (especially if using the median as a summary statistic) (Ryan *et al.*, 2015);

3. It helps to address the linearity principle which requires a minimum number of samples to ensure stochasticity of animal orientation (Simmonds and MacLennan, 2005, p. p191);

4. It creates "elementary distance sampling units" (EDSU) where samples are averaged to reduce the effects of aliasing and local variability (Simmonds and MacLennan, 2005, p. p324).

Bin sizes are often selected based on an EDSU distance measure, e.g. 500 m. If the ship is travelling at 10 knots and the inter ping time $I_T = 2\,\text{s}$ then each bin should include 50 samples. In practice, it is difficult to maintain a constant 10 knots and bin sizes are variable. Ideally bins should have equal numbers of samples, so that $\bar{X} = \bar{Y}$. Data binning is known to be a potential cause of error in statistical analyses (Towers, 2014). Here we show that problems can be substantial when working with fisheries acoustic data.

G.2 Method

Consider an 80.25 km acoustic transect, with backscattering samples (S_v) recorded every 10 m. Set each of the 8025 samples to $-999\,\text{dB}$, except pings 7999 and 8025 which are set to $-60\,\text{dB}$.

Calculate the mean S_v for all samples. Repeat for 250 m bins and 500 m bins.

Repeat the analysis discarding the last 0.25 km partial EDSU.

G.3 Results

Table G.1: The effect of varying bin size on mean volume backscattering coefficient.

Bins	Mean S_v (dB)
None	-96
250 m	-89
500 m	-86

When discarding the last 0.25 km, the result is $-99\,\text{dB}$.

G.4 Discussion

When bins are unequal, choice of bin size made a 10 dB difference to our results. The mean is highly sensitive to outliers, and this is especially true of

acoustic data which has a high dynamic range (usually measured in decibels). Although this example uses synthetic data, we see that failure to remove noise or to include or exclude a bin with Antarctic krill, could make a large difference to results.

Smaller data sizes are easier to work with, using less disk space, memory and computational capacity. In the early days of echosounders, data was processed with primitive computers and lack of computational resources was a legitimate concern. These days, computers have large amounts of memory (16 GB is typical): an 80 km transect recorded to 1000 m might yield approximately 1 GB of data, well within the capability of modern computers.

The linearity principle can be accommodated by blurring data, perhaps using convolution from image processing.

Studies should consider the possible effects of aliasing caused by successive ping beams overlapping, and may wish to reduce the effects of local variability. However, averaging over large elementary distance sampling units is a crude solution. We suggest that computational power is now sufficient to construct geometrically correct echograms which could allow anti-aliasing algorithms to be developed. Maintaining data resolution throughout pre-processing allows the sensitivity of results to subsequent averaging to be carefully assessed.

G.5   Conclusions

Whilst there are legitimate reasons for averaging acoustic data samples, the use of averaging should be considered carefully based on physical principles and survey objectives. In many cases, especially when computing those acoustic metrics measuring patchiness and distribution, it may be advantageous to retain the native resolution of the data.

Appendix H

One hundred ICES fisheries acoustics articles

In Chapters 3 and 6, we examined one hundred journal papers matching the search term "fisheries echogram", published after 2009 in the ICES Journal of Marine Science. Here is that list[1]:

1. Ronan Fablet, Riwal Lefort, Imen Karoui, Laurent Berger, Jacques Massé, Carla Scalabrin, Jean-Marc Boucher, Classifying fish schools and estimating their species proportions in fishery-acoustic surveys, ICES Journal of Marine Science, Volume 66, Issue 6, July 2009, Pages 1136–1142, https://doi.org/10.1093/icesjms/fsp109.

2. Vasilis Trygonis, Zacharias Kapelonis, Corrections of fish school area and mean volume backscattering strength by simulation of an omnidirectional multi-beam sonar, ICES Journal of Marine Science, Volume 75, Issue 4, July-August 2018, Pages 1496–1508, https://doi.org/10.1093/icesjms/fsy009.

3. Paul G. Fernandes, Phillip Copland, Rafael Garcia, Tudor Nicosevici, Ben Scoulding, Additional evidence for fisheries acoustics: small

---

[1] https://github.com/RobBlackwell/hundred-fisheries-acoustic-papers, retrieved November 2019.

cameras and angling gear provide tilt angle distributions and other relevant data for mackerel surveys, ICES Journal of Marine Science, Volume 73, Issue 8, September 2016, Pages 2009–2019, https://doi.org/10.1093/icesjms/fsw091.

4. David A. Demer, Rudy J. Kloser, David N. MacLennan, Egil Ona, An introduction to the proceedings and a synthesis of the 2008 ICES Symposium on the Ecosystem Approach with Fisheries Acoustics and Complementary Technologies (SEAFACTS), ICES Journal of Marine Science, Volume 66, Issue 6, July 2009, Pages 961–965, https://doi.org/10.1093/icesjms/fsp146.

5. Rolf J. Korneliussen, The acoustic identification of Atlantic mackerel, ICES Journal of Marine Science, Volume 67, Issue 8, November 2010, Pages 1749–1758, https://doi.org/10.1093/icesjms/fsq052.

6. Lars G. Rudstam, Sandra L. Parker-Stetter, Patrick J. Sullivan, David M. Warner, Towards a standard operating procedure for fishery acoustic surveys in the Laurentian Great Lakes, North America, ICES Journal of Marine Science, Volume 66, Issue 6, July 2009, Pages 1391–1397, https://doi.org/10.1093/icesjms/fsp014.

7. David N. MacLennan, Reflections on technology and science in fishery research, ICES Journal of Marine Science, Volume 74, Issue 8, September-October 2017, Pages 2069–2075, https://doi.org/10.1093/icesjms/fsx045.

8. Susan B. Fudge, George A. Rose, Passive- and active-acoustic properties of a spawning Atlantic cod (Gadus morhua) aggregation, ICES Journal of Marine Science, Volume 66, Issue 6, July 2009, Pages 1259–1263, https://doi.org/10.1093/icesjms/fsp097.

9. Masahiko Furusawa, Kazuo Amakasu, The analysis of echotrace obtained by a split-beam echosounder to observe the tilt-angle dependence of fish target strength in situ, ICES Journal of Marine Science, Volume 67, Issue 2, March 2010, Pages 215–230, https://doi.org/10.1

093/icesjms/fsp246.

10. Niall G. Fallon, Sophie Fielding, Paul G. Fernandes, Classification of Southern Ocean krill and icefish echoes using random forests, ICES Journal of Marine Science, Volume 73, Issue 8, September 2016, Pages 1998–2008, https://doi.org/10.1093/icesjms/fsw057.

11. Ariel G. Cabreira, Martín Tripode, Adrián Madirolas, Artificial neural networks for fish-species identification, ICES Journal of Marine Science, Volume 66, Issue 6, July 2009, Pages 1119–1129, https://doi.org/10.1093/icesjms/fsp009.

12. Vasilis Trygonis, Stratis Georgakarakos, E. John Simmonds, An operational system for automatic school identification on multibeam sonar echoes, ICES Journal of Marine Science, Volume 66, Issue 5, June 2009, Pages 935–949, https://doi.org/10.1093/icesjms/fsp135.

13. Ruben Patel, Egil Ona, Measuring herring densities with one real and several phantom research vessels, ICES Journal of Marine Science, Volume 66, Issue 6, July 2009, Pages 1264–1269, https://doi.org/10.1093/icesjms/fsp128.

14. Christopher Bassett, Alex De Robertis, Christopher D Wilson, Broadband echosounder measurements of the frequency response of fishes and euphausiids in the Gulf of Alaska, ICES Journal of Marine Science, Volume 75, Issue 3, May-June 2018, Pages 1131–1142, https://doi.org/10.1093/icesjms/fsx204.

15. G. Boyra, U. Martínez, U. Cotano, M. Santos, X. Irigoien, A. Uriarte, Acoustic surveys for juvenile anchovy in the Bay of Biscay: abundance estimate as an indicator of the next year's recruitment and spatial distribution patterns, ICES Journal of Marine Science, Volume 70, Issue 7, November 2013, Pages 1354–1368, https://doi.org/10.1093/icesjms/fst096.

16. Jeroen van der Kooij, Sascha M.M. Fässler, David Stephens, Lisa Readdy, Beth E. Scott, Beatriz A. Roel, Opportunistically recorded

acoustic data support Northeast Atlantic mackerel expansion theory, ICES Journal of Marine Science, Volume 73, Issue 4, March/April 2016, Pages 1115–1126, https://doi.org/10.1093/icesjms/fsv243.

17. Serdar Sakınan, Ali Cemal Gücü, Spatial distribution of the Black Sea copepod, Calanus euxinus, estimated using multi-frequency acoustic backscatter, ICES Journal of Marine Science, Volume 74, Issue 3, March-April 2017, Pages 832–846, https://doi.org/10.1093/icesjms/fsw183.

18. Olav Rune Godø, Nils Olav Handegard, Howard I. Browman, Gavin J. Macaulay, Stein Kaartvedt, Jarl Giske, Egil Ona, Geir Huse, Espen Johnsen, Marine ecosystem acoustics (MEA): quantifying processes in the sea at the spatio-temporal scales on which they occur, ICES Journal of Marine Science, Volume 71, Issue 8, October 2014, Pages 2357–2369, https://doi.org/10.1093/icesjms/fsu116.

19. Joshua M. Lawrence, Eric Armstrong, Jonathan Gordon, Susan Mærsk Lusseau, Paul G. Fernandes, Passive and active, predator and prey: using acoustics to study interactions between cetaceans and forage fish, ICES Journal of Marine Science, Volume 73, Issue 8, September 2016, Pages 2075–2084, https://doi.org/10.1093/icesjms/fsw013.

20. Verena M. Trenkel, Nils Olav Handegard, Thomas C. Weber, Observing the ocean interior in support of integrated management, ICES Journal of Marine Science, Volume 73, Issue 8, September 2016, Pages 1947–1954, https://doi.org/10.1093/icesjms/fsw132.

21. Ben Scoulding, Sven Gastauer, David N. MacLennan, Sascha M. M. Fässler, Phillip Copland, Paul G. Fernandes, Effects of variable mean target strength on estimates of abundance: the case of Atlantic mackerel (Scomber scombrus), ICES Journal of Marine Science, Volume 74, Issue 3, March-April 2017, Pages 822–831, https://doi.org/10.1093/icesjms/fsw212.

22. François Gerlotto, Sixteen lessons from a 40-year quest to understand

the mysterious life of the grey triggerfish, ICES Journal of Marine Science, Volume 74, Issue 9, November/December 2017, Pages 2321–2332, https://doi.org/10.1093/icesjms/fsx086.

23. Sindre Vatnehol, Hector Peña, Nils Olav Handegard, A method to automatically detect fish aggregations using horizontally scanning sonar, ICES Journal of Marine Science, Volume 75, Issue 5, September-October 2018, Pages 1803–1812, https://doi.org/10.1093/icesjms/fsy029.

24. Ian H. McQuinn, Maxime Dion, Jean-François St. Pierre, The acoustic multifrequency classification of two sympatric euphausiid species (Meganyctiphanes norvegica and Thysanoessa raschii), with empirical and SDWBA model validation, ICES Journal of Marine Science, Volume 70, Issue 3, April 2013, Pages 636–649, https://doi.org/10.1093/icesjms/fst004.

25. Carla Scalabrin, Christian Marfia, Jean Boucher, How much fish is hidden in the surface and bottom acoustic blind zones?, ICES Journal of Marine Science, Volume 66, Issue 6, July 2009, Pages 1355–1363, https://doi.org/10.1093/icesjms/fsp136.

26. Carrie C. Wall, J. Michael Jech, Susan J. McLean, Increasing the accessibility of acoustic data through global access and imagery, ICES Journal of Marine Science, Volume 73, Issue 8, September 2016, Pages 2093–2103, https://doi.org/10.1093/icesjms/fsw014.

27. Laurent Berger, Cyrille Poncelet, Verena M. Trenkel, A method for reducing uncertainty in estimates of fish-school frequency response using data from multifrequency and multibeam echosounders, ICES Journal of Marine Science, Volume 66, Issue 6, July 2009, Pages 1155–1161, https://doi.org/10.1093/icesjms/fsp113.

28. Takeshi Nakamura, Akira Hamano, Seasonal differences in the vertical distribution pattern of Japanese jack mackerel, Trachurus japonicus: changes according to age?, ICES Journal of Marine Science, Volume

66, Issue 6, July 2009, Pages 1289–1295, https://doi.org/10.1093/ic
esjms/fsp114.

29. Sébastien Bourguignon, Laurent Berger, Carla Scalabrin, Ronan Fa-
blet, Valérie Mazauric, Methodological developments for improved
bottom detection with the ME70 multibeam echosounder, ICES Jour-
nal of Marine Science, Volume 66, Issue 6, July 2009, Pages 1015–1022,
https://doi.org/10.1093/icesjms/fsp089.

30. Espen Johnsen, Ronald Pedersen, Egil Ona, Size-dependent frequency
response of sandeel schools, ICES Journal of Marine Science, Volume
66, Issue 6, July 2009, Pages 1100–1105, https://doi.org/10.1093/ic
esjms/fsp091.

31. Gary D. Melvin, Observations of in situ Atlantic bluefin tuna (Thun-
nus thynnus) with 500-kHz multibeam sonar, ICES Journal of Ma-
rine Science, Volume 73, Issue 8, September 2016, Pages 1975–1986,
https://doi.org/10.1093/icesjms/fsw077.

32. Teunis Jansen, Kasper Kristensen, Jeroen van der Kooij, Søren Post,
Andrew Campbell, Kjell Rong Utne, Pablo Carrera, Jan Arge Jacob-
sen, Asta Gudmundssdottir, Beatriz A. Roel, Emma M. C. Hatfield,
Nursery areas and recruitment variation of Northeast Atlantic mack-
erel (Scomber scombrus), ICES Journal of Marine Science, Volume
72, Issue 6, July/August 2015, Pages 1779–1789, https://doi.org/10.1
093/icesjms/fsu186.

33. Mathieu Doray, Pierre Petitgas, Laetitia Nelson, Stéphanie Mahévas,
Erwan Josse, Lionel Reynal, The influence of the environment on the
variability of monthly tuna biomass around a moored, fish-aggregating
device, ICES Journal of Marine Science, Volume 66, Issue 6, July 2009,
Pages 1410–1416, https://doi.org/10.1093/icesjms/fsp039.

34. Tim E. Ryan, Rudy J. Kloser, Gavin J. Macaulay, Measurement and
visual verification of fish target strength using an acoustic-optical sys-
tem attached to a trawlnet, ICES Journal of Marine Science, Volume

66, Issue 6, July 2009, Pages 1238–1244, https://doi.org/10.1093/icesjms/fsp122.

35. Steven J. Barbeaux, John K. Horne, Martin W. Dorn, Characterizing walleye pollock (Theragra chalcogramma) winter distribution from opportunistic acoustic data, ICES Journal of Marine Science, Volume 70, Issue 6, September 2013, Pages 1162–1173, https://doi.org/10.1093/icesjms/fst052.

36. Maria Tenningen, Gavin J. Macaulay, Guillaume Rieucau, Héctor Peña, Rolf J. Korneliussen, Behaviours of Atlantic herring and mackerel in a purse-seine net, observed using multibeam sonar, ICES Journal of Marine Science, Volume 74, Issue 1, January-February 2017, Pages 359–368, https://doi.org/10.1093/icesjms/fsw159.

37. M. Pilar Tugores, Magdalena Iglesias, Núria Díaz, Dolores Oñate, Joan Miquel, Ana Giráldez, Latitudinal and interannual distribution of the European anchovy (Engraulis encrasicolus) and sardine (Sardina pilchardus) in the western Mediterranean, and sampling uncertainty in abundance estimates, ICES Journal of Marine Science, Volume 67, Issue 8, November 2010, Pages 1574–1586, https://doi.org/10.1093/icesjms/fsq057.

38. Alex De Robertis, Nils Olav Handegard, Fish avoidance of research vessels and the efficacy of noise-reduced vessels: a review, ICES Journal of Marine Science, Volume 70, Issue 1, January 2013, Pages 34–45, https://doi.org/10.1093/icesjms/fss155.

39. Donhyug Kang, Sungho Cho, Changwon Lee, Jung-Goo Myoung, Jungyul Na, Ex situ target-strength measurements of Japanese anchovy (Engraulis japonicus) in the coastal Northwest Pacific, ICES Journal of Marine Science, Volume 66, Issue 6, July 2009, Pages 1219–1224, https://doi.org/10.1093/icesjms/fsp042.

40. Rudy J. Kloser, Tim E. Ryan, Jock W. Young, Mark E. Lewis, Acoustic observations of micronekton fish on the scale of an ocean basin:

potential and challenges, ICES Journal of Marine Science, Volume 66, Issue 6, July 2009, Pages 998–1006, https://doi.org/10.1093/icesjms/fsp077.

41. Miles J. G. Parsons, Iain M. Parnum, Robert D. McCauley, Visualizing Samsonfish (Seriola hippos) with a Reson 7125 Seabat multibeam sonar, ICES Journal of Marine Science, Volume 70, Issue 3, April 2013, Pages 665–674, https://doi.org/10.1093/icesjms/fst009.

42. Atle Totland, Geir O. Johansen, Olav R. Godø, Egil Ona, Terje Torkelsen, Quantifying and reducing the surface blind zone and the seabed dead zone using new technology, ICES Journal of Marine Science, Volume 66, Issue 6, July 2009, Pages 1370–1376, https://doi.org/10.1093/icesjms/fsp037.

43. Kelly J. Benoit-Bird, The effects of scattering-layer composition, animal size, and numerical density on the frequency response of volume backscatter, ICES Journal of Marine Science, Volume 66, Issue 3, April 2009, Pages 582–593, https://doi.org/10.1093/icesjms/fsp013.

44. Tim E. Ryan, Ryan A. Downie, Rudy J. Kloser, Gordon Keith, Reducing bias due to noise and attenuation in open-ocean echo integration data, ICES Journal of Marine Science, Volume 72, Issue 8, September/October 2015, Pages 2482–2493, https://doi.org/10.1093/icesjms/fsv121.

45. Paul G. Fernandes, Classification trees for species identification of fish-school echotraces, ICES Journal of Marine Science, Volume 66, Issue 6, July 2009, Pages 1073–1080, https://doi.org/10.1093/icesjms/fsp060.

46. Thomas Axenrot, Martin Ogonowski, Alfred Sandström, Tomas Didrikas, Multifrequency discrimination of fish and mysids, ICES Journal of Marine Science, Volume 66, Issue 6, July 2009, Pages 1106–1110, https://doi.org/10.1093/icesjms/fsp131.

47. Tim E. Ryan, Rudy J. Kloser, Improved estimates of orange roughy biomass using an acoustic-optical system in commercial trawlnets,

ICES Journal of Marine Science, Volume 73, Issue 8, September 2016, Pages 2112–2124, https://doi.org/10.1093/icesjms/fsw009.

48. Amanda M. Kaltenberg, Kelly J. Benoit-Bird, Intra-patch clustering in mysid swarms revealed through multifrequency acoustics, ICES Journal of Marine Science, Volume 70, Issue 4, July 2013, Pages 883–891, https://doi.org/10.1093/icesjms/fst034.

49. G Boyra, G Moreno, B Orue, B Sobradillo, I Sancristobal, In situ target strength of bigeye tuna (Thunnus obesus) associated with fish aggregating devices, ICES Journal of Marine Science, Volume 76, Issue 7, December 2019, Pages 2446–2458, https://doi.org/10.1093/icesjms/fsz131.

50. Tanya R. Graham, James T. Harvey, Scott R. Benson, Josiah S. Renfree, David A. Demer, The acoustic identification and enumeration of scyphozoan jellyfish, prey for leatherback sea turtles (Dermochelys coriacea), off central California, ICES Journal of Marine Science, Volume 67, Issue 8, November 2010, Pages 1739–1748, https://doi.org/10.1093/icesjms/fsq112.

51. Shale Rosen, Arill Engås, Anders Fernö, Terje Jörgensen, The reactions of shoaling adult cod to a pelagic trawl: implications for commercial trawling, ICES Journal of Marine Science, Volume 69, Issue 2, March 2012, Pages 303–312, https://doi.org/10.1093/icesjms/fsr199.

52. Nils Olav Handegard, Geir Pedersen, Ole Brix, Estimating tail-beat frequency using split-beam echosounders, ICES Journal of Marine Science, Volume 66, Issue 6, July 2009, Pages 1252–1258, https://doi.org/10.1093/icesjms/fsp003.

53. Geir O. Johansen, Olav R. Godø, Morten D. Skogen, Terje Torkelsen, Using acoustic technology to improve the modelling of the transportation and distribution of juvenile gadoids in the Barents Sea, ICES Journal of Marine Science, Volume 66, Issue 6, July 2009, Pages 1048–1054, https://doi.org/10.1093/icesjms/fsp081.

54. Richard L. O'Driscoll, Peter de Joux, Richard Nelson, Gavin J. Macaulay, Adam J. Dunford, Peter M. Marriott, Craig Stewart, Brian S. Miller, Species identification in seamount fish aggregations using moored underwater video, ICES Journal of Marine Science, Volume 69, Issue 4, May 2012, Pages 648–659, https://doi.org/10.1093/icesjms/fss010.

55. Myounghee Kang, Takeshi Nakamura, Akira Hamano, A methodology for acoustic and geospatial analysis of diverse artificial-reef datasets, ICES Journal of Marine Science, Volume 68, Issue 10, November 2011, Pages 2210–2221, https://doi.org/10.1093/icesjms/fsr141.

56. Geir Pedersen, Rolf J. Korneliussen, The relative frequency response derived from individually separated targets of northeast Arctic cod (Gadus morhua), saithe (Pollachius virens), and Norway pout (Trisopterus esmarkii), ICES Journal of Marine Science, Volume 66, Issue 6, July 2009, Pages 1149–1154, https://doi.org/10.1093/icesjms/fsp070.

57. Gavin J. Macaulay, Rudy J. Kloser, Tim E. Ryan, In situ target strength estimates of visually verified orange roughy, ICES Journal of Marine Science, Volume 70, Issue 1, January 2013, Pages 215–222, https://doi.org/10.1093/icesjms/fss154.

58. Viacheslav A. Ermolchev, Methods and results of in situ target-strength measurements of Atlantic cod (Gadus morhua) during combined trawl-acoustic surveys, ICES Journal of Marine Science, Volume 66, Issue 6, July 2009, Pages 1225–1232, https://doi.org/10.1093/icesjms/fsp024.

59. Peter C. Davison, J. Anthony Koslow, Rudy J. Kloser, Acoustic biomass estimation of mesopelagic fish: backscattering from individuals, populations, and communities, ICES Journal of Marine Science, Volume 72, Issue 5, May/June 2015, Pages 1413–1424, https://doi.org/10.1093/icesjms/fsv023.

60. Guillermo Boyra, Gala Moreno, Bea Sobradillo, Isabel Pérez-Arjona, Igor Sancristobal, David A Demer, Target strength of skipjack tuna (Katsuwanus pelamis) associated with fish aggregating devices (FADs), ICES Journal of Marine Science, Volume 75, Issue 5, September-October 2018, Pages 1790–1802, https://doi.org/10.1093/icesjms/fsy041.

61. Georg Skaret, Aril Slotte, Herring submesoscale dynamics through a major spawning wave: duration, abundance fluctuation, distribution, and schooling, ICES Journal of Marine Science, Volume 74, Issue 3, March-April 2017, Pages 717–727, https://doi.org/10.1093/icesjms/fsw180.

62. Mareike Volkenandt, Simon Berrow, Ian O'Connor, Jean-Marc Guarini, Ciaran O'Donnell, Prespawning herring distribution in the Irish Celtic Sea between 2005 and 2012, ICES Journal of Marine Science, Volume 72, Issue 2, January/February 2015, Pages 498–507, https://doi.org/10.1093/icesjms/fsu143.

63. Ryan A. Saunders, Ciaran O'Donnell, Rolf J. Korneliussen, Sascha M. M. Fässler, Maurice W. Clarke, Afra Egan, Dave Reid, Utility of 18-kHz acoustic data for abundance estimation of Atlantic herring (Clupea harengus), ICES Journal of Marine Science, Volume 69, Issue 6, July 2012, Pages 1086–1098, https://doi.org/10.1093/icesjms/fss059.

64. Lise Doksæter, Olav R. Godø, Erik Olsen, Leif Nøttestad, Ruben Patel, Ecological studies of marine mammals using a seabed-mounted echosounder, ICES Journal of Marine Science, Volume 66, Issue 6, July 2009, Pages 1029–1036, https://doi.org/10.1093/icesjms/fsp130.

65. Sindre Vatnehol, Hector Peña, Egil Ona, Estimating the volumes of fish schools from observations with multi-beam sonars, ICES Journal of Marine Science, Volume 74, Issue 3, March-April 2017, Pages 813–821, https://doi.org/10.1093/icesjms/fsw186.

66. George A. Rose, Variations in the target strength of Atlantic cod during vertical migration, ICES Journal of Marine Science, Volume 66, Issue 6, July 2009, Pages 1205–1211, https://doi.org/10.1093/icesjms/fsp085.

67. Jason D. Stockwell, Thomas C. Weber, Adam J. Baukus, J. Michael Jech, On the use of omnidirectional sonars and downwards-looking echosounders to assess pelagic fish distributions during and after mid-water trawling, ICES Journal of Marine Science, Volume 70, Issue 1, January 2013, Pages 196–203, https://doi.org/10.1093/icesjms/fss139.

68. Richard L. O'Driscoll, Stéphane Gauthier, Jennifer A. Devine, Acoustic estimates of mesopelagic fish: as clear as day and night?, ICES Journal of Marine Science, Volume 66, Issue 6, July 2009, Pages 1310–1317, https://doi.org/10.1093/icesjms/fsp015.

69. Alex De Robertis, Christopher D. Wilson, Silent ships sometimes do encounter more fish. 2. Concurrent echosounder observations from a free-drifting buoy and vessels, ICES Journal of Marine Science, Volume 67, Issue 5, July 2010, Pages 996–1003, https://doi.org/10.1093/icesjms/fsp301.

70. L. G. S. Mello, G. A. Rose, The acoustic dead zone: theoretical vs. empirical estimates, and its effect on density measurements of semi-demersal fish, ICES Journal of Marine Science, Volume 66, Issue 6, July 2009, Pages 1364–1369, https://doi.org/10.1093/icesjms/fsp099.

71. J. Michael Jech, Gareth L. Lawson, Andone C. Lavery, Wideband (15–260 kHz) acoustic volume backscattering spectra of Northern krill (Meganyctiphanes norvegica) and butterfish (Peprilus triacanthus), ICES Journal of Marine Science, Volume 74, Issue 8, September-October 2017, Pages 2249–2261, https://doi.org/10.1093/icesjms/fsx050.

72. Alex De Robertis, Noah Lawrence-Slavas, Richard Jenkins, Ivar Wan-

gen, Calvin W Mordy, Christian Meinig, Mike Levine, Dave Peacock, Heather Tabisola, Long-term measurements of fish backscatter from Saildrone unmanned surface vehicles and comparison with observations from a noise-reduced research vessel, ICES Journal of Marine Science, Volume 76, Issue 7, December 2019, Pages 2459–2470, https://doi.org/10.1093/icesjms/fsz124.

73. Pierre Petitgas, Anne Goarant, Jacques Massé, Paul Bourriau, Combining acoustic and CUFES data for the quality control of fish-stock survey estimates, ICES Journal of Marine Science, Volume 66, Issue 6, July 2009, Pages 1384–1390, https://doi.org/10.1093/icesjms/fsp007.

74. Samuel S. Urmy, John K. Horne, David H. Barbee, Measuring the vertical distributional variability of pelagic fauna in Monterey Bay, ICES Journal of Marine Science, Volume 69, Issue 2, March 2012, Pages 184–196, https://doi.org/10.1093/icesjms/fsr205.

75. Mathieu Doray, Laurent Berger, Naig Le Bouffant, Jean Yves Coail, Jean Philippe Vacherot, Xavier de La Bernardie, Pierre Morinière, Elisabeth Lys, Romain Schwab, Pierre Petitgas, A method for controlled target strength measurements of pelagic fish, with application to European anchovy (Engraulis encrasicolus), ICES Journal of Marine Science, Volume 73, Issue 8, September 2016, Pages 1987–1997, https://doi.org/10.1093/icesjms/fsw084.

76. Rolf J. Korneliussen, Yngve Heggelund, Inge K. Eliassen, Ola K. Øye, Tor Knutsen, John Dalen, Combining multibeam-sonar and multifrequency-echosounder data: examples of the analysis and imaging of large euphausiid schools, ICES Journal of Marine Science, Volume 66, Issue 6, July 2009, Pages 991–997, https://doi.org/10.1093/icesjms/fsp092.

77. Donhyug Kang, Jusam Park, Seom-Kyu Jung, Sungho Cho, Estimates of acoustic target strength for giant jellyfish Nemopilema nomurai Kishinouye in the coastal Northwest Pacific, ICES Journal of Marine Science, Volume 71, Issue 3, March/April 2014, Pages 597–603, https:

//doi.org/10.1093/icesjms/fst182.

78. David A. Demer, George R. Cutter, Josiah S. Renfree, John L. Butler, A statistical-spectral method for echo classification, ICES Journal of Marine Science, Volume 66, Issue 6, July 2009, Pages 1081–1090, https://doi.org/10.1093/icesjms/fsp054.

79. Michael A. Soule, Ian Hampton, Marek R. Lipiński, Estimating the target strength of live, free-swimming chokka squid Loligo reynaudii at 38 and 120 kHz, ICES Journal of Marine Science, Volume 67, Issue 7, October 2010, Pages 1381–1391, https://doi.org/10.1093/icesjms/fsq058.

80. Rokas Kubilius, Egil Ona, Target strength and tilt-angle distribution of the lesser sandeel (Ammodytes marinus), ICES Journal of Marine Science, Volume 69, Issue 6, July 2012, Pages 1099–1107, https://doi.org/10.1093/icesjms/fss093.

81. Gavin J Macaulay, Ben Scoulding, Egil Ona, Sascha M M Fässler, Comparisons of echo-integration performance from two multiplexed echosounders, ICES Journal of Marine Science, Volume 75, Issue 6, November-December 2018, Pages 2276–2285, https://doi.org/10.1093/icesjms/fsy111.

82. Alexey B Ryabov, Geraint A Tarling, Scaling of size, shape and surface roughness in Antarctic krill swarms, ICES Journal of Marine Science, Volume 76, Issue 4, July-August 2019, Pages 1177–1188, https://doi.org/10.1093/icesjms/fsz005.

83. Makoto Tomiyasu, Wan-Yu Kao, Koki Abe, Kenji Minami, Taro Hirose, Michio Ogawa, Kazushi Miyashita, The relationship between body angle and target strength of ribbonfish (Trichiurus japonicus) displaying a vertical swimming motion, ICES Journal of Marine Science, Volume 73, Issue 8, September 2016, Pages 2049–2057, https://doi.org/10.1093/icesjms/fsw095.

84. Marian Peña, Mesopelagic fish avoidance from the vessel dynamic

positioning system, ICES Journal of Marine Science, Volume 76, Issue 3, May-June 2019, Pages 734–742, https://doi.org/10.1093/icesjms/fsy157.

85. Josiah S. Renfree, David A. Demer, Optimizing transmit interval and logging range while avoiding aliased seabed echoes, ICES Journal of Marine Science, Volume 73, Issue 8, September 2016, Pages 1955–1964, https://doi.org/10.1093/icesjms/fsw055.

86. Peter H. Wiebe, Gareth L. Lawson, Andone C. Lavery, Nancy J. Copley, Erich Horgan, Albert Bradley, Improved agreement of net and acoustical methods for surveying euphausiids by mitigating avoidance using a net-based LED strobe light system, ICES Journal of Marine Science, Volume 70, Issue 3, April 2013, Pages 650–664, https://doi.org/10.1093/icesjms/fst005.

87. Olav Rune Godø, Ruben Patel, Geir Pedersen, Diel migration and swimbladder resonance of small fish: some implications for analyses of multifrequency echo data, ICES Journal of Marine Science, Volume 66, Issue 6, July 2009, Pages 1143–1148, https://doi.org/10.1093/icesjms/fsp098.

88. Peter H. Wiebe, Dezhang Chu, Stein Kaartvedt, Anna Hundt, Webjorn Melle, Egil Ona, Paola Batta-Lona, The acoustic properties of Salpa thompsoni, ICES Journal of Marine Science, Volume 67, Issue 3, April 2010, Pages 583–593, https://doi.org/10.1093/icesjms/fsp263.

89. Sandra L. Parker-Stetter, John K. Horne, Mariko M. Langness, The influence of midwater hypoxia on nekton vertical migration, ICES Journal of Marine Science, Volume 66, Issue 6, July 2009, Pages 1296–1302, https://doi.org/10.1093/icesjms/fsp006.

90. ICES Journal of Marine Science, Volume 71, Issue 8, October 2014, Pages 1989–2369, https://doi.org/10.1093/icesjms/fsu171.

91. Alex De Robertis, Christopher D. Wilson, Neal J. Williamson, Michael A. Guttormsen, Sarah Stienessen, Silent ships sometimes do

encounter more fish. 1. Vessel comparisons during winter pollock surveys, ICES Journal of Marine Science, Volume 67, Issue 5, July 2010, Pages 985–995, https://doi.org/10.1093/icesjms/fsp299.

92. Kirsten A. Simonsen, Patrick H. Ressler, Christopher N. Rooper, Stephani G. Zador, Spatio-temporal distribution of euphausiids: an important component to understanding ecosystem processes in the Gulf of Alaska and eastern Bering Sea, ICES Journal of Marine Science, Volume 73, Issue 8, September 2016, Pages 2020–2036, https://doi.org/10.1093/icesjms/fsv272.

93. Vaneeda Allken, Nils Olav Handegard, Shale Rosen, Tiffanie Schreyeck, Thomas Mahiout, Ketil Malde, Fish species identification using a convolutional neural network trained on synthetic data, ICES Journal of Marine Science, Volume 76, Issue 1, January-February 2019, Pages 342–349, https://doi.org/10.1093/icesjms/fsy147.

94. Bart Buelens, Tim Pauly, Raymond Williams, Arthur Sale, Kernel methods for the detection and classification of fish schools in single-beam and multibeam acoustic data, ICES Journal of Marine Science, Volume 66, Issue 6, July 2009, Pages 1130–1135, https://doi.org/10.1093/icesjms/fsp004.

95. Geir Pedersen, Nils Olav Handegard, Egil Ona, Lateral-aspect, target-strength measurements of in situ herring (Clupea harengus), ICES Journal of Marine Science, Volume 66, Issue 6, July 2009, Pages 1191–1196, https://doi.org/10.1093/icesjms/fsp121.

96. Jarrod A. Santora, Stephen Ralston, William J. Sydeman, Spatial organization of krill and seabirds in the central California Current, ICES Journal of Marine Science, Volume 68, Issue 7, July 2011, Pages 1391–1402, https://doi.org/10.1093/icesjms/fsr046.

97. O. P. Pedersen, T. Pedersen, K. S. Tande, D. Slagstad, Integrating spatial and temporal mortality from herring on capelin larvae: a study in the Barents Sea, ICES Journal of Marine Science, Volume 66, Issue

10, December 2009, Pages 2183–2194, https://doi.org/10.1093/icesjms/fsp192.

98. Alex De Robertis, Christopher D. Wilson, Silent ships do not always encounter more fish (revisited): comparison of acoustic backscatter from walleye pollock recorded by a noise-reduced and a conventional research vessel in the eastern Bering Sea, ICES Journal of Marine Science, Volume 68, Issue 10, November 2011, Pages 2229–2239, https://doi.org/10.1093/icesjms/fsr146.

99. Robert A. McConnaughey, Stephen E. Syrjala, Statistical relationships between the distributions of groundfish and crabs in the eastern Bering Sea and processed returns from a single-beam echosounder, ICES Journal of Marine Science, Volume 66, Issue 6, July 2009, Pages 1425–1432, https://doi.org/10.1093/icesjms/fsp147.

100. Adrián Madirolas, Federico A. Membiela, Juan D. Gonzalez, Ariel G. Cabreira, Matías dell'Erba, Igor S. Prario, Silvia Blanc, Acoustic target strength (TS) of argentine anchovy (Engraulis anchoita): the nighttime scattering layer, ICES Journal of Marine Science, Volume 74, Issue 5, May-June 2017, Pages 1408–1420, https://doi.org/10.1093/icesjms/fsw185.

References

Aad, G. *et al.* (2012) 'Observation of a new particle in the search for the Standard Model Higgs boson with the ATLAS detector at the LHC', *Physics Letters B.* Elsevier, 716(1), pp. 1–29. doi: 10.1016/j.physletb.2012.08.020.

Abadi, M. *et al.* (2016) 'Tensorflow: Large-scale machine learning on heterogeneous distributed systems', *arXiv preprint arXiv:1603.04467.* Available at: https://arxiv.org/abs/1603.04467.

Akyildiz, I. F., Pompili, D. and Melodia, T. (2005) 'Underwater acoustic sensor networks: Research challenges', *Ad hoc networks.* Elsevier, 3(3), pp. 257–279. doi: 10.1016/j.adhoc.2005.01.004.

Amblas, D. *et al.* (2016) 'Real-time lossless compression of multibeam echosounder water column data', in *7th international workshop on marine technology martech.* Available at: https://upcommons.upc.edu/handle/2117/99929.

Anderson, C., Brierley, A. and Armstrong, F. (2005) 'Spatio-temporal variability in the distribution of epi-and meso-pelagic acoustic backscatter in the Irminger Sea, North Atlantic, with implications for predation on Calanus finmarchicus', *Marine Biology.* Springer, 146(6), pp. 1177–1188. doi: 10.1007/s00227-004-1510-8.

Asper, V. *et al.* (2011) 'Using gliders to study a phytoplankton bloom in the Ross Sea, Antarctica', in *OCEANS 2011.* IEEE, pp. 1–7. doi: 10.23919/OCEANS.2011.6107082.

Atkinson, A. *et al.* (2019) 'Krill (Euphausia superba) distribution contracts southward during rapid regional warming', *Nature Climate Change.* Nature Publishing Group, 9(2), pp. 142–147. doi: 10.1038/s41558-018-0370-z.

Atkinson, A. *et al.* (2006) 'Natural growth rates in Antarctic krill (Euphausia superba): II. Predictive models based on food, temperature, body length, sex, and maturity stage', *Limnology and Oceanography.* Wiley Online Library, 51(2), pp. 973–987. doi: 10.4319/lo.2006.51.2.0973.

Atkinson, A. *et al.* (2009) 'A re-appraisal of the total biomass and annual production of Antarctic krill', *Deep Sea Research Part I: Oceanographic Research Papers.* Elsevier, 56(5), pp. 727–740. doi: 10.1016/j.dsr.2008.12.007.

Atkinson, A. *et al.* (2004) 'Long-term decline in krill stock and increase in salps within the Southern Ocean', *Nature.* Nature Publishing Group, 432(7013), pp. 100–103. doi: 10.1038/nature02996.

Atkinson, A. *et al.* (2008) 'Oceanic circumpolar habitats of Antarctic krill', *Marine Ecology Progress Series*, 362, pp. 1–23. doi: 10.3354/meps07498.

Bakker, D. C. E. *et al.* (2020) 'Big Data in Marine Science, Future Science Brief 6 of the European Marine Board, Ostend, Belgium'. Available at: https://www.marineboard.eu/sites/marineboard.eu/files/public/publication/EMB_FSB6_BigData_Web_0.pdf.

Barange, M. (1994) 'Acoustic identification, classification and structure of biological patchiness on the edge of the Agulhas Bank and its relation to frontal features', *South African Journal of marine science.* Taylor & Francis, 14(1), pp. 333–347. doi: 10.2989/025776194784286969.

Baylor, D. (1995) 'Colour mechanisms of the eye', in Lamb, T. and Bourriau, J. (eds) *Colour: Art and science.* Cambridge University Press, Cambridge, UK, p. 103. Available at: https://isbn.nu/9780521499637.

Beaudoin, J. (2010) 'Application of JPEG 2000 wavelet compression to multibeam echosounder mid-water acoustic reflectivity measurements', in *Canadian Hydrographic Conference, Quebec City (Canada).* Available at:

http://www.omg.unb.ca/omg/papers/beaudoin_watercolumn_compression.pdf.

Bekkadal, F. (2009) 'Emerging maritime communications technologies', in *2009 9th international conference on intelligent transport systems telecommunications,(ITST)*. IEEE, pp. 358–363. Available at: https://www.tib.eu/en/search/id/TIBKAT%3A623723778/2009-9th-International-Conference-on-Intelligent/.

Belcher, A. *et al.* (2019) 'Krill faecal pellets drive hidden pulses of particulate organic carbon in the marginal ice zone', *Nature communications*. Nature Publishing Group, 10(1), p. 889. doi: [10.1038/s41467-019-08847-1](https://doi.org/10.1038/s41467-019-08847-1).

Benoit-Bird, K. J. and Lawson, G. L. (2016) 'Ecological insights from pelagic habitats acquired using active acoustic techniques', *Annual review of marine science*. Annual Reviews, 8, pp. 463–490. doi: [10.1146/annurev-marine-122414-034001](https://doi.org/10.1146/annurev-marine-122414-034001).

Benoit-Bird, K. *et al.* (2018) 'Equipping an underwater glider with a new echosounder to explore ocean ecosystems', *Limnology and Oceanography: Methods*. Wiley Online Library, 16(11), pp. 734–749. doi: [10.1002/lom3.10278](https://doi.org/10.1002/lom3.10278).

Bezanson, J. *et al.* (2017) 'Julia: A fresh approach to numerical computing', *SIAM review*. SIAM, 59(1), pp. 65–98. doi: [10.1137/141000671](https://doi.org/10.1137/141000671).

Blackwell, R. E. *et al.* (2019) 'Colour maps for fisheries acoustic echograms.', *ICES Journal of Marine Science*. doi: [10.1093/icesjms/fsz242](https://doi.org/10.1093/icesjms/fsz242).

Blackwell, R. *et al.* (2019) 'Aliased seabed detection in fisheries acoustic data', *arXiv preprint arXiv:1904.10736*. Available at: https://arxiv.org/abs/1904.10736.

Borkin, M. *et al.* (2011) 'Evaluation of artery visualizations for heart disease diagnosis', *IEEE transactions on visualization and computer graphics*. IEEE, 17(12), pp. 2479–2488. doi: [10.1109/TVCG.2011.192](https://doi.org/10.1109/TVCG.2011.192).

Borland, D. and Ii, R. M. T. (2007) 'Rainbow color map (still) considered

harmful', *IEEE computer graphics and applications.* IEEE, 27(2), pp. 14–17. doi: 10.1109/MCG.2007.323435.

Bourguignon, S. *et al.* (2009) 'Methodological developments for improved bottom detection with the ME70 multibeam echosounder', *ICES Journal of Marine Science: Journal du Conseil.* Oxford University Press, Oxford, UK, 66(6), pp. 1015–1022. doi: 10.1093/icesjms/fsp089.

Brainard, D. H. (2003) 'Color appearance and color difference specification', *The Science of Color*, 2(191-216), p. 5. doi: 10.1016/B978-044451251-2/50006-4.

Brautaset, O. *et al.* (2020) 'Acoustic classification in multifrequency echosounder data using deep convolutional neural networks', *ICES Journal of Marine Science.* doi: 10.1093/icesjms/fsz235.

Breiman, L. (2001) 'Random forests', *Machine learning.* Springer, New York, USA, 45(1), pp. 5–32. Available at: https://link.springer.com/content/pdf/10.1023/A:1010933404324.pdf.

Brewer, C. (2015) *Designing better Maps: A Guide for GIS users.* ESRI Press, Redlands, California, USA. Available at: https://isbn.nu/9781589484405.

Brito, M., Smeed, D. and Griffiths, G. (2014) 'Underwater glider reliability and implications for survey design', *Journal of Atmospheric and Oceanic Technology*, 31(12), pp. 2858–2870. doi: 10.1175/JTECH-D-13-00138.1.

Campbell, F. W. and Robson, J. (1968) 'Application of Fourier analysis to the visibility of gratings', *The Journal of physiology.* Wiley Online Library, 197(3), pp. 551–566. doi: 10.1113/jphysiol.1968.sp008574.

Catipovic, J. A. (1990) 'Performance limitations in underwater acoustic telemetry', *IEEE Journal of Oceanic Engineering.* IEEE, New York, USA, 15(3), pp. 205–216. doi: 10.1109/48.107149.

Chollet, F. and others (2015) 'Keras'. Available at: https://keras.io.

Clarke, J. H. (2006) 'Applications of multibeam water column imaging for

hydrographic survey', *Hydrographic Journal.* The Hydrographic Society, UK, 120, p. 3. Available at: https://pdfs.semanticscholar.org/b49b/426a 9bbd9e84163892cf22bac8c7480cf8f0.pdf.

Cochrane, N. *et al.* (1991) 'Multiple-frequency acoustic backscattering and zooplankton aggregations in the inner scotian shelf basins', *Canadian Journal of Fisheries and Aquatic Sciences.* NRC Research Press, 48(3), pp. 340–355. doi: 10.1139/f91-046.

Coetzee, J. (2000) 'Use of a shoal analysis and patch estimation system (shapes) to characterise sardine schools', *Aquatic Living Resources.* EDP Sciences, 13(1), pp. 1–10. doi: 10.1016/S0990-7440(00)00139-X.

Constable, A. J. *et al.* (2016) 'Developing priority variables ("ecosystem Essential Ocean Variables"—eEOVs) for observing dynamics and change in Southern Ocean ecosystems', *Journal of Marine Systems.* Elsevier, Amsterdam. Netherlands, 161, pp. 26–41. doi: 10.1016/j.jmarsys.2016.05.003.

Constable, A. J. *et al.* (2014) 'Climate change and Southern Ocean ecosystems I: how changes in physical habitats directly affect marine biota', *Global Change Biology.* Wiley Online Library, 20(10), pp. 3004–3025. doi: 10.1111/gcb.12623.

Conti, S. G. and Demer, D. A. (2006) 'Improved parameterization of the SDWBA for estimating krill target strength', *ICES Journal of Marine Science.* Oxford University Press, 63(5), pp. 928–935. doi: 10.1016/j.icesjms.2006.02.007.

Cover, T. and Hart, P. (1967) 'Nearest neighbor pattern classification', *IEEE transactions on information theory.* IEEE, 13(1), pp. 21–27. doi: 10.1109/TIT.1967.1053964.

Cury, P. M. *et al.* (2005) 'Viability theory for an ecosystem approach to fisheries', *ICES journal of marine science.* Oxford University Press, 62(3), pp. 577–584. doi: 10.1016/j.icesjms.2004.10.007.

Davis, L. B. *et al.* (2017) 'Distributions of krill and Antarctic silver-

fish and correlations with environmental variables in the western Ross Sea, Antarctica', *Marine Ecology Progress Series*, 584, pp. 45–65. doi: 10.3354/meps12347.

D'elia, M. *et al.* (2016) 'Diel variation in the vertical distribution of deep-water scattering layers in the Gulf of Mexico', *Deep Sea Research Part I: Oceanographic Research Papers.* Elsevier, 115, pp. 91–102. doi: 10.1016/j.dsr.2016.05.014.

Demer, D. A. *et al.* (2015) 'Calibration of acoustic instruments, ICES Cooperative Research Report No. 326'. International Council for the Exploration of the Sea (ICES), Copenhagen, Denmark. doi: 10.25607/OBP-185.

Demer, D. A. and Conti, S. G. (2005) 'New target-strength model indicates more krill in the Southern Ocean', *ICES Journal of Marine Science.* Oxford University Press, 62(1), pp. 25–32. doi: 10.1016/j.icesjms.2004.07.027.

De Robertis, A. *et al.* (2019) 'Amplifier linearity accounts for discrepancies in echo-integration measurements from two widely used echosounders', *ICES Journal of Marine Science.* doi: 10.1093/icesjms/fsz040.

De Robertis, A. and Higginbottom, I. (2007) 'A post-processing technique to estimate the signal-to-noise ratio and remove echosounder background noise', *ICES Journal of Marine Science*, 64(6), pp. 1282–1291. doi: 10.1093/icesjms/fsm112.

Dickey, T. D. (1991) 'The emergence of concurrent high-resolution physical and bio-optical measurements in the upper ocean and their applications', *Reviews of Geophysics.* Wiley Online Library, 29(3), pp. 383–413. doi: 10.1029/91RG00578.

Eriksen, C. C. *et al.* (2001) 'Seaglider: A long-range autonomous underwater vehicle for oceanographic research', *IEEE Journal of oceanic Engineering.* IEEE, 26(4), pp. 424–436. doi: 10.1109/48.972073.

Everson, I. (2008) *Krill: Biology, ecology and fisheries.* John Wiley & Sons, Hoboken, New Jersey, USA. Available at: https://isbn.nu/9780470999486.

Fallon, N. G., Fielding, S. and Fernandes, P. G. (2016) 'Classification of Southern Ocean krill and icefish echoes using random forests', *ICES Journal of Marine Science.* Oxford University Press, 73(8), pp. 1998–2008. doi: 10.1093/icesjms/fsw057.

Fassler, S. *et al.* (2015) *VIP report, Use of new broadband echosounder.* IMARES. Available at: https://library.wur.nl/WebQuery/wurpubs/fullte xt/371565.

Fernandes, P. G. (2009) 'Classification trees for species identification of fish-school echotraces', *ICES Journal of Marine Science.* Oxford University Press, 66(6), pp. 1073–1080. doi: 10.1093/icesjms/fsp060.

Fernandes, P. G. *et al.* (2002) 'Acoustic applications in fisheries science: the ICES contribution', in. ICES. Available at: https://imr.brage.unit.no/imr-xmlui/bitstream/handle/11250/107495/sym_2002_215b.pdf?sequence=1.

Fielding, S. *et al.* (2012) 'Acoustic determination of the distribution of fish and krill across the Scotia Sea in spring 2006, summer 2008 and autumn 2009', *Deep Sea Research Part II: Topical Studies in Oceanography.* Elsevier, 59, pp. 173–188. doi: 10.1016/j.dsr2.2011.08.002.

Fielding, S. *et al.* (2014) 'Interannual variability in Antarctic krill (Euphausia superba) density at South Georgia, Southern Ocean: 1997–2013', *ICES Journal of Marine Science.* ICES/CIEM, 71(9), pp. 2578–2588. doi: 10.1093/icesjms/fsu104.

Flexer, A. (1996) 'Statistical evaluation of neural network experiments: Minimum requirements and current practice', *Cybernetics and Systems Research.* Citeseer, pp. 1005–1008. Available at: http://citeseerx.ist.psu.edu/viewdo c/download?doi=10.1.1.34.924&rep=rep1&type=pdf.

Flores, H. *et al.* (2012) 'Impact of climate change on Antarctic krill', *Marine Ecology Progress Series*, 458, pp. 1–19. doi: 10.3354/meps09831.

Folt, C. L. and Burns, C. W. (1999) 'Biological drivers of zooplankton patchiness', *Trends in Ecology & Evolution.* Elsevier, 14(8), pp. 300–305.

doi: 10.1016/S0169-5347(99)01616-X.

Food and Agriculture Organization of the United Nations (2018) 'The state of world fisheries and aquaculture 2018'. Food; Agriculture Organization of the United Nations. Available at: http://www.fao.org/3/i9540en/i9540en.pdf.

Foote, K. G., Aglen, A. and Nakken, O. (1986) 'Measurement of fish target strength with a split-beam echo sounder', *The Journal of the Acoustical Society of America.* ASA, 80(2), pp. 612–621. doi: 10.1121/1.394056.

Foote, K. G. *et al.* (1991) 'Postprocessing system for echo sounder data', *The Journal of the Acoustical Society of America.* ASA, 90(1), pp. 37–47. doi: 10.1121/1.401261.

Fowler, J., Cohen, L. and Jarvis, P. (1998) *Practical statistics for field biology.* 2nd edn. John Wiley & Sons, Hoboken, New Jersey, USA. Available at: https://isbn.nu/9780471982968.

Francois, R. and Garrison, G. (1982) 'Sound absorption based on ocean measurements. Part II: Boric acid contribution and equation for total absorption', *The Journal of the Acoustical Society of America.* ASA, 72(6), pp. 1879–1890. doi: 10.1121/1.388673.

Fung, J. and Mann, S. (2005) 'OpenVIDIA: parallel GPU computer vision', in *Proceedings of the 13th annual acm international conference on multimedia*, pp. 849–852. doi: 10.1145/1101149.1101334.

Gegenfurtner, K. R., Bloj, M. and Toscani, M. (2015) 'The many colours of "the dress"', *Current Biology.* Elsevier, 25(13), pp. R543–R544. doi: 10.1016/j.cub.2015.04.043.

Giering, S. L. *et al.* (2014) 'Reconciliation of the carbon budget in the ocean's twilight zone', *Nature.* Nature Publishing Group, 507(7493), pp. 480–483. doi: 10.1038/nature13123.

Godø, O. *et al.* (2014) 'Commercial fishing vessel as research vessels in the Antarctic–requirements and solutions exemplified with a new vessel',

CCAMLR Science. CCAMLR, 21, pp. 11–17. Available at: http://nora.n erc.ac.uk/id/eprint/508483.

Greene, C. H. *et al.* (2014) 'A wave glider approach to fisheries acoustics: Transforming how we monitor the nation's commercial fisheries in the 21st century', *Oceanography.* JSTOR, 27(4), pp. 168–174. Available at: https://www.jstor.org/stable/24862221.

Greenstreet, S. P. *et al.* (2006) 'Variation in the abundance of sandeels Ammodytes marinus off southeast Scotland: an evaluation of area-closure fisheries management and stock abundance assessment methods', *ICES Journal of Marine Science.* Oxford University Press, 63(8), pp. 1530–1550. doi: 10.1016/j.icesjms.2006.05.009.

Griffiths, G. (ed.) (2002) *Technology and applications of autonomous underwater vehicles.* CRC Press, Boca Raton, Florida, USA. Available at: https://isbn.nu/9780415301541.

Guihen, D. (2018) 'High-resolution acoustic surveys with diving gliders come at a cost of aliasing moving targets', *PloS one.* Public Library of Science, 13(8). doi: 10.1371/journal.pone.0201816.

Guihen, D. *et al.* (2014) 'An assessment of the use of ocean gliders to undertake acoustic measurements of zooplankton: the distribution and density of Antarctic krill (Euphausia superba) in the Weddell Sea', *Limnol. Oceanogr.: Methods*, 12, pp. 373–389. doi: 10.4319/lom.2014.12.373.

Gutt, J. *et al.* (2015) 'The Southern Ocean ecosystem under multiple climate change stresses-an integrated circumpolar assessment', *Global Change Biology.* Wiley Online Library, 21(4), pp. 1434–1453. doi: 10.1111/gcb.12794.

Hall, J. K. (2006) 'GEBCO Centennial Special Issue–Charting the secret world of the ocean floor: the GEBCO project 1903–2003', *Marine Geophysical Researches.* Springer, 27(1), pp. 1–5. doi: 10.1007/s11001-006-8181-4.

Haralabous, J. and Georgakarakos, S. (1996) 'Artificial neural networks

as a tool for species identification of fish schools', *ICES Journal of Marine Science.* Oxford University Press, 53(2), pp. 173–180. doi: 10.1006/jmsc.1996.0019.

Harrison, L.-M. K. *et al.* (2015) 'The R package EchoviewR for automated processing of active acoustic data using Echoview', *Frontiers in Marine Science.* Frontiers, 2, p. 15. doi: 10.3389/fmars.2015.00015.

Hasler, D. and Süsstrunk, S. E. (2003) 'Measuring colorfulness in natural images', in *Human vision and electronic imaging viii.* International Society for Optics; Photonics, pp. 87–96. doi: 10.1117/12.477378.

Henson, S. A., Beaulieu, C. and Lampitt, R. (2016) 'Observing climate change trends in ocean biogeochemistry: When and where', *Global change biology.* Wiley Online Library, 22(4), pp. 1561–1571. doi: 10.1111/gcb.13152.

Hill, S. L., Phillips, T. and Atkinson, A. (2013) 'Potential climate change effects on the habitat of antarctic krill in the weddell quadrant of the southern ocean', *PloS one.* Public Library of Science, 8(8). doi: 10.1371/journal.pone.0072246.

Hilliard Jr, E. (1960) *Electromagnetic radiation in sea water.* DTIC Document. Available at: https://apps.dtic.mil/dtic/tr/fulltext/u2/a046687.pdf.

HM Government (2015) 'Merseyside beats global competition to build £200 million polar research ship'. https://www.gov.uk/government/news/merseyside-beats-global-competition-to-build-200-million-polar-research-ship.

Hofmann, E. E. *et al.* (1998) 'Krill transport in the Scotia Sea and environs', *Antarctic Science.* Cambridge University Press, Cambridge, UK, 10(4), pp. 406–415. doi: 10.1017/S0954102098000492.

Hogg, O. T. *et al.* (2016) 'Landscape mapping at sub-Antarctic South Georgia provides a protocol for underpinning large-scale marine protected areas', *Scientific reports.* Nature Publishing Group, 6. doi: 10.1038/srep33163.

Holland, P. R. (2014) 'The seasonality of Antarctic sea ice trends', *Geophys-*

ical Research Letters. Wiley Online Library, 41(12), pp. 4230–4237. doi: 10.1002/2014GL060172.

Horne, J. K. (2000) 'Acoustic approaches to remote species identification: A review', *Fisheries Oceanography.* Wiley Online Library, 9(4), pp. 356–371. doi: 10.1046/j.1365-2419.2000.00143.x.

Huffman, D. A. (1952) 'A method for the construction of minimum-redundancy codes', *Proceedings of the IRE.* IEEE, 40(9), pp. 1098–1101. doi: https://doi.org/10.1109/JRPROC.1952.273898.

Hunter, J. D. (2007) 'Matplotlib: A 2D graphics environment', *Computing In Science & Engineering.* IEEE COMPUTER SOC, 9(3), pp. 90–95. doi: 10.1109/MCSE.2007.55.

ICES (2013) 'A Metadata Convention for Processed Acoustic Data from Active Acoustic Systems, SISP 3 TG-AcMeta'. ICES WGFAST Topic Group, TG-AcMeta: 35. Available at: https://archimer.ifremer.fr/doc/00587/69903/67808.pdf.

ICES (2018) 'Interim Report of the Working Group on Fisheries Acoustics, Science and Technology (WGFAST) 20-23 March 2018 Seattle, USA.' ICES CM 2018/EOSG:11. Available at: https://archimer.ifremer.fr/doc/00585/69760/67650.pdf.

Inman, H. F. and Bradley Jr, E. L. (1989) 'The overlapping coefficient as a measure of agreement between probability distributions and point estimation of the overlap of two normal densities', *Communications in Statistics-Theory and Methods.* Taylor & Francis, 18(10), pp. 3851–3874. doi: 10.1080/03610928908830127.

Jech, J. M. and Michaels, W. L. (2006) 'A multifrequency method to classify and evaluate fisheries acoustics data', *Canadian Journal of Fisheries and Aquatic Sciences.* NRC Research Press, 63(10), pp. 2225–2235. doi: 10.1139/f06-126.

Jefferson, L. and Harvey, R. (2006) 'Accommodating color blind com-

puter users', in *Proceedings of the 8th International ACM SIGACCESS Conference on Computers and Accessibility.* ACM, pp. 40–47. doi: 10.1145/1168987.1168996.

Judd, D. B. and Wyszecki, G. (1975) *Color in Business, Science, and Industry.* Hoboken, New Jersey, USA: John Wiley; Sons, Inc. Available at: https://isbn.nu/9780471452126.

Kanji, G. K. (2006) *100 statistical tests.* Third. Sage. Available at: https://isbn.nu/9781412923767.

Kennicutt, M. C. *et al.* (2014) 'Polar research: Six priorities for Antarctic science', *Nature.* Macmillan Publishers Ltd., London, England, 512(7512), pp. 23–25. doi: 10.1038/512023a.

Kingma, D. P. and Ba, J. (2014) 'Adam: A method for stochastic optimization', *arXiv preprint arXiv:1412.6980.* Available at: https://arxiv.org/abs/1412.6980.

Kjellsson, J. *et al.* (2015) 'Model sensitivity of the Weddell and Ross seas, Antarctica, to vertical mixing and freshwater forcing', *Ocean Modelling.* Elsevier, 94, pp. 141–152. doi: 10.1016/j.ocemod.2015.08.003.

Klein, E. S. *et al.* (2018) 'Impacts of rising sea temperature on krill increase risks for predators in the Scotia Sea', *PloS one.* Public Library of Science, 13(1), p. e0191011. doi: 10.1371/journal.pone.0191011.

Klinck, H. *et al.* (2012) 'Near-real-time acoustic monitoring of beaked whales and other cetaceans using a Seaglider™', *PloS one.* Public Library of Science, 7(5). doi: 10.1371/journal.pone.0036128.

Kloser, R. J. *et al.* (2009) 'Acoustic observations of micronekton fish on the scale of an ocean basin: Potential and challenges', *ICES Journal of Marine Science.* Oxford University Press, 66(6), pp. 998–1006. doi: 10.1093/icesjms/fsp077.

Kock, K.-H. (2000) *Understanding ccamlr's approach to management.* CCAMLR Hobart, Australia. Available at: https://www.ccamlr.org/en/

document/publications/understanding-ccamlr%E2%80%99s-approach-management.

Kolmogorov, A. N. (1963) 'On tables of random numbers', *Sankhyā: The Indian Journal of Statistics, Series A*. JSTOR, pp. 369–376. Available at: https://www.jstor.org/stable/25049284.

Korb, R. *et al.* (2008) 'Magnitude and maintenance of the phytoplankton bloom at south georgia: A naturally iron-replete environment', *Marine Ecology Progress Series*, 368, pp. 75–91. doi: 10.3354/meps07525.

Korneliussen, R. J. (ed.) (2018) 'Acoustic target classification. ICES cooperative research report no. 344'. International Council for the Exploration of the Sea (ICES). doi: 10.17895/ices.pub.4567.

Korneliussen, R. J. *et al.* (2016) 'Acoustic identification of marine species using a feature library', *Methods in Oceanography*. Elsevier, 17, pp. 187–205. doi: 10.1016/j.mio.2016.09.002.

Korneliussen, R. J. and Ona, E. (2003) 'Synthetic echograms generated from the relative frequency response', *ICES Journal of Marine Science: Journal du Conseil*. Oxford University Press, 60(3), pp. 636–640. doi: 10.1016/S1054-3139(03)00035-3.

Krafft, B. A. *et al.* (2019) 'Report from a krill focused survey with RV Kronprins Haakon and land-based predator work in Antarctica during 2018/2019', *Rapport fra havforskningen*. Havforskningsinstituttet. doi: 10.13140/RG.2.2.19165.05603.

Krafft, B. A. *et al.* (2018) 'Summer distribution and demography of Antarctic krill Euphausia superba Dana, 1850 (Euphausiacea) at the South Orkney Islands, 2011–2015', *Journal of Crustacean Biology*. Oxford University Press US, 38(6), pp. 682–688. doi: 10.1093/jcbiol/ruy061.

Lake, B. M. *et al.* (2017) 'Building machines that learn and think like people', *Behavioral and Brain Sciences*. Cambridge University Press, 40. doi: 10.1017/S0140525X16001837.

Lavery, A. C. *et al.* (2017) 'Exploiting signal processing approaches for broadband echosounders', *ICES Journal of Marine Science.* Oxford University Press, 74(8), pp. 2262–2275. doi: 10.1093/icesjms/fsx155.

LeCun, Y., Bengio, Y. and Hinton, G. (2015) 'Deep learning', *Nature.* Nature Publishing Group, 521(7553), p. 436. doi: 10.1038/nature14539.

Lee, K.-H. *et al.* (2012) 'Parallel data processing with mapreduce: A survey', *AcM sIGMoD Record.* ACM New York, NY, USA, 40(4), pp. 11–20. doi: 10.1145/2094114.2094118.

Leung, H. K. N. and White, L. (1990) 'A study of integration testing and software regression at the integration level', in *Proceedings. Conference on software maintenance 1990*, pp. 290–301. doi: 10.1109/ICSM.1990.131377.

Liblik, T. *et al.* (2016) 'Potential for an underwater glider component as part of the Global Ocean Observing System', *Methods in Oceanography.* Elsevier, 17, pp. 50–82. doi: 10.1016/j.mio.2016.05.001.

Lindstrom, E. *et al.* (2012) 'A framework for ocean observing', *Proceedings of the Ocean Information for Society: Sustaining the Benefits, Realizing the Potential, Venice, Italy*, 2125. doi: 10.5270/OceanObs09-FOO.

Lovenduski, N. S. and Gruber, N. (2005) 'Impact of the Southern Annular Mode on Southern Ocean circulation and biology', *Geophysical Research Letters.* Wiley Online Library, 32(11). doi: 10.1029/2005GL022727.

Lysogor, I. I., Voskov, L. S. and Efremov, S. G. (2018) 'Survey of data exchange formats for heterogeneous LPWAN-satellite IoT networks', in *2018 moscow workshop on electronic and networking technologies (mwent).* IEEE, pp. 1–5. doi: 10.1109/MWENT.2018.8337257.

Macaulay, G. and Peña, H. (2018) 'The SONAR-netCDF4 convention for sonar data, Version 1.0, ICES Cooperative Research Report No. 2341'. International Council for the Exploration of the Sea (ICES), Copenhagen, Denmark. doi: 10.17895/ices.pub.4392.

MacKay, D. J. (2003) *Information theory, inference and learning algorithms.*

Cambridge University Press, Cambridge, UK. Available at: http://www.in
ference.org.uk/mackay/itila/book.html.

MacLennan, D. *et al.* (2004) 'Experiments on the discrimination of fish and
seabed echoes', *ICES Journal of Marine Science.* Oxford University Press,
61(2), pp. 201–210. doi: 10.1016/j.icesjms.2003.09.005.

Madureira, L. S., Everson, I. and Murphy, E. J. (1993) 'Interpretation of
acoustic data at two frequencies to discriminate between antarctic krill (Eu-
phausia superba Dana) and other scatterers', *Journal of Plankton Research.*
Oxford University Press, 15(7), pp. 787–802. doi: 10.1093/plankt/15.7.787.

Mankins, J. C. (1995) 'Technology readiness levels'. Advanced Concepts
Office, Office of Space Access and Technology, NASA; NASA. Available at:
https://aiaa.kavi.com/apps/group_public/download.php/2212/TRLs_M
ankinsPaper_1995.pdf.

Manley, J. E. (2008) 'Unmanned surface vehicles, 15 years of development',
in *OCEANS 2008.* IEEE, pp. 1–4. doi: 10.1109/OCEANS.2008.5152052.

Maral, G. and Bousquet, M. (2011) *Satellite communications systems: Sys-
tems, techniques and technology.* John Wiley & Sons. Available at: https:
//isbn.nu/9780470714584.

Maxwell, S. M. *et al.* (2015) 'Dynamic ocean management: Defining and
conceptualizing real-time management of the ocean', *Marine Policy.* Else-
vier, 58, pp. 42–50. doi: 10.1016/j.marpol.2015.03.014.

Mayer-Schönberger, V. and Cukier, K. (2013) *Big data: A revolution that
will transform how we live, work, and think.* Houghton Mifflin Harcourt.
Available at: https://isbn.nu/9781848547902.

McClatchie, S. *et al.* (2000) 'Ground truth and target identification for
fisheries acoustics', *Fisheries Research.* Elsevier, 47(2-3), pp. 173–191. doi:
10.1016/S0165-7836(00)00168-5.

McKinney, W. (2010) 'Data structures for statistical computing in python',
in *Proceedings of the 9th Python in Science Conference. (SCIPY 2010).*,

pp. 51–56. Available at: http://conference.scipy.org/proceedings/scipy20
10/pdfs/mckinney.pdf.

McQuinn, I. H. *et al.* (2005) 'Description of the ICES HAC standard data
exchange format, version 1.60, ICES Cooperative Research Report No. 278'.
International Council for the Exploration of the Sea (ICES), Copenhagen,
Denmark. doi: 10.17895/ices.pub.5482.

Meredith, M. P. *et al.* (2008) 'On the interannual variability of ocean
temperatures around South Georgia, Southern Ocean: Forcing by El Niño/-
Southern Oscillation and the southern annular mode', *Deep Sea Research
Part II: Topical Studies in Oceanography.* Elsevier, 55(18-19), pp. 2007–
2022. doi: 10.1016/j.dsr2.2008.05.020.

Meredith, M. P. *et al.* (2013) 'The vision for a Southern Ocean observing
system', *Current Opinion in Environmental Sustainability.* Elsevier, 5(3-4),
pp. 306–313. doi: 10.1016/j.cosust.2013.03.002.

Mitson, R. (1983) *Fisheries Sonar:(incorporating Underwater Observation
Using Sonar by DG Tucker).* Fishing News Books Farnham, Surray, England.
Available at: https://isbn.nu/0852381247.

Moline, M. A. *et al.* (2015) 'Integration of scientific echo sounders with
an adaptable autonomous vehicle to extend our understanding of animals
from the surface to the bathypelagic', *Journal of Atmospheric and Oceanic
Technology*, 32(11), pp. 2173–2186. doi: 10.1175/JTECH-D-15-0035.1.

Moll, C. A. van, Ainslie, M. A. and Vossen, R. van (2009) 'A simple
and accurate formula for the absorption of sound in seawater', *IEEE
Journal of Oceanic Engineering.* IEEE, 34(4), pp. 610–616. doi:
10.1109/JOE.2009.2027800.

Mordy, C. W. *et al.* (2017) 'Advances in Ecosystem Research: Saildrone
Surveys of Oceanography, Fish, and Marine Mammals in the Bering Sea',
Oceanography. JSTOR, 30(2), pp. 113–115. doi: 10.5670/oceanog.2017.230.

Murphy, E. J. *et al.* (2016) 'Understanding the structure and functioning

of polar pelagic ecosystems to predict the impacts of change', *Proceedings of the Royal Society B: Biological Sciences.* The Royal Society, 283(1844), p. 20161646. doi: 10.1098/rspb.2016.1646.

Murphy, E. *et al.* (2012) 'Spatial and temporal operation of the scotia sea ecosystem', *Antarctic Ecosystems: An Extreme Environment in a Changing World.* Wiley Online Library, pp. 160–212. doi: 10.1002/9781444347241.ch6.

Murphy, E. *et al.* (2007) 'Spatial and temporal operation of the scotia sea ecosystem: A review of large-scale links in a krill centred food web', *Philosophical Transactions of the Royal Society B: Biological Sciences.* The Royal Society London, 362(1477), pp. 113–148. doi: 10.1098/rstb.2006.1957.

Nair, V. and Hinton, G. E. (2010) 'Rectified linear units improve restricted boltzmann machines', in *Proceedings of the 27th international conference on machine learning (icml-10)*, pp. 807–814. Available at: https://www.cs.toronto.edu/~hinton/absps/reluICML.pdf.

Nicol, S. and Foster, J. (2016) 'The Fishery for Antarctic Krill: Its Current Status and Management Regime', in *Biology and ecology of antarctic krill.* Springer, pp. 387–421. doi: 10.1007/978-3-319-29279-3_11.

Otsu, N. (1979) 'A threshold selection method from gray-level histograms', *IEEE transactions on systems, man, and cybernetics.* IEEE, 9(1), pp. 62–66. Available at: http://webserver2.tecgraf.puc-rio.br/~mgattass/cg/trbImg/Otsu.pdf.

Overton, M. L. (2001) *Numerical computing with ieee floating point arithmetic.* Siam. Available at: https://isbn.nu/0898714826.

Pearson, K. (1901) 'LIII. On lines and planes of closest fit to systems of points in space', *The London, Edinburgh, and Dublin Philosophical Magazine and Journal of Science.* Taylor & Francis, 2(11), pp. 559–572. doi: 10.1080/14786440109462720.

Pedregosa, F. *et al.* (2011) 'Scikit-learn: Machine learning in Python',

Journal of Machine Learning Research, 12, pp. 2825–2830. Available at: http://www.jmlr.org/papers/v12/pedregosa11a.

Piontkovski, S. A. *et al.* (2017) 'Subsurface algal blooms of the northwestern Arabian Sea', *Marine Ecology Progress Series*, 566, pp. 67–78. doi: 10.3354/meps11990.

Poynton, C. A. (1996) *A technical introduction to digital video.* Wiley New York. Available at: https://isbn.nu/9780471122531.

Pratt, S. R. *et al.* (1999) 'An operational and performance overview of the IRIDIUM low earth orbit satellite system', *IEEE Communications Surveys.* IEEE, 2(2), pp. 2–10. doi: 10.1109/COMST.1999.5340513.

Quetin, L. B. and Ross, R. M. (1991) 'Behavioral and physiological characteristics of the Antarctic krill, Euphausia superba', *American Zoologist.* Oxford University Press UK, 31(1), pp. 49–63. doi: 10.1093/icb/31.1.49.

Razavi, S. and Gupta, H. V. (2015) 'What do we mean by sensitivity analysis? The need for comprehensive characterization of "global" sensitivity in Earth and Environmental systems models', *Water Resources Research.* Wiley Online Library, 51(5), pp. 3070–3092. doi: 10.1002/2014WR016527.

Reid, K. *et al.* (2010) 'Krill population dynamics at South Georgia: implications for ecosystem-based fisheries management', *Marine Ecology Progress Series*, 399, pp. 243–252. doi: 10.3354/meps08356.

Reiss, C. S. *et al.* (2008) 'Variations in the biomass of Antarctic krill (Euphausia superba) around the South Shetland Islands, 1996–2006', *ICES Journal of Marine Science.* Oxford University Press, 65(4), pp. 497–508. doi: 10.1093/icesjms/fsn033.

Renfree, J. S. and Demer, D. A. (2016) 'Optimizing transmit interval and logging range while avoiding aliased seabed echoes', *ICES Journal of Marine Science.* Oxford University Press, 73(8), pp. 1955–1964. doi: 10.1093/icesjms/fsw055.

Robertson, A. R. (1977) 'The CIE 1976 color-difference formulae', *Color*

Research & Application. Wiley Online Library, 2(1), pp. 7–11. doi: 10.1002/j.1520-6378.1977.tb00104.x.

Robertson, A. R. (1990) 'Historical development of CIE recommended color difference equations', *Color Research & Application.* Wiley Online Library, 15(3), pp. 167–170. doi: 10.1002/col.5080150308.

Robotham, H. *et al.* (2010) 'Acoustic identification of small pelagic fish species in chile using support vector machines and neural networks', *Fisheries Research.* Elsevier, 102(1-2), pp. 115–122. doi: 10.1016/j.fishres.2009.10.015.

Roemmich, D. *et al.* (2009) 'The Argo Program: Observing the global ocean with profiling floats'. Oceanography Society. Available at: https://www.jstor.org/stable/24860957.

Rogers, A. *et al.* (2019) 'Antarctic futures: an assessment of climate-driven changes in ecosystem structure, function, and service provisioning in the Southern Ocean', *Annual review of marine science.* Annual Reviews, 12. doi: 10.1146/annurev-marine-010419-011028.

Rogowitz, B. E. and Kalvin, A. D. (2001) 'The which blair project: A quick visual method for evaluating perceptual color maps', in *Proceedings of the conference on visualization'01.* IEEE Computer Society, pp. 183–190. doi: 10.1109/VISUAL.2001.964510.

Rogowitz, B. E., Treinish, L. A. and Bryson, S. (1996) 'How not to lie with visualization', *Computers in Physics.* AIP, 10(3), pp. 268–273. doi: 10.1063/1.4822401.

Rosenblatt, F. (1958) 'The perceptron: A probabilistic model for information storage and organization in the brain.', *Psychological review.* American Psychological Association, 65(6), p. 386. doi: 10.1037/h0042519.

Ross, T., Keister, J. E. and Lara-Lopez, A. (2013) 'On the use of high-frequency broadband sonar to classify biological scattering layers from a cabled observatory in saanich inlet, british columbia', *Methods in Oceanog-*

raphy. Elsevier, 5, pp. 19–38. doi: 10.1016/j.mio.2013.05.001.

Rudnick, D. L. (2016) 'Ocean research enabled by underwater gliders', *Annual review of marine science.* Annual Reviews, 8, pp. 519–541. doi: 10.1146/annurev-marine-122414-033913.

Rumelhart, D. E., Hinton, G. E. and Williams, R. J. (1986) 'Learning representations by back-propagating errors', *Nature.* Nature Publishing Group, 323(6088), p. 533. doi: 10.1038/323533a0.

Runeson, P. (2006) 'A survey of unit testing practices', *IEEE software.* IEEE, 23(4), pp. 22–29. doi: 10.1109/MS.2006.91.

Ryan, T. E. *et al.* (2015) 'Reducing bias due to noise and attenuation in open-ocean echo integration data', *ICES Journal of Marine Science.* Oxford University Press, 72(8), pp. 2482–2493. doi: 10.1093/icesjms/fsv121.

Samek, W., Wiegand, T. and Müller, K.-R. (2017) 'Explainable artificial intelligence: Understanding, visualizing and interpreting deep learning models', *arXiv preprint arXiv:1708.08296.* Available at: https://arxiv.org/abs/1708.08296.

Santora, J. A. *et al.* (2012) 'Krill space: A comparative assessment of mesoscale structuring in polar and temperate marine ecosystems', *ICES Journal of Marine Science.* Oxford University Press, 69(7), pp. 1317–1327. doi: 10.1093/icesjms/fss048.

Saunders, R. *et al.* (2007) 'Intra-annual variability in the density of Antarctic krill (Euphausia superba) at South Georgia, 2002–2005: within-year variation provides a new framework for interpreting previous annual estimates of krill density', *CCAMLR Sci*, 14, pp. 27–41. Available at: http://www.ccamlrscience.com/index.php/ccamlrscience/article/viewFile/95/95.

Schiermeier, Q. (2010) 'Ecologists fear Antarctic krill crisis', *Nature*, 467. doi: 10.1038/467015a.

Shannon, C. E. (1948) 'A mathematical theory of communication', *The Bell System Technical Journal*, 27, pp. 379–423, 623–656. doi:

10.1145/584091.584093.

Siegel, V. (2016) 'Introducing Antarctic krill Euphausia superba Dana, 1850', in *Biology and ecology of antarctic krill.* Springer, pp. 1–19. doi: 10.1007/978-3-319-29279-3_1.

Silk, J. R. *et al.* (2016) 'Environmental correlates of Antarctic krill distribution in the Scotia Sea and southern Drake Passage', *ICES Journal of Marine Science.* Oxford University Press, 73(9), pp. 2288–2301. doi: 10.1093/icesjms/fsw097.

Simmonds, J. E., Armstrong, F. and Copland, P. J. (1996) 'Species identification using wideband backscatter with neural network and discriminant analysis', *ICES Journal of Marine Science: Journal du Conseil.* Oxford University Press, 53(2), pp. 189–195. doi: 10.1006/jmsc.1996.0021.

Simmonds, J. and MacLennan, D. N. (2005) *Fisheries acoustics: Theory and practice.* John Wiley & Sons. doi: 10.1002/9780470995303.

Simrad (2012) *Simrad EK60 Context sensitive on-line help.* Release 2.4.x. Kongsberg Maritime AS; http://www.simrad.net/ek60_ref_english/default.htm.

Soille, P. (2013) *Morphological image analysis: Principles and applications.* Springer Science & Business Media. Available at: https://isbn.nu/9783540429883.

Sozer, E. M., Stojanovic, M. and Proakis, J. G. (2000) 'Underwater acoustic networks', *IEEE journal of oceanic engineering.* IEEE, 25(1), pp. 72–83. doi: 10.1109/48.820738.

Spalding, J. A. (1999) 'Colour vision deficiency in the medical profession', *British Journal of General Practice.* Royal College of General Practitioners, 49(443), pp. 469–475. Available at: https://bjgp.org/content/49/443/469.

Spiegelhalter, D. (2019) *The art of statistics: How to learn from data.* Penguin, Random House, UK. Available at: https://isbn.nu/9780241398630.

Stammerjohn, S. E. *et al.* (2008) 'Trends in Antarctic annual sea ice retreat

and advance and their relation to El Niño–Southern Oscillation and Southern Annular Mode variability', *Journal of Geophysical Research: Oceans.* Wiley Online Library, 113(C3). doi: 10.1029/2007JC004269.

Stenseth, N. C. *et al.* (2002) 'Ecological effects of climate fluctuations', *Science.* American Association for the Advancement of Science, 297(5585), pp. 1292–1296. doi: 10.1126/science.1071281.

Steyerl, H. (2016) 'A sea of data: Apophenia and pattern (Mis-) Recognition', *E-flux Journal*, 72. Available at: https://www.e-flux.com/journal/72/60480/a-sea-of-data-apophenia-and-pattern-mis-recognition/.

Suberg, L. *et al.* (2014) 'Assessing the potential of autonomous submarine gliders for ecosystem monitoring across multiple trophic levels (plankton to cetaceans) and pollutants in shallow shelf seas', *Methods in Oceanography.* Elsevier, 10, pp. 70–89. doi: 10.1016/j.mio.2014.06.002.

Sumaila, U. R. (2012) 'Seas, oceans and fisheries: A challenge for good governance', *The Round Table.* Taylor & Francis, 101(2), pp. 157–166. doi: 10.1080/00358533.2012.661532.

Sun, C. *et al.* (2017) 'Revisiting unreasonable effectiveness of data in deep learning era', in *Proceedings of the ieee international conference on computer vision*, pp. 843–852. doi: 10.1109/ICCV.2017.97.

Sund, O. (1935) 'Echo sounding in fishery research', *Nature.* Nature Publishing Group, 135(3423), p. 953. doi: 10.1038/135953a0.

Tarling, G. A. *et al.* (2009) 'Variability and predictability of antarctic krill swarm structure', *Deep Sea Research Part I: Oceanographic Research Papers.* Elsevier, 56(11), pp. 1994–2012. doi: 10.1016/j.dsr.2009.07.004.

Testor, P. *et al.* (2019) 'OceanGliders: a component of the integrated GOOS', *Frontiers in Marine Science.* Frontiers, 6, p. 422. doi: 10.3389/fmars.2019.00422.

Thyng, K. M. *et al.* (2016) 'True colors of oceanography', *Oceanography*, 29(3), p. 10. doi: 10.5670/oceanog.2016.66.

Towers, S. (2014) 'Potential fitting biases resulting from grouping data into variable width bins', *Physics Letters B*. Elsevier, 735, pp. 146–148. doi: 10.1016/j.physletb.2014.06.023.

Trathan, P. *et al.* (1995) 'Krill biomass in the Atlantic', *Nature*. Nature Publishing Group, 373(6511), pp. 201–202. doi: 10.1038/373201b0.

Trathan, P. N. and Hill, S. L. (2016) 'The importance of krill predation in the Southern Ocean', in *Biology and ecology of antarctic krill*. Springer, pp. 321–350. doi: 10.1007/978-3-319-29279-3_9.

Trenkel, V. M. *et al.* (2009) 'Overview of recent progress in fisheries acoustics made by Ifremer with examples from the Bay of Biscay', *Aquatic Living Resources*. EDP Sciences, 22(4), pp. 433–445. doi: 10.1051/alr/2009027.

Tufte, E. R. (1983) *The visual display of quantitative information*. Graphics Press Cheshire, CT. Available at: https://isbn.nu/9780961392109.

Tukey, J. W. (1962) 'The future of data analysis', *The annals of mathematical statistics*. JSTOR, 33(1), pp. 1–67. Available at: https://www.jstor.org/stable/2237638.

Upton, E. and Halfacree, G. (2014) *Raspberry Pi user guide*. John Wiley & Sons. Available at: https://isbn.nu/1118921666.

Urick, R. J. (1967) *Principles of underwater sound for engineers*. Tata McGraw-Hill Education. Available at: https://isbn.nu/0070660859.

Urmy, S. S., Horne, J. K. and Barbee, D. H. (2012) 'Measuring the vertical distributional variability of pelagic fauna in Monterey Bay', *ICES Journal of Marine Science: Journal du Conseil*. Oxford University Press, 69(2), pp. 184–196. doi: 10.1093/icesjms/fsr205.

Vaseghi, S. V. (2008) *Advanced digital signal processing and noise reduction*. John Wiley & Sons. Available at: https://isbn.nu/9780470754061.

Villalobos, H. (2017) 'An open source tool for echogram visualization and analysis', in *2017 ieee/oes acoustics in underwater geosciences symposium (rio acoustics)*. IEEE, pp. 1–4. doi: 10.1109/RIOAcoustics.2017.8349734.

Von Alt, C. (2003) 'Autonomous underwater vehicles', in *Autonomous underwater lagrangian platforms and sensors workshop*. Available at: https://auvac.org/uploads/publication_pdf/AUVs%20WHOI%202003.pdf.

Vujović, V. and Maksimović, M. (2015) 'Raspberry Pi as a Sensor Web node for home automation', *Computers & Electrical Engineering*. Elsevier, 44, pp. 153–171. doi: 10.1016/j.compeleceng.2015.01.019.

Wall, C. C., Jech, J. M. and McLean, S. J. (2016) 'Increasing the accessibility of acoustic data through global access and imagery', *ICES Journal of Marine Science*. Oxford University Press, 73(8), pp. 2093–2103. doi: 10.1093/icesjms/fsw014.

Wallace, G. K. (1992) 'The jpeg still picture compression standard', *IEEE transactions on consumer electronics*. IEEE, 38(1), pp. xviii–xxxiv. doi: 10.1109/30.125072.

Ware, C. (1988) 'Color sequences for univariate maps: Theory, experiments and principles', *IEEE Computer Graphics and Applications*. IEEE, 8(5), pp. 41–49. doi: 10.1109/38.7760.

Watkins, J. L. *et al.* (2004) 'The CCAMLR 2000 Survey: a multinational, multi-ship biological oceanography survey of the Atlantic sector of the Southern Ocean', *Deep Sea Research Part II: Topical Studies in Oceanography*, 51(12), pp. 1205–1213. doi: 10.1016/j.dsr2.2004.06.010.

Watkins, J. *et al.* (2016) 'The use of fishing vessels to provide acoustic data on the distribution and abundance of Antarctic krill and other pelagic species', *Fisheries Research*. Elsevier, 178, pp. 93–100. doi: 10.1016/j.fishres.2015.07.013.

Weill, A., Scalabrin, C. and Diner, N. (1993) 'MOVIES-b: An acoustic detection description software. Application to shoal species' classification', *Aquatic Living Resources*. EDP Sciences, 6(3), pp. 255–267. doi: 10.1051/alr:1993026.

Whitehouse, M. *et al.* (2008) 'Rapid warming of the ocean around South

Georgia, Southern Ocean, during the 20th century: forcings, characteristics and implications for lower trophic levels', *Deep Sea Research Part I: Oceanographic Research Papers.* Elsevier, 55(10), pp. 1218–1228. doi: 10.1016/j.dsr.2008.06.002.

Whitehouse, M., Priddle, J. and Brandon, M. (2000) 'Chlorophyll/nutrient characteristics in the water masses to the north of South Georgia, Southern Ocean', *Polar Biology.* Springer, 23(6), pp. 373–382. doi: 10.1007/s003000050458.

Wiedenmann, J., Cresswell, K. and Mangel, M. (2008) 'Temperature-dependent growth of Antarctic krill: predictions for a changing climate from a cohort model', *Marine Ecology Progress Series*, 358, pp. 191–202. doi: 10.3354/meps07350.

Wild, C. J. and Pfannkuch, M. (1999) 'Statistical thinking in empirical enquiry', *International statistical review.* Wiley Online Library, 67(3), pp. 223–248. doi: https://doi.org/10.1111/j.1751-5823.1999.tb00442.x.

Witt, K. (2007) 'CIE color difference metrics', in *Colorimetry: Understanding the cie system.* Hoboken, NJ: John Wiley & Sons, pp. 79–100. Available at: https://isbn.nu/0470175621.

Woodd-Walker, R. S., Kingston, K. S. and Gallienne, C. P. (2001) 'Using neural networks to predict surface zooplankton biomass along a 50°N to 50°S transect of the Atlantic', *Journal of plankton research.* Oxford University Press, 23(8), pp. 875–888. doi: 10.1093/plankt/23.8.875.

Wu, L., Zielinski, A. and Bird, J. S. (1997) 'Lossless compression of hydroacoustic image data', *IEEE journal of oceanic engineering.* IEEE, 22(1), pp. 93–101. doi: 10.1109/48.557543.

Wynn, R. B. *et al.* (2014) 'Autonomous Underwater Vehicles (AUVs): Their past, present and future contributions to the advancement of marine geoscience', *Marine Geology.* Elsevier, 352, pp. 451–468.

Ziv, J. and Lempel, A. (1977) 'A universal algorithm for sequential data

compression', *IEEE Transactions on information theory.* IEEE, 23(3), pp. 337–343. doi: 10.1109/TIT.1977.1055714.

Ziv, J. and Lempel, A. (1978) 'Compression of individual sequences via variable-rate coding', *IEEE transactions on Information Theory.* IEEE, 24(5), pp. 530–536. doi: 10.1109/TIT.1978.1055934.